

1-1-1980

Synthesis and properties of electrically conducting polymers.

Gary Edmund Wnek
University of Massachusetts Amherst

Follow this and additional works at: https://scholarworks.umass.edu/dissertations_1

Recommended Citation

Wnek, Gary Edmund, "Synthesis and properties of electrically conducting polymers." (1980). *Doctoral Dissertations 1896 - February 2014*. 656.
<https://doi.org/10.7275/k31e-qg53> https://scholarworks.umass.edu/dissertations_1/656

This Open Access Dissertation is brought to you for free and open access by ScholarWorks@UMass Amherst. It has been accepted for inclusion in Doctoral Dissertations 1896 - February 2014 by an authorized administrator of ScholarWorks@UMass Amherst. For more information, please contact scholarworks@library.umass.edu.



312066 0015 5663 0

SYNTHESIS AND PROPERTIES OF
ELECTRICALLY CONDUCTING
POLYMERS

A Dissertation Presented

By

GARY EDMUND WNEK

Submitted to the Graduate School of the
University of Massachusetts in partial fulfillment
of the requirements for the degree of

DOCTOR OF PHILOSOPHY

September 1980

Polymer Science and Engineering

©

Gary Edmund Wnek

1980

All Rights Reserved

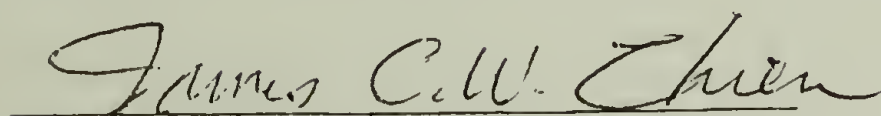
SYNTHESIS AND PROPERTIES OF ELECTRICALLY
CONDUCTING POLYMERS

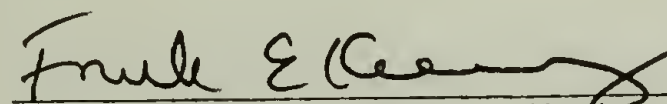
A Dissertation Presented

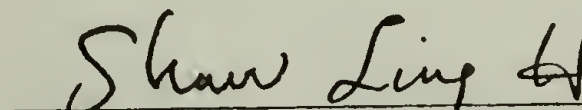
by

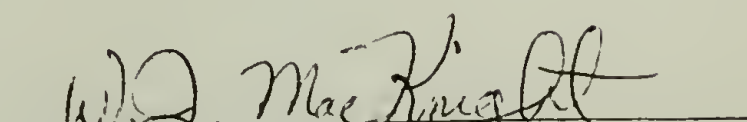
GARY EDMUND WNEK

Approved as to style and content by


Prof. James C.W. Chien,
Chairperson of Committee


Prof. Frank E. Karasz, Member


Prof. Shaw L. Hsu, Member


Prof. William J. MacKnight, Head
Department of Polymer Science and
Engineering

DEDICATION

To the most influential people in my life - my parents, my wife and Professors James C. W. Chien and James W. Pavlik.

ACKNOWLEDGEMENT

I wish to express my sincere appreciation to Prof. James C. W. Chien for his inspiration and advice during the course of this dissertation work. I was truly influenced by the fundamental enthusiasm for science which he possesses. I am indebted to him for his continuous interest in my scientific career.

The members of my Thesis Committee, Prof. Frank E. Karasz and Prof. S. L. Hsu, provided invaluable advice, support and encouragement. I enjoyed working with them and the entire faculty of the Polymer Science and Engineering Department. Collaboration with Prof. C. P. Lillya was enjoyable and stimulating. I am grateful to Dr. L. C. Dickinson for his time spent in offering me advice and support concerning a variety of subjects.

The friendship and good humor of my colleagues in the laboratory created a pleasant and stimulating environment in which to work. Furthermore, they all contributed in no small way to the successful completion of this dissertation work. Special thanks is due to Jim Capistran for assisting with innumerable experiments and for valuable suggestions concerning experimental techniques. Jack Hirsch provided invaluable assistance as the dissertation work neared completion. Without his help, the copolymer project would not have reached fruition. I am grateful to Dr. Richard Gable for assistance with four-probe conductivity measurements and to Dr. Robert Galkiewicz, Louis Raboin and Richard Nathhorst for obtaining electron micrographs. I also wish to thank Dr. K. Yao, R. Good-

ing and M. Samolis for their synthetic efforts in the aromatic polymers project.

This dissertation work would not have been accomplished without the collaboration of the conducting polymers group at the University of Pennsylvania under the direction of Profs. A. G. MacDiarmid and A. J. Heeger. It was a privilege and a pleasure to work with them. In particular, thanks is due to Mark Druy for making available to our group experimental techniques concerning doping (Chapter III) and $(CH)_x$ film preparations (Chapter IV), for collaboration on the variable-density $(CH)_x$ project and for his hospitality during my visits to Philadelphia.

Our laboratory would have been immobilized without the efforts of Joe Walas, Jr., Gordon Good and Larry Williams in the UMASS glassblowing laboratory. Their assistance is gratefully acknowledged.

Words cannot express my appreciation for my parents, without whose continuous support this work would have not been possible. I can never repay them for their love and their desire to foster my education.

Finally, I am grateful to my wife, Maria, for her continuous love and support. She willingly endured many evenings alone and spent several hours drawing the figures in this dissertation.

ABSTRACT

SYNTHESIS AND PROPERTIES OF
ELECTRICALLY CONDUCTING POLYMERS

(September 1980)

Gary E. Wnek, B.S. Worcester Polytechnic Institute, 1977
Ph.D. University of Massachusetts, Amherst, 1980

Directed by: Professor James C.W. Chien

The recent demonstration of high electrical conductivity upon chemical doping of polyacetylene, $(CH)_x$, has generated a fundamental interest in this material. The objective of this dissertation work was to employ several approaches in the context of applied polymer science to the characterization and synthetic chemical modification of polyacetylene.

Following a brief introduction which summarizes appropriate aspects of the electrical properties of materials and reviews the field of polyacetylene chemistry, details of laboratory techniques concerning the purification of materials, doping procedures and the preparation of polyacetylene films are described.

Electron microscopy studies of $(CH)_x$ obtained with the $Ti(OBu)_4/Et_3Al$ catalyst system demonstrate that ca. 200 Å diameter fibrils dominate the nascent morphology. Surface area measurements are consistent with the morphology.

Electron paramagnetic resonance (EPR) investigations of in-situ acetylene polymerization demonstrate that paramagnetism is not an intrinsic property of cis $(CH)_x$. The polymerization mechanism and

vii

possible structures of catalyst species in the $\text{Ti}(\text{OBu})_4/\text{Et}_3\text{Al}$ system are discussed. Additional EPR studies emphasize the dependence of line width, line shape asymmetry and saturation behavior on the dopant concentration in cis $[\text{CH}(\text{AsF}_5)_y]_x$. The results indicate that paramagnetism increases upon AsF_5 doping; the opposite is observed in the case of iodine doping. The phenomenon of microwave heating of doped samples as a function of power is also discussed.

The synthesis of $(\text{CH})_x$ gels provides an intermediate for the production of variable-density $(\text{CH})_x$. Various synthetic techniques are described which broaden the scope of the processibility of $(\text{CH})_x$. Electrical transport studies of pristine and doped variable-density $(\text{CH})_x$ demonstrate that intrinsic electrical properties are not dependent upon changes in the bulk density of the material.

Copolymerization is shown to be an effective method for the modification of chemical, physical and electrical properties of $(\text{CH})_x$. The synthesis of acetylene/methyl acetylene copolymer films is described. Studies of EPR line width as a function of acetylene content in these materials suggest that they are true copolymers rather than homopolymer mixtures. The electrical conductivity of the doped copolymers decreases as the acetylene content of the copolymers decreases.

Finally, aromatic polymers are evaluated in terms of the electrical conductivities attainable through chemical doping. In particular, studies of poly(p-phenylene vinylene), or PPV, are emphasized.

IR and EPR studies substantiate the contention that PPV assumes metal-like properties upon doping with AsF_5 . The conductivity is found

to be essentially independent of the degree of polymerization of PPV. This result and the observation that only the surfaces of several aromatic polymers and model compounds become doped upon exposure to AsF_5 suggest that polymerization occurs in conjunction with doping.

TABLE OF CONTENTS

DEDICATION	iv
ACKNOWLEDGEMENT	v
ABSTRACT	vii
Chapter	
I. INTRODUCTION	1
Statement of the Problem	1
Electrical Properties of Materials	2
General considerations; metals, semiconductors and insulators	2
Semimetals; dimensionality	8
Electrical conductivity in organic molecules and polymers	11
Charge transfer complexes; "organic metals"	15
Polyacetylene, $(CH)_x$; Historical Survey	19
The laboratory curiosity	19
Polyacetylene films	21
Cis and trans $(CH)_x$; isomerization	22
Comments on the electrical conductivity of "pristine" $(CH)_x$	28
Doped polyacetylene	29
The semiconductor-metal transition	32
Electrical transport studies	37
Partially oriented films; anisotropic electrical and optical properties	38
The function of the dopant	39
The conduction mechanism	43
Applications of doped $(CH)_x$	44
References	45
II. EQUIPMENT AND PURIFICATION OF MATERIALS	51
Equipment	51
Vacuum line	51
Schlenk tubes	53
Gas storage bulbs	53

TABLE OF CONTENTS (continued)

Syringes	56
Glove bag and dry box.	56
Sample storage; EPR tubes.	56
Purification of Materials.	58
Inert gas.	58
Solvents	58
Acetylene.	64
Methylacetylene.	66
Polymerization catalyst components	66
References	68
III. ELECTRICAL CONDUCTIVITY MEASUREMENTS AND DOPING	
METHODS.	69
Conductivity Measurements.	69
General considerations	69
Experimental methods	71
Doping Methods	71
Apparatus.	71
Iodine	77
Arsenic pentafluoride.	79
Sodium naphthalide	82
Other dopants.	84
IV. SYNTHESIS OF <u>cis</u> (CH) _x FILMS	85
The apparatus.	85
Preparation of the catalyst.	88
The polymerization reaction.	91
Washing of <u>cis</u> (CH) _x film.	92
Transfer and storage of <u>cis</u> (CH) _x film	93
Orientation; quality of <u>cis</u> (CH) _x films.	94
Isomerization.	97
Cleaning the reactor	97
References	100

TABLE OF CONTENTS (continued)

V.	NASCENT MORPHOLOGY OF POLYACETYLENE	101
	Experimental	101
	Results	103
	Discussion	110
	Conclusions	112
	References	113
VI.	ELECTRON PARAMAGNETIC RESONANCE STUDY OF ACETYLENE POLYMERIZATION	114
	Experimental	116
	Results	120
	Discussion	127
	Inherent paramagnetism of $(CH)_x$	127
	Influence of oxygen on the resonance	127
	Interpretation of the EPR resonances from the catalyst	129
	Conclusions	133
	References	134
VII.	ELECTRON PARAMAGNETIC RESONANCE STUDY OF PRISTINE AND DOPED <u>CIS</u> $(CH)_x$	136
	Experimental	138
	AsF ₅	139
	Iodine	141
	EPR spectra	141
	Results	142
	EPR saturation	143
	Undoped $(CH)_x$	143
	AsF ₅ -doped $(CH)_x$	143
	Iodine doping	163
	Discussion	168
	Saturation behavior; undoped $(CH)_x$	168
	AsF ₅ doping	169
	Iodine doping	172
	Microwave heating	173

TABLE OF CONTENTS (continued)

Conclusions	174
References	176
VIII. POLYACETYLENE GELS AND VARIABLE DENSITY CONDUCTING POLYMERS	178
Experimental	181
Preparation of $(CH)_x$ gels	181
Processing of $(CH)_x$ gels; pressed films	182
Processing of $(CH)_x$ gels; foam-like $(CH)_x$	183
Variable density $(CH)_x$	185
Observations concerning gel preparations	185
Doping and electrical measurements	186
Morphology	187
Results	187
Discussion	195
Morphology	195
Electrical transport studies	197
Conclusions	200
References	202
IX. ACETYLENE-METHYL ACETYLENE COPOLYMER FILMS	205
Experimental	207
Comonomer feed	207
Copolymer film synthesis	209
Preparation of poly (methylacetylene), $(C_3H_4)_x$	212
Doping	215
Spectra	215
Results	215
Copolymer compositions	215
Qualitative comparisons	218
Miscellaneous properties	229
Electrical conductivity	237
Discussion	241

TABLE OF CONTENTS
(continued)

Conclusions	245
References	247
X. AROMATIC CONDUCTING POLYMERS	249
Experimental	252
Preparation of samples for doping and spectroscopy	258
EPR spectra	260
Results	260
PPV	260
Model compounds and PPV derivatives	275
Discussion	276
Conclusions	281
References	283
IX. CONCLUSIONS	285

LIST OF TABLES

1. Conductivities and compositions of selected $(CH)_x$ derivatives . .	31
2. Surface areas of $(CH)_x$ film from B.E.T. measurements	109
3. EPR data of <u>in situ</u> acetylene polymerization in the presence of $Ti(OBu)_4/4Et_3Al$ at $-78^\circ C$	121
4. EPR relaxation data (T_1, T_2) for <u>cis</u> and <u>trans</u> $(CH)_x$ and <u>cis</u> $[CH(AsF_5)]_y$	159
5. Conductivity and thermopower data for pristine and doped pressed film and foam-like $(CH)_x$	190
6. Comonomer feed and copolymer compositions for acetylene methyl acetylene copolymer films	216
7. Conductivities and compositions of selected doped copolymer films	238
8. Effect of elongation ratio (l/l_0) on σ for an AMA-11 copolymer film doped with iodine	241
9. Elemental analyses of selected polymers	257
10. Room temperature conductivity of AsF_5 -doped PPV	261
11. Conductivity and EPR data for doped aromatic polymers and model compounds	263

LIST OF FIGURES

1. Electronic band descriptions of materials	4
2. Electrical conductivity as a function of dopant concentration for polyacetylene doped with I_2 , Br_2 and AsF_5	34
3. Comparisons of electrical conductivities of various materials	36
4. Vacuum line	52
5. Schlenk tube	54
6. Gas storage bulb	55
7. Sample storage and EPR tubes	57
8. Solvent still	61
9. Solvent storage tube	63
10. Acetylene purification system	65
11. Schematic diagram of four-probe electronics	72
12. Four-probe apparatus	74
13. Apparatus for the synthesis of $(CH)_x$ films	87
14. Apparatus for orientation of <u>cis</u> $(CH)_x$ films	96
15. Infrared spectrum of <u>cis</u> $(CH)_x$	99
16. Electron micrographs of thin $(CH)_x$ films on gold grids	105
17. Electron micrographs of $(CH)_x$ films on grids and as-grown films	107
18. Apparatus for polymerization of acetylene in an EPR sample tube	118
19. EPR spectra of $Ti(OBu)_4/4Et_3Al$ at $-78^\circ C$	123
20. EPR spectra of $Ti(OBu)_4/4Et_3Al$ in the presence of C_2H_2 at room temperature	125
21. EPR saturation plots of <u>cis</u> and <u>trans</u> $(CH)_x$	145
22. EPR spectra of <u>cis</u> $[CH(AsF_5)_y]_x$	147
23. Plot of EPR lineshape asymmetry (A/B) <u>vs.</u> y for <u>cis</u> $[CH(AsF_5)_y]_x$	151
24. Plot of ΔH_{pp}° <u>vs.</u> y for <u>cis</u> $[CH(AsF_5)_y]_x$	153
25. EPR saturation plots of <u>cis</u> $[CH(AsF_5)_y]_x$	155
26. Plots of sample temperature <u>vs.</u> microwave power for <u>cis</u> $[CH(AsF_5)_y]_x$	158

LIST OF FIGURES
(continued)

27. EPR spectra of <u>cis</u> (CH) _x lightly doped with AsF ₅	162
28. EPR spectra as a function of microwave power of <u>cis</u> (CH) _x lightly doped with AsF ₅	165
29. EPR saturation plots of <u>cis</u> [CHI _y] _x	167
30. Electron micrographs of pressed film and foam-like (CH) _x	189
31. Plot of conductivity <u>vs.</u> density for iodine-doped (CH) _x	192
32. Normalized temperature dependence of the conductivity for undoped and doped pressed film and foam-like (CH) _x	194
33. Plot of comonomer feed <u>vs.</u> copolymer composition	217
34. Electron micrographs of (CH) _x film prepared using high concentrations of Ti(OBu) ₄ /Et ₃ Al	221
35. Electron micrographs of AMA-31 copolymer film.	223
36. Electron micrographs of AMA-11 and AMA-13 copolymer films.	225
37. Infrared spectrum of poly (methylacetylene).	228
38. Plot of EPR linewidth as a function of acetylene content in copolymer films	231
39. Infrared spectra of AMA-11 film	234
40. TGA curves of (CH) _x , (C ₃ H ₄) _x and AMA-11.	236
41. Plot of conductivity <u>vs.</u> copolymer composition for films coped with iodine and AsF ₅	240
42. Structures of aromatic polymers and model compounds.	254
43. Infrared spectra of undoped and AsF ₅ -doped PPV	268
44. EPR spectra of PPV doped with AsF ₅	270
45. EPR saturation plots of AsF ₅ -doped PPV	272
46. EPR saturation plots of AsF ₅ -doped model compounds	274

CHAPTER I

INTRODUCTION

Statement of the Problem

High electrical conductivity has always been regarded as a property specific to the metallic elements. Materials such as organic molecules and polymers, on the other hand, are typically insulators. However, it has been known for several years that significantly improved conductivity can be achieved in organic materials through charge transfer interactions. In fact, certain charge transfer complexes exhibit extremely high conductivity and have been classified as "organic metals" or "synthetic metals." Such high conductivity was unknown in organic polymer systems until the discovery of doped polyacetylene only four years ago. This discovery clearly indicated that polyacetylene is an extremely unusual material, which in turn demonstrated the need for fundamental research concerning its detailed macromolecular structure and physical properties in an effort to understand the conduction mechanism.

The characterization problem is unfortunately complicated by the extreme intractability of polyacetylene, although certain techniques such as electron paramagnetic resonance suggested the potential for a great deal of structural and mechanistic information concerning the polymerization reaction, free spin generation and dopant-polymer interactions. Synthetic chemical modification, besides offering entirely new classes of conducting polymers, also suggested promise as an indirect method for the elucidation of factors which influence electrical trans-

port in polyacetylene. Thus, the principal objective of this dissertation work was to attempt to characterize and modify polyacetylene, in the context of applied polymer science, in an effort to gain understanding about the relationship between structure and properties of this novel and interesting material.

Electrical Properties of Materials

General considerations: metals, semiconductors and insulators.^{1a,b} Materials are generally classified into three categories depending upon their ability to conduct electricity. Metals are excellent conductors and insulators are very poor conductors, while semiconductors display intermediate behavior. The response of a material to an applied electric field is governed by the energies of the electrons in the atoms and bonds of the material. This relationship is perhaps best understood by considering the electronic structure formed when several atoms are brought together to form a molecular entity. Simple molecular orbital, or band, theory provides a useful description of this electronic structure. Three important results of the theory are the following:

- i. Orbitals are conserved in creating molecules from atoms; n atomic orbitals lead to the formation of n molecular orbitals
- ii. If n is very large, the difference in energy between molecular orbitals is extremely small and these orbitals effectively form a continuous band of energy levels.
- iii. Each band can accommodate $2n$ electrons.

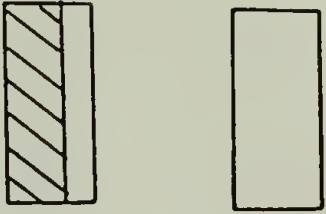
In metals, energy bands are incompletely filled (Figure 1a). For

Figure 1. Electronic energy band descriptions of materials.

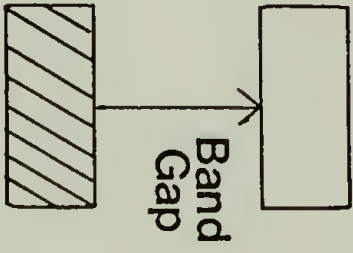
- A Metal
- B Intrinsic semiconductor
- C Extrinsic semiconductor
- D Insulator
- E Semimetal

Filled Levels Empty Levels

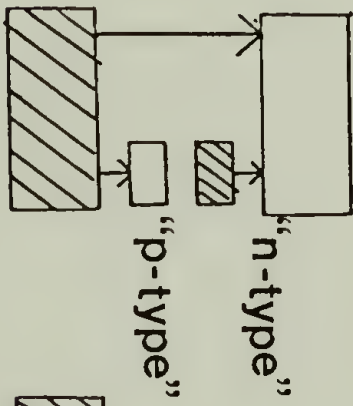
A



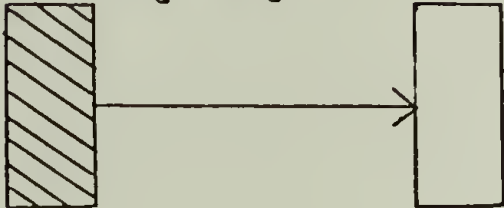
B



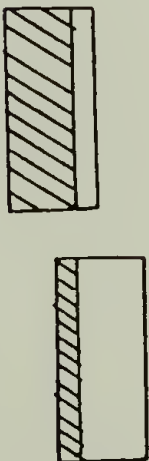
C



D



E



example, in the case of sodium, the 3s orbitals form a band which is only half filled since sodium possesses only one valence electron. The valence electrons in the highest filled energy levels are easily excited to unoccupied levels that are only infinitesimally higher in energy. Thus, the valence electrons are free to migrate within the metal lattice, giving rise to electrical conductivity. Since these electrons are not associated with a particular bond having a characteristic energy, they easily absorb and re-emit light at a variety of wavelengths, accounting for the luster of metals. The electrical conductivity of metals characteristically decreases with increasing temperature as the result of scattering due to thermally-induced lattice fluctuations.

Semiconductors and insulators differ from metals in that every energy band is either completely filled or completely empty (Figures 1b and 1d). The absence of partially filled low energy states is a direct consequence of the fact that all low energy states are used in the formation of covalent bonds. In an intrinsic semiconductor, electrons from the filled valence band are excited by heat or light to empty, high energy states in order to achieve free carriers for electrical conductivity. The energy barrier which must be crossed in the excitation process is referred to as the band gap. It should be noted that two carriers are created upon excitation; the electron in the previously vacant conduction band and a positive "hole" in the previously filled valence band.

Another class of semiconductor is the extrinsic, or "doped", semiconductor (Figure 1c). In this case, substitutional impurities or "dopants" supply charge carriers. For example, silicon is an intrinsic

semiconductor whose conductivity can be increased upon doping. Substitution of small amounts of gallium (a group III element) for silicon (a group IV element) in a silicon framework provides acceptor sites which allow the formation of charge deficiencies or positive holes in the valence band of silicon. Since electron holes, with their positive charges, are responsible for conduction, these materials are referred to as p-type semiconductors. On the other hand, partial replacement of silicon by arsenic (a group V element) provides donor sites and thus a small excess of electrons in the empty conduction band of silicon. Such a material is referred to as an n-type semiconductor. Three important points concerning extrinsic semiconductors should be noted. First, the donor and acceptor states (Figure 1c) are usually very close to the conduction and valence bands, respectively, allowing electron promotion to occur nearly completely at room temperature. Second, these materials have only one type of carrier, i.e., electrons or holes, in contrast to intrinsic semiconductors, which possess both. This aspect is extremely important in semiconductor device applications. Finally, the impurity states are localized, and hence are nonconducting.

In semiconductors, the electrical conductivity (σ) depends upon the concentration of charge carriers (n), their charge (e) and mobility (μ) according to

$$\sigma = ne\mu.$$

Increasing the temperature of an intrinsic semiconductor results in a concomitant increase in n , since more electrons obtain the energy necessary to cross the band gap, and a decrease in μ as the result of

scattering from lattice vibrations. At most practical temperatures the increase in n is dominant and the conductivity increases with increasing temperature, in contrast to metals. Extrinsic semiconductors show a less pronounced dependence on temperature than the intrinsic variety since most of the impurity states are ionized at room temperature.

Insulators (Figure 1d) differ from intrinsic semiconductors in that the band gap of insulators is very large. Hence, essentially no electron promotion across the energy gap occurs at ordinary temperatures.

It is worthwhile to note that the band gap of a material can substantially decrease or even "disappear" by compressing the material as a consequence of decreasing internuclear distances and increasing orbital overlap. Diamond, an insulator at room temperature, displays metallic properties when subjected to pressures of 600,000 atmospheres.

The electrical conductivities of common metals, semiconductors and insulators are compared in Figure 3. In general, the conductivity of metals is $\gtrsim 10^2 \Omega^{-1} \text{ cm}^{-1}$ while that of insulators is $\lesssim 10^{-9} \Omega^{-1} \text{ cm}^{-1}$; semiconductors fall within these limits. It should be noted that the absolute magnitude of the conductivity is not rigorously appropriate for distinguishing between metals and semiconductors. Several materials, in particular organic charge transfer complexes to be discussed shortly, may possess the high conductivity characteristic of metals but may differ in other respects, i.e., the temperature dependence of the conductivity.

The electrical conductivity of a particular material may vary depending on the quality of the specimen. Thus, the conductivity of sin-

gle crystals is generally higher than that of compacted powders, since interparticle contacts such as grain boundaries present in the latter introduce defection sites for electrons and provide resistance to electron flow. The experimentally measurable conductivity may be well below the intrinsic conductivity of the material. It is often desirable to examine intrinsic electrical properties, especially in the case of organic conductors, when single crystals are not easily obtained, and measurement of the thermopower provides a method for doing so. If one end of a material is heated, electrons in this region of the specimen gain energy and tend to migrate to the cold end. When this occurs, a potential difference, ΔV , is established between the two ends of the material and is known as the thermal electromotive force or thermopower. The thermopower coefficient, S , is the ratio of the voltage and temperature gradients:

$$S = \Delta V / \Delta T .$$

S is a zero-current transport coefficient and therefore does not depend on factors such as interparticle contact resistances. Since S can be viewed as the entropy per charge carrier, semiconductors typically yield large values of S (few carriers with many possible states per carrier) while metals, with many carriers, show small values of S . Furthermore, the sign of S indicates the nature of the carriers (positive for hole conduction and negative for electron conduction). The thermopower is a particularly useful parameter in studies of electrically conducting polymers where disorder is typically very large.

Semimetals; dimensionality. A limited number of materials exist in

which, in principle, all low energy states in the valence band are filled due to the formation of covalent bonds, although the filled valence bands and empty conduction bands overlap to generate two incompletely filled bands. This is illustrated in a simple manner in Figure 1e. The presence of partially filled bands allows metal-like conductivity in such materials, which are referred to as semimetals.

The most common example of a semimetal is an allotroph of carbon known as graphite.² In graphite, sp^2 hybridized orbitals constituting σ -bonds are formed into a planar hexagonal network while the remaining p_z orbital, the π -bond, loosely holds the planes together. This weak bonding between planes allows them to easily "slide" relative to each other and accounts for the lubricating properties of graphite. The conductivity of graphite is $\sim 10^4 \Omega^{-1} \text{ cm}^{-1}$ at room temperature and increases with decreasing temperature as does a metal. The electrical conductivity of graphite is anisotropic, being greater in the planes of hexagonal rings than perpendicular to the planes as a direct consequence of the greater bond strengths and orbital overlap within the planes. The anisotropy, $\sigma_{||}/\sigma_{\perp}$, is $\sim 10^4$ at room temperature.

This example of anisotropy serves to introduce the concept of dimensionality in discussions of electrically conducting materials. Common metals such as sodium are isotropic and thus conductivity is uniform in all directions; these are simply referred to as three-dimensional metals. On the other hand, conductivity in graphite preferentially occurs within the hexagonal planes. Hence, graphite is termed a two-dimensional metal. As dimensionality decreases, electrical conductivity

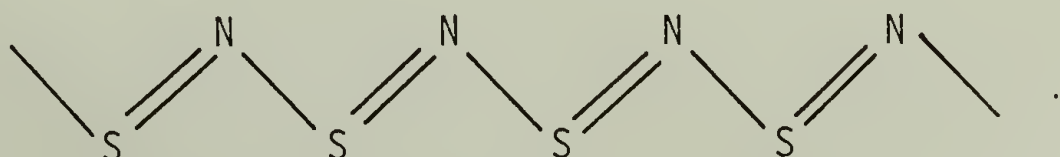
becomes progressively more sensitive to defects and disorder within the material.

The conductivity of graphite can be further increased² upon doping with electron donors (metals) or acceptors (non-metal molecular species such as Br_2 , HNO_3 , etc.) with the graphite lattice acting like a giant anion or cation, respectively. The dopants intercalate between the hexagonal planes in stages, the stage referring to the number of dopant layers between the planes. A large expansion results in the direction perpendicular to the planes and the stage can be determined from the lattice repeat distance.

Extremely high electrical conductivity is observed for selected graphite intercalation compounds. The most notable³ system is graphite- SbF_5 which possesses a conductivity ($\sim 10^6 \Omega^{-1} \text{ cm}^{-1}$); i.e., greater than that of copper or silver at room temperature. The anisotropy in such systems is also high ($\sigma_{\parallel}/\sigma_{\perp} \sim 10^6$).

Intercalated graphite fiber/polymer composites are being investigated as materials which provide high strength, light weight and conductivity for applications such as aircraft structural members.

Another interesting semimetal is polythiazyl,⁴ commonly referred to as poly(sulfur nitride) or $(\text{SN})_x$, having the structure



The high conductivity of single crystals of $(\text{SN})_x$ is the result of strong overlap of orbitals along the polymer chain. The conductivity is anisotropic, being greatest along the polymer chain axis. Thus,

$(\text{SN})_x$ is referred to as a one-dimensional metal. The anisotropy is relatively small ($\sigma_{11}/\sigma_{\perp} \sim 15$ at room temperature) indicating that there is significant overlapping of orbitals between chains. The temperature dependency of the conductivity resembles that of metals. Furthermore, $(\text{SN})_x$ becomes a superconductor⁵ at temperatures below 0.3K.

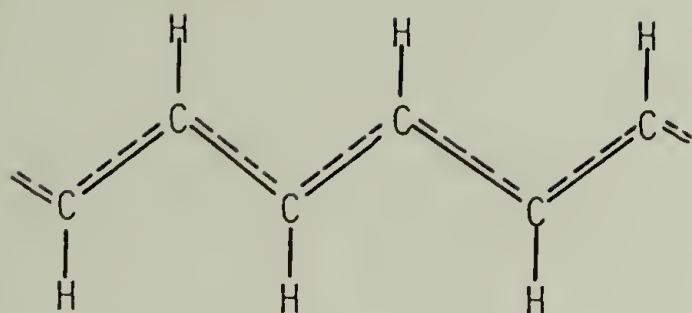
Exposure of $(\text{SN})_x$ to halogens⁴ (e.g., Br_2) increases its conductivity by about an order of magnitude with the materials having compositions such as $(\text{SNBr}_{0.4})_x$. Raman spectroscopy shows that Br_3^- is present in the brominated $(\text{SN})_x$, suggesting that bromine acts as an electron acceptor. The positive sign of the thermopower is consistent with this result. X-ray diffraction studies suggest that the bromine intercalates between $(\text{SN})_x$ chains. Reactions with I_2 , ICl and IBr have also been investigated. Due to the extreme intractability of $(\text{SN})_x$ and derivatives, it is doubtful that these materials will be technologically useful, although Schottky barriers and solar cells have been fabricated.⁴

Electrical conductivity in organic molecules and polymers.^{1b,5} Most organic molecules in the solid state are widely separated and held together by weak Van der Waals forces. These weak intermolecular interactions necessarily preclude strong orbital overlap between molecules and concomitant formation of energy bands. Thus, any potential charge carriers cannot move freely within an energy band, but rather "hop" from molecule to molecule by thermally activated processes. The mobility of these carriers is expected to be extremely low since the carriers will reside for long periods of time on the individual molecules. Certain organic molecules, however, do display strong intermolecular interactions. In

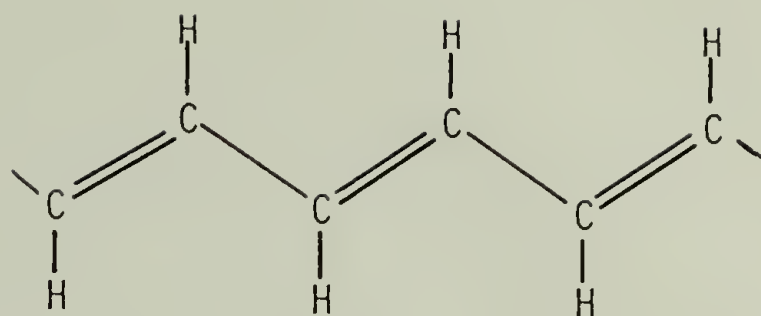
solid anthracene, for example, strong intermolecular π -orbital overlap essentially allows the formation of energy bands, and carriers can move freely through the bands. In fact, the mobility of anthracene is quite high ($\mu \sim 1 \text{ cm}^2 \text{ V}^{-1} \text{ s}^{-1}$). However, such aromatic molecules are usually devoid of charge carriers. Thus, as a general rule, organic molecules are insulators.

An internal conduction path of high mobility is envisioned if carriers can be delocalized within a conjugated system. Thus, polymers containing conjugated double bonds are known to be semiconductors, with carriers formed by activation of π -bonding electrons. It has been predicted that the activation energy for carrier formation decreases, and that the conductivity increases, with increasing conjugated chain length. This appears to be born out in a study of a series of poly(thiophene vinylenes) by Kossmehl et al.⁶ The dependence of conductivity on conjugation length suggests that carrier transport is anisotropic and occurs mainly along the polymer chain. Thus, conjugated polyenes appear to be pseudo-one-dimensional in terms of conduction.

A true polyene of sufficiently high molecular weight, such as polyacetylene, is expected to approach metal-like conductivity in the absence of bond alternation. This can be explained by noting that in polyacetylene three of the four valence electrons are in sp^2 hybridized orbitals; two of the σ bonds are links in the backbone while the third forms a bond with the hydrogen substituent. The remaining electron resides in a π -orbital which delocalizes along the chain. In terms of molecular orbital theory, the formation of a $(\text{CH})_x$ chain results in the



equal chain bond lengths
(metallic)



alternating chain bond lengths
(semiconducting)

trans polyacetylene

formation of an energy band for the π -electrons which is half-filled since each CH unit contains one valence electron. This is formally analogous to a band description of a "chain" of sodium atoms; each atom has one valence electron and thus the valence band is half-filled (Figure 1a). Contrary to expectations, however, polyacetylene is not a metal; the conductivity of trans polyacetylene is $\sim 10^5 \Omega^{-1} \text{ cm}^{-1}$ at room temperature. This has been rationalized by suggesting⁷ that any one-dimensional conductor is susceptible to an instability that alters the periodic spacing of the lattice (Peierls instability). Under certain conditions, the energy of the electrons in such a system can be reduced if an energy gap is created at the highest occupied level of the partially filled band. The gap can be introduced by a periodic distortion of the lattice. In the simplest sense such a distortion in polyacetylene can occur if units of the chain "clump" together in pairs so as to form alternating double and single bonds (see above). This chain structure will have a filled valence band and accounts for the fact that polyacetylene is a band gap semiconductor. The band gap for perfect

bond alternation in trans polyacetylene has been calculated⁸ to be ~ 2.3 eV while optical studies⁹ of this material yield $\sim 1.5 - 1.9$ eV. Thus, the real polyacetylene chain is intermediate in character between non-alternating and completely alternating bond lengths.

The Peierls instability is frequently used to explain other phenomena such as anomalous temperature dependencies of conductivity in one-dimensional conductors.

Placement of substituents on a polyene chain generally results in a decrease in conductivity due to steric interactions which cause a twisting of the chain and a reduction in the effective conjugation length. As an example, the conductivity of poly(phenyl acetylene)¹⁰ is $\sim 10^{-15} \Omega^{-1} \text{ cm}^{-1}$.

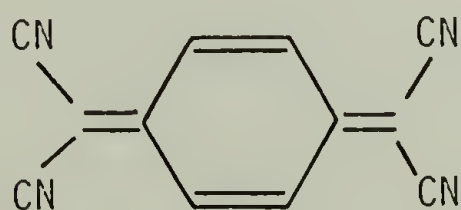
An interesting class of perfectly conjugated, macroscopic single-crystal polymers, the poly(diacetylenes), were first prepared by Wegner¹¹ by solid-state polymerization of diacetylene monomers. Although highly conjugated, most of these polymers are insulators ($\sigma \sim 10^{-10} \Omega^{-1} \text{ cm}^{-1}$). Electron spin resonance studies¹² have shown that the polymers have no measureable carrier concentration. It has been postulated¹³ that carrier generation in conjugated polyenes initially involves chain rotation to break double bonds, and that this mechanism is not possible in poly(diacetylenes) where the chain is locked in the crystal lattice. The optical properties¹¹ of polydiacetylenes have generated considerable interest.

Conjugated ladder polymers, such as polyacene quinones,¹⁴ display semiconducting properties although these materials are highly intract-

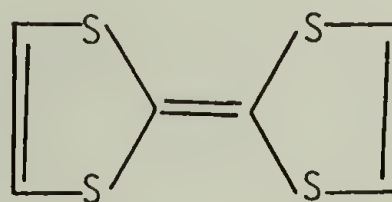
able.

Charge transfer complexes; "organic metals".^{1b,5} Certain organic materials are known to display unusually high electrical conductivity and, in most cases, extremely anisotropic conductivity. The anisotropy reflects the fundamental structure of these materials; namely, many parallel stacks of molecules in which orbital overlap is strong along the direction of the stacks. Since the greatest degrees of intermolecular overlap between orbitals of organic molecules result from π -electron clouds, most of these materials are comprised of aromatic molecules. As mentioned previously, these molecules have essentially no carriers for conductivity, although specific combinations of molecules are able to produce sufficient carriers through an important mechanism known as charge transfer. These molecular combinations are known as charge transfer complexes and, since very high conductivity can be achieved in selected cases, are sometimes referred to as one-dimensional conductors or "organic metals". A few examples will serve to illustrate their structure and function.

Perhaps the most well known of such materials is the stoichiometric complex¹⁵ of tetracyanoquinodimethane (TCNQ) and tetrathiafulvalene (TTF). The complex is comprised of alternating, parallel columns of TTF



TCNQ



TTF

and TCNQ molecules. Overlap of π -orbitals is strong in the direction of the stacks and anisotropic energy bands are formed. This is not the total picture, since these energy bands will be completely filled or completely empty, and hence no conductivity can occur. However, TTF is an electron donor and TCNQ is an electron acceptor, resulting in partial charge transfer between the stacks and creation of radical ions. The consequence is to partially fill the empty conduction band of TCNQ and partially empty the filled valence band of TTF. Since there is very little orbital interaction between stacks, conductivity between stacks is inefficient. Single crystals of TTF - TCNQ have a room temperature conductivity of $\sim 650 \Omega^{-1} \text{ cm}^{-1}$ parallel to the stack direction, with $\sigma_{\parallel}/\sigma_{\perp} \sim 500$. The negative sign of the thermopower indicates that the acceptor stacks dominate the conductivity.

The temperature dependence of the conductivity of TTF - TCNQ is metal-like down to $\sim 58\text{K}$ where a sharp maximum occurs, followed by a dramatic decrease in conductivity with temperature, corresponding to a metal-insulator transition. This unusual temperature dependence is not easily explained by simple band models. Charge density waves have been implicated as a possible rationale, although these are beyond the scope of this discussion. An excellent account of anomalous temperature dependencies in one-dimensional metals is given in Reference 1b.

It has long been recognized¹⁶ that aromatic molecules such as perylene form donor acceptor complexes with iodine. Again, it appears that individual, parallel stacks of each species are present in the complexes and that partial charge transfer between the donor (aromatic molecule)

and the acceptor (iodine) occurs. As a typical example,¹⁷ the conductivity of a perylene-4I₂ complex is $\sim 10^{-2} \Omega^{-1} \text{ cm}^{-1}$ in the stack direction with $\sigma_{\parallel}/\sigma_{\perp} \sim 10^3$. Other systems, such as perylene-nickel maleonitriledithiolate, appear to form mixed stacks, i.e., both donors and acceptors alternate in each individual stack.

Radical cation salts of perfluoronaphthalene have been recently reported by Bartlett et al.,¹⁸ and these are anticipated to be conductors. In fact, recent studies¹⁹ of radical anion salts of di-(tetramethyltetraselenafulvalene) and PF₆⁻, AsF₆⁻, etc., have demonstrated that conductivities as high as ca. $800 \Omega^{-1} \text{ cm}^{-1}$ can be achieved. Furthermore, at a pressure of 12 Kbar and a temperature of 0.9 K, the PF₆⁻ salt becomes superconducting.²⁰ This represents the first example of superconductivity in a synthetic organic material.

Aside from virtually creating a scientific revolution concerning the kinds of materials which can possess the high conductivity characteristic of metals, organic conductors offer a potentially large advantage over elemental metals. The latter are not very flexible in terms of electrical properties, although variations in conductivity can be afforded by various metal alloys. On the other hand, considering the possible subtle variations in structure of organic metals by synthetic chemical methods, fine-tuning of electrical properties can be anticipated depending primarily upon the imagination of the chemist. For example,¹⁵ substitution of selenium for sulfur in TTF raises the room temperature conductivity of TTF-TCNQ, lowers the metal-insulator transition and allows the donor stack to dominate electrical transport properties. Fur-

thermore, bulky substituents on TTF and/or TCNQ increases the distance between the stacks with a corresponding increase in anisotropy. A number of other synthetic modifications of this system have recently been described.¹⁵

Several organic polymer charge transfer complexes have been made although the conductivities are quite low ($\sim 10^3 \Omega^{-1} \text{ cm}^{-1}$), presumably due to the inherent microscopic disorder of polymers precluding efficient stacking of donor and acceptor species. Some examples⁵ of these complexes are poly(N-vinylpyridine)-iodine, poly(vinyl-tetrathiafulvalene)-TCNQ and poly(vinyl-phenothiazine)-2, 4, 5, 7 - tetranitrofluorenone. Charge carriers (radical ions) can be generated in poly(N-vinyl carbazole) upon exposure to light, and the photoconductivity of this material has found practical applications in electronic copying machines. Organometallic polymers based on ferrocene are typically insulators, although increased conductivities are observed upon partial oxidation of ferrocene (Fe^{2+}) to ferrocinium (Fe^{3+}) units. A comprehensive review of polymeric charge transfer complexes is given in Reference 5.

The low conductivity observed in polymer systems is disappointing in view of the fact that polymers are the most versatile of all materials. Besides control of electrical properties through structural modifications, important properties such as flexibility, light weight and ease of production are anticipated to offer significant advantages over low molecular weight organic conductors and even traditional metals. However, the recent discovery of doped, highly conducting polyacetylene²¹ has stirred considerable interest concerning the structure and proper-

ties of this unique material and has provided renewed promise that construction of materials which combine high conductivity and polymer versatility can be achieved.

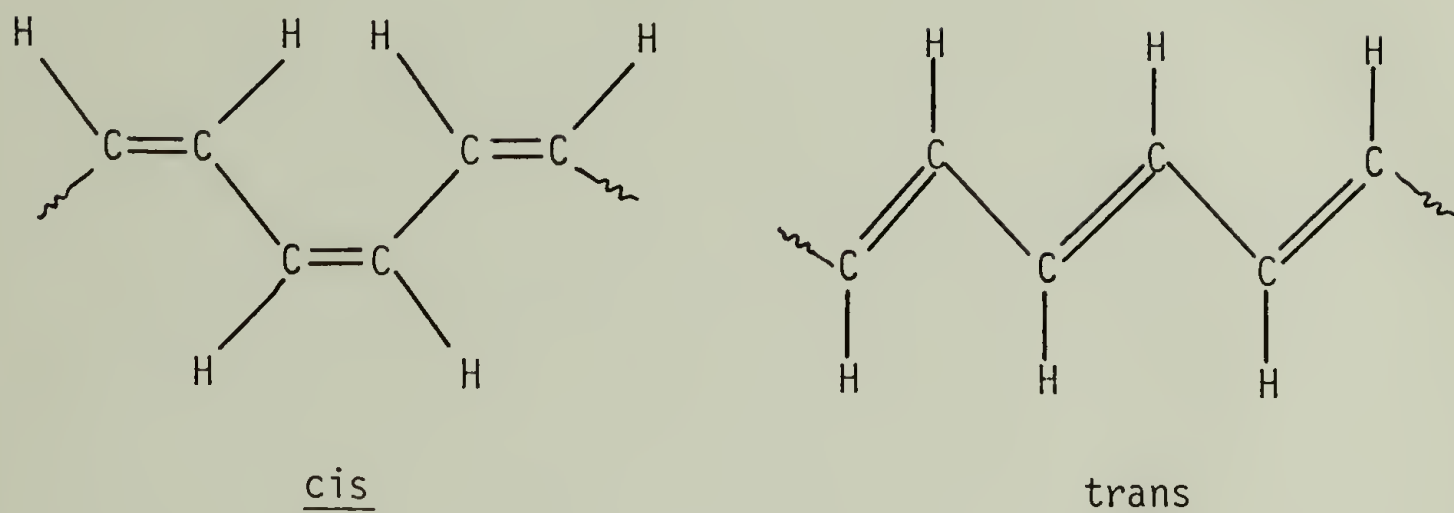
Prerequisite to the interpretation of the unique electrical characteristics of polyacetylene is an understanding of its structure and properties in the context of macro-molecular science and is the foremost objective of this dissertation work.

Polyacetylene, $(CH)_x$: Historical Survey

The discussion to be presented below is a comprehensive account of studies concerning the chemical and physical properties of polyacetylene and doped derivatives. The discovery of doped polyacetylene has generated fundamental interest in the properties of the parent material which were previously ignored. Thus, for the sake of coherence, the historical survey will not necessarily be chronological; rather, studies of pristine and doped polyacetylene will be treated separately.

The laboratory curiosity. Acetylene was first polymerized to a linear conjugated polymer by Natta and coworkers in 1958,²² and over the next several years numerous catalyst systems²³⁻²⁸ were reported for the synthesis of $(CH)_x$. The material formed was usually a gray or black powder with crystallinity depending on the catalyst employed. Polyacetylene can exist as the cis or trans isomer (or a mixture) depending on the polymerization temperature. This relationship will be discussed in more detail shortly, but suffice it to say that most syntheses employed relatively high reaction temperatures ($\sim 50^\circ \text{C}$), with the resulting polymers

having predominantly the trans structure.



Unfortunately, polyacetylene is insoluble and does not melt, thus precluding rigorous characterization at the molecular level. Consequently, fundamental properties such as molecular weight and degree of chain branching cannot be determined by conventional methods. Although the intractable $(\text{CH})_x$ was for the most part considered to be a laboratory curiosity, it was soon recognized to be a semiconductor,²³ having a typical conductivity of ca. $10^{-5} \Omega^{-1} \text{ cm}^{-1}$. The temperature dependence of the conductivity indicated that $(\text{CH})_x$ is an intrinsic band-gap semiconductor. The material was also found to be paramagnetic from electron spin resonance measurements.²³

Hatano et al.²³ showed that the electrical conductivity of $(\text{CH})_x$ increased with the crystallinity of the sample. Polyacetylene, which is of course rich in carbon-carbon double bonds, was found to be very susceptible to oxidation. Berets and Smith²⁷ found that the oxygen content of $(\text{CH})_x$ is important; samples having the lowest oxygen contents yielded the highest conductivities. These workers also discovered that a small increase in conductivity (ca. 0.3×10^{-5} to $1.7 \times 10^{-5} \Omega^{-1} \text{ cm}^{-1}$) could

be achieved upon exposure to a compressed pellet of $(CH)_x$ to chlorine. It is perhaps unfortunate that chlorine, which easily adds across the double bonds in $(CH)_x$ and hence destroys conjugation, was used in their experiment. Nevertheless, this represents the first attempt at modifying the conductivity of polyacetylene through the addition of a chemical impurity, or dopant.

Polyacetylene films. Any polymeric material in film form is more amenable to study, especially in terms of electrical properties. Polyacetylene was reportedly prepared²⁹ as a film by glow discharge polymerization although such films were extremely thin and rather impractical for study. In the early 1970's, however, an important synthetic procedure was developed by Shirakawa and coworkers.³⁰⁻³² They succeeded in synthesizing flexible, continuous films of $(CH)_x$ using a soluble Ziegler-Natta catalyst based on titanium tetrabutoxide and triethyl aluminum. These workers also developed techniques for controlling the cis-trans content of $(CH)_x$. The polymer film grows on all surfaces wetted with the catalyst solution. The surface of the film which grows on the face of a glass reactor wall displays a coppery or silvery luster, while the backside of the film possesses a dull maroon or gray coloration representative of cis or trans material, respectively. Electron microscopy studies³² indicate that the films are comprised of random, twisted fibrils about 200 \AA in diameter. The bulk density is typically 0.4 g/cc as compared to 1.2 g/cc obtained from floatation measurements,³³ indicating that the polymer fills only about one-third of the total volume of the sample. X-ray diffraction^{34,35} has determined that the films are

partially crystalline, possessing degrees of crystallinity as high as ca. 0.7.³⁵ The thermal stability³⁶ of the films in vacuo is quite good with the onset of decomposition observed near 325° C. Films of the cis isomer are extremely flexible and can be stretched³⁷ to extension ratios as high as 3.3 with concomitant partial orientation of the fibrils. Trans (CH)_x films are rather brittle and thus can be stretched only to a small extent. The tensile properties of (CH)_x films have been recently investigated in detail by Druy et al.³⁷

Several attempts have been made to convert polyacetylene to a more tractable form through post-polymerization reactions such as hydrogenation.^{38,39} The most successful of these has been the hydrogenation of (CH)_x films pre-treated with sodium naphthalide,³⁹ yielding partially soluble "polyethylene", a result which implies that the original (CH)_x is highly linear. The number-average molecular weight (\bar{M}_n) of the soluble fraction was found to be ~6,000. More recently,⁴⁰ a study of acetylene polymerization using radiotagging methods has yielded values of \bar{M}_n in the range 20,000 - 30,000.

It should be noted that (CH)_x films have also been prepared by Hsu and coworkers⁴¹ using (C₅H₄)(C₅H₅)₃Ti₂, although Shirakawa's method remains the simplest and most straightforward synthetic approach.

Cis and trans (CH)_x isomerization. Shirakawa et al.³⁰⁻³² carried out the first systematic study of the dependence of the cis-trans isomeric composition on the polymerization temperature. They found that the cis content of (CH)_x is > 90% when the polymerization is carried out at

-78° C, and $\leq 5\%$ at temperatures above 150° C. Furthermore, cis (CH)_x can be irreversibly converted to trans (CH)_x upon heating. These results indicate that the polymerization proceeds through cis opening of the acetylene triple bond to yield cis (CH)_x followed by isomerization, the initial degree of which is dependent on the polymerization temperature. The thermodynamic stability of the trans isomer is attributable to reduction of steric interactions between hydrogen atoms on every other carbon-carbon double bond along the polymer chain. Furthermore, these steric interactions probably cause a "twist" around the carbon-carbon single bonds in cis (CH)_x, thus reducing the effective conjugation length as the result of poorer π -orbital overlap. In fact, uv-visible spectra³¹ of thin films show that λ_{max} for the cis isomer is ca. 590 nm while that of the trans isomer is ca. 710 nm, in agreement with this prediction. The electrical conductivity⁴² of cis (CH)_x is ca. $10^{-9} \Omega^{-1} \text{cm}^{-1}$ as compared to ca. $10^{-5} \Omega^{-1} \text{cm}^{-1}$ for trans (CH)_x, again implying that conjugation is enhanced in the case of the trans isomer. The band gaps of the cis and trans isomers, which correspond to the energies of the onset of the $\pi \rightarrow \pi^*$ transitions in the visible spectra, are ca. 2.0 and ca. 1.5 eV, respectively.⁴³

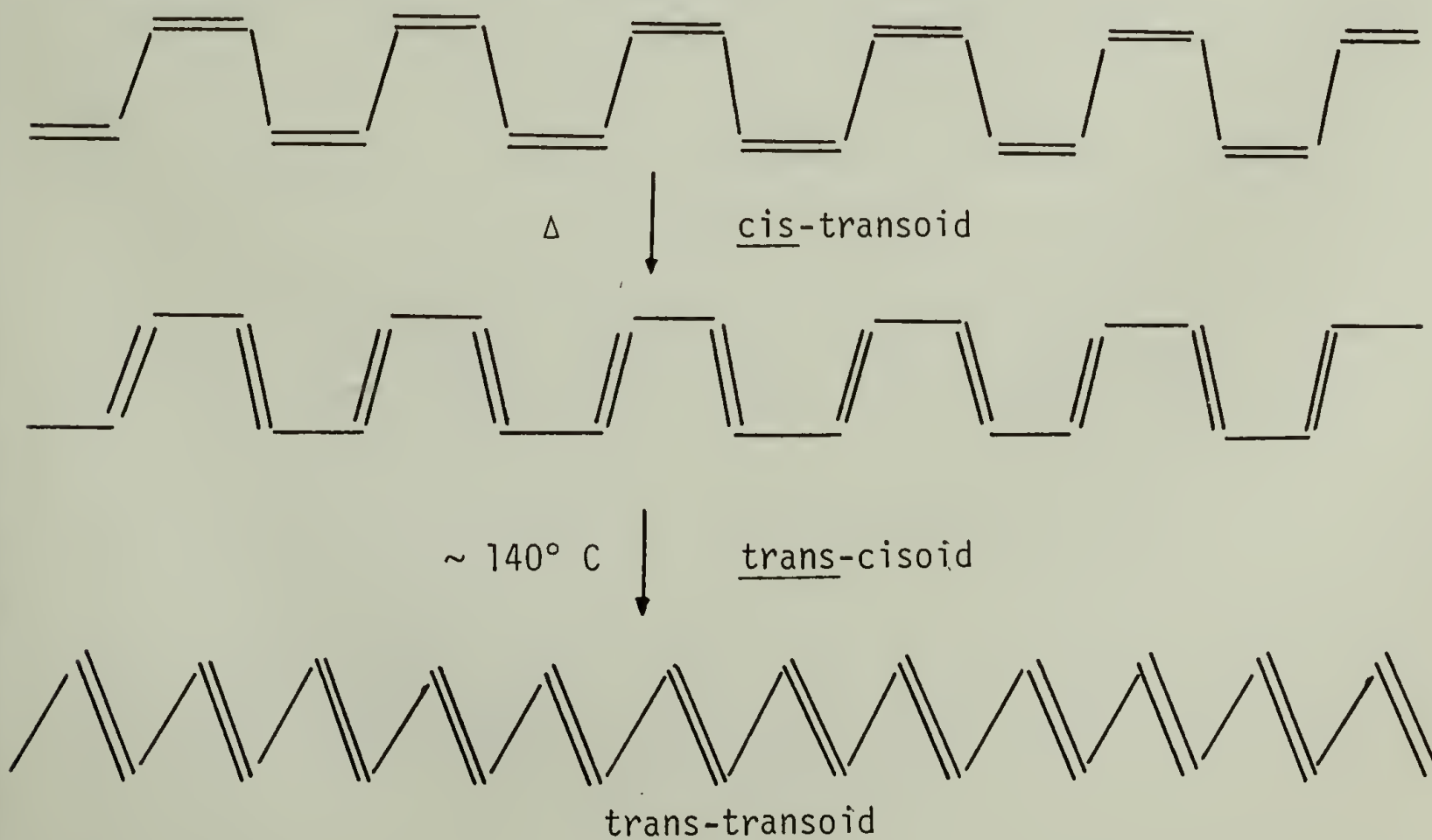
The cis-trans content is readily determined³² by infrared spectroscopy according to

$$\% \text{ cis } = \frac{1.3 A_{\text{cis}}}{1.3 A_{\text{cis}} + A_{\text{trans}}} \quad (100)$$

where A_{cis} and A_{trans} are the absorbances of the cis and trans IR bands

(at 730 and 1010 cm^{-1}) respectively. Vibrational assignments from IR and Raman spectroscopic studies have been reported.^{30,31} Solid state ^{13}C NMR spectra⁴⁴ of both cis and trans films have confirmed their isomeric composition.

Infrared spectroscopy has also been used to study the kinetics of the isomerization process.³⁶ It is interesting to note that whereas IR spectroscopy shows a continual change in cis-trans content as a sample of $(\text{CH})_x$ is heated (for example, from 25° C to 150° C), differential scanning calorimetry indicates an irreversible exothermic transition at ca. 145° C. These results suggest that besides simple bond rearrangements occurring on heating, a major "phase transition" occurs near 145° C. In fact, it has recently been demonstrated³⁷ that samples of partially oriented cis $(\text{CH})_x$ show a ca. 20% increase in length when heated under stress to ca. 140 - 150° C. A plausible mechanism for the isomerization process is as follows:⁴⁵



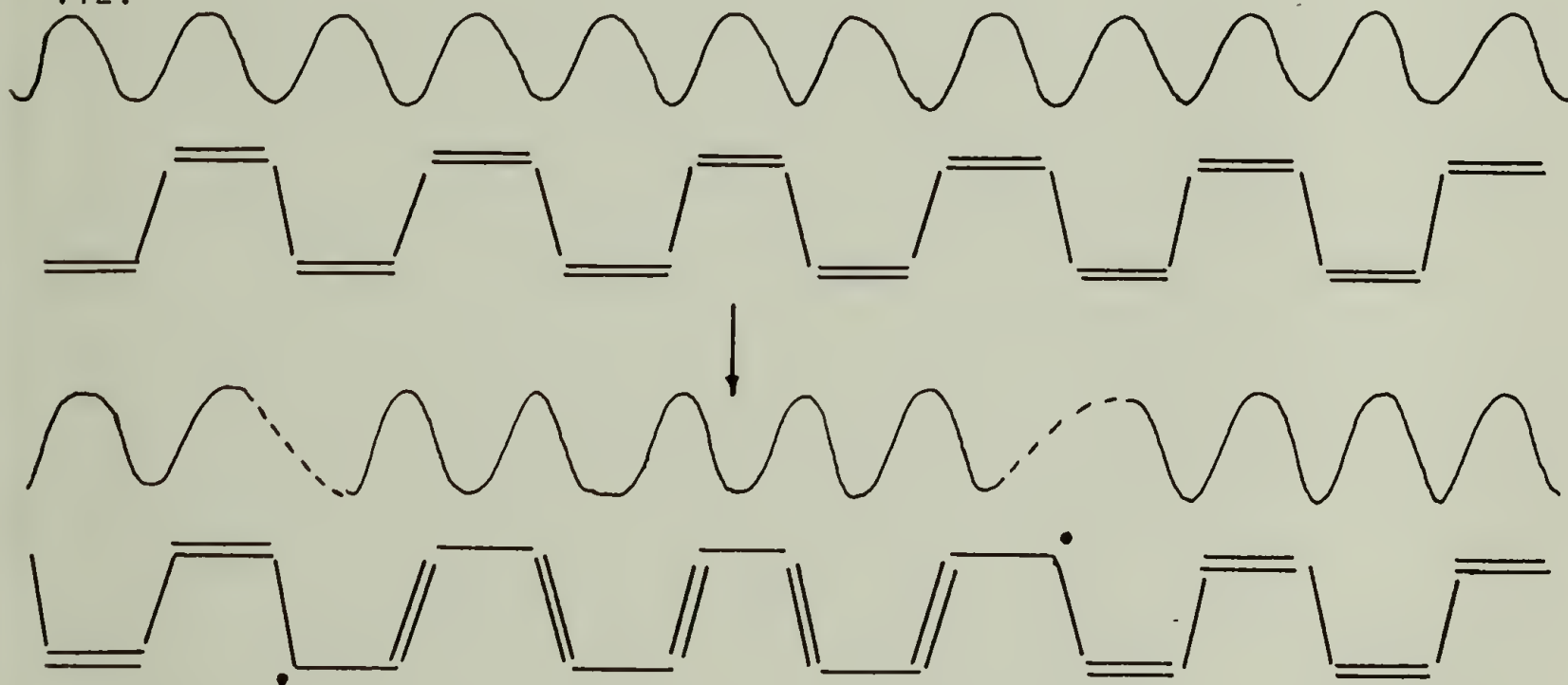
The trans-transoid structure is the most extended form of the polymer chain and reasonably accounts for the increase in length near 150° C. The more formal designations of the configurations of the double and single bonds in the polymer chain (e.g., cis-transoid, etc.) are necessary in the mechanism described above. However, for simplicity and consistency with nomenclature in the literature, previous and future discussions employ only the designations cis or trans. It should be noted that most trans (CH)_x samples studied have been thermally treated above 150° C and are probably best represented by the trans-transoid structure depicted above.

Electron paramagnetic resonance (EPR) studies. EPR spectroscopy has been used extensively to study the formation and nature of the unpaired electrons in (CH)_x. The paramagnetism of (CH)_x was first recognized by Hatano et al.,²³ who observed a Lorentzian lineshape with a g-value close to that of the free electron, indicating that the free spins are π -electron radicals rather than σ -electron radicals. Spin concentrations ranged from 10^{17} - 10^{19} spins/gram, depending on the degree of crystallinity and oxygen content.

Several recent studies have focused on (CH)_x films, especially concerning the relationship between EPR signal intensity and linewidth and cis-trans isomer content. Shirakawa and coworkers⁴² found that the EPR linewidth decreased from ca. 7G to ca. 1G as the cis content decreased from ca. 90% to ca. 5%. Thus, it was suggested that the free electrons are more delocalized, or mobile, in trans (CH)_x. This proposal is in agreement with uv-visible spectroscopic studies³¹ which indicate that

trans $(CH)_x$ is the more conjugated of the two isomers. Furthermore, these workers found that the spin concentration increases with increasing trans content. Thus, thermal cis-trans isomerization resulted in a ca. ten-fold increase in the number of free spins. This observation suggests that spin formation is intimately related to isomerization and is undoubtedly the result of random, non-concerted bond rearrangements,

viz:



This mechanism is qualitatively analogous to that proposed by Holob et al.¹³ for unpaired spin generation in poly(phenyl acetylene). In the simplest sense, such free spins can be considered as "mistakes" formed on the $(CH)_x$ chain as the result of random bond rearrangements. A more formal definition is that the free radical is a "neutral defect" on the chain at which point the π -wave function amplitude vanishes⁴⁵⁻⁴⁸ (note dotted line above). The radical is referred to as a neutral defect since it is uncharged. Recent studies⁴⁹ have shown that the EPR line-width increases from 1.5G to 5.5G as the temperature is lowered from 298° K to 4° K, indicating that the radical is more mobile at higher

temperatures. From these results, it is estimated that the free electron is delocalized over about fifteen lattice units at 298° K. Such an electron is referred to as a "soliton". It should be noted that the EPR linewidth of $(\text{CD})_x$ ⁴⁹ is narrower than that of $(\text{CH})_x$, implying that unresolved hyperfine interactions play an important role in determining the observed linewidths.

Hatano et al.²³ demonstrated that the electrical conductivity of polyacetylene is activated and increases with increasing temperature, as expected for an intrinsic band gap semiconductor. Pople and Walmsley⁵⁰ have proposed that the presence of unpaired electrons in a long, conjugated polyene may facilitate semiconduction processes in neutral polyene molecules. It is thus tempting to rationalize the higher conductivity of trans $(\text{CH})_x$ as compared to cis $(\text{CH})_x$ as being due to the greater number of free electrons in the former material. However, Shirakawa et al.⁴² found that the relative intensity of the EPR signals of both cis and trans $(\text{CH})_x$ decreased with increasing temperature. Since the signal intensity is proportional to the magnetic susceptibility, this Curie Law temperature dependence suggests that the observable unpaired electrons in $(\text{CH})_x$ cannot be carriers for electrical conduction. This argument is further supported by the fact that electrical conductivity of trans $(\text{CH})_x$ falls by more than four orders of magnitude⁵¹ upon exposure to the donor, NH_3 , although no change in the EPR spectrum is observed.⁴⁶ The NH_3 apparently compensates impurities such as catalyst residues. These rather baffling results can be rationalized by considering that the energy required for formation of a neutral defect,

or soliton, has been estimated⁴⁸ to be ca. 0.4 eV, whereas the energy required to create a conduction electron (or hole) is $E_g/2$, where E_g is the band gap of cis $(CH)_x$ (ca. 2.0 eV). Thus, soliton formation is energetically more favorable. In fact, a recent kinetic study⁴⁵ of unpaired spin formation in $(CH)_x$ yields an activation energy very close to 0.4 eV. A complete isomerization mechanism has also been proposed.⁴⁵

Comments on the electrical conductivity of "pristine" $(CH)_x$. In view of the sensitivity of $(CH)_x$ to impurities as demonstrated by doping experiments (see below), its intrinsic conductivity is likely to be considerably lower than the measured values of ca. 10^{-9} and ca. $10^{-5} \Omega^{-1} \text{cm}^{-1}$ for cis and trans material, respectively. As mentioned previously, exposure of trans $(CH)_x$ to NH_3 vapor causes its conductivity to fall more than four orders of magnitude without detectable weight increase. Apparently, NH_3 compensates traces of impurities such as catalyst residues. Thermoelectric power studies⁵² indicate that both nascent cis and trans $(CH)_x$ are p-type semiconductors. The effect of impurities is also realized in optical absorption studies⁹ where the energy gap of $(CH)_x$ is ca. 1.5 - 2.0 eV, considerably greater than 0.3 - 0.5 eV obtained from electrical conductivity measurements.⁴²

Traces of aluminum and titanium compounds in $(CH)_x$ films remaining from the Ziegler-Natta catalyst can be detected by spark emission spectroscopy.⁵³ This result is not surprising upon consideration of the synthesis of $(CH)_x$ films. It is well recognized that polymerization with Ziegler-Natta catalysts involves insertion of monomer at a metal-polymer bond and this bond is commonly cleaved by materials containing

active hydrogens (e.g., methanol/HCl solution). Since such materials are rigorously excluded in the synthesis and handling of $(\text{CH})_x$ films, most chain ends are likely to remain covalently bonded to titanium and aluminum compounds. Treating $(\text{CH})_x$ films with methanol/HCl is expected to remove these catalyst residues but will not yield a more "pure" $(\text{CH})_x$ in terms of intrinsic electrical conductivity since HCl can partially dope $(\text{CH})_x$.

Doped polyacetylene. In a series of studies concerning halogenation of polyacetylene films, Shirakawa and Ikeda⁵⁴ noted a dramatic decrease in infrared transmission ($4000 - 400 \text{ cm}^{-1}$) of $(\text{CH})_x$ when it was exposed to small quantities of Cl_2 or Br_2 without any visible change in appearance of the films. Extensive exposure yielded eg. $(\text{CHBr})_x$, with the white films again displaying high infrared transmission. Since metals in general highly absorb infrared radiation, the initial reduction in infrared transmission suggested that the halogen-doped $(\text{CH})_x$ films may have interesting electrical properties.

In collaboration with MacDiarmid, Heeger and coworkers at the University of Pennsylvania, it was indeed demonstrated^{55,56} that large increases in electrical conductivity of $(\text{CH})_x$ films result from exposure to Cl_2 , Br_2 , and I_2 , with values as high as $350 \Omega^{-1} \text{ cm}^{-1}$ for cis $(\text{CH})_x$ doped with I_2 .⁵⁷ It was subsequently found that other electron acceptors such as AsF_5 , BF_3 , H_2SO_4 , etc., and electron donors such as Na or K ⁵⁸ also yield highly conducting derivatives. Conductivities as high as ca. $1.2 \times 10^3 \Omega^{-1} \text{ cm}^{-1}$ are obtained upon doping of cis $(\text{CH})_x$ with

AsF_5 or H_2SO_4 ⁵³ and are comparable to those of the best "organic metals" such as TTF/TCNQ. Electron donors and acceptors yield n-type and p-type $(\text{CH})_x$, respectively, and the two types of dopants can compensate one another.⁵⁸ The conductivity is electronic and not ionic in all cases; no polarization with concomitant increase in resistance is observed after passage of current through the samples for several hours.

The methods of introducing dopants into polyacetylene fall into three chief categories:⁵³

i. Exposure of $(\text{CH})_x$ film to a known vapor pressure of a volatile dopant (e.g., I_2 , AsF_5) for a given time period.

ii. Treatment of $(\text{CH})_x$ with a solution of the dopant in an appropriate solvent (e.g., I_2 in pentane, sodium naphthalide in THF).

iii. Electrochemical doping,⁵⁹ e.g., use of $(\text{CH})_x$ as the anode in an electrochemical cell with aqueous KI solution to yield I_2 -doped $(\text{CH})_x$.

Perhaps the most unique and important property of $(\text{CH})_x$ is that its conductivity can be selectively controlled by the nature and amount of dopant employed. The accessible range of conductivity, up to twelve orders of magnitude in the case of the cis isomer, is compared to common metals, semiconductors and insulators in Figure 3. Representative conductivities and compositions for several doped $(\text{CH})_x$ films are listed in Table 1. The designations cis and trans refer to the isomer employed before doping. In general, the maximum conductivity of doped cis $(\text{CH})_x$ is three to five times greater than the corresponding conductivity of doped trans $(\text{CH})_x$, although the undoped conductivity of

TABLE 1
CONDUCTIVITIES AND COMPOSITIONS OF
SELECTED $(CH)_x$ DERIVATIVES ⁵³

Sample	Conductivity, $\Omega^{-1}cm^{-1}$
<u>cis</u> $(CH)_x$	1.7×10^{-9}
<u>trans</u> $(CH)_x$	4.4×10^{-5}
A. p-type dopants	
<u>trans</u> $[CHCl_{0.02}]_x$	1×10^{-4}
<u>trans</u> $[CHB_{0.23}]_x$	4×10^{-1}
<u>cis</u> $[CHI_{0.30}]_x$	5.5×10^2
<u>trans</u> $[CHI_{0.20}]_x$	1.6×10^2
<u>trans</u> $[CH(AsF_5)_{0.10}]_x$	4×10^2
<u>cis</u> $[CH(AsF_5)_{0.10}]_x$	1.2×10^3
<u>cis</u> $[CH(SbCl_5)_{0.022}]_x$	2
<u>cis</u> $[CH(ClO_4)_{0.0645}]_x$	9.7×10^2
<u>cis</u> $[CH(BF_2)_{0.09}]_x$	1×10^2
<u>cis</u> $[CH(H_2SO_4)_{0.106}(H_2O)_{0.070}]_x$	1.2×10^3
B. n-type dopants	
<u>cis</u> $[K_{0.16}(CH)]_x$	5.0×10^1
<u>cis</u> $[Na_{0.21}(CH)]_x$	2.5×10^1
<u>trans</u> $[Na_{0.28}(CH)]_x$	8.0×10^1

cis $(\text{CH})_x$ is four orders of magnitude lower than that of trans $(\text{CH})_x$. At least for the case of iodine doping, optical absorption,⁴³ thermopower⁵² and NMR studies⁶⁰ indicate that cis-trans isomerization takes place during doping. It is not yet clear to what extent other dopants induce a similar isomerization. The higher conductivities obtained with cis starting material suggests that doping induced isomerization leads to higher quality trans material than thermal isomerization with subsequent doping.⁶²

The conductivity of acceptor-doped $(\text{CH})_x$ typically decreases slowly over a period of several days upon exposure to air as the result of oxidation of the polymer and dopant. On the other hand, the conductivity of donor-doped $(\text{CH})_x$ decreases rapidly under similar conditions. The oxidation can be retarded by coating samples with wax or polymer films.⁵³ The thermal stability of films doped with I_2 or AsF_5 is fairly good; samples can be heated up to ca. 100°C with only a small decrease in conductivity.⁵³

The semiconductor-metal transition. Typical results for the dependence of the conductivity, σ , on the dopant concentration, y , are shown in Figure 2. Inspection of these plots indicates that the maximum conductivity at a particular value of y depends on the dopant species. More importantly, however, is the observation that σ is critically dependent on y during the early stages of doping but becomes essentially independent of y above $y \sim 0.02$. Such a relationship is common to all dopants investigated suggesting that an important transition occurs near $y \sim 0.02$; namely, a semiconductor-metal transition. This conclusion is

Figure 2. Electrical conductivity as a function of dopant concentration for $(\text{CH})_x$ doped with I_2 , Br_2 , and AsF_5 .⁵³

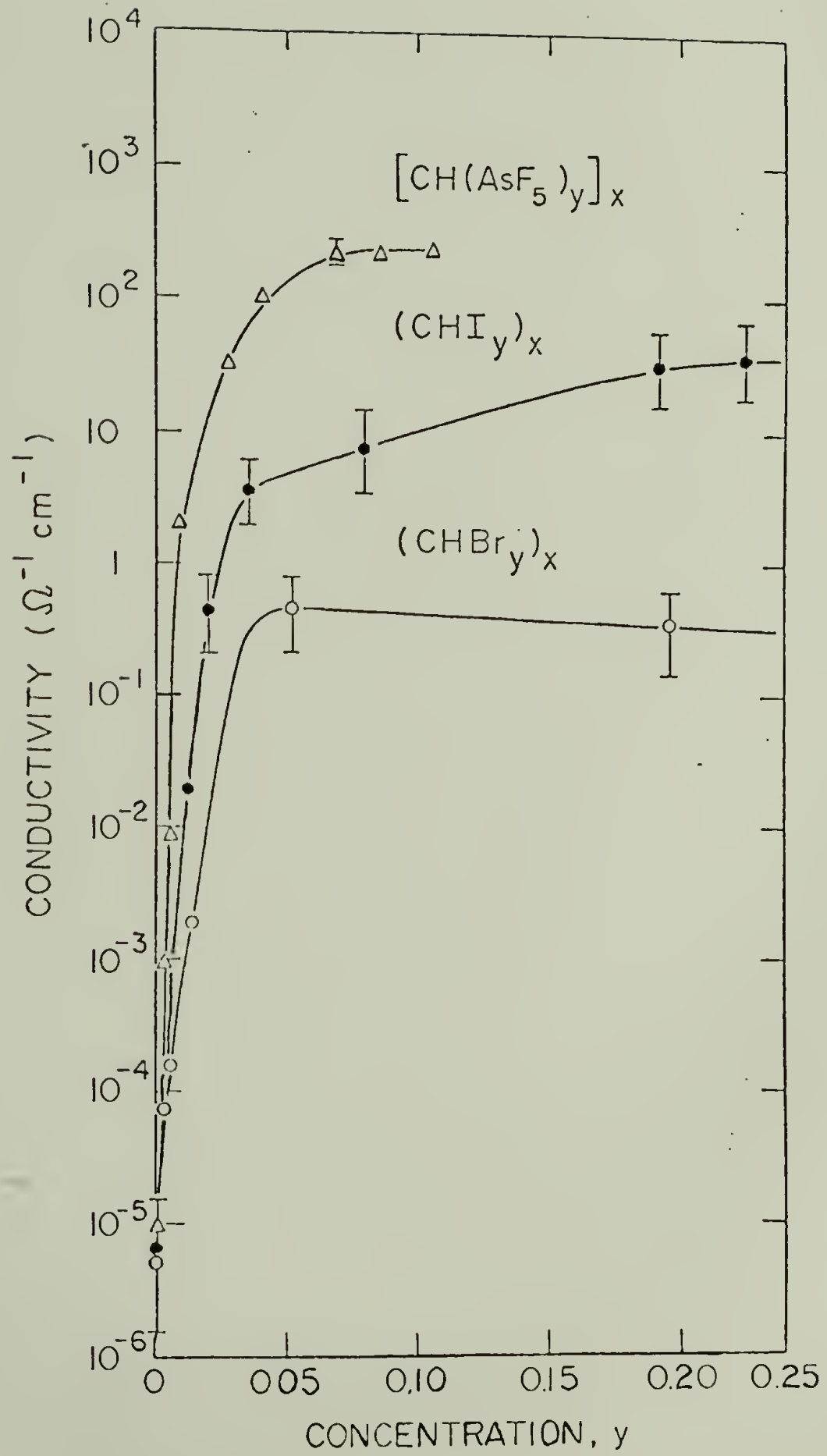
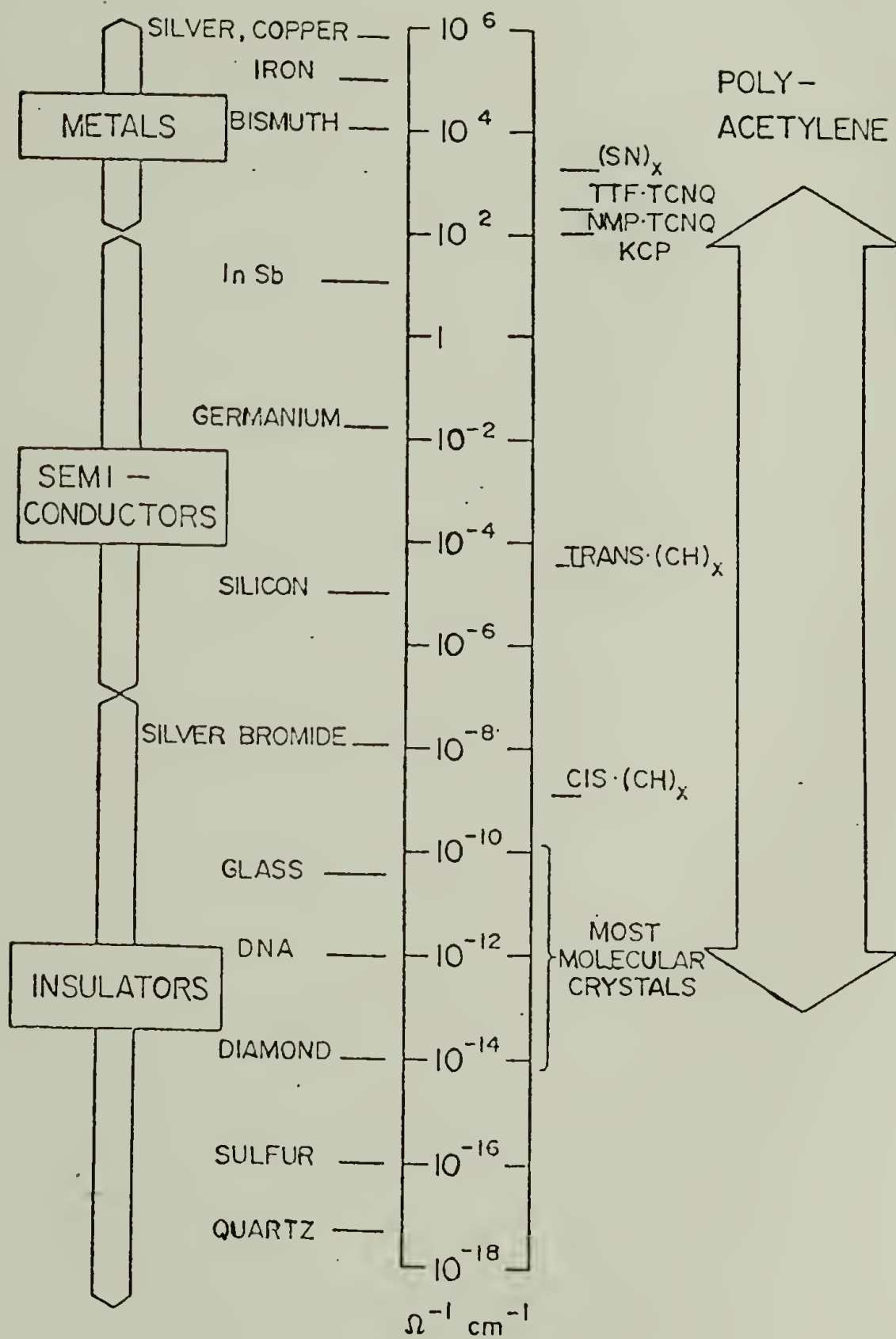


Figure 3. Comparison of electrical conductivities
of metals, semiconductors and insulators.⁵³



supported by infrared transmission studies⁵¹ as a function of y which demonstrate a dramatic decrease in transmission, characteristic of a metal, above $y \sim 0.02$. The activation energy for the electrical conductivity of doped $(\text{CH})_x$, obtained from temperature dependence studies,⁵⁶ is observed to decrease markedly up to $y \sim 0.02$, beyond which it is essentially unchanged. The thermoelectric power (S) also shows a dramatic decrease⁵² in S up to $y \sim 0.02$ and becomes essentially constant at higher values of y . The magnitude of the thermopower in the heavily doped regime ($\sim 10 - 20 \mu\text{V/K}$) is consistent with metallic behavior. Electron paramagnetic resonance spectra of trans $(\text{CH})_x$ heavily doped with AsF_5 ⁴⁶ show an asymmetric (Dysonian) lineshape characteristic of a metal-like material. Thus, several independent methods have demonstrated the attainment of metallic properties at high dopant levels (i.e., $y > 0.02$).

Electrical transport studies. The conductivity of doped $(\text{CH})_x$ decreases with increasing temperature⁶¹ even for samples in the "metallic" regime in contrast to "true" metals. Plots of $\ln \sigma$ vs. $T^{-1/4}$ (or $T^{-1/2}$) give nearly straight line behavior, comparable to that observed in non-crystalline inorganic semiconductors such as amorphous silicon. Although X-ray diffraction has suggested that $(\text{CH})_x$ films are highly crystalline, the random fibrillar morphology indicates significant disorder and probably accounts for the observed temperature dependence. However, the temperature dependence of the thermopower for heavily doped $(\text{CH})_x$ implies intrinsic metallic behavior down to 2°K . Interparticle contact resistances undoubtedly play a limiting role in the observed con-

ductivities of doped $(\text{CH})_x$. The intrinsic conductivity of metallic AsF_5 -doped $(\text{CH})_x$ has been estimated⁶² to be ca. $4 \times 10^4 \Omega^{-1} \text{cm}^{-1}$.

In the dilute regime ($y < 0.001$) the activation energy for conductivity is insensitive to y and the thermopower is temperature-independent, implying that transport is via carrier hopping.⁶² The conductivity in this regime is apparently due to a temperature-independent carrier concentration (proportional to y) and an activated mobility. The mobility in the metallic regime has been estimated⁶² to be $> 60 \text{ cm}^2/\text{V-sec}$ and is surprisingly large in view of the extensive disorder of the polymer, especially if doped $(\text{CH})_x$ is quasi-one-dimensional. Spectroscopic studies of short chain polyenes lead to the conclusion that interchain transfer integrals are on the order of 2.0 - 2.5 eV; i.e., orbital overlap between chains is small. Thus, $(\text{CH})_x$ is anticipated to have a highly anisotropic band structure with corresponding anisotropic electrical transport, analogous to behavior in other "synthetic metals" such as TTF/TCNQ and $(\text{SN})_x$. One-dimensionality in $(\text{CH})_x$ has been inferred from transport,⁶³ optical^{9,43} and NMR⁶⁴ studies.

Partially oriented films; anisotropic electrical and optical properties.^{63,9}

As mentioned previously, films of cis $(\text{CH})_x$ are flexible and can be stretched to extension ratios as high as ~ 3.3 . Electron micrographs of stretched films show some degree of alignment of the fibrils although the orientation is at best modest. The electrical conductivity of doped, partially oriented films is anisotropic, with higher conductivities being observed in the stretch direction. Typical values of

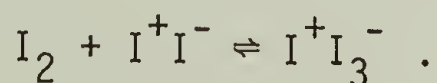
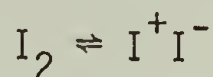
$\sigma_{11}/\sigma_{\perp}$ for metallic $(CH)_x$ are in the range 8 - 16 depending upon the dopant. Films doped with AsF_5 display the largest anisotropies. Furthermore, σ_{11} is two-to-four times greater than σ of the corresponding doped, unoriented film. The highest value of the conductivity of doped $(CH)_x$ reported to date is ca. $2,500 \Omega^{-1} \text{ cm}^{-1}$ for $[CH(AsF_5)_{0.1}]_x$ with $l/l_0 \sim 3$. The magnitude of σ is comparable to single crystals of $(SN)_x$.

It is tempting to ascribe the electrical anisotropy obtained by partial orientation to chain orientation of $(CH)_x$. Although X-ray diffraction photographs of stretched films do suggest a small degree of chain orientation, the electrical anisotropy can also be explained in terms of macroscopic morphological changes, i.e., a decrease in interfibril contact resistance in the stretch direction. The anisotropic optical reflectance from partially aligned films and the increased optical anisotropy upon doping are suggested as evidence for quasi-one-dimensional behavior in pure and doped $(CH)_x$. However, highly ordered materials having various morphologies are necessary to reach definitive conclusions.

The function of the dopant. By analogy with the requirements for electrical conductivity in "organic metals" such as TTF/TCNQ, it was initially believed that carriers were introduced in $(CH)_x$ by charge transfer between the polymer and dopant. Hsu et al.⁴¹ were the first to report structural information concerning iodine-doped $(CH)_x$ using Raman and X-ray photoelectron spectroscopy (XPS). These workers found that the principal iodine species existing in the doped polymer are I_3^- and

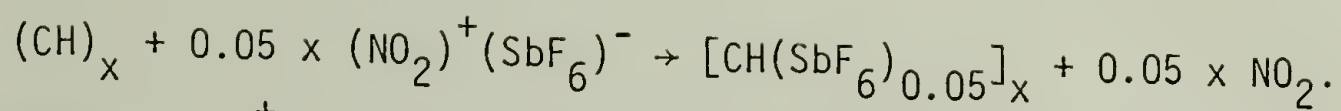
I_5^- , consistent with a charge transfer doping mechanism. More recent XPS studies⁶⁵ suggest that I_5^- is the predominant species. Additional Raman studies⁶⁶ have demonstrated that Br_3^- and Br_5^- are present in bromine-doped $(CH)_x$. Thus, electron acceptors apparently partially oxidize the $(CH)_x$ π -system and provide anions to stabilize the polycarbenium ion chain.

Consideration of a typical composition of I_2 -doped $(CH)_x$, e.g., $(CHI_{0.18})_x$, leads to the formulation of the polymer-dopant species as $[(CH)^{+0.06} (I_3^-)_{0.06}]$, $[(CH)^{+0.036} (I_5^-)_{0.035}]$ or species having intermediate compositions depending on the I_3^-/I_5^- ratio. Although no specific mechanism of oxidation of the $(CH)_x$ chain by iodine has been proposed, it may be that doping proceeds via the iodonium ion, viz.,



Iodine is known to initiate cationic polymerization reactions and species such as $I^+ I_3^-$ have been invoked as the actual initiators. Bromine is much more reactive than iodine, and bromine addition to $(CH)_x$ double bonds apparently occurs at high doping levels as evidenced by a decrease in conductivity near $y \sim 0.1$ (Figure 2). It is well established that bromination of simple olefins proceeds via the bromonium ion (Br^+). This species may well be involved in the doping process. Partial substitution of bromine for hydrogen on the $(CH)_x$ backbone can be accomplished by appropriate thermal treatment of bromine-doped $(CH)_x$.⁶⁷

Salts containing the $(NO)^+$ or $(NO_2)^+$ ions act as good dopants,⁶⁸ viz.

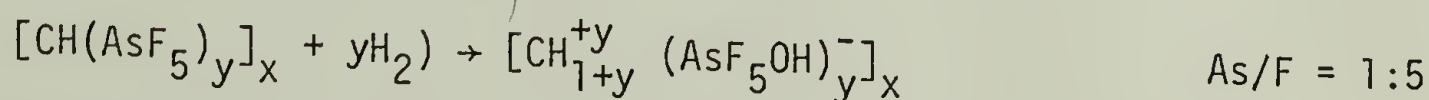
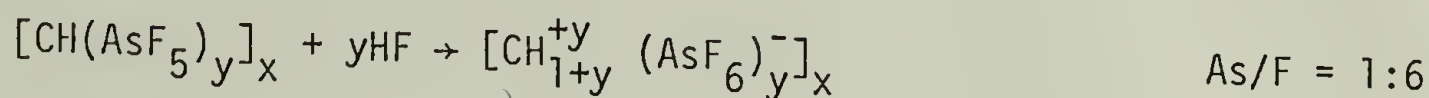


Thus, $(\text{NO}_2)^+$ is reduced and $(\text{CH})_x$ is partially oxidized in this process.

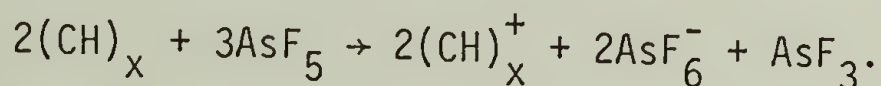
Protonic acids such as H_2SO_4 and HClO_4 are among the best dopants for $(\text{CH})_x$ ⁶⁸ ($\sigma \sim 10^3 \Omega^{-1} \text{cm}^{-1}$). It is believed that protonic acids are also involved in other dopant species.⁵³ For example, BCl_3 and PF_3 behave as poor dopants, but if traces of moisture are added before these gases contact the $(\text{CH})_x$, they both dope $(\text{CH})_x$ rapidly to the metallic regime. The doping mechanism involving protonic acids is unclear. It may be that H^+ increases conduction by partially withdrawing electrons from the $(\text{CH})_x$ chain or that a proton adds to the chain forming a polycarbenium ion. The latter possibility seems unlikely since interruption of the π -system of $(\text{CH})_x$ is expected to be detrimental to the conductivity. More detailed studies are required to elucidate this doping mechanism.

Doping of $(\text{CH})_x$ with AsF_5 has been extensively studied although conclusions concerning the mechanism are controversial. MacDiarmid and coworkers have found^{53,69} that upon treatment of $(\text{CH})_x$ with very pure AsF_5 , elemental analyses yield an arsenic to-fluorine ratio of 1:5. Since EPR⁴⁶ and magnetic susceptibility⁷⁰ studies show that AsF_5^- , the radical anion anticipated from electron transfer between $(\text{CH})_x$ and AsF_5 , is not present, it has been suggested⁵³ that the AsF_5^- species may dimerize to produce the previously unreported diamagnetic $\text{As}_2\text{F}_{10}^{=}$. Treatment of films having compositions of $[\text{CH}(\text{AsF}_5)_y]_x$ with HF vapor or H_2O yield $[\text{CH}_{1+y}^+(\text{AsF}_6)^-]_x$ and $[\text{CH}_{1+y}^+(\text{AsF}_5\text{OH})_y^-]_x$, respectively. Apparently, reactions of the AsF_5 in the polymer with HF and H_2O yield H^+AsF_6^- .

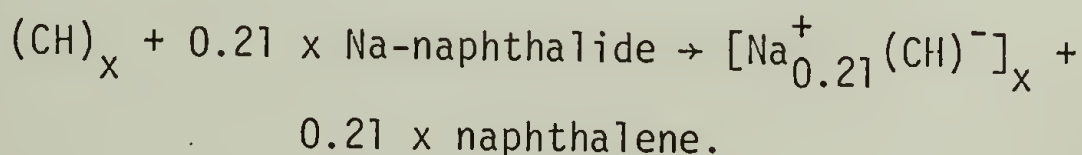
$\text{H}^+\text{AsF}_5\text{OH}^-$, respectively, and these protonic acids proceed to dope the remaining $(\text{CH})_x$ portion of the film. The reactions may be summarized as follows:⁵³



Street and coworkers⁷¹ have shown that AsF_6^- is the principal species from infrared and X-ray absorption studies. However, these workers have proposed that AsF_6^- is the result of disproportion of AsF_5 in a manner analogous to that suggested by Bartlett et al.⁷² for AsF_5 -graphite intercalation compounds, viz.



Electron donor dopants have received much less attention. Electron transfer from the dopant to $(\text{CH})_x$ occurs to form a polycarbonium ion chain:⁵³



The well-known sensitivity of carbonium ions to moisture and oxygen accounts for the fact that the conductivity of n-type $(\text{CH})_x$ decays rapidly upon exposure to atmospheric constituents. This extreme sensitivity will seriously limit the potential applications of donor-doped $(\text{CH})_x$.

The homogeneity of dopant placement within the $(\text{CH})_x$ fibrils has received considerable attention. Hsu and coworkers,⁴¹ on the basis of X-ray diffraction studies, suggest that species such as I_3^- intercalate

between $(\text{CH})_x$ chains in a manner similar to dopant placement in graphite. XPS⁶⁵ and NMR⁶⁰ studies suggest that iodine is distributed throughout the fibril bulk. Lefrant and coworkers⁶⁶ observed that doping with bromine and iodine is inhomogeneous; doping to a greater extent occurs on the dull (higher surface area) side of the $(\text{CH})_x$ film. Additional XPS studies⁷³ of AsF_5 -doped $(\text{CH})_x$ indicate that the AsF_5 resides primarily on the surface of the fibrils. The question of surface vs. bulk conductivity will remain a topic of considerable debate. It is curious, however, that calculation of the amount of AsF_5 required to form a monolayer⁷¹ on 200 Å diameter $(\text{CH})_x$ fibrils corresponds to $[\text{CH}(\text{AsF}_5)_{0.02}]_x$; i.e., very close to, though perhaps fortuitously, the semiconductor-metal transition.

The conduction mechanism. Perhaps the most fundamental property of doped $(\text{CH})_x$ which needs to be thoroughly understood is the mechanism of electron transport. The most simplified proposal invokes band theory, with dopants either withdrawing electrons from the filled valence band of $(\text{CH})_x$ (acceptors) or donating electrons to the empty conduction band by analogy with conventional semiconductors. However, unlike the latter, the dopants in $(\text{CH})_x$ cannot be looked upon as "substitutional" impurities. Chiang et al.⁵¹ suggest that acceptor doping creates localized holes in the band gap, while Street and coworkers⁷⁴ propose that the acceptor level is at an energy which falls within the valence band. Although conduction is assumed to be along the chain, one may consider the possibility of conduction primarily between chains through chain-dopant-chain stacks as in some radical ion salts of organic molecules.

Magnetic susceptibility studies⁷⁰ indicate that the carriers in AsF₅-doped (CH)_x are non-magnetic, supporting the hypothesis that charged solitons^{47,48} are responsible for the conductivity. Furthermore, recent studies have provided additional evidence of a soliton doping mechanism and will be discussed in Chapter VII. It is apparent that theories of conduction mechanisms will continue to challenge scientists for the next several years. Concomitant with the importance of theories are more detailed experimental studies of the structure and functions of dopants in polyacetylene.

Applications of doped (CH)_x. Doped polyacetylene has been used in the fabrication of various electronic devices. Rectifying p - n⁵⁸ and Schottky barrier junctions⁷⁵ have been demonstrated. Photovoltaic devices⁷⁵ which may be potential and economical solar cells, and light weight, rechargeable batteries⁷⁶ have also been prepared and studied.

Polyacetylene is far from an ideal material in terms of practical applications for several reasons. First, the polymer is intractable and therefore processibility is impossible. Also, the material is air sensitive, thus precluding any applications under environmental conditions without the use of protective coatings and/or stabilizers. However, valuable information may be gained from studies of (CH)_x and applied to the development of other conducting polymer systems which are more tractable. Thus, investigations of the properties of (CH)_x are expected to continue with vigor over the course of the next several years.

References

1. Cf. a.) G. C. Demitras, C. R. Russ, J. G. Salmon, J. H. Weber and G. S. Weiss, Inorganic Chemistry, Prentice Hall, Englewood Cliffs, Ch. 7 (1972); b.) A. J. Epstein and J. S. Miller, Sci. Amer., 241 (4), 52 (1979)
2. F. L. Vogel, Molecular Metals, W. E. Hatfield, ed., Plenum Press, New York, p. 261-279 (1979)
3. F. L. Vogel, J. Mat. Sci., 12, 982 (1977)
4. Cf. G. B. Street and W. D. Gill, Molecular Metals, W. E. Hatfield, ed., Plenum Press, New York, p. 301-326 (1979)
5. E. P. Goodings, Chem. Soc. Revs., 5 (1), 95 (1976)
6. M. Hartel, G. Kossmehl, G. Manecke, W. Willie, D. Wöhrle and D. Zerpner, Angew. Makromol. Chem., 29, 307 (1973)
7. R. E. Peierls, Quantum Theory of Solids, Clarendon Press, Oxford, p. 108 (1955)
8. P. M. Grant and I. P. Batra, Solid State Comm., 29, 225 (1979)
9. C. R. Fincher, Jr., D. L. Peebles, A. J. Heeger, M. A. Dray, Y. Matsumura, A. G. MacDiarmid, H. Shirakawa and S. Ikeda, Solid State Comm., 27, 489 (1978)
10. A. G. Hankin and A. M. North, Trans. Faraday Soc., 63, 1525 (1967)
11. G. Wegner, Z. Naturforschg., 24b, 824 (1969); G. Wegner, Molecular Metals, W. E. Hatfield, ed., Plenum Press, New York, p. 203-242 (1979)
12. D. Bloor, D. J. Ando, F. H. Preston and G. C. Stevens, Chem. Phys. Lett., 24, 407 (1974)

13. G. M. Holob, P. Ehrlich and R. D. Allendoerfer, Macromolecules, 5, 569 (1972)
14. R. D. Hartman and H. A. Pohl, J. Polym. Sci., Part A-1, 6, 1116 (1968)
15. Cf. A. F. Garito and A. J. Heeger, Accts. Chem. Res., 7, 232 (1974); Molecular Metals, W. E. Hatfield, ed., Plenum Press, New York, p. 1-160 (1979)
16. J. H. Perlstein, Angew. Chem. Int. Ed. Engl., 16, 519 (1977)
17. H.-C. I. Kao, M. Jones and M. M. Lbaes, J. Chem. Soc. Chem. Comm., 329 (1979)
18. N. Bartlett, R. N. Biagioni, G. McCarron, B. McQuillan and F. Tanzella, Molecular Metals, W. E. Hatfield, ed., Plenum Press, New York, 293 (1979)
19. K. Bechgaard, C. S. Jacobsen, K. Mortensen, H. J. Pederson and N. Thorup, Solid State Comm., 33, 1119 (1980)
20. D. Jerome, A. Mazaud, M. Ribault and K. Bechgaard, J. Physique Lett., 41, L95 (1980)
21. A. G. MacDiarmid and A. J. Heeger, Molecular Metals, W. E. Hatfield, ed., Plenum Press, New York, 161 (1979)
22. G. Natta, G. Mazzanti and P. Corradini, Atti. Acad. Nazl. Lincei Reud. Classe Sci. Fis. Mat. Nat., 25, 3 (1958)
23. M. Hatano, S. Kambara and S. Okamoto, J. Polym. Sci., 51, S26 (1961)
24. L. B. Luttinger, J. Org. Chem., 27, 1591 (1962)
25. I. V. Nicolescu and E. Angelescu, J. Polym. Sci. A., 3, 1227 (1965)
26. I. V. Nicolescu and E. Angelescu, J. Polym. Sci. A-1, 4, 2963 (1966)

27. D. J. Berets and D. S. Smith, Trans. Faraday Soc., 64, 823 (1968)
28. F. D. Kleist and N. R. Byrd, J. Polym. Sci. A-1, 7, 3419 (1969)
29. A. Bradley and J. P. Hammes, J. Electrochem. Soc., 110, 15 (1963)
30. H. Shirakawa and S. Ikeda, Polym. J., 2, 231 (1971)
31. H. Shirakawa, T. Ito and S. Ikeda, Polym. J., 4, 460 (1973)
32. T. Ito, H. Shirakawa and S. Ikeda, J. Polym. Sci., Polym. Chem. Ed., 12, 11 (1974)
33. T. Ito, H. Shirakawa and S. Ikeda, Kobunshi Ronbunshu, Eng. Ed., 5, 470 (1976)
34. R. H. Baughman, S. L. Hsu, G. P. Pez and A. J. Signorelli, J. Chem. Phys., 68, 5405 (1978)
35. T. Akaishi, K. Miyasaka, K. Ishikawa, H. Shirakawa and S. Ikeda, J. Polym. Sci., Polym. Phys. Ed., 18, 745 (1980)
36. T. Ito, H. Shirakawa and S. Ikeda, J. Polym. Sci., Polym. Chem. Ed., 13, 1943 (1975)
37. M. A. Druy, C. H. Tsang, N. Brown, A. J. Heeger and A. G. MacDiarmid, J. Polym. Sci., Polym. Phys. Ed., 18, 429 (1980)
38. B. Chacko, J. C. W. Chien, F. E. Karasz, A. G. MacDiarmid and A. J. Heeger, Bull. Amer. Phys. Soc., 24, 480 (1979)
39. H. Shirakawa, M. Sato, A. Hamano, S. Kawakami, K. Soga and S. Ikeda, Macromolecules, 13, 459 (1980)
40. J. C. W. Chien, J. D. Capistran, L. C. Dickinson and F. E. Karasz, in preparation
41. S. L. Hsu, A. J. Signorelli, G. P. Pez and R. H. Baughman, J. Chem. Phys., 69, 106 (1978)

42. H. Shirakawa, T. Ito and S. Ikeda, Makromol. Chem., 179, 1565 (1978)
43. C. R. Fincher, Jr., M. Ozaki, M. Tanaka, D. Peebles, L. Lauchlan, A. J. Heeger and A. G. MacDiarmid, Phys. Rev. B, 20, 1589 (1979)
44. M. M. Maricq, J. S. Waugh, A. G. MacDiarmid, H. Shirakawa and A. J. Heeger, J. Amer. Chem. Soc., 100, 7729 (1978)
45. J. C. W. Chien, F. E. Karasz and G. E. Wnek, Nature, 285, 391 (1980)
46. I. B. Goldberg, H. P. Crowe, P. R. Newman, A. J. Heeger and A. G. MacDiarmid, J. Chem. Phys., 70, 1132 (1979)
47. M. J. Rice, Phys. Lett., A71, 152 (1979)
48. W. P. Su, J. R. Schreiffer and A. J. Heeger, Phys. Rev. Lett., 42, 1698 (1979)
49. B. R. Weinberger, E. Ehrenfreund, A. Pron, A. J. Heeger and A. G. MacDiarmid, J. Chem. Phys., 72, 4749 (1980)
50. J. A. Pople and S. H. Walmsley, Mol. Phys., 5, 15 (1962)
51. C. K. Chiang, C. R. Fincher, Jr., Y. W. Park, A. J. Heeger, H. Shirakawa, E. J. Louis, S. C. Gau and A. G. MacDiarmid, Phys. Rev. Lett., 39, 1098 (1977)
52. Y. W. Park, A. Denenstein, C. K. Chiang, A. J. Heeger and A. G. MacDiarmid, Solid State Comm., 29, 747 (1979)
53. A. G. MacDiarmid and A. J. Heeger, Synth. Metals, 1, 101 (1979/80)
54. H. Shirakawa and S. Ikeda, unpublished results (1976)
55. H. Shirakawa, E. J. Louis, A. G. MacDiarmid, C. K. Chiang and A. J. Heeger, J. Chem. Soc. Chem. Comm., 578 (1978)
56. C. K. Chiang, Y. W. Park, A. J. Heeger, H. Shirakawa, E. J. Louis and A. G. MacDiarmid, J. Chem. Phys., 69, 5098 (1978)

57. C. K. Chiang, M. A. Druy, S. C. Gau, A. J. Heeger, E. J. Louis, A. G. MacDiarmid and Y. W. Park, J. Amer. Chem. Soc., 100, 1013 (1978)
58. C. K. Chiang, C. S. Gau, C. R. Fincher, Jr., Y. W. Park, A. G. MacDiarmid and A. J. Heeger, Appl. Phys. Lett., 33, 18 (1978)
59. P. J. Nigrey, A. G. MacDiarmid and A. J. Heeger, J. Chem. Soc. Chem. Comm., 594 (1978)
60. L. Mihaly, S. Pekker and A. Janossy, J. Synth. Metals, in press
61. Cf. A. G. MacDiarmid and A. J. Heeger, Molecular Metals, W. E. Hatfield, ed., Plenum Press, New York, 180 (1979)
62. Y. W. Park, A. J. Heeger, M. A. Druy and A. G. MacDiarmid, submitted for publication
63. Y. W. Park, M. A. Druy, C. K. Chiang, A. J. Heeger, A. G. MacDiarmid, H. Shirakawa and S. Ikeda, J. Polym. Sci., Polym. Lett. Ed., 17, 195 (1979)
64. M. Nechtstein, F. Devereaux, R. L. Greene, T. C. Clarke and G. B. Street, Phys. Rev. Lett., 44, 356 (1980)
65. W. R. Salaneck, H. R. Thomas, R. W. Bigelow, C. B. Duke, E. W. Plummer, A. J. Heeger and A. G. MacDiarmid, J. Chem. Phys., 72, 3674 (1980)
66. S. Lefrant, L. S. Lichtman, H. Temkin, D. B. Fitchen, D. C. Miller, G. E. Whitwell and J. M. Burlitch, Solid State Comm., 29, 191 (1979)
67. M. J. Kletter, T. Woerner, A. Pron, A. G. MacDiarmid, A. J. Heeger and Y. W. Park, J. Chem. Soc. Chem. Comm., 426 (1980)

68. S. C. Gau, J. Milliken, A. Pron, A. G. MacDiarmid and A. J. Heeger, J. Chem. Soc. Chem. Comm., 662 (1979)
69. A. Pron, A. G. MacDiarmid, A. J. Heeger, D. C. Weber, J. Decorpo and F. E. Saalfeld, submitted for publication
70. B. R. Weinberger, J. Kaufer, A. J. Heeger, A. Pron and A. G. MacDiarmid, Phys. Rev. B, in press
71. T. C. Clarke, R. H. Geiss, W. D. Gill, P. M. Grant, J. W. Macklin, H. Morawitz, J. F. Rabolt, D. Sayres and G. B. Street, J. Chem. Soc. Chem. Comm., 332 (1979)
72. N. Bartlett, R. N. Biagionni, B. W. McQuillan, A. S. Robertson and A. C. Thompson, J. Chem. Soc. Chem. Comm., 200 (1978)
73. W. R. Salaneck, H. R. Thomas, C. B. Duke, A. Paton, E. W. Plummer, A. J. Heeger and A. G. MacDiarmid, J. Chem. Phys., 71, 2044 (1979)
74. R. L. Greene, T. C. Clarke, W. D. Gill, P. M. Grant, J. F. Kwak and G. B. Street, Molecular Metals, W. E. Hatfield, ed., Plenum Press, New York, 203 (1979)
75. M. Ozaki, D. L. Peebles, B. R. Weinberger, C. K. Chiang, S. C. Gau, A. J. Heeger and A. G. MacDiarmid, Appl. Phys. Lett., in press
76. P. J. Nigrey, A. G. MacDiarmid and A. J. Heeger, in preparation

C H A P T E R II

EQUIPMENT AND PURIFICATION OF MATERIALS

The use of Ziegler-Natta catalysts in the preparation of polyacetylene and derivatives combined with the inherent oxidative instability of the polymers necessitates the routine use of specialized laboratory equipment and rigorously dried, oxygen-free solvents and gases. Thus, it is useful to devote one Chapter to the description of apparatus and purification procedures, since these will be frequently referred to throughout the course of this dissertation.

Equipment

Vacuum line. A typical glass vacuum line for transfer of gases and solvents in polymer syntheses, doping, etc., is described in Figure 4. Ground glass, high vacuum stopcocks (greased with Apiezon "L" or "N") were commonly employed, although manifolds equipped with high vacuum Teflon stopcocks were used when handling corrosive materials (e.g., halogens, arsenic pentafluoride, etc.). The narrow sub-manifold was always used for the synthesis of polyacetylene and copolymers, the advantage being minimal expansion (pressure reduction) of gaseous monomers before entering the polymerization reactor.

The quality of a vacuum obtained was determined using a Tesla coil. The absence of a visible glow discharge in the manifold suggests pressures in the micron range. As a general rule, a bright red glow discharge indicates the presence of air in the system. All vacuum line manipulations were performed only after no glow discharge was observed.

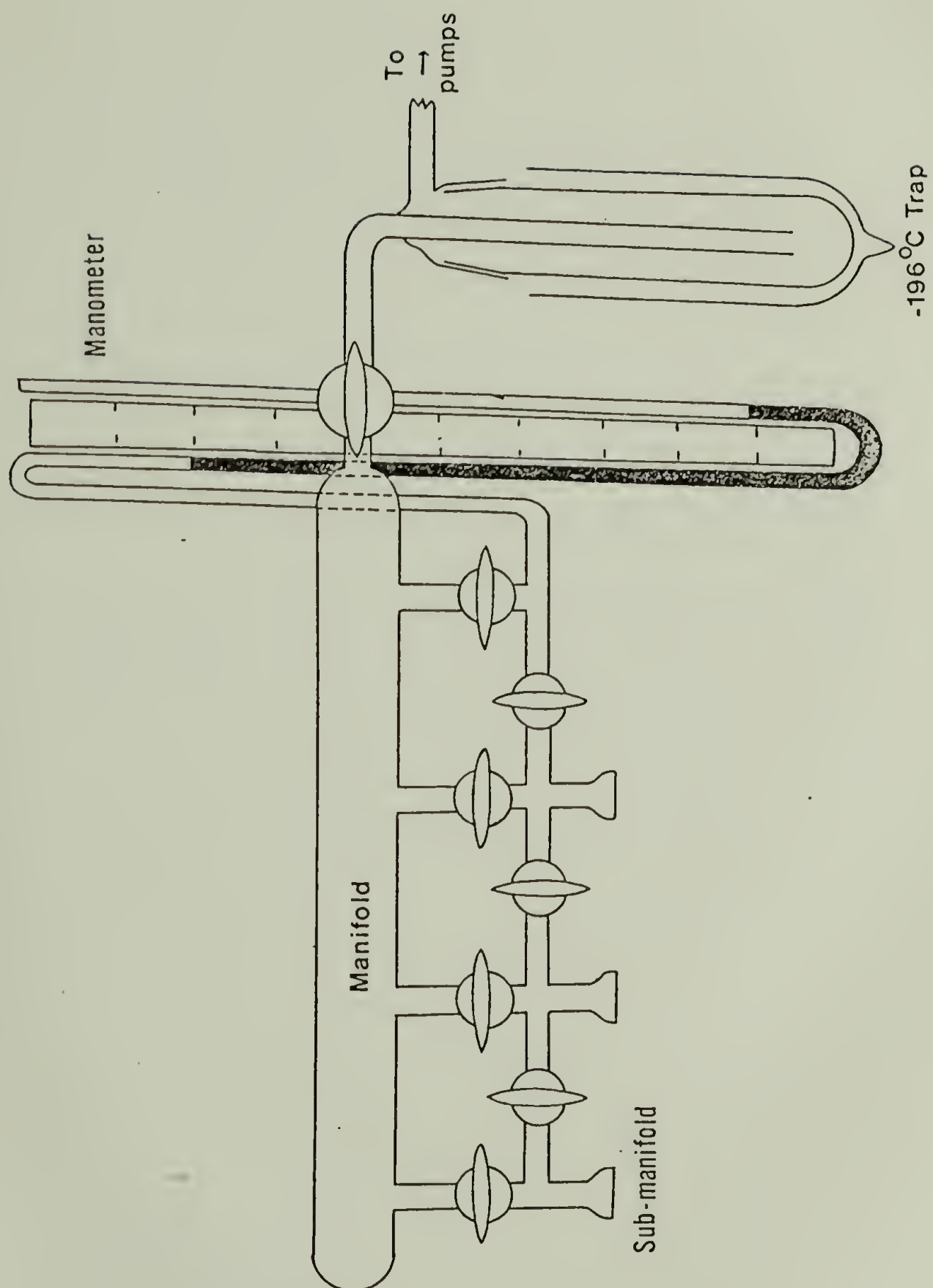


Figure 4. Vacuum line.

It is perhaps worth mentioning that dry ice-acetone cold traps were employed on the vacuum lines during preliminary work involving $(CH)_x$ film and gel preparations. Small amounts of mercury vapor from the diffusion pumps were present in the manifolds as evidenced by a light blue glow discharge from a Tesla coil. However, its effect on the quality of materials prepared is not considered to be significant.

Schlenk tubes. A Schlenk tube (Figure 5) was the most common piece of apparatus employed in the synthesis and storage of air sensitive materials. Although a variety of shapes and sizes were used, the essential features common to all tubes are 1.) a side arm with a ground glass, high vacuum stopcock for introduction of inert gas and 2.) a ground glass joint to which could be attached a top for evacuation. Typically, the tube was pumped on a high vacuum line and flame-dried with a gas-oxygen torch. The side arm stopcock usually had a small hole blown in the bottom of the cup, permitting one-step purging of the arm before filling with inert gas. Apiezon "N" or "L" grease was used for the stopcocks and ground glass joints.

Gas storage bulbs. A typical glass bulb for gas storage is shown in Figure 6. Bulbs typically possessed either a one or two liter capacity and were fitted with cold fingers for freezing of gases followed by pumping on the vacuum line to remove traces of air which may have entered the bulb during gas transfer operations. Stopcocks generally employed Teflon plugs fitted with Viton o-rings. In many cases, gases were stored in bulbs for several weeks before use. Since leakage of air at the stopcock is always a possibility, at least one freeze-pump-

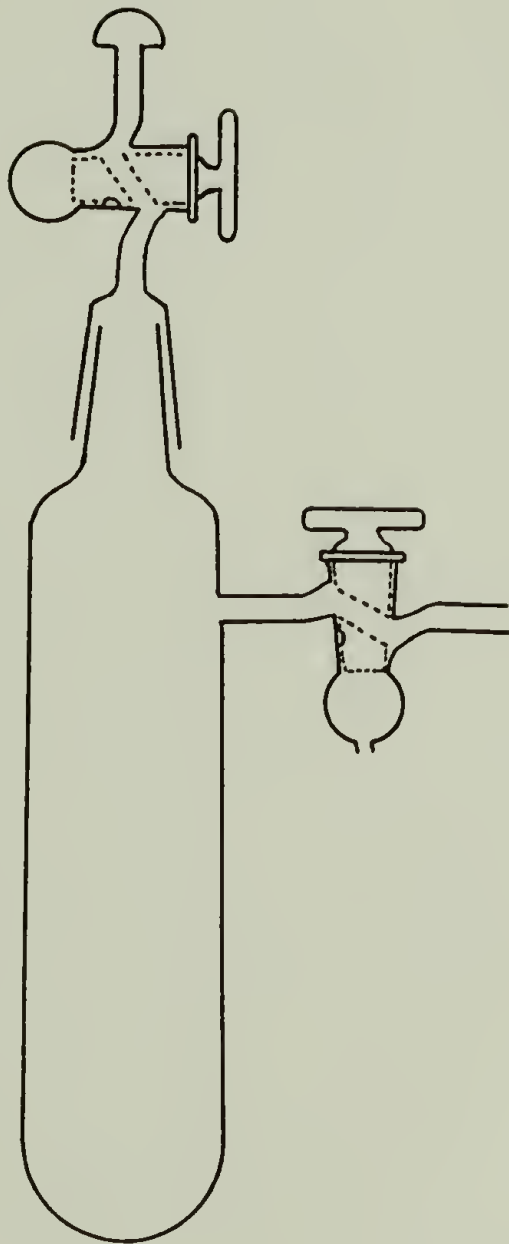


Figure 5. Schlenk tube.

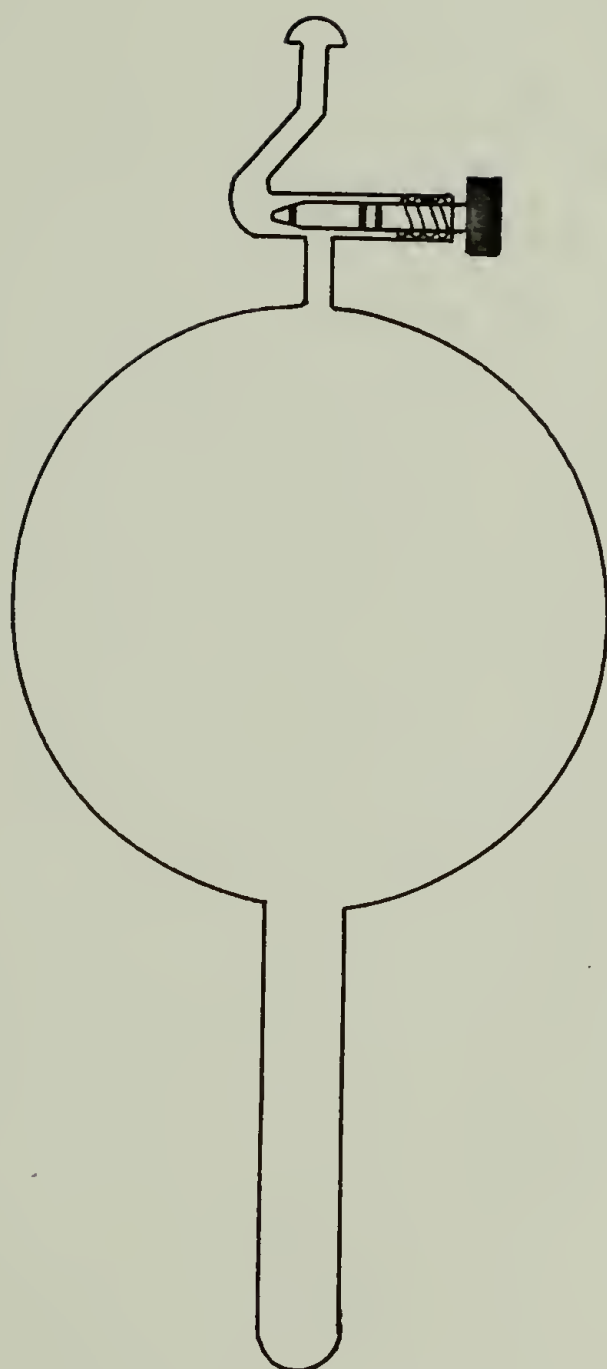


Figure 6. Gas storage bulb.

thaw cycle was performed immediately prior to use of the gas. In general, leakage during storage was not found to be a problem. All bulbs were covered thoroughly with electrical tape to contain the glass in the event of an explosion.

Syringes. Matched plug and barrel syringes equipped with Luer-Lok tips were used to transfer air sensitive liquids. Stainless steel needles were employed. The syringe was purged by drawing in argon several times and expelling before beginning transfers. The Luer-Lok tips were wrapped with Teflon tape to minimize air leakage during drawing of liquids into the syringe. All syringes were stored in an oven at ca. 80°C until use.

Glove bag and dry box. A polyethylene glove bag (I^2R), having an atmosphere of purified nitrogen, was used for most transfers of air sensitive solids. The bag was purged at least three times by filling with N_2 and expelling before beginning work. The dry box (Vacuum Atmospheres Corp.), being a relatively new addition to our laboratory, was extensively used only in handling of acetylene/methyl acetylene copolymers (Chapter IX).

Sample storage; EPR tubes. A Schlenk tube was commonly used for storage of large quantities of air sensitive polymers. However, for long term storage of small amounts of unique samples (e.g., doped polymers) or for materials to be sent for microanalysis, it was convenient to seal these in glass tubes under vacuum. Typically, samples were placed in glass tubes fitted with o-ring joints (Figure 7a) in a glove bag, pumped on a vacuum line and sealed at the constriction. It was useful to coat the seal with a black hydrocarbon wax (Apiezon "W") while the

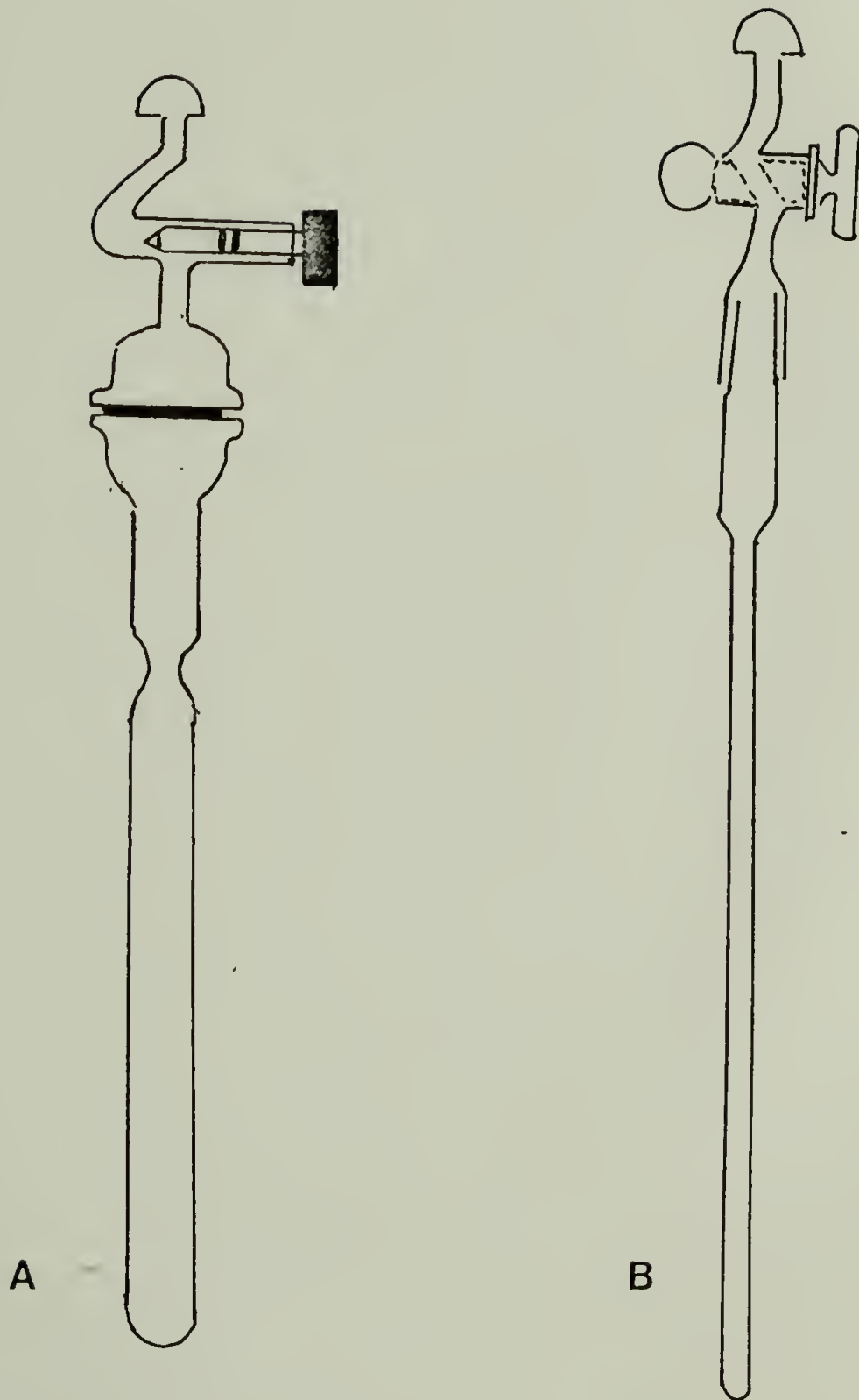


Figure 7. (A) Sample storage and (B) EPR tubes.

seal was warm to prevent leakage if thin spots were present in the seal.

Samples were transferred to quartz EPR tubes (Figure 7b) and evacuated before recording spectra. The EPR tubes could be reused or, if long term sample storage was necessary, sealed with a torch.

Purification of Materials

Inert gas. Argon was the inert gas of choice for polymer syntheses. Argon (Linde) was purified by passing the gas through a 50 cm x 4.5 cm heated column (ca. 110 - 120° C) of "BTS" supported copper catalyst (BASF Corp.) for removal of oxygen, followed by two 60 cm x 3 cm columns containing molecular sieves and KOH pellets, respectively, and small amounts of indicating Drierite for moisture removal. Connections between the columns and gas outlets employed Tygon tubing. A mercury bubbler was connected to the system between the argon cylinder and BTS column via a 3-way stopcock to prevent overpressurization of the gas line.

The two drying columns described were not used in initial $(CH)_x$ film and gel preparations; rather, a u-tube containing P_2O_5 and a sulfuric acid bubbler were employed. Although the molecular sieve/KOH system is presumably more efficient for moisture removal, differences between the two methods were not considered to be significant.

Prepurified nitrogen (Merriam Graves) for use in glove bags was usually passed through two columns of anhydrous $CaSO_4$.

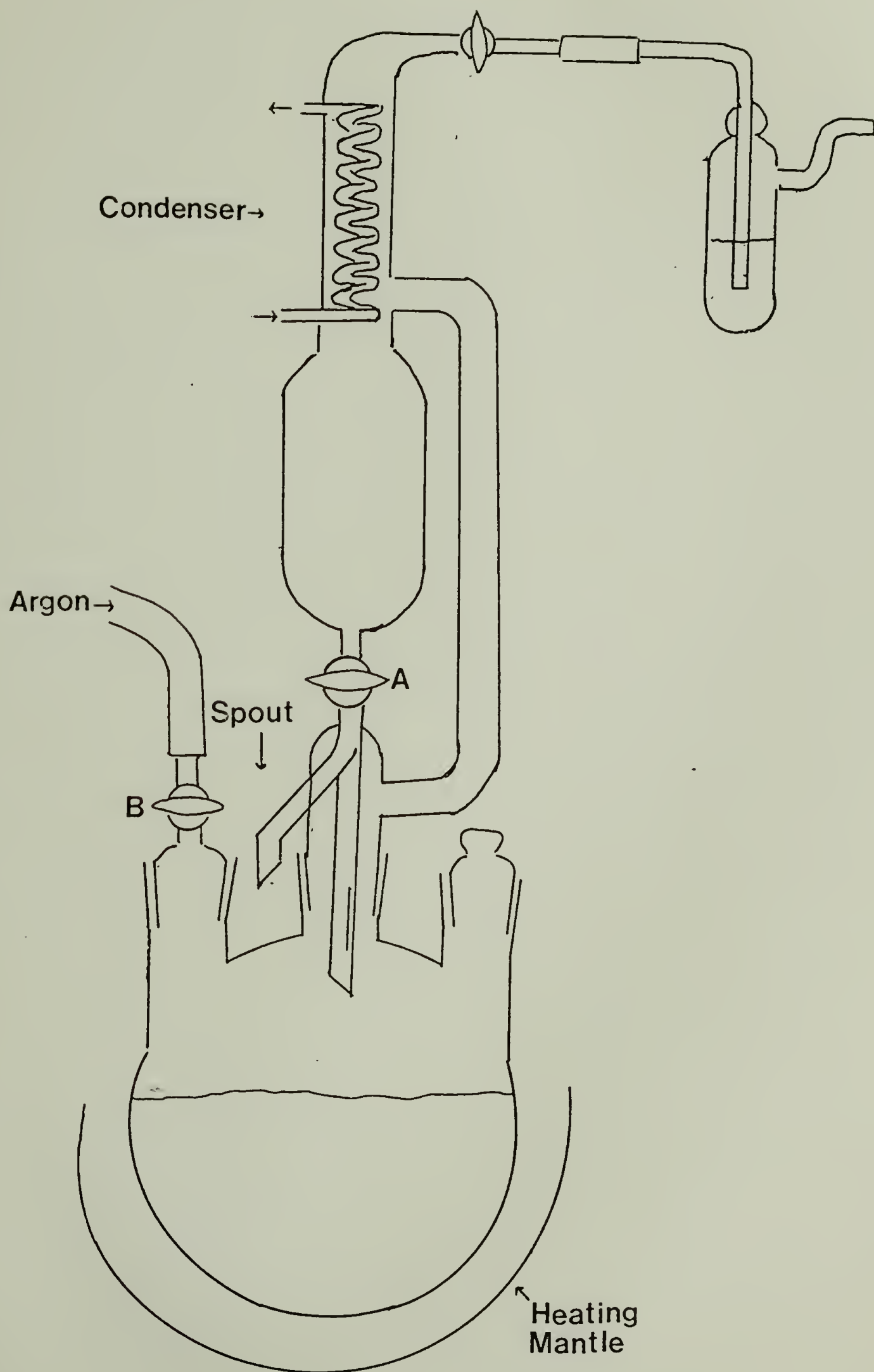
Solvents. The most common solvents used in synthetic preparations were toluene and pentane. They were purified as follows.

Two liters of toluene (Fisher) or pentane (Eastman Kodak white label) were placed in a 4 L erlenmeyer flask along with ca. 400 mL concentrated H_2SO_4 and stirred with a magnetic bar overnight. The concentrated H_2SO_4 served to remove traces of olefins. It was important that in the case of toluene the stirring with H_2SO_4 was not allowed to proceed for more than ca. 16 hours, in order to prevent sulfonation of the toluene. The brown H_2SO_4 layer was then removed using a 4 L separatory funnel and the solvent was stirred overnight once more with fresh concentrated H_2SO_4 . After separation of the H_2SO_4 layer, the solvent was washed in a 4 L separatory funnel with two 500 mL portions of distilled H_2O , three 300 mL portions of aqueous 10% NaOH and then with more distilled H_2O until the aqueous layer was neutral to litmus paper. The solvent was dried over anhydrous MgSO_4 overnight.

The solvent was then filtered to remove MgSO_4 and transferred to a still containing CaH_2 (Figure 8) under a stream of argon, and brought to reflux. A slow stream of argon was passed through the still at least overnight to remove oxygen. After this time, the stopcock to the argon line was closed, although the solvent was always kept under continuous reflux. It should be noted that the still was grease-free; stopcocks were fitted with Teflon plugs, and Teflon sleeves provided seals at the ground glass joints of the three-neck flask.

Transfer of a desired amount of solvent was accomplished as follows. A moderate amount of solvent was collected in the still by turning stopcock A (Figure 8) to the closed position, followed by increasing the temperature of the heating mantle. Meanwhile, a known amount of vola-

Figure 8. Solvent Still.



tile solvent (e.g., acetone) was added to a desired vessel (usually a Schlenk tube), and a mark was made at the liquid level with a wax pencil. The liquid was discarded and the tube was pumped on a high vacuum line, flame-dried and filled with argon. The spout of the still was then purged with argon by means of a short length of 4 mm O.D. Tygon tubing. With a strong argon flow through the Schlenk tube, the spout end was placed in the mouth of the Schlenk tube, and the 4 mm O.D. Tygon tubing was pulled from the spout. Argon was also introduced into the distiller via stopcock B, and then stopcock A was appropriately turned allowing solvent to flow into the Schlenk tube under argon. The Schlenk tube was capped, and the solvent in the still was cooled to a mild reflux under a slow stream of argon.

For certain experiments, it was desirable to have solvents for distillation directly on the vacuum line, affording more rigorous exclusion of moisture and oxygen. Thus, toluene or pentane was transferred from a still into a ca. 300 mL capacity solvent storage tube (Figure 9) with argon flow via the balljoint. The tube contained ca. 0.5 mL triethyl aluminum for toluene or ca. 5g CaH_2 for pentane. The tubes were degassed on a vacuum line by 3 - 5 freeze-pump-thaw cycles at -196°C and kept under vacuum. Since the tubes were disconnected from the vacuum line when not in use, a check for air leakage was always made before transfers. Thus, a small amount of solvent was introduced into the vacuum line and the manifold on the pumping side of the liquid nitrogen trap was sparked with a Tesla coil. If a glow discharge was observed here, the solvent was degassed before proceeding.



Figure 9. Solvent storage tube.

Acetylene. A purification train (Figure 10) containing two bubblers of concentrated H_2SO_4 (for removal of acetone and phosphine) and a u-tube containing P_2O_5 (for moisture removal) was used. The inlet of the train was connected to a tank of nitrogen (Merriam Graves prepurified) and a cylinder of acetylene (Matheson or Union Carbide purified grade) via a 3-way stopcock. The outlet was connected, via a 3-way stopcock, to butyl rubber pressure tubing which led to the fume hood and to a ball-joint for attachment to the vacuum line.

A 1 L or 2 L bulb equipped with a cold finger and Teflon stopcock was attached to the sub-manifold of the vacuum line, pumped and flame-dried. The manometer and the short piece of rubber tubing connecting the train to the line was also pumped. The train was purged with N_2 for ca. 15 minutes (exiting via the fume hood) followed by acetylene (by turning stopcock A) for ca. 15 minutes. The sub-manifold was isolated from the rest of the vacuum line and then stopcock B was turned to allow the acetylene to fill the storage bulb to a pressure of 700 - 750 torr. (Important:¹ under no circumstances should the acetylene pressure exceed 1 atm. (760 torr.); acetylene may spontaneously explode at pressures near 2 atm.). The acetylene flow was then once again directed to the fume hood, the bulb was closed and the acetylene supply was turned off. The train was purged with N_2 for ca. 15 minutes and, after closing off the N_2 supply, stopcocks at both ends of the train were turned so as to keep the train under N_2 .

The acetylene in the bulb was condensed into the cold finger at -196°C and pumped to remove traces of N_2 or air which may have entered

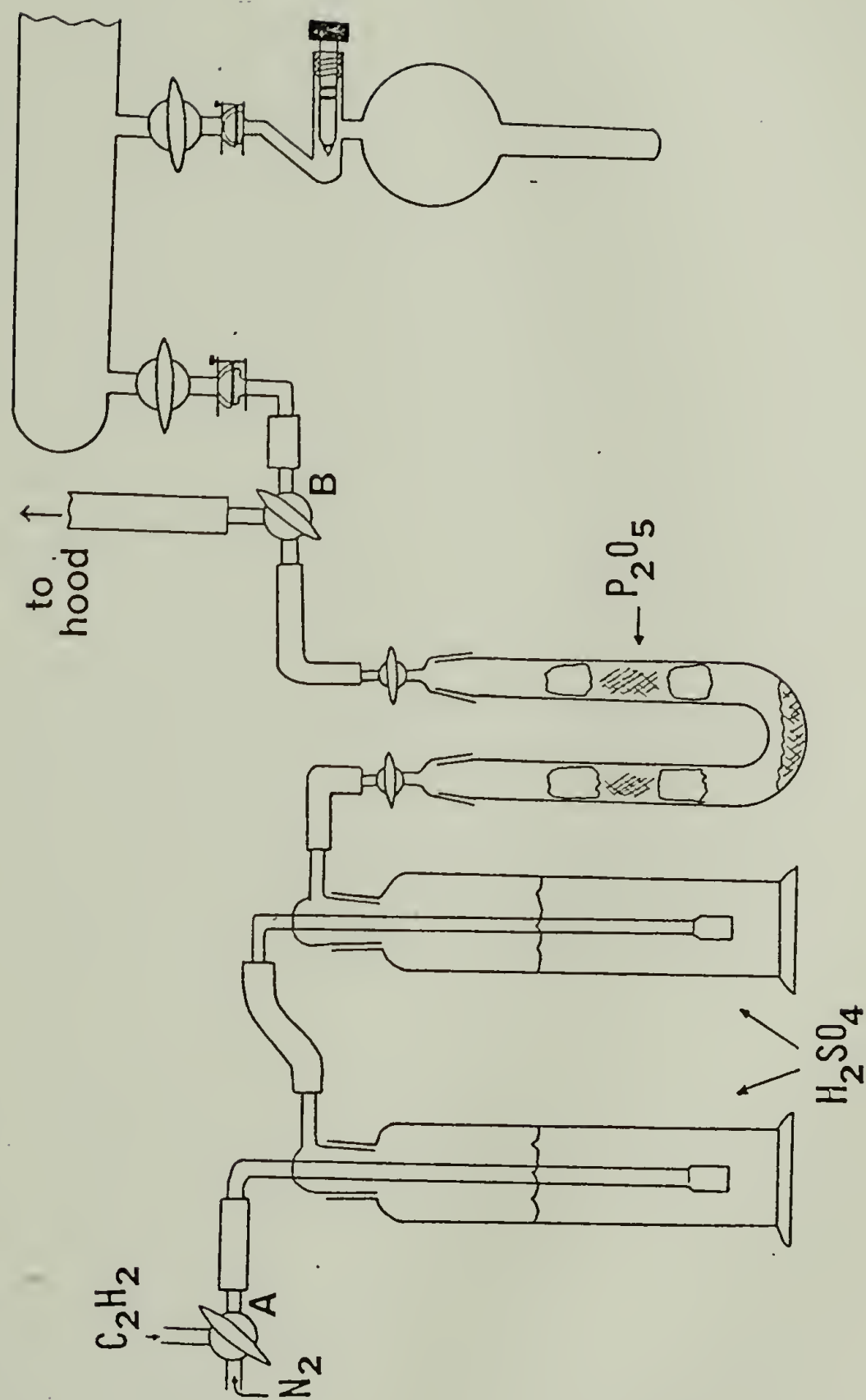


Figure 10. Acetylene purification system.

the system during the transfer. The degassing was repeated at least once.

Methyl acetylene. A cylinder of methyl acetylene (Air Products and Chemicals, Inc.) was connected via butyl rubber tubing and a balljoint to the sub-manifold of a vacuum line along with an evacuated 1 L or 2 L bulb and an evacuated Schlenk tube containing 5 - 10 g P_2O_5 . After evacuating the tubing and manometer and isolating the sub-manifold from the remainder of the vacuum line, the bulb was filled to the desired pressure (never > 1 atm.). The methyl acetylene cylinder was closed and isolated from the vacuum line, and the Schlenk tube was opened. The methyl acetylene in the bulb was dried by condensing it as a liquid over the P_2O_5 in the Schlenk tube at $-78^\circ C$ for 20 - 30 minutes. After warming the Schlenk tube to room temperature, the gas was condensed back into the bulb at $-196^\circ C$ and pumped to remove traces of air which may have entered the system during the transfer. The degassing was repeated at least once.

Polymerization catalyst components. Titanium tetrabutoxide (Alfa Inorganics) was purified by reduced pressure distillation under a slow argon bleed using standard techniques. A standard high vacuum line was used as the vacuum source. The outlet of the distillation apparatus had a glass "Y-tube" fitted with ground glass joints for attachment of Schlenk tubes as receiving flasks. A low boiling, colorless liquid (presumably n-butanol) was collected and discarded. The titanium tetrabutoxide was distilled as a light yellow, viscous liquid and was stored under argon

in the Schlenk tube. The tube was usually wrapped with black electrical tape to protect the solution from light.

Triethyl aluminum (Ethyl Corp.) was used as received. It was shipped and stored in an Alkyltainer under argon, which is essentially a metal Schlenk tube. It is reported² to contain ca. 1% AlH_3 and ca. 7% triisobutyl aluminum.

References

1. Matheson Gas Products, Acetylene Data Sheet (1971)
2. Ethyl Corp., telephone conversation

CHAPTER III

ELECTRICAL CONDUCTIVITY MEASUREMENTS AND DOPING METHODS

Conductivity Measurements

General considerations. The intrinsic electrical transport of materials is governed by Ohm's Law,

$$V = IR$$

where V is the potential difference, I the current and R the resistance of the sample. The resistance is a function of sample dimensions and can be expressed as

$$R = \frac{\rho L}{A}$$

where ρ is the electrical resistivity and L and A are the length and cross section of the sample, respectively. The reciprocal of ρ is the electrical conductivity, σ :

$$\sigma = \frac{L}{RA}.$$

Both σ and ρ are properties of the material and do not depend on its size or shape. The electrical conductivity rather than the resistivity is the more common parameter reported and is usually expressed in units of $\Omega^{-1}\text{cm}^{-1}$.

Experimental methods. The values of σ for polymers studied in this dissertation were determined by measuring sample dimensions and resistance. Typically, rectangular polymer films (length and width ca. 2 cm and 0.2 cm, respectively) were employed although in certain instances compressed pellets (ca. 1.25 cm diameter) of powdered samples were used.

Sample thickness was measured using a micrometer (sensitive to 0.0001") while length and width were obtained using a caliper (sensitive to 0.001").

In order to measure R , four parallel platinum wires were attached to the sample using a graphite cement (Electrodag 502, Acheson Colloids Co.). Platinum was employed since it is inert toward reactive and corrosive dopants. The four-probe cell is described in the following section of this chapter.

For samples of very high resistance (ca. $10^7 - 10^{11} \Omega$), R was measured directly using two of the platinum probe wires (usually the inner two) and a Keithley 610A electrometer. The electrometer or a simple ohm-meter (Simpson or Radio Shack) was employed for samples of intermediate resistance (ca. $10^3 - 10^7 \Omega$). The value of L was simply the distance between the two probe wires on the sample. However, the use of the two-probe method for samples having smaller resistances can be misleading due to the contribution of contact resistance of the Electrodag. In other words, the value of R obtained from a two-probe measurement can be considerably greater than the actual R of the sample. This problem was circumvented by using the four-probe method. In this case, a current (I) was applied across the outer two electrodes and the potential difference (V) was measured across the inner electrodes. Since no current flows through the inner two electrodes, the effect of contact resistance is eliminated and V is dependent only upon I and the sample resistance. It is important to note that the value of the sample length used in the determination of σ is that between the inner two probes.

The electrical apparatus used in this work employed a 1.5 V battery as the current source. The potential difference was measured across a known reference resistor and the sample using a Keithley 149 millivoltmeter. The reference resistors ranged from 1 - 10,000 Ω in decade increments. The exact value of I was not necessary due to the reference resistor network and was assumed to be constant during the measurement. A circuit diagram of the apparatus is shown in Figure 11.

The two equations (Ohm's Law) describing the circuits of interest are:

$$V_{\text{reference}} = I R_{\text{reference}}$$

$$V_{\text{sample}} = I R_{\text{sample}}$$

Since I is constant, these relations reduce to

$$R_{\text{sample}} = \frac{V_{\text{sample}}}{V_{\text{reference}}} \cdot R_{\text{reference}}$$

The largest reference resistor was $10^4 \Omega$; thus, for samples having values of R greater than this, the two-probe method was used. Contact resistances were found to vary from ca. $10^1 - 10^3 \Omega$, so R was always measured by the four-probe method when in the accessible range of the instrument.

Doping Methods

Apparatus. Typical apparatus used for simultaneous doping and monitoring electrical conductivity of polymer samples are shown in Figure 12.

Two basic designs were used and are designated as type I or type II.

Although both designs were of the four-probe variety, two-probe measure-

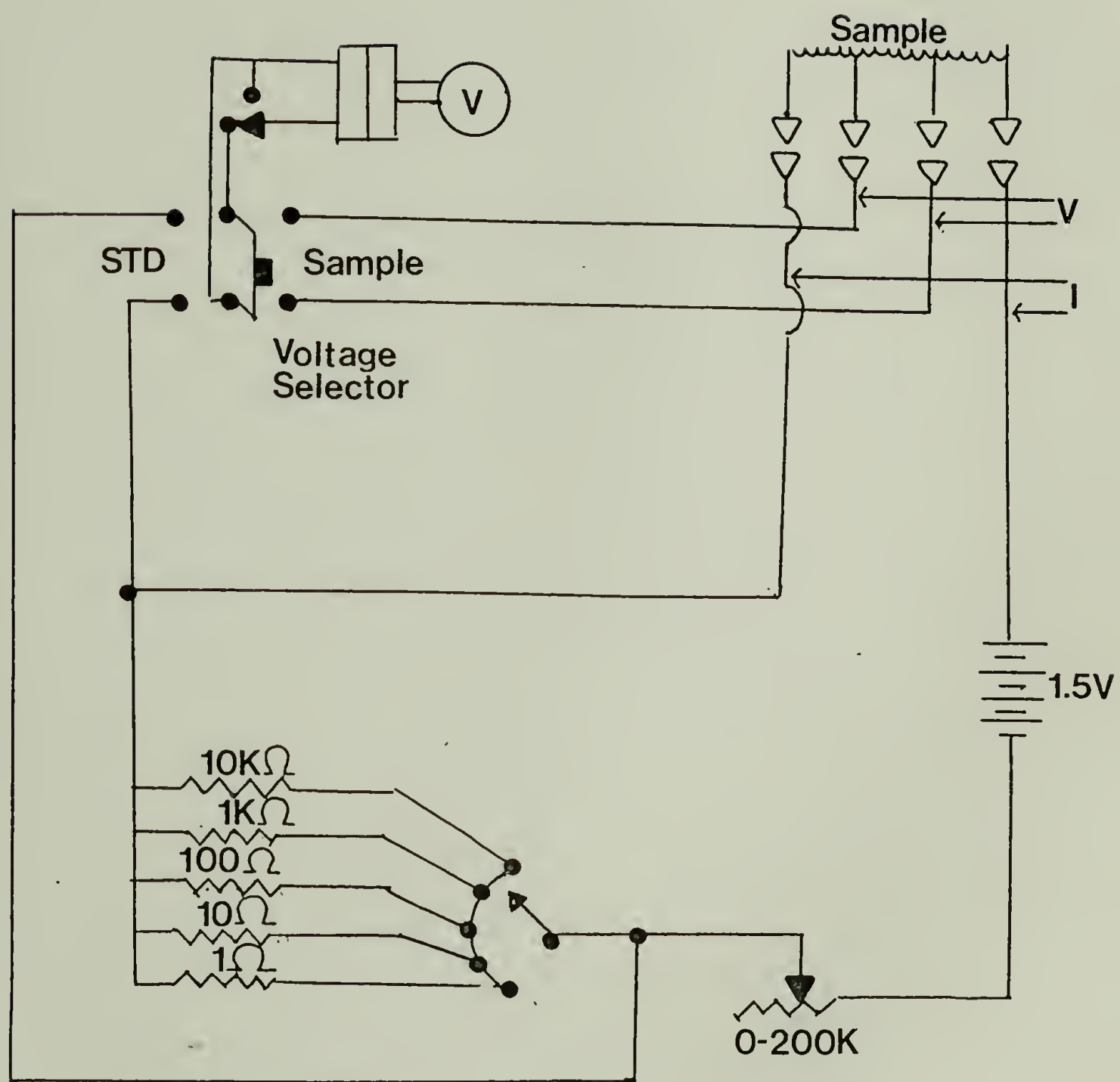


Figure 11. Schematic diagram of four-probe electronics.

Figure 12. Four-probe apparatus.

(a) - type I

(b) - type II

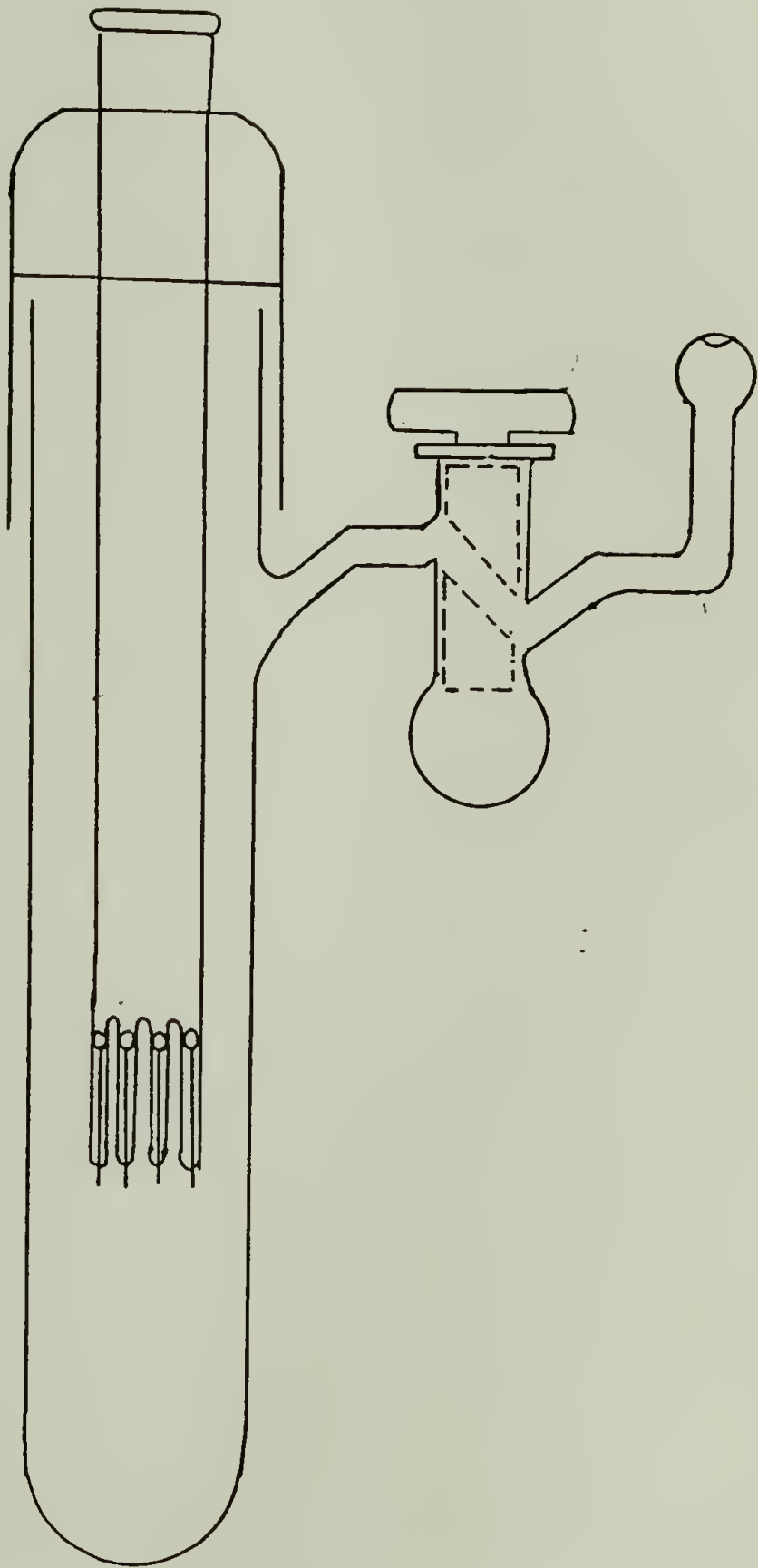


Figure 12a.

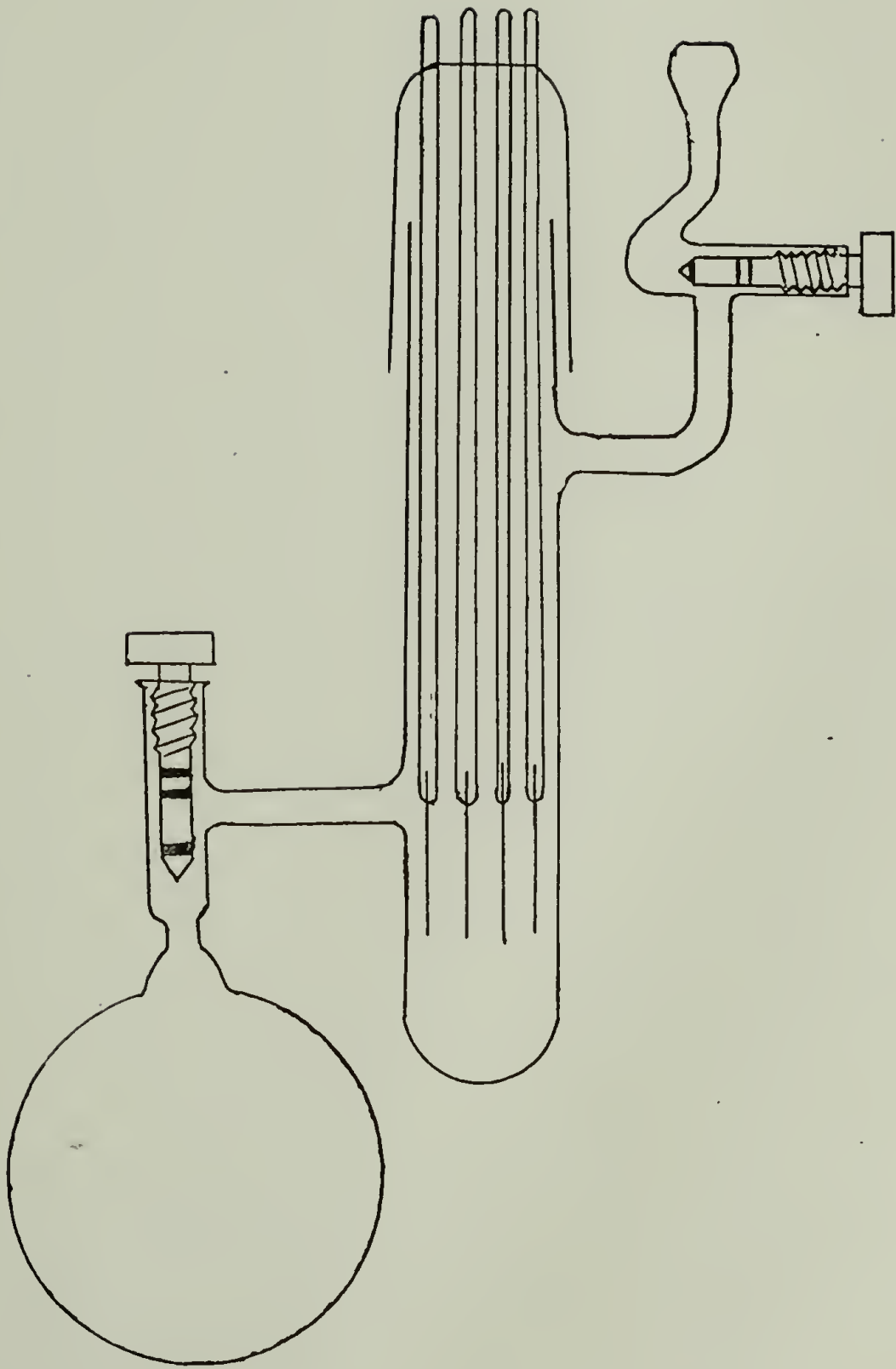


Figure 12b.

ments were easily accomplished when appropriate. The apparatus were constructed of glass and employed either high vacuum ground glass or Teflon o-ring stopcocks. The tips of the four glass fingers were melted around the platinum wires. Since platinum and Pyrex glass are rather incompatible, a small quantity of blue cobalt glass was employed at the finger tips to make these seals vacuum-tight. These seals were still subject to leaks on occasion. Rather than reworking the glass at the fingertips, it was found useful to drop small chips of black hydrocarbon wax (Apiezon W) into the bottom of the fingers followed by melting of the wax through gentle heating with a gas flame. This method was usually very successful. The apparatus was demonstrated to be leak free (Tesla coil check) before use.

Contacts to external electrical instruments were made by filling the fingers with mercury followed by placing appropriate lengths of copper wire into the fingers. Contacts between the copper wires and instruments were made with "alligator" clips. The wires were sheathed with thin glass tubing to provide insulation. The type II four-probe apparatus employed four isolated pieces of glass tubing which served as both fingers for sealing the platinum wires and insulation for the copper wires.

Polymer samples were typically mounted on the platinum wires in air with exposure kept to a minimum unless stated otherwise. It should be noted that in the type-I four-probe the platinum wires were usually turned up from the bottoms of the fingers and then twisted around small glass knobs near the tops of the fingers (See Figure 12a). This design

facilitated easy sample mounting since the sample could rest on the glass fingers during application of the Electrodeag. In the case of the type-II apparatus, the sample was usually rested on a stack of microscope slides during mounting. A pre-weighed sample was usually placed in the bottom of the apparatus for determination of uptake of dopant along with additional samples (for EPR, etc.) when necessary. The apparatus was pumped on a vacuum line for at least one hour before beginning doping experiments to dry the Electrodeag (methylethyl ketone solvent).

Iodine. A type-II four-probe was used for most iodine doping experiments. The side bulb contained several iodine crystals (Fisher resublimed) and was pumped several times at -196°C to remove air. The degassing was always done before the sample under study was mounted on the probe wires. Typically, after pumping the four-probe chamber thoroughly, the stopcock connecting the bulb was opened quickly several times if fairly low doping levels were desired or was simply left open to dope the sample rapidly to the metallic regime. Better control of the extent of doping could be accomplished by concomitant control of the iodine vapor pressure using appropriate slush baths. After doping to the desired level, the apparatus was usually pumped at least ten minutes before handling the sample for any reason.

In certain cases where only doping of moderately air-sensitive samples to the saturation conductivity was desired, it was found convenient to pass iodine-bearing inert gas over the sample. In this case, a four-probe sample holder was constructed from a #6 rubber stopper,

open-ended melting point tubes and platinum wire. A few millimeters of a short piece of platinum wire (ca. 25 mm total length) was placed in the end of a melting point tube and the tube end was sealed with a gentle gas flame. While still warm, the outside of the platinum-glass seal was covered with Apiezon W black wax. Four such tubes were prepared and inserted through four small holes in the stopper with the remaining open ends of the tubes on the wide-diameter side of the stopper. The tubes were filled to a depth of ca. 1 cm with mercury and thin copper wires were dipped into the mercury reservoirs to provide contacts between the probes and external instruments. The assembled rubber stopper four-probe, which also contained a hole (ca. 5 mm-diameter) to accommodate a disposable pipette tip, was fitted onto a glass tube of the appropriate diameter (ca. 10 cm length) which served as the doping chamber. The bottom of this tube contained a glass wool plug and a constriction to allow attachment of 1/4" Tygon tubing. The remaining end of this tubing was connected to a small mineral oil bubbler. As usual, the sample was mounted across the four platinum wires with Electrodag.

A stream of purified argon was passed through a glass tube containing iodine crystals and then into the doping chamber via a disposable pipette tip inserted into the four-probe rubber stopper. Connections between the iodine and doping tubes were made with Tygon tubing. The doping rate of the sample was easily controlled by the argon flow rate. Reference samples for weight uptake were rested on the glass wool plug at the bottom of the doping chamber. Due to the toxicity of iodine, the system was only used in a fume hood.

This method has three disadvantages concerning the "quality" of

the doped samples. First, controlled doping is more difficult as compared to doping in vacuo since the vapor pressure and hence the amount of iodine introduced in the latter method is easier to regulate. Second, the flow method is objectionable if samples must be rigorously kept from exposure to air since transfer of samples into and out of the doping chamber is performed in air. Finally, if it is necessary to monitor conductivity changes which may occur upon pumping of excess iodine from the sample, the flow system clearly cannot be employed.

Evaluation of the potential conductivity of samples which have never been previously investigated is a major application of the flow method since the doping is rapid and sophisticated glassware is not required.

Arsenic pentafluoride. Note: AsF_5 is extremely hazardous and should be stored and used in a hood at all times.

It is worthwhile to point out that AsF_5 is a very powerful dopant for materials such as polyacetylene and thus warrants the transfer of minute quantities of the gas. It is usually very easy to dope beyond a desired level and corresponding conductivity. Other materials may not be as sensitive to AsF_5 and greater amounts may be required to produce dramatic changes in conductivity. Thus, in terms of future reference, selection of the best route to AsF_5 doping of a given material will need to be determined. However, the "slow-doping" method described below which was the most common route employed for samples studied in this dissertation is recommended as a general initial method for AsF_5 -doping of new materials. Specific deviations from this method will be mentioned throughout the text where appropriate.

An AsF_5 cylinder (Ozark Mahoning Co.) was fitted with a CGA-660 stainless steel valve; the outlet of the valve was attached to the metal end of a glass-to-metal seal with silver solder. The glass end was connected to a ground glass, high vacuum stopcock and a balljoint for attachment to a vacuum line fitted with Teflon stopcocks and located in a hood. Typically, a 1 L gas storage bulb was filled to a pressure of ca. 300 - 500 torr AsF_5 on the vacuum line. The gas was condensed into the cold finger of the bulb (-196°C) and pumped to remove air which may have entered the system during the transfer. The bulb was stored in the hood and the AsF_5 was always degassed immediately prior to use.

A type-I four-probe was employed in most AsF_5 doping experiments. After flame-drying the vacuum line, degassing the AsF_5 and pumping the four-probe at least two hours, the cold finger of the bulb was cooled to ca. -95 to -100°C using a methanol or toluene slush bath. This bath provided a low vapor pressure (ca. 20 - 30 torr) of AsF_5 for easier control of sample doping and also served to trap traces of HF which may result from the reaction of AsF_5 with traces of moisture in the bulb and vacuum line.

After opening the manometer and isolating the manifold from the remainder of the vacuum line, the stopcock to the four-probe was closed. Next, the stopcock isolating the bulb from the manifold was closed and the stopcock of the bulb was opened for ca. 1 - 3 seconds, allowing AsF_5 to fill this small volume of the system. With the bulb closed, the stopcock between the bulb and manifold was opened to allow the AsF_5 to expand into the manifold with a corresponding large decrease in pres-

sure. This pressure was usually < 0.5 torr. The stopcock to the four-probe was opened allowing the AsF_5 to contact the sample. The conductivity of the sample was allowed to reach a nearly constant value and then another small dose of AsF_5 was transferred as described above. This process was repeated several times. In general, as the particular sample became doped with AsF_5 , the conductivity changes became progressively less dramatic. A point was usually reached when addition of these small doses produced little change in conductivity. Thus, the amount of AsF_5 was progressively increased, usually in increments of 2 - 3 torr, until no further conductivity change was observed, and this was considered to be the saturation conductivity of the sample. The AsF_5 in the vacuum line and four-probe was condensed back into the bulb at -196°C and the four-probe was pumped for a minimum of 15 minutes before handling the sample.

The pressure of the AsF_5 , particularly in the later stages of doping, was usually measured with a double-arm mercury manometer. A problem arose in recording the mercury level in the arm of the manometer in contact with the vacuum line since AsF_5 reacts with mercury to coat the manometer with a golden film. Thus, the pressure was approximated by noting the change in mercury level in the arm exposed to the atmosphere and multiplying by two. It should be emphasized that an accurate measurement of the AsF_5 pressure was not critical for the experiments. Conductivities obtained in several dopings of a particular sample were very reproducible so long as the slow-doping method described above was employed.

Sodium naphthalide. The procedure for doping with ca. 1 M sodium naphthalide radical anion was as follows. Ca. 50 mL dry THF which was refluxed over CaH_2 in a solvent still (courtesy of Professor M. Raush, UMass Chemistry Dept.) was transferred to a Schlenk tube under argon. A piece of sodium metal (coated with paraffin oil) was dipped into pentane to remove the oil and cut into a cube (ca. 1.28 g). The sodium was flattened into a sheet with a hammer and, while holding the sheet above the mouth of the Schlenk tube containing the THF, small pieces were cut with scissors and dropped into the tube under argon flow. The suspension was stirred with a magnetic bar, and ca. 6.4 g naphthalene (Fisher) was poured into the tube under argon. The solution became deep green-black, characteristic of the sodium naphthalide radical anion, and was allowed to stir overnight to insure solubilization of the components.

The sample to be doped was mounted on the probes of a type-II four-probe apparatus. The apparatus was pumped overnight on a vacuum line. Argon was introduced through the balljoint of the four-probe and the Teflon plug of stopcock attached to the bulb was removed. The sodium naphthalide/THF solution was transferred to the bulb under argon using a syringe. A small magnetic bar was dropped into the bulb, the stopcock was replaced and the four-probe was closed off from the argon supply. It is recommended that the operations described above be carried out in a dry-box if one is available.

The apparatus was connected to a vacuum line and the doping chamber was pumped at least one hour. The sodium naphthalide/THF solution

was frozen at -196°C and pumped for several minutes until no Tesla coil discharge was observed. This freeze-pump-thaw process was repeated at least twice. After disconnecting the apparatus from the vacuum line, the bottom of the doping chamber was cooled to -196°C for several seconds and then the stopcock to the bulb was opened. The sodium naphthalide/THF solution was then immediately poured into the doping chamber to cover the sample connected to the probe wires. The initial cooling of the bottom of the chamber was done in order to facilitate the transfer of the solution. The conductivity was monitored initially by a simple ohmmeter (two-probe) and finally by using the four-probe method described previously. For samples studied in this work, the conductivity usually reached saturation within a few minutes.

The sample and doping vessel was washed of excess sodium naphthalide as follows. After reaching the saturation conductivity of the sample, the bulb was cooled to -196°C and the solution in the doping chamber was poured into the bulb. The solution in the bulb was stirred vigorously and pure THF was distilled into the doping chamber by cooling the bottom of the chamber with liquid nitrogen. After warming the THF to room temperature, it was poured back into the bulb and this process was repeated until the THF in the chamber was colorless. The stopcock to the bulb was then closed. The solution could be re-used as long as it still possessed a deep green coloration. A light brown solution suggested significant decomposition due to interaction with moisture and/or air, and in this case the solution was discarded by decomposing it in a large quantity of t-butyl alcohol.

Since samples doped with sodium are inordinately sensitive to

traces of moisture or air, no attempt was made to handle these samples as a drybox was unavailable for most of this dissertation work.

Other dopants. In a few cases, less common dopants such as bromine and H_2SO_4 were used and are described only briefly. The technique for bromine doping was similar to that used for iodine doping. Typically, a few milliliters of bromine (Fisher Reagent A.C.S.) were added to the bulb of a type-II four-probe and was degassed on a vacuum line. The sample was exposed in vacuo to a known vapor pressure of bromine (using appropriate slush baths) and doped to the desired level. Upon completion of the doping, the bromine in the doping chamber was condensed back into the bulb at -196°C .

Doping with H_2SO_4 was accomplished as follows. After mounting the sample in either a type-I or type-II four-probe and pumping to dry the Electrode contacts, the apparatus was opened in air and ca. 0.5 mL H_2SO_4 (Fisher Reagent A.C.S., 98%) was placed in the bottom of the doping chamber. The apparatus was connected to the vacuum line and pumped dynamically for several hours, allowing the H_2SO_4 vapor to contact and dope the sample.

For future reference, the doping procedures outlined in this chapter can be adapted, with perhaps slight modifications, to experiments employing essentially any gaseous or liquid dopant. It is emphasized that slow, controlled doping usually affords higher conductivities, especially when dealing with $(\text{CH})_x$, as compared to rapid doping.

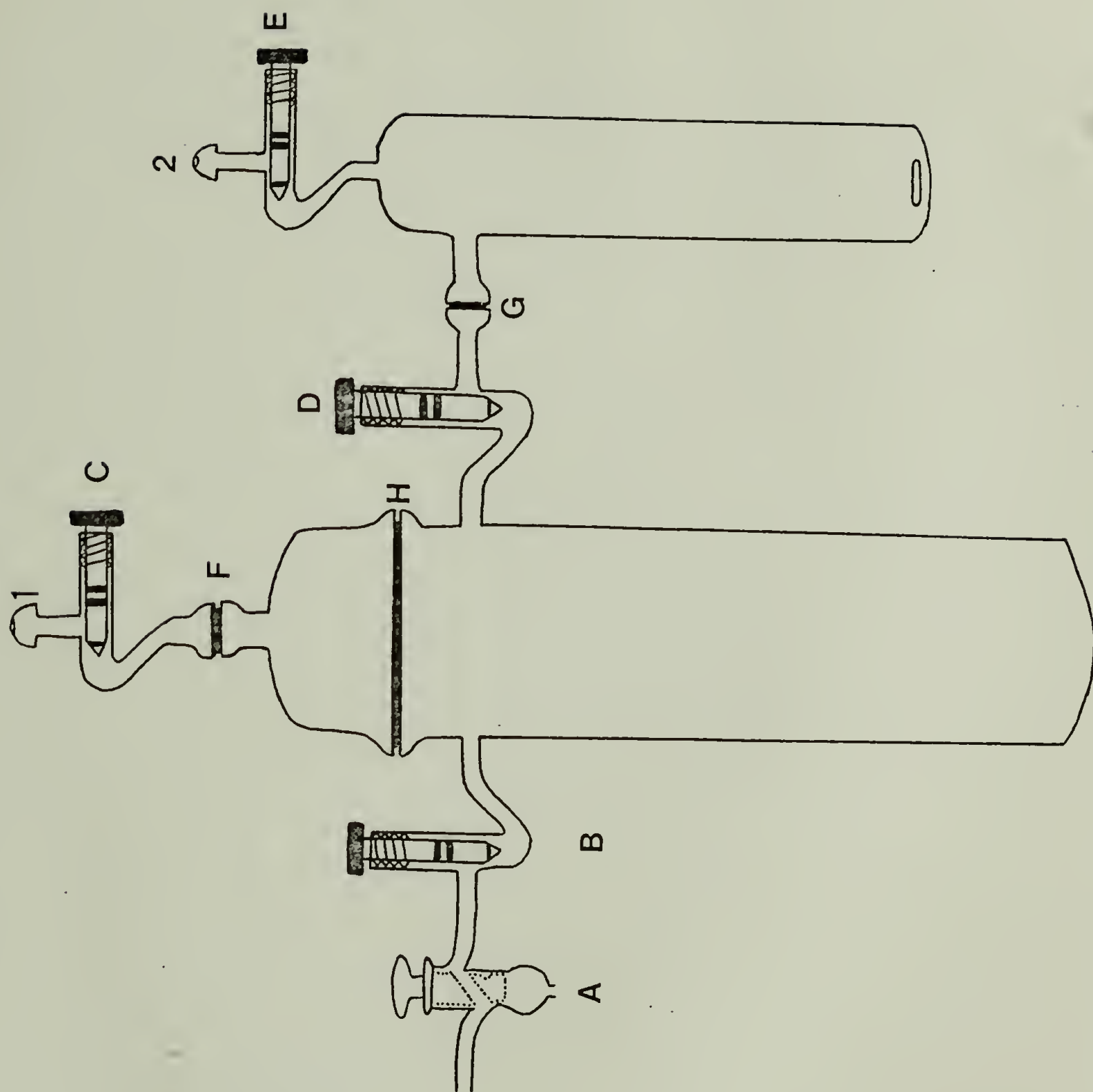
CHAPTER IV

SYNTHESIS OF CIS $(CH)_x$ FILMS

Acetylene was first polymerized to a linear polymer in 1958¹, although the resulting black, intractable powder remained a scientific curiosity until Shirakawa et al.²⁻⁵ demonstrated the formation of a continuous polyacetylene film using a Ziegler-Natta catalyst based on titanium tetrabutoxide and triethyl aluminum. This form of $(CH)_x$ is much more amenable to studies of electrical transport properties. The experimental procedure developed by Shirakawa et al. for the synthesis of $(CH)_x$ films has been modified⁶ by workers at the University of Pennsylvania in order to produce analytically pure material. This is important in view of the sensitivity of the electrical properties of $(CH)_x$ to impurities.⁷ Since this modified procedure is the basis for the synthesis of all $(CH)_x$ films studied in this dissertation, it will be described in detail. A few additional refinements have been developed in our laboratory. Although the cis-trans isomer content can be controlled by the polymerization temperature,⁵ it is much more convenient to prepare cis $(CH)_x$ at low temperatures followed by thermal isomerization if trans $(CH)_x$ is desired. Thus, the procedures described below apply specifically to the synthesis of cis $(CH)_x$ films. The reader is referred to Chapter II for details concerning the purification of materials used in this preparation.

The apparatus. The apparatus used for the synthesis of $(CH)_x$ films is shown in Figure 13. The apparatus consists of a reactor, which is essen-

Figure 13. Apparatus for the synthesis
of $(\text{CH})_x$ films.



tially a Schlenk tube, and a washing arm for collection of catalyst residues. All o-rings (Viton) were covered with a thin film of silicone grease prior to assembly of the apparatus. In order to eliminate the possibility of extraction of stopcock grease by solvents used in the $(CH)_x$ film preparation and washing, stopcocks B - E employed Teflon plugs equipped with Viton o-rings. However, a ground glass stopcock (A) was used for introduction of inert gas, and Apiezon "L" or "N" grease was employed here.

The assembled apparatus was connected to a high vacuum line via ball-joint #1 and pumped at least two hours with stopcocks B - D open. A Tesla coil was used to check for leaks. Next, the apparatus was isolated from the vacuum line by closing stopcock C; stopcock D was then closed and the apparatus was allowed to remain under vacuum for at least three hours. After this time, a Tesla coil was used to verify the presence of a good vacuum. Any leaks were usually the result of poor seals at o-ring joints. It was important for the apparatus to maintain a good static vacuum before proceeding. The apparatus was then left to pump on the vacuum line overnight (stopcocks B - D open).

The next morning, the apparatus was flame-dried (using a gas-oxygen torch) while under dynamic vacuum.

Preparation of the catalyst. After the apparatus cooled to room temperature and stopcocks B and D were closed, the bottom of the reactor was cooled to $-196^\circ C$ and 20 mL toluene was distilled in directly from a solvent storage tube containing ca. 0.5% triethyl aluminum (20 mL toluene corresponded to a depth of 8 mm in the solvent storage tube). As a

precaution, upon completion of the distillation the reactor was pumped for a few minutes while the toluene was still frozen to remove any traces of air which may have entered the system during the transfer. A Tesla coil was used to check the quality of the vacuum.

The apparatus was disconnected from the vacuum line after closing stopcock C, and the frozen toluene was allowed to warm to room temperature. Next, purified argon was introduced at stopcock A (after purging), and stopcocks B and C were opened. The top of the reactor was removed at o-ring F. Using a syringe, 1.7 mL titanium tetrabutoxide (stored in a Schlenk tube under argon) was added to the toluene in the reactor. The bottom of the reactor was then cooled to -78°C (dry ice - acetone bath), and 2.7 mL triethyl aluminum (from Alkyltainer, Ethyl Corp.) was added dropwise via a syringe to the titanium tetrabutoxide/toluene solution over a period of about one minute. During the addition, the color of the solution changed from light yellow to deep orange-red. The tip of the syringe needle was used to occasionally stir the solution as the triethyl aluminum was added. If this was not done, a deep red-orange "layer" was observed on the top of the catalyst solution while the bottom remained light yellow, suggesting inhomogeneous reduction of the titanium tetrabutoxide.

The reactor was capped at o-ring F and, while stopcock C remained open, the argon flow was turned down to a low rate, after which stopcocks C, B and A were immediately closed. The argon flow reduction was important since the pressure in the reactor will increase due to the formation of gaseous catalyst reaction products and warming of the solu-

tion (see below). On occasion, failure of an o-ring occurred due to the excess pressure.

The reactor was removed from the -78°C bath and the catalyst solution was allowed to warm to room temperature. The solution was then allowed to "age" for 30 minutes at room temperature. The color of the solution changed from deep red-orange to dark brown during the aging period. In the meantime, a 2 L bulb of purified acetylene (ca. 700 - 740 torr) was attached to the vacuum line and degassed one final time at -196°C . (Note: It is recommended that the acetylene pressure in the bulb be close to, but below, 760 torr. Films prepared with low acetylene pressures generally yield lower tensile strengths than those prepared with acetylene pressures near 760 torr⁸).

After the aging period, the reactor was immersed up to the stopcock "arms" in a dry ice - acetone bath. A white vapor or "smoke" was observed on the surface of the catalyst solution, presumably due to the condensation of toluene vapor during cooling. The reactor was then connected to the vacuum line (balljoint #1) via a 12 - 18 cm length of flexible stainless-steel tubing equipped with Swagelok fittings, having a ball and socket joint on either end. The ball and socket each were tapered with 1/4" O.D. glass tubing for connection to the fittings. The metal tubing was pumped out, and then stopcock C was opened to pump away argon and gaseous catalyst reaction products. The reactor was shaken gently to promote degassing of the catalyst solution (as evidenced by bubbling of the solution) and pumping was continued until essentially no bubbling was observed (ca. 30 - 90 minutes). A Tesla coil was played

over the vacuum line past the liquid nitrogen trap to verify the absence of non-condensable gases. Stopcock C was then closed. It is worthwhile to note that the catalyst solution became progressively more viscous during the degassing process.

The polymerization reaction. After evacuating the entire sub-manifold of the vacuum line including the manometer, the sub-manifold was isolated from the main manifold and the acetylene bulb was opened. The reactor was removed from the dry ice - acetone bath and shaken in order to wet the walls with the catalyst solution. The reactor was then immediately placed back into the -78°C bath and stopcock C was opened, allowing acetylene to enter. All surfaces wet with the catalyst solution and which were below the -78°C bath level immediately became bright red due to the formation of cis $(\text{CH})_x$. The red film on the reactor walls developed a coppery luster within a few minutes. A more silvery film (higher in trans isomer content) was observed on surfaces above the level of the bath. The film thickness was very dependent upon the interval of time between wetting the reactor walls with catalyst and introduction of the acetylene. For thin (ca. 30 - 50 μm) films suitable for infrared spectroscopy, at least 30 seconds should elapse before introducing the acetylene. Typical reaction times were 10 - 30 minutes, with uptake of acetylene in the range 100 - 200 torr. After the desired time period, stopcock C was closed and the remaining acetylene in the sub-manifold was condensed back into the bulb at -196°C .

The apparatus (at -78°C) was disconnected from the manifold and argon was introduced, after which the top was removed at o-ring F. The

argon flow removed the remaining acetylene in the reactor. A 50 mL syringe with a long needle was used to punch several holes in the $(\text{CH})_x$ film which had grown on the surface of the catalyst solution at the bottom of the reactor. The catalyst solution under this film was then drawn into the syringe and discarded. The top was replaced and all stopcocks were closed.

Washing of *cis* $(\text{CH})_x$ film. The apparatus (with the reactor at -78°C) was attached to the vacuum line and evacuated (stopcocks C and D open) to remove all argon and residual acetylene. Next, 30 - 50 mL pentane (kept in vacuo over CaH_2 in a solvent storage tube) was distilled into the reactor. A small frit filter equipped with ball and socket joints was placed between the pentane tube and manifold to prevent bumping of the CaH_2 into the manifold. The pentane was stirred with a magnetic bar to facilitate transfer. After the distillation, stopcock C was closed and the apparatus was disconnected from the manifold.

The reactor was then removed from the -78°C bath and the washing arm was placed in the bath for several seconds. With stopcock D open, the apparatus was turned upside down several times allowing the brown pentane/catalyst solution to flow into the washing arm. Stopcock D was then closed and the reactor was placed back in the cold bath. The solution in the side arm was then stirred with a magnetic bar and stopcock D was opened slowly, allowing fresh pentane to distill back into the reactor. The distillation rate was controlled by the stirring rate and the size of the opening at stopcock D. This washing procedure was repeated until the pentane in the reactor was colorless (ca. 8 - 12 cycles).

If the glass surfaces were clean, much of the film separated from the reactor walls during washing. After every five or so cycles, the reactor was connected to the vacuum line and pumped briefly. A Tesla coil was used to check for the presence of non-condensables in the region of the vacuum line past the liquid nitrogen trap. It was important that air (red glow discharge from the Tesla coil) was not present in the system. On occasion, residual argon (blue glow discharge) was observed. It should be noted that the washing arm was equipped with a stopcock (E). In the event of a leak in this portion of the apparatus, which would most likely be at o-ring G, the washing arm could be disconnected and the o-ring replaced, followed by connection of a clean washing arm. The arm could then be pumped out via stopcock E, followed by distillation of fresh pentane from the storage tube. However, this process was seldom necessary.

Once the pentane in the reactor was colorless, it was poured into the washing arm and stopcock D was closed.

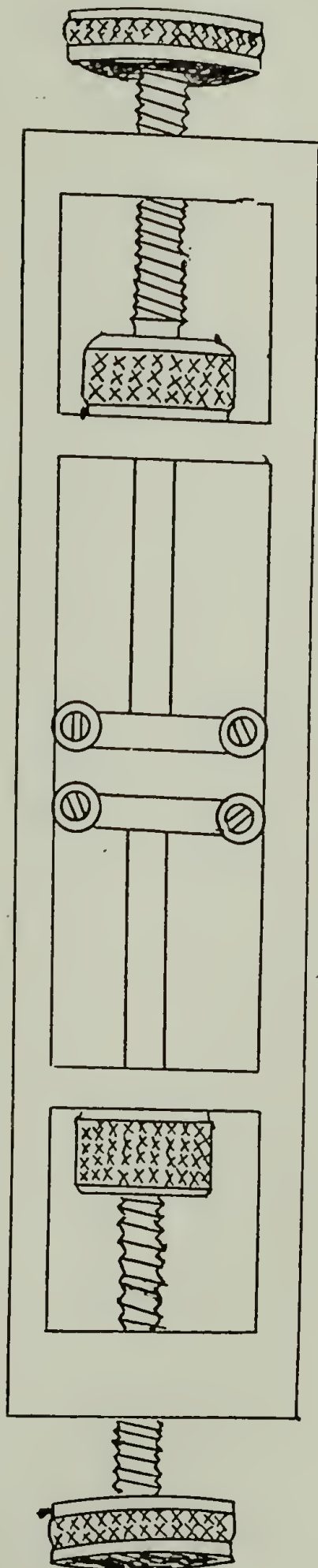
Transfer and storage of *cis* (CH)_x film. The reactor was removed from the -78° C bath and allowed to warm to room temperature. The washing arm was disconnected and the catalyst solution was decomposed by pouring it into a large quantity of methanol. All moisture was wiped from the outside of the reactor, and it was then placed in a glove bag or drybox along with scissors, a long spatula and forceps, and a long Schlenk tube (with 29/42 ground glass joints) which has been previously evacuated.

In the glove bag or drybox, the large o-ring (H) of the reactor

was disconnected and a long spatula was gently played along the reactor wall to free the cis $(CH)_x$ film. Forceps were used to pull the film (in one piece) from the reactor. The side of the film which grew on the surface of the reactor wall displayed a coppery luster, while the backside was dull maroon. The bottom of the film (shiny green) which grew on the surface of the catalyst reservoir was cut away with scissors, along with any silvery film which was formed above the level of the dry ice - acetone bath. The remaining cis $(CH)_x$ film was cut into small pieces (ca. 3 cm x 1 cm) and placed in the long Schlenk tube. At this time, samples were cut for microanalysis, doping, etc. The Schlenk tube was capped in the glove bag or drybox and then stored in a Dewar at -78°C to preserve the cis-isomer content of the film. Subsequent removal of film for any reason was performed in the glove bag or drybox. (Note: It is advisable, especially when a glove bag is used, to pump the Schlenk tube on a vacuum line in order to remove any traces of air before placing it in the storage Dewar.)

Orientation; quality of cis $(CH)_x$ films. Cis $(CH)_x$ films have been noted to be quite flexible^{8,9} if prepared properly. Thus, a piece of freshly prepared film was stretched in the apparatus shown in Figure 14. Extension ratios (l/l_0 , where l is the length after stretching and l_0 is the initial length of the film) approached 3.0 for the best films, but more typical values were in the range 2.0 - 2.6. Extension ratios much below this suggested that the film may have isomerized during handling, although a more likely possibility is that oxygen was present during some stage of the preparation. In all cases, samples were analyzed

Figure 14. Apparatus for orientation
of cis (CH)_x films.



for C H content. Total C H should be $> 98\%$ for high quality films, and the C H ratio should correspond exactly to the formula $(CH)_x$.

Isomerization. Films of cis $(CH)_x$ were easily isomerized to the trans form as follows. A quantity of cis $(CH)_x$ was placed (in a glove bag or drybox) into a tube equipped with an o-ring joint, and the tube was capped with a top having an o-ring joint, stopcock and balljoint. The tube was pumped on the vacuum line, and an oil bath ($180 - 200^\circ C$) was placed around the tube for a period of 1 - 2 hours while pumping. Within a few minutes, the shiny side of the film became silvery, while the dull side became gray-black. Trans $(CH)_x$ is brittle as compared to cis $(CH)_x$. An infrared spectrum of cis $(CH)_x$ (ca. 85% cis content) is shown in Figure 15.

Cleaning the reactor. A clean reactor was essential for the synthesis of cis $(CH)_x$ films. Thus, immediately after removing a freshly prepared film from the reactor, it was cleaned by soaking overnight with aqua regia ($1:3 HNO_3/HCl$) or $1:1 HNO_3/H_2SO_4$ followed by several rinses with distilled H_2O , 1% aqueous HF, and more distilled H_2O). It is recommended that basic solutions (e.g., KOH/ethanol) not be used, since such solutions may etch the surfaces of the reactor.

Figure 15. Infrared spectrum of cis (CH)_x.



References

1. G. Natta, G. Mazzanti and P. Corradini, Atti. Acad. Nazl. Lincei Rend. Classe Sic. Fis. Mat. Nat., 25, 3 (1958)
2. H. Shirakawa and S. Ikeda, Polym. J., 2, 231 (1971)
3. H. Shirakawa, T. Ito and S. Ikeda, Polym. J., 4, 460 (1973)
4. T. Ito, H. Shirakawa and S. Ikeda, J. Polym. Sci., Polym. Chem. Ed., 12, 11 (1974)
5. T. Ito, H. Shirakawa and S. Ikeda, J. Polym. Sci., Polym. Chem. Ed., 13, 1943 (1975)
6. M. A. Druy, A. G. MacDiarmid and A. J. Heeger, personal communications (1978, 1979)
7. Cf. C. K. Chiang, M. A. Druy, S. C. Gau, A. J. Heeger, E. J. Louis, A. G. MacDiarmid and Y. W. Park, J. Amer. Chem. Soc., 100, 1013 (1978)
8. M. A. Druy, C. H. Tsang, N. Brown, A. J. Heeger and A. G. MacDiarmid, J. Polym. Sci., Polym. Phys. Ed., 18, 429 (1980)
9. H. Shirakawa and S. Ikeda, unpublished results.

CHAPTER V

NASCENT MORPHOLOGY OF POLYACETYLENE

The high conductivity obtained upon doping¹⁻⁴ of polyacetylene, $(CH)_x$, has truly generated interest in several fundamental aspects of the parent material. Of particular importance in any polymeric material, and especially in the case of $(CH)_x$ where surface properties are anticipated to have a great deal of influence on polymer-dopant interactions, is the morphology. Although electron microscopy studies have revealed fibrous structures in unoriented⁵ and partially oriented (stretch-elongated)⁶ polyacetylene films, it has been suggested that the observed morphology might be misleading, possibly resulting from post-polymerization handling of the film or perhaps an artifact as the result of ultra-sonication. In view of these discrepancies, a short study was undertaken to examine the true nascent morphology of $(CH)_x$ through the polymerization of acetylene directly onto thin electron microscope grids. In addition, the surface area of conventional $(CH)_x$ films was determined from B.E.T. measurements. An account of this work has been reported elsewhere.⁷

Experimental

A Schlenk tube was used as the reaction vessel for the polymerization of acetylene onto thin electron microscope (EM) grids (3 mm disks of 300-mesh gold screen). The Schlenk tube top possessed a ca. 3 mm diameter glass rod of sufficient length so that the end of the rod was

ca. 3 cm from the bottom of the tube when the tube and top were joined. The glass rod possessed several small glass "ears" in order to support the grids. Several grids were soldered with small amounts of indium to a length of platinum wire and the wire was looped around the "ears" on the glass rod. The grids and platinum wire were rinsed several times with acetone and dried under a stream of argon immediately before use.

The catalyst was prepared directly in the reaction vessel. Ca. 10 mL of dry toluene was added from the solvent still followed by the addition of 1.0 mL $\text{Ti}(\text{OBu})_4$ and 1.4 mL Et_3Al using syringes. All transfers were carried out under argon. The catalyst solution was aged for ca. 30 minutes at room temperature prior to polymerization reactions. A 200 mL gas storage bulb was filled to a pressure of ca. 700 torr (Chapter II).

The reaction vessel was connected to a vacuum line via a ca. 12 cm length of flexible stainless steel tubing equipped with ball and socket joints. The solution was cooled to -78°C (dry ice-acetone bath) and pumped at least 20 minutes with occasional shaking to accomplish degassing. The solution (-78°C) was then shaken vigorously in order to coat the grids. Initial pressures of acetylene ranging from ca. 10 to ca. 700 torr were then admitted into the reaction vessel. The reaction was terminated at a desired time period (usually < 1 minute) by evacuating the vessel. The grids were washed of excess catalyst by dipping them into a beaker of dry pentane under a stream of argon. The grids were finally dried under the argon flow.

A film of cis polyacetylene was prepared using techniques

described in the previous chapter. The film thickness was ca. 120 μm .

Electron micrographs were obtained using a JEOL 100 cx Temscan electron microscope. The three modes of observation were transmission (TEM), scanning (SEM) and scanning transmission (STEM). The polymerized film was observed by the first mode; gold coated films were examined with the remaining modes. Gold coatings were applied either by sputtering or evaporation with thicknesses carefully controlled and kept in the 3-7 nm range. All micrographs were obtained by Dr. R. Galkiewicz.

The surface area of as-grown $(\text{CH})_x$ film was obtained from single-point Brunauer-Emmett-Teller (B.E.T.) measurements using nitrogen gas, using identical techniques and apparatus as described in Reference 8. A sample of Kaiser Al_2O_3 (surface area $\approx 380 \text{ m}^2/\text{g}$) was used as a check for sensitivity. The experiment yielded a surface area of ca. 290-300 m^2/g , i.e., ca. 20% lower than anticipated, although it was an acceptable result.

Results

Figure 16a is a STEM image of a thin $(\text{CH})_x$ film (55 torr C_2H_2 for ≈ 30 seconds) on a gold grid at low magnification (10^4). The fibrous, web-like structure of the specimen is clearly visible. Figures 16b and 16c are STEM images of the same portion of the sample in which voids appear black (and white), respectively, demonstrating that the film is only a few fibrils in thickness. At 10^5 magnification (Figure 16d) individual fibrils are clearly discernable. Fibril diameters ranged

Figure 16. Electron micrographs of thin
(CH)_x films on gold grids.

55 torr acetylene for 30 seconds

a) x10,000 in STEM mode; b) Same sample as in (a) at
x50,000 SEM; c) Same as for (b) but in STEM mode; d) Same
sample as in (a) showing 100,000 STEM

700 torr acetylene for 1 minute

e) x1,500; f) x15,000; g) x100,000

Scale bars: a, 1 μm; b,c, 0.2 μm; d, 0.1 μm; e, 10 μm;
f, 1 μm; g, 0.1 μm

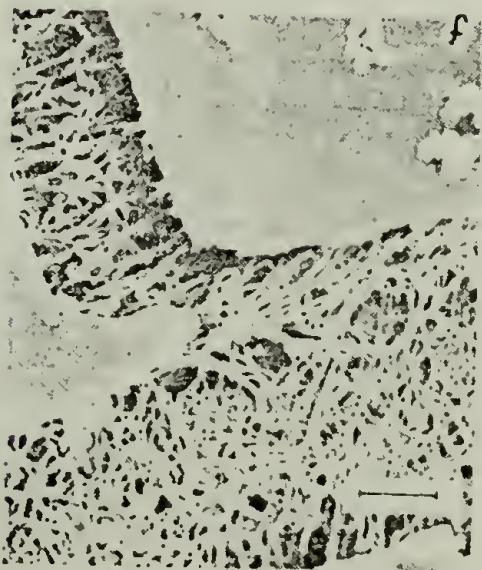
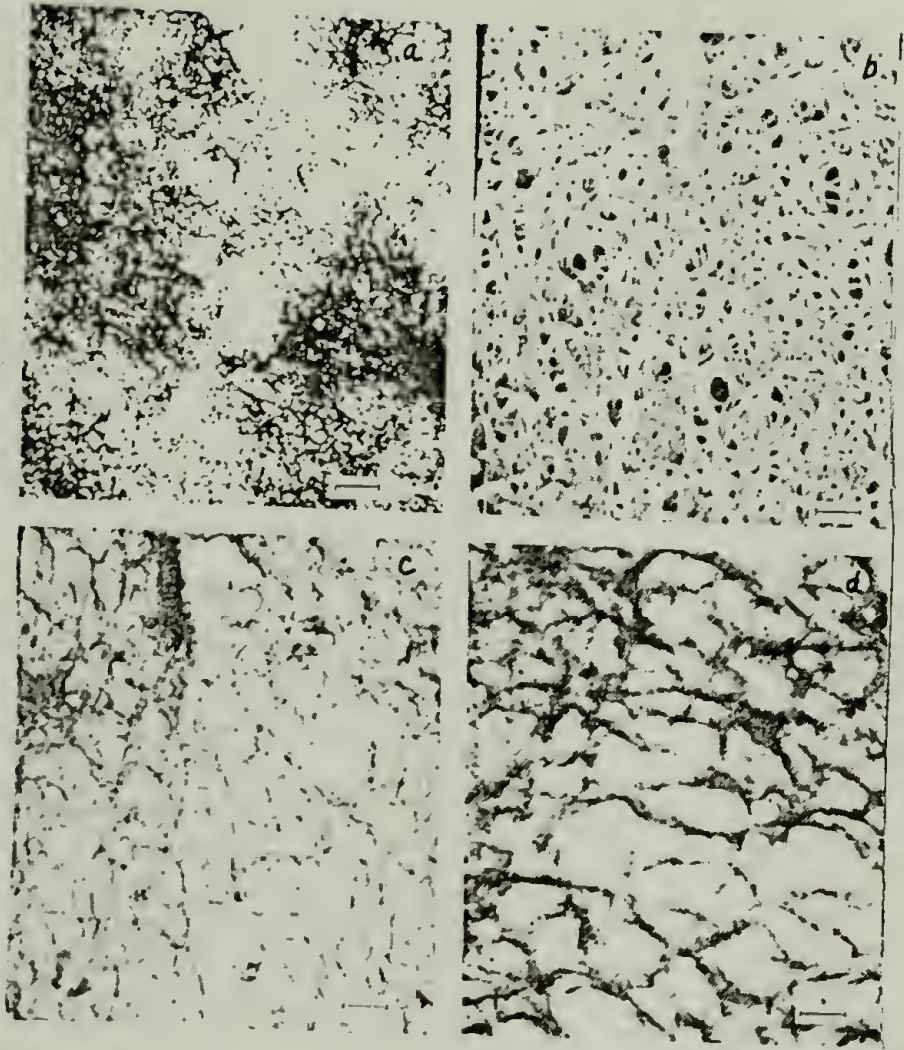


Figure 17. SEM micrographs of $(\text{CH})_x$ film.

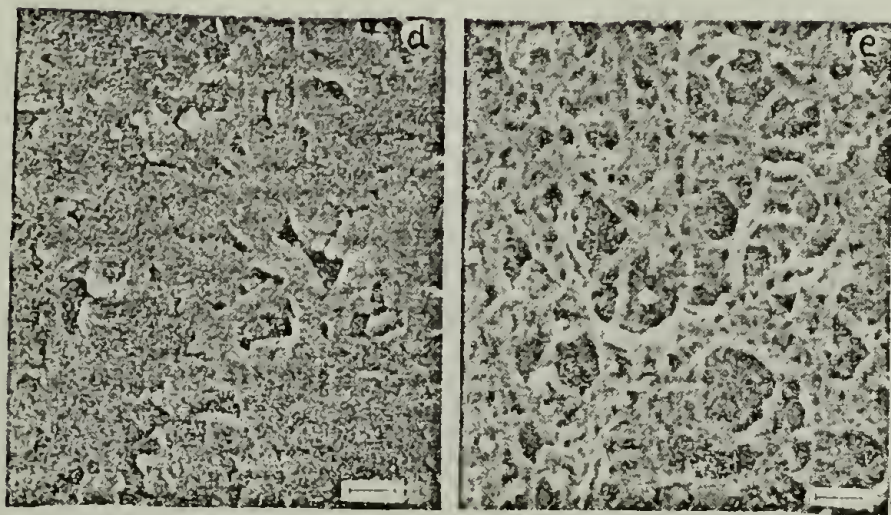
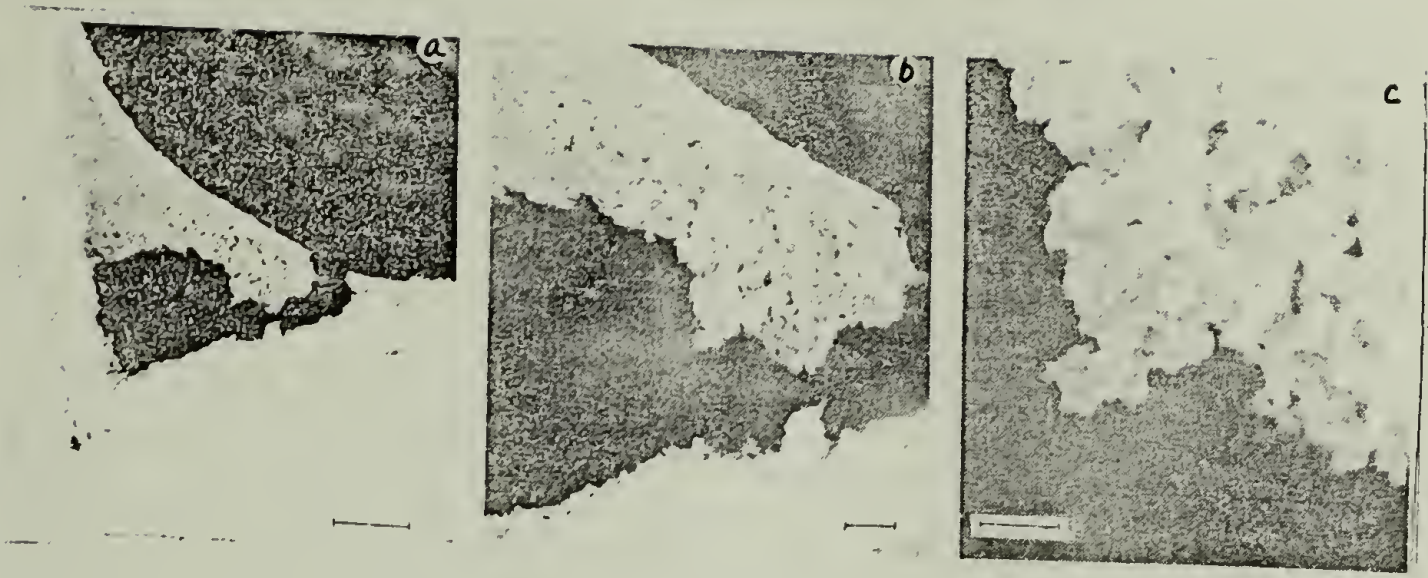
Film at a grid edge

a) x3,000; b) x8,000; c) x30,000.

As-grown film

d) x50,000 (shiny side); e) x50,000 (dull side)

Scale bars: a, 5 μm ; b, 1.25 μm ; c, 0.5 μm .



from ca. 5 to 40 nm with 20 nm fibrils being the most abundant.

Polymerizations at higher acetylene pressures (ca. 700 torr for \approx 1 minute) yielded very smooth $(CH)_x$ film on grids. These films possessed surface cracks and fractures (Figure 16e) in which were observed partially aligned fibrils (Figure 16f). Interestingly, occasional regions were found to possess highly-oriented 10 nm diameter fibrils (Figure 16g).

The surface of the smooth film (Figure 16f) was observed to possess occasional globular structures. These were more prominent in areas where a portion of the $(CH)_x$ film apparently separated from the grid edge (Figures 17a-c).

The fibrous morphology described above was also observed with typical as-grown $(CH)_x$ films. Such films display a shiny, metallic-like surface which grew on the glass reactor wall (Figure 17d) and a more dull surface on the opposite side (Figure 17e). The morphology of the latter surface is identical to that shown in Figures 16a-d. This morphology is apparently preserved on the shiny side although the fibrils appear to be flattened or merged into larger entities.

The results of the surface area measurements concerning the as-grown $(CH)_x$ film are given in Table 2.

The theoretical surface area of $(CH)_x$ film, assuming the fibril diameter (d) to be 200 Å, was determined as follows. First, we take the length (l) of the fibrils to be, say, 2000 Å. This choice is completely arbitrary and any other value will lead to the same final result. The surface area (S_A) of one such fibril is given by

TABLE 2
SURFACE AREAS OF $(\text{CH})_x$ FILM
FROM B.E.T. MEASUREMENTS

$(\text{CH})_x$ Sample	Surface Area, m^2/g
1	55.6
2	70.6
3	72.5
Average = 66.0	

$$S_A = \pi d l$$

Hence, $S_A = \pi(2 \times 10^{-8} \text{ m})(2 \times 10^{-7} \text{ m}) = 1.25 \times 10^{-14} \text{ m}^2$. The volume of the fibril is simply $\pi r^2 l$ or $\pi(1 \times 10^{-8} \text{ m})^2(2 \times 10^{-7} \text{ m}) = 6.3 \times 10^{-23} \text{ m}^3$. The amount of $(\text{CH})_x$ in such a fibril, taking the density (floatation)⁹ to be 1.2 g cm^3 , is

$$\begin{aligned} \text{Amount } (\text{CH})_x &= 1.2 \text{ g/cm}^3 \times 10^6 \text{ cm}^3/\text{m}^3 \times 6.3 \times 10^{-23} \text{ m}^3 \\ &= 7.6 \times 10^{-17} \text{ g/fibril.} \end{aligned}$$

The surface area in m^2/g is

$$\frac{1.25 \times 10^{-14} \text{ m}^2}{7.6 \times 10^{-17} \text{ g}} = 165 \text{ m}^2/\text{g}$$

However, the bulk density of $(\text{CH})_x$ is only 0.4 g/cc , indicating that the fibrils fill only about one-third of the total volume of the sample. The surface area then is

$$165 \text{ m}^2/\text{g} \times \frac{0.4 \text{ g/cm}^3}{1.2 \text{ g/cm}^3} \approx 55 \text{ m}^2/\text{g}$$

This value is in very good agreement with the average obtained ($\approx 66 \text{ m}^2/\text{g}$) experimentally, considering the crudeness of the calculation.

Discussion

The fractures observed in smooth films polymerized on grids at high acetylene pressures (Figures 16e-g) are most likely formed during the washing procedure and are due either to the displacement of one diluent (toluene) with another (pentane) or to the potential thermal contraction occurring upon warming the sample from -78°C to room temperature. The globular structures shown in Figures 17a-c combined with the

apparent separation of the material from the grid might suggest melting contraction due to the exothermic polymerization reaction. A more likely possibility is that the globular structures are catalyst residues which became insoluble due to partial oxidation before completely washing unreacted catalyst from the samples.

The fibrillar morphology of the ultra-thin samples is preserved in the as-grown films (Figures 17d,e). The shiny side of the film displays apparent fibrils which have been flattened or merged into larger entities. Similar results have been observed from the surfaces of pressed film $(CH)_x$ derived from gels (Chapter VIII) suggesting that the fibrils, at least initially in the presence of solvent, are somewhat "ductile" and can be flattened by application of mechanical pressure. The potential pressure at the surface of a $(CH)_x$ film due to rapid growth at the glass reactor wall reasonably accounts for the observed "shiny side" morphology.

Fibrillar morphologies have been previously observed in materials such as polyethylene¹⁰ and polypropylene¹¹ when selected heterogeneous catalysts were employed in their syntheses. The $Ti(OBu)_4/Et_3Al$ system used in this work, on the other hand, is a well-known homogeneous (soluble) Ziegler-Natta catalyst. Although it might be possible for this system to be somewhat heterogeneous at the concentrations employed in $(CH)_x$ film syntheses, characteristic fibrillar morphologies were also observed using significantly lower catalyst concentrations (see Chapter VIII). Thus, at least for the $Ti(OBu)_4/Et_3Al$ catalyst system, it appears that acetylene polymerizes directly into fibrils, possibly

due to the rigidity of the resulting conjugated polymer backbone.

Conclusions

The nascent morphology of $(\text{CH})_x$ has been shown to be fibrillar with small variations in local morphologies (globular, smooth surfaces) depending upon the details of the polymerization reaction. Surface area measurements are consistent with the fibrillar morphology.

References

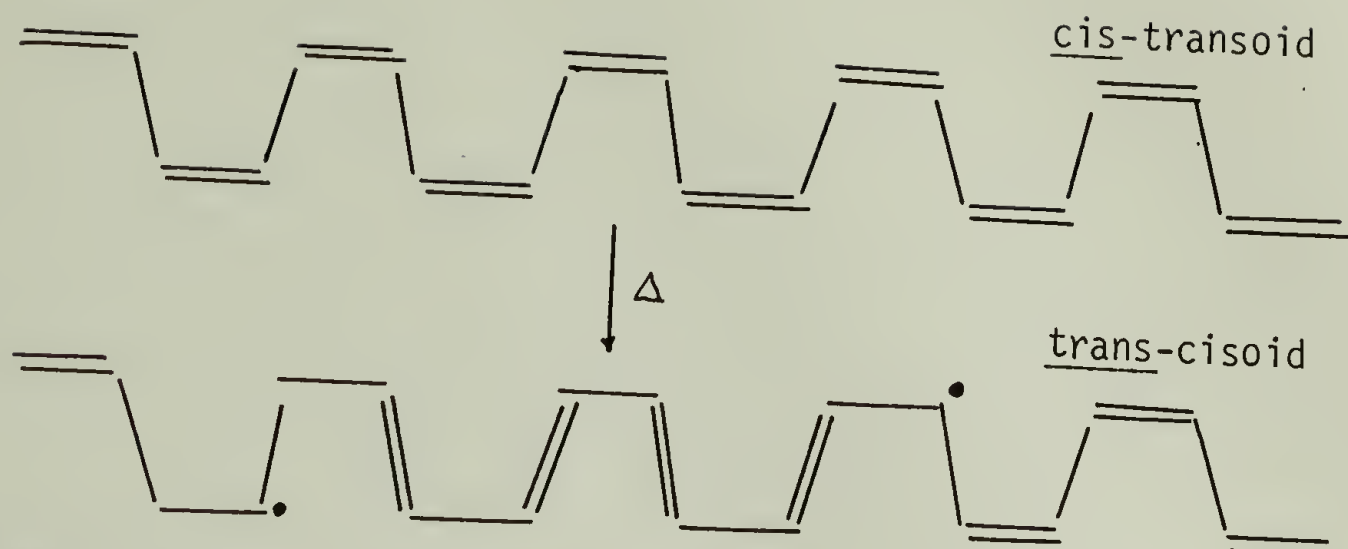
1. H. Shirakawa, E.J. Louis, A.G. MacDiarmid, C.K. Chiang and A.J. Heeger, J. Chem. Soc. Chem. Comm., 578 (1977).
2. C.K. Chiang, C.R. Fincher, Jr., Y.W. Park, A.J. Heeger, H. Shirakawa, E.J. Louis, S.C. Gau and A.G. MacDiarmid, Phys. Rev. Lett., 39, 1098 (1977).
3. C.K. Chiang, M.A. Druy, S.C. Gau, A.J. Heeger, E.J. Louis, A.G. MacDiarmid and Y.W. Park, J. Amer. Chem. Soc., 100, 1013 (1978).
4. C.K. Chiang, S.C. Gau, C.R. Fincher, Jr., Y.W. Park, A.G. MacDiarmid and A.J. Heeger, Appl. Phys. Lett., 33, 18 (1978).
5. T. Ito, H. Shirakawa and S. Ikeda, J. Polym. Sci. Polym. Lett. Ed., 12, 11 (1974).
6. M.A. Druy, C.H. Tsang, N. Brown, A.J. Heeger and A.G. MacDiarmid, J. Polym. Sci. Polym. Phys. Ed., 18, 429 (1980).
7. F.E. Karasz, J.C.W. Chien, R. Galkiewicz, G.E. Wnek, A.J. Heeger and A.G. MacDiarmid, Nature, 282, 286 (1979).
8. Z.K. Jelinek, Particle Size Determination, Halsted Press, New York, p. 140 (1974).
9. T. Ito, H. Shirakawa and S. Ikeda, Kobunshi Ronbunshu, Eng. Ed., 5, 470 (1976).
10. P. Ingram and A. Schindler, Makromol. Chem., 111, 267 (1968).
11. J.Y. Guttman and J.E. Guillet, Polym. Preprints, 30, 177 (1970).

CHAPTER VI

ELECTRON PARAMAGNETIC RESONANCE STUDY OF ACETYLENE POLYMERIZATION

Recent demonstration¹⁻³ of high electrical conductivity upon doping of polyacetylene, $(CH)_x$, has generated fundamental interest concerning the properties and electronic structure of this material. A thorough understanding of the pristine polymer is necessary before a rational approach can be made toward an interpretation of the conduction mechanism in doped derivatives. A few of the many basic aspects of polyacetylene chemistry which need to be understood, namely, the source of the inherent paramagnetism, the influence of oxygen on the paramagnetism, and the mechanism of polymerization, are addressed in this Chapter.

The paramagnetism of undoped $(CH)_x$ has been recognized for several years⁴ although it has only recently become a property studied in detail.⁵⁻⁸ Polyacetylene typically displays an electron paramagnetic resonance (EPR) signal having a Lorentzian line shape and a g value (ca. 2.0024) close to that of the free electron (ca. 2.003). The g value precisely identifies⁶ the unpaired spins as being due to π -electron radicals. Shirakawa et al.⁵ observed a ten-fold increase in spin concentration upon thermal cis-trans isomerization, suggesting that spin generation and isomerization are intimately related. A reasonable mechanistic interpretation⁹ involves random, non-concerted bond rearrangements, viz.,



The unpaired spin is rigorously defined as a spatially extended, neutral magnetic defect⁸ and is referred to as a soliton.^{10,11} The term "defect" is very appropriate since the spins are "mistakes" which result from the random bond rearrangements. The cis-trans isomerization process is irreversible. The greater thermodynamic stability of the trans isomer is attributable to a reduction of steric interactions between neighboring hydrogen atoms on the polymer backbone.

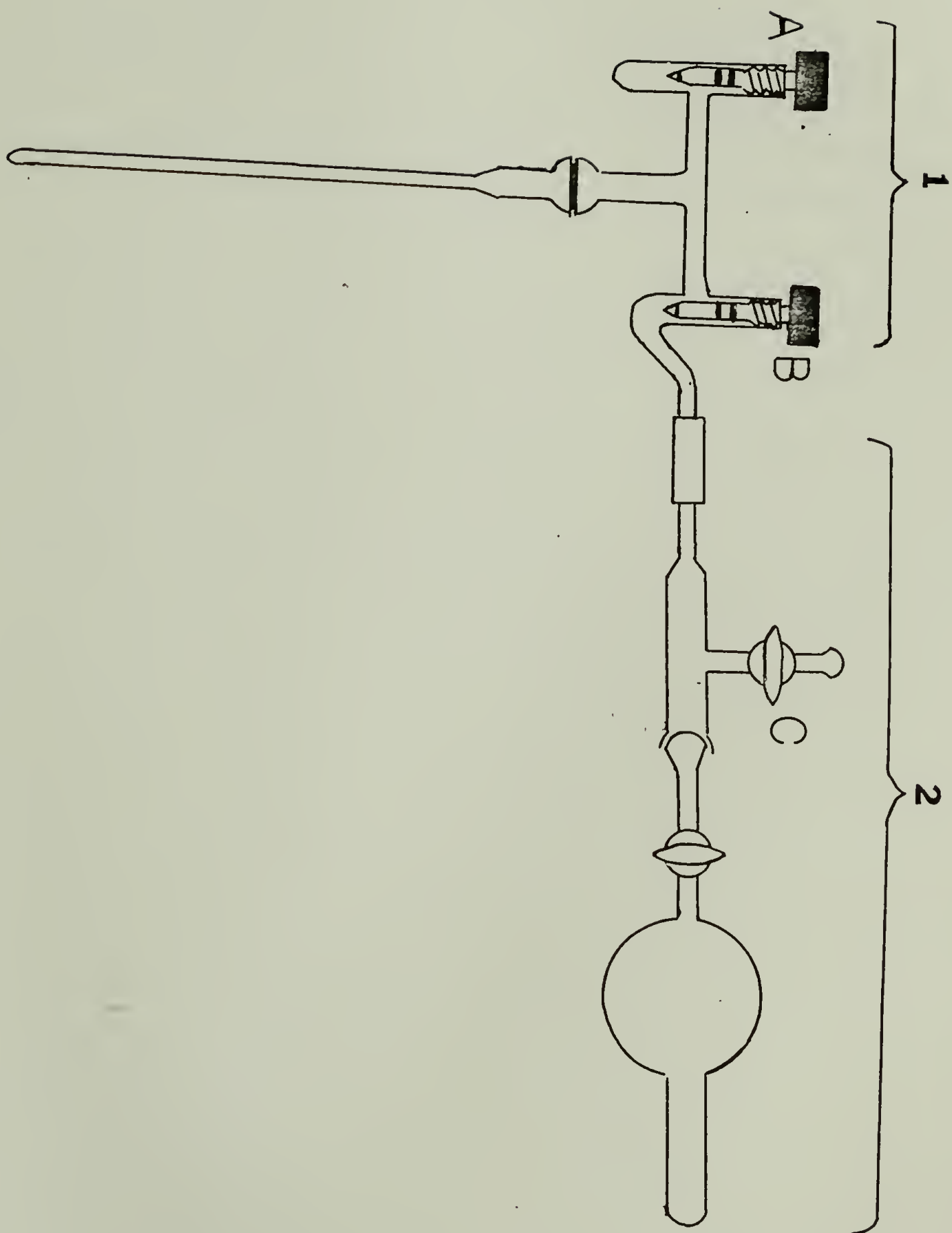
Although the mechanism depicted above assumes that spin formation is exclusively the result of thermally-induced isomerization, it was of interest to investigate the potential contributions of the polymerization in either directly creating unpaired spins or inducing the isomerization process. A technique was developed for the polymerization of acetylene directly in an EPR sample tube at low temperatures in order to monitor spin formation during polymerization. This technique, by virtue of the paramagnetic nature of the Ziegler-Natta catalyst, also afforded simultaneous study of the polymerization reaction itself. An account of this work has been published elsewhere.¹² Similar studies have been recently reported by Snow et al.⁷ and Bernier et al.¹³

Experimental

The parent catalyst was prepared in a Schlenk tube by adding 1.7 mL $\text{Ti}(\text{OBu})_4$ and 2.7 mL Et_3Al to dry toluene (from the solvent still) under argon at room temperature. The solution was aged for ca. 30 minutes at room temperature. The catalyst used in the EPR experiments was obtained by syringing 1 mL of this catalyst (under argon) into another Schlenk tube containing ca. 30 mL dry toluene. This dilution was carried out in order to insure slower polymerization of acetylene and to reduce the possibility of signal broadening due to the paramagnetic catalyst species. It should be noted that this catalyst concentration is essentially the same as that used to prepare polyacetylene gels (Chapter VIII).

The apparatus employed for the in-situ polymerization of acetylene is shown in Figure 18. The apparatus was initially connected to a vacuum line for pumping and flame-drying of the EPR sample tube and catalyst reservoir via the free balljoint. The bulb containing ca. 700 torr of acetylene was not connected during this process; the socket joint for attachment to the bulb was capped with a closed-end balljoint. After pumping, stopcocks A and B were closed and section 2 along with the butyle rubber tubing was disconnected from section 1. A pipette tip was used to purge the glass tubing leading to stopcock B with argon and then the end of the tube was quickly capped with the tubing from the argon line. With stopcock B open, the Teflon plug of stopcock A was removed and, while argon was flowing through the apparatus and the Schlenk tube containing the catalyst, ca. 0.5 mL of the catalyst was transferred

Figure 18. Apparatus for in-situ polymerization of acetylene in an EPR sample tube.



via a syringe into the reservoir at the bottom of stopcock A. The plug was replaced and stopcock B was closed.

The vessel was tipped to allow enough catalyst solution to fill the EPR tube to a depth of ca. 2 cm and stopcock A was closed. The various components of the apparatus were then assembled (Figure 18) followed by attachment to a vacuum line. The catalyst solution in the EPR tube was cooled to -78°C and the apparatus (stopcocks B and C open) was pumped for ca. 15 minutes. The apparatus was occasionally agitated to promote degassing of the solution. Stopcocks B and C were closed and the EPR tube was then allowed to warm to room temperature.

A Varian E-9 X-band spectrometer equipped with a dual microwave cavity and a variable-temperature probe was used to obtain the EPR spectra. For in-situ polymerizations, the probe was pre-cooled to ca. -70°C by circulation of prepurified nitrogen through a metal coil immersed in liquid nitrogen. Additional nitrogen gas (room temperature) was circulated through the microwave cavity to prevent the accumulation of moisture. The EPR sample tube was then inserted into the probe; the acetylene bulb and section 2 were maintained in a horizontal position by clamping the cold finger of the bulb to a tall ring stand. After allowing ca. 10 minutes for the catalyst solution to reach thermal equilibrium with the probe, a spectrum was recorded. The stopcock of the acetylene bulb was opened and the polymerization was monitored by EPR. A sample of diphenyl picryl hydrazyl (DPPH) was maintained in the remaining cavity and was used as a reference signal for the determination of g values.

The g values were calculated according to

$$g_s = \frac{g_D H_D}{H_s}$$

where g_s and H_s are the g value and magnetic field strength at resonance (determined at the center of the derivative EPR signal) for the particular signal; g_D and H_D are similarly defined for the DPPH reference signal.

Results

Figure 19a shows a typical EPR spectrum of the catalyst solution at ca. -70°C . The resonances are due to Ti^{3+} species obtained from the reduction of $\text{Ti}(\text{OBu})_4$ by Et_3Al . Four resonances with g values of 1.981 (1), 1.976 (2), 1.965 (3) and 1.945 (4) and respective linewidths of 5.0 ± 0.5 , 5.0 ± 0.5 , 20 ± 2 and ca. 57 ± 5 G were observed. The linewidth of resonance 4 is only an estimated value since the line was never completely resolved. Even though five catalyst samples were identically prepared according to techniques described in the experimental section, there were significant variations in the relative intensities of the four resonances (Table 3). It has been well documented¹⁴⁻¹⁶ that the EPR signals of the $\text{Ti}(\text{OBu})_4/\text{Et}_3\text{Al}$ system are very sensitive to Al/Ti ratios, temperature and length of aging. In fact, up to eleven different Ti^{3+} resonances have been observed. It should be noted that in all five cases exposure of the catalyst solution to acetylene resulted in the formation of polymer.

Signal 1, upon warming to room temperature, displayed 21 hyperfine

TABLE 3

EPR DATA OF IN-SITU ACETYLENE POLYMERIZATION IN THE
 PRESENCE OF $\text{Ti}(\text{OBu})_4/4\text{Et}_3\text{Al}$ AT -78°C

Relative EPR Intensities Peak to Peak*				
	Species 1 ~	Species 2 ~	Species 3 ~	Species 4 ~
g value	1.981	1.976	1.965	1.945
<u>Sample A</u>				
initial	1	0.29	0.23	0.52
+ C_2H_2 (60 min)	0.65	0.06	0.06	0.52
<u>Sample B</u>				
initial	1	0.02	1.43	0.12
+ C_2H_2 (60 min)	0.35	0.02	0.15	0.49
<u>Sample C</u>				
initial	1	3.89	2.0	0.2
+ C_2H_2 (25 min)	0.62	1.38	0.89	0.24
<u>Sample D</u>				
initial	1	1.05	0	1.87
+ C_2H_2 (20 min)	0.89	shoulder	shoulder	1.87
<u>Sample F</u>				
initial	1	0	5.0	0
+ C_2H_2 (10 min)	0.71	shoulder	3.0	0

*The signal for species 1 is taken to be unity for each preparation.

Figure 19. EPR spectra of $\text{Ti}(\text{OBu})_4/4 \text{ Et}_3\text{Al}$ at -78°C .

(A) catalyst only; (B) spectrum after exposure to acetylene for 20 minutes; (C) Bringing (B) to 25°C under anaerobic conditions followed by cooling to -78°C ; (D) spectrum after addition of air to a sample previously warmed to 25°C under anaerobic conditions.

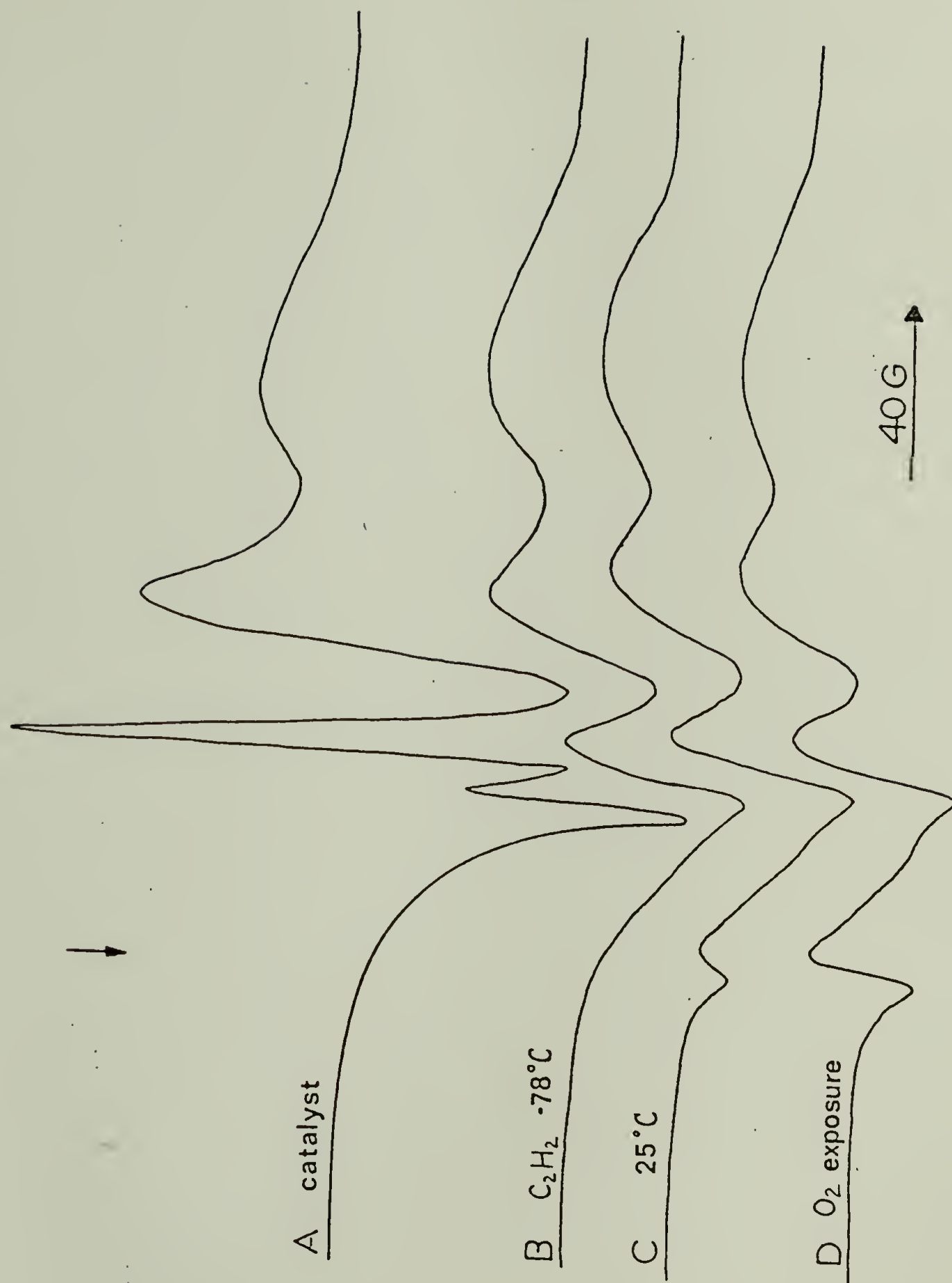
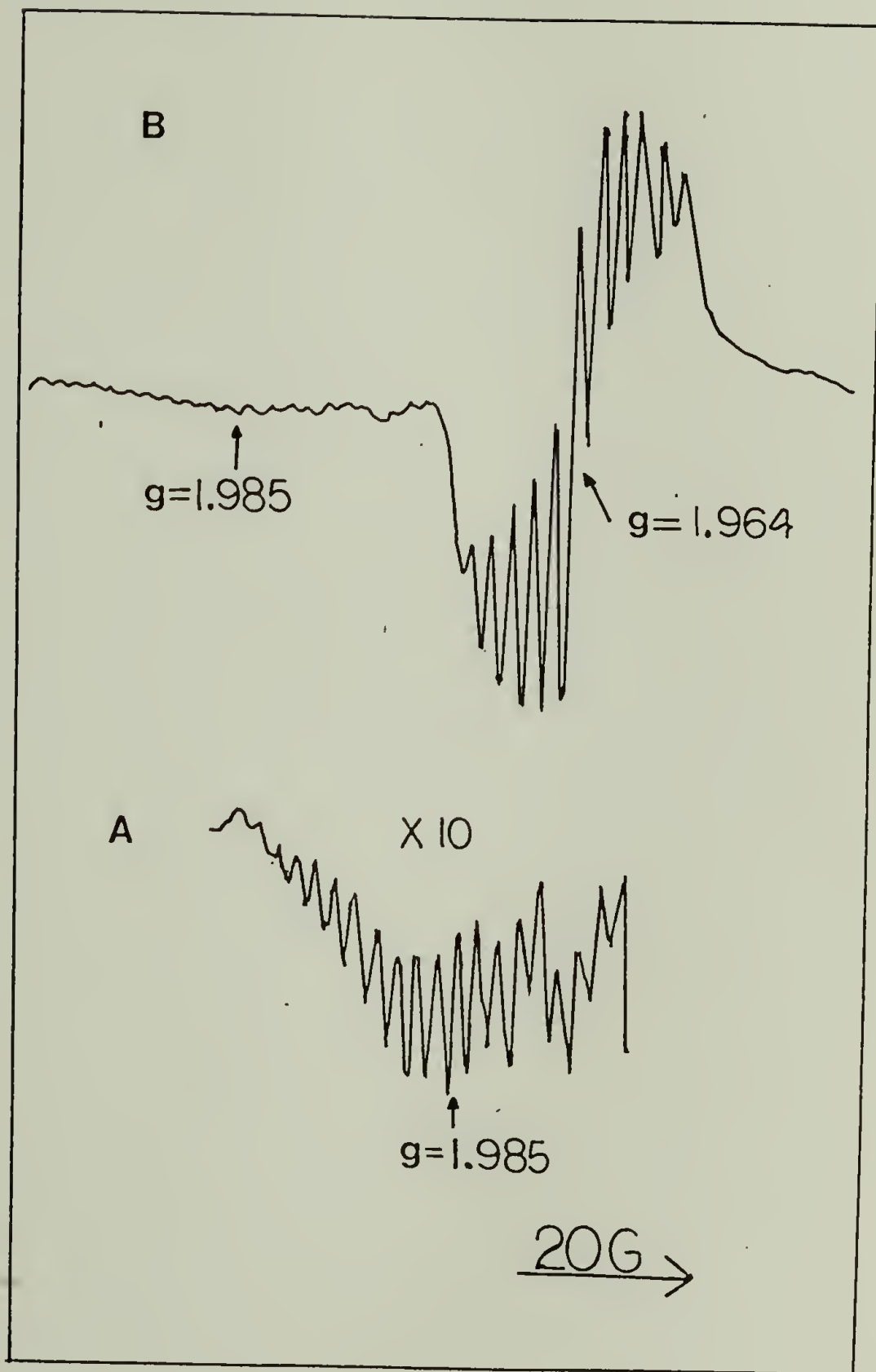


Figure 20. EPR spectra of $\text{Ti}(\text{C}_2\text{H}_5)_4/4 \text{ Et}_3\text{Al}$ in the presence of C_2H_2 at room temperature. (A) species 1 at high gain; (B) species 2 at low gain.



lines (Figure 20a) with a splitting of 2 - 4 G; no resolved hyperfine structure for signal 2 was observed. It was once considered¹⁷ that signals 1 and 2 are the result of a pair of hyperfine doublets from Ti^{3+} coupled to an $I = 1/2$ nucleus (I is the spin quantum number). However, this assignment appears to be incorrect since the resonances of species 1 and 2 seldomly appeared with equal intensities¹⁴ (Table 3). At 25° C, species 3 displayed a well resolved hyperfine structure consisting of 11 lines with a coupling constant of 2.6 G (Figure 20b). No hyperfine structures were observed from resonance 4.

Exposure of the catalyst at -70° C to acetylene (Figure 19b) resulted in a decrease of the intensity of the catalyst resonances. No signal characteristic of the $g = 2.002$ $(CH)_x$ resonance was observed. This result was initially thought to be due to insufficient formation of polymer, although upon removal of the tube from the probe, a reasonable amount of $(CH)_x$ was observed near the surface of the catalyst solution. Placement of the tube back into the probe (still at ca. - 70° C) afforded spectrum C (Figure 19). The $(CH)_x$ signal at $g = 2.002$, though weak, is clearly visible. Identical results were observed in three additional experiments. Furthermore, exposure of such a sample to air resulted in a three-to-five-fold increase in the $(CH)_x$ signal intensity (Figure 19d). This observation was also reproducible. Finally, exposure of the sample polymerized and held at ca. -70° C (Figure 19b) to air produced an observable $(CH)_x$ resonance similar to that shown in Figure 19c.

Discussion

Inherent paramagnetism of $(\text{CH})_x$. The EPR spectrum shown in Figure 19b demonstrates that pristine cis $(\text{CH})_x$ is devoid of a measurable number of free carriers even during the polymerization itself. A brief warming period at room temperature results in a visible EPR signal (Figure 19c) and demonstrates without question that free spin formation in $(\text{CH})_x$ is purely a thermal phenomenon and undoubtedly results from random bond rearrangements as described previously. Thus, paramagnetism is not an intrinsic characteristic of cis $(\text{CH})_x$. This conclusion has been recently confirmed by the similar experiments of Bernier et al.¹³

Influence of oxygen on the resonance. The large increase in free spins upon exposure of air to an in-situ polymerization mixture previously warmed to room temperature and cooled again to -70°C or the generation of spins in an in-situ polymerization mixture at -70°C previously devoid of spins upon similar exposure demonstrates the extreme sensitivity of $(\text{CH})_x$ to oxygen. It should be noted that the effect is irreversible; no decrease of the signal was observed upon evacuating the sample. In similar studies, Snow et al.⁷ also observed this irreversibility but in addition found that subsequent oxygen exposures followed by evacuation resulted in reversible broadening of the EPR line.

Two rationalizations can be offered concerning the role of oxygen in modifying the paramagnetism of $(\text{CH})_x$. First, since oxygen is a weak electron acceptor, partial doping of $(\text{CH})_x$ may result with a concomitant increase in the number of free carriers. In fact, Pochan and co-

workers¹⁸ recently found that oxygen can cause an initial increase of several orders of magnitude in the conductivity of cis and trans $(CH)_x$ films. Furthermore, this effect was partially reversible upon pumping in vacuo. This probably accounts for the observations of Snow et al.⁷ and Goldberg et al.⁶ concerning the reversible EPR line broadening upon exposure to oxygen followed by pumping. However, the initial irreversible increase in the number of spins upon oxygen exposure is perhaps best explained as the result of irreversible cis-trans isomerization. Bernier et al.,¹³ from studies of the increase of in-situ $(CH)_x$ EPR signal with time upon oxygen exposure, concluded that oxygen (initially) merely serves to catalyze isomerization. These workers also found that thermal isomerization followed by oxidation leads to the same EPR behavior (ca. 2.5 G linewidth) as pre-oxidation of cis $(CH)_x$ followed by thermal isomerization. In addition, it has been reported that the initial increase in the spin concentration of $(CH)_x$ upon exposure to oxygen results in a concomitant increase in the trans isomer content as determined by infrared spectroscopy.²² (Note added in proof: we have recently examined EPR spectra of cis $(CH)_x$ films which were carefully prepared and handled in a drybox, although these were handled at room temperature for several hours. No apparent increase in the EPR signal intensity of the films was observed on exposure to oxygen. Thus, oxygen presumably catalyzes the isomerization to a cis-trans equilibrium mixture characteristic of that mixture obtained by purely warming the sample to room temperature for a sufficient time period.)

Interpretation of the EPR resonances from the catalyst. The EPR spectra can be analyzed by¹⁹

$$\mathcal{H} = g\beta H_0 S + AS \cdot I \quad (1)$$

for a species with one paramagnetic ion and by

$$\mathcal{H} = g\beta H_0 S + A(S_1 \cdot I_1 + S_2 \cdot I_2) + JS_1 \cdot S_2$$

for a species with two paramagnetic ions, where \mathcal{H} is the Hamiltonian operator, g is the g value, β is the Bohr magneton, H_0 is the applied magnetic field, S and I are the spin and nuclear angular momentum, respectively, A is the isotropic hyperfine coupling or Fermi contact interaction and J is the fine structure splitting constant.

The structures of the species which display hyperfine splittings are considered first. Species 3 has 11 hyperfine lines (Figure 20a) and is most likely a single Ti^{3+} species coupled to two ^{27}Al nuclei ($I = 5/2$) since the number of peaks in the fine structure will be $2nI + 1$. Species 1 has 21 hyperfine lines (Figure 20b). In this case, two interpretations are possible. The first and the preferred one is that there are two Ti^{3+} species in the molecule with rapid exchange between them (i.e., $J \gg A$). In this case, there should be $4I + 1 = 4(5) + 1$ lines with intensities 1:2:3:2I:2I-1...3:2:1, in agreement with Figure 3b. The second possibility is that the catalyst species possesses one Ti^{3+} coupled to two ^{27}Al nuclei and an additional nucleus with $I = 1/2$ such as a hydride ion or the α -hydrogen atom of the propagating chain. However, the catalyst solution was found to display the 21 line spectrum of species 1 at room temperature even in the absence of acetylene. Thus, it appears that the first interpretation is the more likely one.

The interpretation of the EPR spectra can be further enhanced upon consideration of g values. For the case of a single electron in a non-degenerate d orbital, the isotropic g value (assuming rapid tumbling of the species in the solution) is given by²⁰

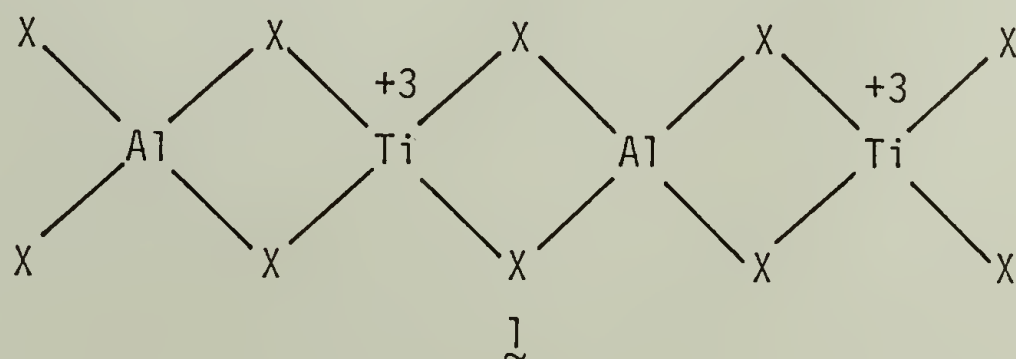
$$g = g_0 \pm \frac{n\lambda}{\Delta E}$$

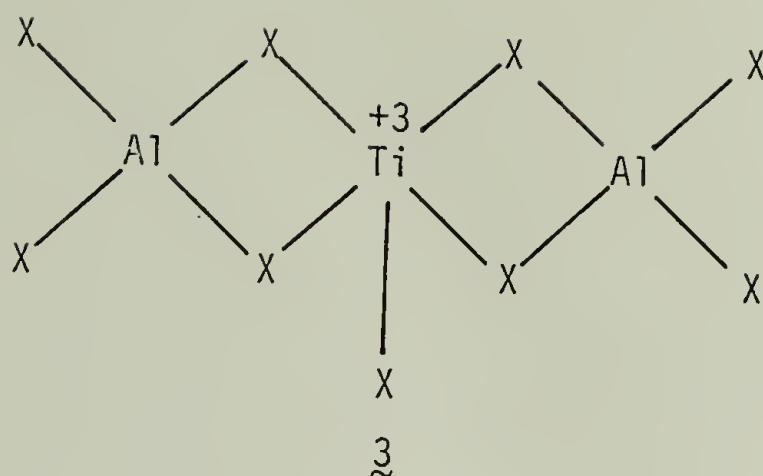
where $g_0 = 2.0023$, λ is the spin-orbit coupling constant and ΔE is the energy separation between the orbital containing the unpaired electron and the orbital with which it may mix by spin-orbit coupling. The value of the coefficient n depends upon the orbitals under consideration. In the case of Ti^{3+} (a d^1 system) this relation becomes

$$g = 2.0023 - \frac{8\lambda}{\Delta E(d_{x^2-y^2} - d_{xy})}$$

Therefore, smaller separations between the ground state and excited state (smaller ΔE) result in smaller g values. This condition corresponds to small values of the crystal field splitting energy (i.e., 10 Dq). By inference, the paramagnetic species with small g values are coordinately more saturated and should also have short spin-lattice relaxation times and broad line widths.

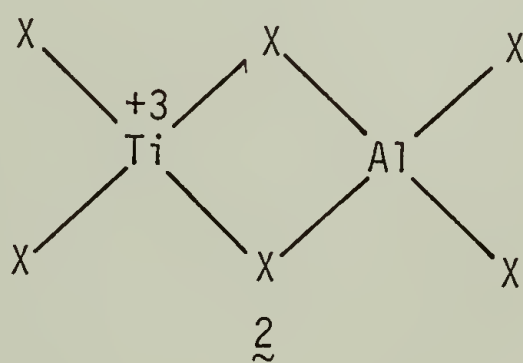
With the above considerations, the following structures are assigned to species 1 and 3:



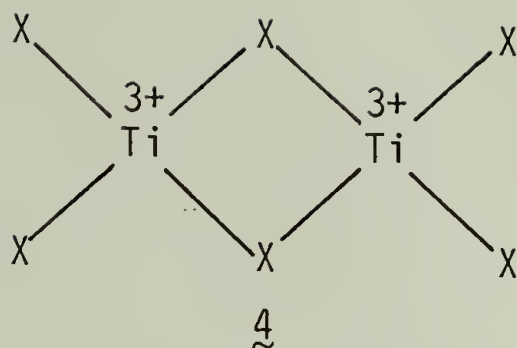


where is either OBu or Et. EPR cannot differentiate between these ligands. However, since OBu is unhindered and is a better bridging ligand than Et., the groups bridging Al and Ti are most likely to be OBu with the remainder being either OBu or Et depending on the Al/Ti ratio. The more coordinately saturated Ti^{3+} in species 3 is favored due to the relatively low g value of the signal and its rather broad line width. The structure of species 3 is analogous to that proposed by Djabien et al.²¹

The assignments of species 2 and 4 are much more speculative. Species 2 might be:



A similar structure with a g value close to that of 2 has been previously proposed.¹⁴ Species 4 has the broadest line width and may have a structure such as

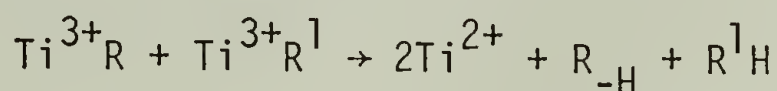


The spin-lattice relaxation time of $\tilde{4}$ is expected to be small due to the proximity of the two Ti^{3+} atoms and reasonably accounts for the broad linewidth. The small g value might additionally indicate the presence of coordinative saturation.

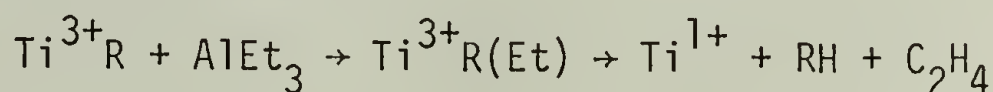
The formation of $(\text{CH})_x$ having primarily the cis configuration at low temperatures and our observation that pristine cis $(\text{CH})_x$ is devoid of unpaired spins suggests that the polymerization proceeds through cis-opening of the acetylene triple bond. Trans-sequences are formed upon warming of the material or upon exposure to oxygen.

It is by no means certain but probable that species $\tilde{1}$, $\tilde{2}$ and $\tilde{3}$ are catalytically active. These signals all decrease in intensity (Table 3) to varying degrees during the course of the polymerization (Figure 19b). Three possible reactions are:

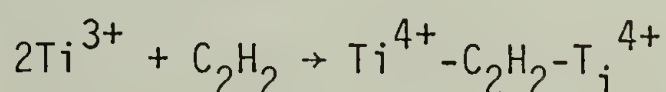
- i. Reduction by bimolecular termination



- ii. Reduction by alkylation



- iii. Oxidative coupling



In these reactions the Ti^{3+} species can be any one of the species $\tilde{1}$, $\tilde{2}$, or $\tilde{3}$.

Conclusions

EPR studies have shown that paramagnetism is not an intrinsic property of $(\text{CH})_x$. The paramagnetism is very sensitive to oxygen. Apparently, oxygen catalyzes the cis-trans isomerization process. Analysis of EPR spectra of the $\text{Ti}(\text{OBu})_4/\text{Et}_3\text{Al}$ system has led to proposals concerning the structures of the catalyst species responsible for acetylene polymerization.

References

1. H. Shirakawa, E. J. Louis, A. G. MacDiarmid, C. K. Chiang and A. J. Heeger, J. Chem. Soc. Chem. Comm., 578 (1977)
2. C. K. Chiang, C. R. Fincher, Jr., Y. W. Park, A. J. Heeger, H. Shirakawa, E. J. Louis, S. C. Gau and A. G. MacDiarmid, Phys. Rev. Lett., 39, 1098 (1977)
3. C. K. Chiang, M. A. Druy, S. C. Gau, A. J. Heeger, E. J. Louis, A. G. MacDiarmid, Y. W. Park and H. Shirakawa, J. Amer. Chem. Soc., 100, 1013 (1978)
4. M. Hatano, S. Karnbara and S. Okamoto, J. Polym. Sci., 51, S26 (1961)
5. H. Shirakawa, T. Ito and S. Ikeda, Makromol. Chem., 179, 1565 (1978)
6. I. B. Goldberg, H. R. Crowe, P. R. Newman, A. J. Heeger and A. G. MacDiarmid, J. Chem. Phys., 70, 1132 (1979)
7. A. Snow, P. Brant, D. Weber and N. L. Yang, J. Polym. Sci., Polym. Lett. Ed., 17, 263 (1979)
8. B. R. Weinberger, E. Ehrenfreund, A. Pron, A. J. Heeger and A. G. MacDiarmid, J. Chem. Phys., 72, 4749 (1980)
9. J. C. W. Chien, F. E. Karasz and G. E. Wnek, Nature, 285, 391 (1980)
10. M. J. Rice, Phys. Lett., 71A, 152 (1979)
11. W. P. Su, J. R. Schrieffer and A. J. Heeger, Phys. Rev. Lett., 42, 1698 (1979)
12. J. C. W. Chien, F. E. Karasz, G. E. Wnek, A. G. MacDiarmid and A. J. Heeger, J. Polymer. Sci., Polym. Lett. Ed., 18, 53 (1980)

13. P. Bernier, M. Rolland, C. Linaya, M. Disi, J. Sledz, F. Schue, J. M. Fabre and L. Giral, to be published
14. M. Takeda, K. Iimura, Y. Nozawa, M. Hisatome and N. Koide, J. Polym. Sci. C, 23, 741 (1968)
15. H. Hirai, K. Hiraki, I. Noguchi and S. Makishima, J. Polym. Sci. A-1, 8, 147 (1972)
16. H. Hiraki, S. Kaneko and H. Hirai, J. Polym. Sci. Polym. Lett. Ed., 10, 199 (1972)
17. P. E. M. Allen, J. K. Brown and R. M. S. Obaid, Trans. Faraday Soc., 85, 1808 (1973)
18. J. M. Pochan, H. W. Gibson and F. C. Bailey, J. Polym. Sci. Polym. Lett. Ed., 18, 447 (1980)
19. B. A. Goodman and J. B. Raynor, Adv. Inorg. Chem. and Radiochem., H. J. Emeleus and A. G. Sharpe, eds., 13, p. 149 (1970)
20. Ibid, p. 188
21. T. S. Djabiev, R. D. Sabirova and A. E. Shilov, Kinetika i Kataliz, 5, 441 (1964)
22. Reference 13 and references therein

C H A P T E R V I I

ELECTRON PARAMAGNETIC RESONANCE STUDY OF PRISTINE AND DOPED CIS $(CH)_x$

The tremendous increases in electrical conductivity upon doping of polyacetylene with electron donors or acceptors¹ can be depicted in the broadest sense as being due to charge transfer between the dopant and the polymer. Evidence for such interactions has been obtained from spectroscopic studies. In the case of iodine doping, for example, species such as I_3^- and I_5^- have been identified using Raman and x-ray photoelectron techniques.^{2,3} Similar species involving polybromide ions have been observed in bromine-doped $(CH)_x$.⁴ However, although charge transfer interactions can be considered to be well-established, mechanistic interpretations are either completely lacking or highly controversial.

The persistent presence of unpaired spins⁵⁻⁹ in $(CH)_x$ coupled with anticipated changes in their number and/or nature upon doping has prompted the application of electron paramagnetic resonance (EPR) spectroscopy to studies of $(CH)_x$ dopant interactions. The system given the most attention to date has been trans $(CH)_x/AsF_5$. Goldberg et al.⁹ studied the in situ doping of trans $(CH)_x$ using relatively high pressures (ca. 60-120 torr) of AsF_5 . These workers found that the paramagnetism of $(CH)_x$ increased upon doping due to the creation of charge carriers (radical cations). The g value of the resonance did not change upon doping demonstrating that the free carriers were associated with $(CH)_x$ and not AsF_5 . Furthermore, the EPR lineshape became asymmetric

(Dysonian) at high doping levels, a result which is consistent with metallic behavior.

However, the recent studies of Weinberger et al.¹⁰ indicate that controlled doping of trans (CH)_x with AsF₅ results in anomalously small Curie contributions to the total magnetic susceptibility, χ , which is proportional to the double integral of the EPR signal. Thus, it was concluded that the charge carriers in lightly doped trans (CH)_x are spinless (referred to as charged solitons). This conclusion has been supported by NMR studies¹¹ which show that the proton spin-lattice relaxation time (T_1) of trans (CH)_x decreases by a factor of ca. 20 upon light doping with AsF₅ suggesting that paramagnetism is quenched by doping.

Studies of the cis isomer, on the other hand, have been limited. It is important to note^{10,12} that χ of cis (CH)_x (ca. 2.7×10^{-8} emu/mole-C) is nearly two orders of magnitude lower than that of the trans isomer (ca. 1.2×10^{-6} emu/mole-C) as a direct consequence of the fewer paramagnetic centers in cis (CH)_x. Tomkiewicz and coworkers¹² found that χ for cis [CH(AsF₅)_{0.009}]_x is an order of magnitude greater than that of the pristine material. The magnitude of this increase, these workers claim, would be undetectable against the background χ of pristine trans (CH)_x. Thus, they concluded that the absence of an apparent increase in χ upon light doping of trans (CH)_x reported by Weinberger et al.¹⁰ was simply a matter of sensitivity and suggested that the conductivity in doped (CH)_x arises from randomly distributed (inhomogeneous) highly conducting regions.

The importance of the cis isomer in view of its greater conductivity upon doping¹ and the limited amount of information available concerning doped derivatives as compared to trans $(CH)_x$ suggested that additional EPR studies would be very worthwhile. The AsF_5 doping technique described in Chapter III, used routinely in several laboratories,¹³ was employed in this work. Of particular interest was the influence of dopant concentration on linewidth, lineshape and saturation behavior. Saturation studies of cis and trans $(CH)_x$ and iodine-doped cis $(CH)_x$ were investigated for comparative purposes. In addition, the curious phenomenon of microwave heating of heavily doped samples with increasing microwave power was studied.

Experimental

A film of analytically pure* cis $(CH)_x$ was prepared according to techniques described in Chapter IV and was stored in vacuo at $-78^\circ C$ until use.

The experiments to be described below required three individual samples for measurement of electrical conductivity, weight uptake of dopant and EPR spectroscopy. Samples for four-probe conductivity measurements were mounted in air with Electrodag. A reference film for weight uptake was weighed in air and placed in the four-probe apparatus. The apparatus was pumped ca. 1 hour on a vacuum line to dry the Electrodag

* Galbraith Laboratories, Inc., Knoxville, Tenn. Anal. Calcd. for $(CH)_x$: C, 92.26%; H, 7.74%. Found: C, 91.26%; H, 7.92%. Total: 99.18%

and remove air and then was taken into a glove bag. An additional piece of cis $(\text{CH})_x$ film for EPR studies (large enough for ca. twelve 15 mm x 2 mm strips) was placed in the apparatus. Thus, EPR samples were never exposed to air. The four-probe was then pumped for ca. 1 hour before beginning doping experiments.

The EPR studies of AsF_5 -doped $(\text{CH})_x$ usually employed standard quartz tubes (Chapter II) with a top comprised of a 10/30 joint, high vacuum stopcock and ball joint for attachment to the vacuum line. In addition, this top had a short side-arm at the end of which was a socket joint. A thermocouple (copper constantan) of sufficient length was threaded through a matching ball joint in order that the tip of the thermocouple rested ca. 3 cm from the bottom of the EPR tube when the ball and socket joints and the tube and top were joined. The ball-joint had a narrow constriction to minimize the free space around the thermocouple wires. This space was made vacuum tight by sealing with an epoxy resin.

AsF_5 . The slow-doping method outlined in Chapter III was employed. The sample was doped to the desired level by comparison of the conductivity to a calibration curve of σ vs. y for AsF_5 doping of $(\text{CH})_x$ (Cf. Figure 2, Chapter I). [It should be noted that the weight uptakes of the samples were in excellent agreement with this curve.] After reaching the desired doping level, the apparatus was pumped ca. 30 minutes and then taken into a glove bag along with EPR tubes and appropriate tops. The reference sample was weighed in air and placed back into the apparatus in the glove bag. A small strip (ca. 15 mm x 2 mm)

was cut from the sample designated for EPR and placed on a stack of microscope slides. The tip of a copper-constantan thermocouple (connected to an EPR tube top as described previously) was attached to the "dull" side of the $(\text{CH})_x$ film with a drop of Electrodag. After allowing the Electrodag to dry for a few minutes, the thermocouple was threaded into an EPR tube and the tube was capped. The four-probe apparatus, containing the reference and EPR samples, was once again attached to a vacuum line and pumped at least 30 minutes before continuing the doping. The EPR tube was also attached to a vacuum line and pumped at least 20 minutes before recording EPR spectra.

In certain cases, it was of interest to dope cis $(\text{CH})_x$ to very low levels directly in an EPR tube (referred to as in situ doping in the text, although this was done on a vacuum line and not while the tube was in the EPR probe). Extremely small quantities of gas were metered as follows. With the AsF_5 bulb cold finger cooled to -95°C and the stopcock between the bulb and manifold closed, the stopcock of the bulb was opened briefly allowing AsF_5 (ca. 30 torr at -95°C) to fill this small volume. The bulb was then closed, the gas was expanded into the manifold and the stopcock isolating the bulb and the manifold was closed. The AsF_5 in the manifold was pumped away and the extremely small portion of AsF_5 remaining between the bulb and manifold was then allowed to contact the film in the EPR tube. The tube was then disconnected from the vacuum line and a spectrum was recorded. A few such consecutive dopings were sometimes required to yield the desired results (see below). Compensation experiments were carried out with

ca. 50-100 torr of dry, degassed NH_3 contained in a glass bulb.

Iodine. Samples of cis $(\text{CH})_x$ were doped with iodine using the in vacuo method described in Chapter III. The doping rate was kept fairly slow by pre-cooling the bulb of the four-probe apparatus containing iodine crystals to -196°C and allowing the bulb to slowly warm to room temperature. The level of doping was obtained from the conductivity by comparison with a calibration curve (Cf. Chapter I, Figure 2). Identical techniques to those previously described for AsF_5 -doped materials were employed for sample transfers although the thermocouple was not used while recording EPR spectra.

EPR spectra. All EPR spectra were obtained using a Varian E-9 X-band spectrometer equipped with a dual microwave cavity. Signal amplitudes and linewidths were monitored as a function of microwave power. Typically, initial powers were 0.7-1.0 mW. A spectrum was recorded after each incremental increase (usually 2-5 mW) of the power. The maximum power available from the instrument was 200 mW. The detector current output was always adjusted so as to maintain its value at 250 μA . The modulation amplitude was maintained at a value which was at most one-quarter of the EPR linewidth. The determination of g values has been described in the preceeding chapter.

In the case of AsF_5 -doped samples with the attached thermocouple, the placement of the EPR tube in the microwave cavity was adjusted so that the thermocouple tip was approximately centered in the cavity. Such placement yielded maximum sample temperatures. The temperatures

were measured using a Leeds and Northrup 8686 millivolt potentiometer. Potentiometer readings were converted to temperature ($^{\circ}\text{C}$) from well-established copper constantan thermocouple data.

Saturation behaviors of pristine cis and trans $(\text{CH})_x$ were investigated for comparative purposes.

Results

EPR saturation. Signal amplitudes (Y') were plotted as a function of the square root of the microwave power (P_w). The saturation point was defined as the power at the amplitude maximum in such a plot if a maximum was observed. The saturation maximum was used to compute the spin-lattice relaxation time (T_1) according to¹⁴

$$T_1 = 1.97 \times 10^{-7} \Delta H_{pp}^{\circ} / g (H_1)^2 \quad \underline{1}$$

where ΔH_{pp}° is the resonance linewidth below saturation, g is the g value and H_1 is the rf magnetic field amplitude. The spin-spin relaxation time was determined from the linewidth by¹⁴

$$T_2 = 1.31 \times 10^{-7} / (\Delta H_{pp}^{\circ}) g \quad \underline{2}$$

The value of $(H_1)^2$ in equation 1 is proportional to the incident power level,

$$(H_1)^2 = K P_w,$$

where P_w is the power level and K is a proportionality constant which needs to be experimentally determined. Attempts were made to measure K (by L.C. Dickinson and J.M. Warakomski) according to techniques described by Poole,¹⁵ and K was found to be ≈ 0.2 . The credibility of this value is somewhat questionable in view of the fact that certain

experiments (see below) yielded $T_2 > T_1$, a relationship which is theoretically impossible. However, although the absolute values of T_1 and T_2 may be in error, their relative values are anticipated to be reasonably accurate.

Undoped (CH)_x. A saturation plot of cis (CH)_x is shown in Figure 21a. A well-defined maximum is observed at ca. 3.4 mW. After heating the sample at ca. 200°C (in vacuo) for ca. 1 minute to convert the material to predominantly the trans configuration, Figure 21b was obtained. This plot is identical to that obtained from a sample subjected to prolonged isomerization (ca. 200°C for 1 hour). The saturation maximum is identical to that of cis (CH)_x although Y' in the tail of the curve at high powers is more nearly dependent upon $1/p^{1/2}$ for trans (CH)_x. Values of T_1 and T_2 for cis and trans (CH)_x are given in Table 4.

AsF₅-doped (CH)_x. Four general types of lineshapes were observed throughout the course of the EPR study as a function of dopant concentration, y . The spectra in Figures 22a-d are representative of a.) undoped cis (CH)_x, b.) lightly doped ($y \approx 0.005$) material, c.) samples doped in the range $0.008 \leq y \leq 0.02$, and d.) heavily doped, "metallic" (CH)_x. The relationship between signal intensity and y was not examined quantitatively, although the intensities were noticeably greater as y increased from 0-ca. 0.02 for approximately the same size of the sample. Beyond $y \approx 0.02$, it is difficult to comment even qualitatively about this relationship due to skin depth effects.⁹ The ratio of the signal amplitudes above and below the baseline (A/B ratio) was found to be

Figure 21. EPR saturation plots of cis (●)
and trans (▲) $(CH)_x$.

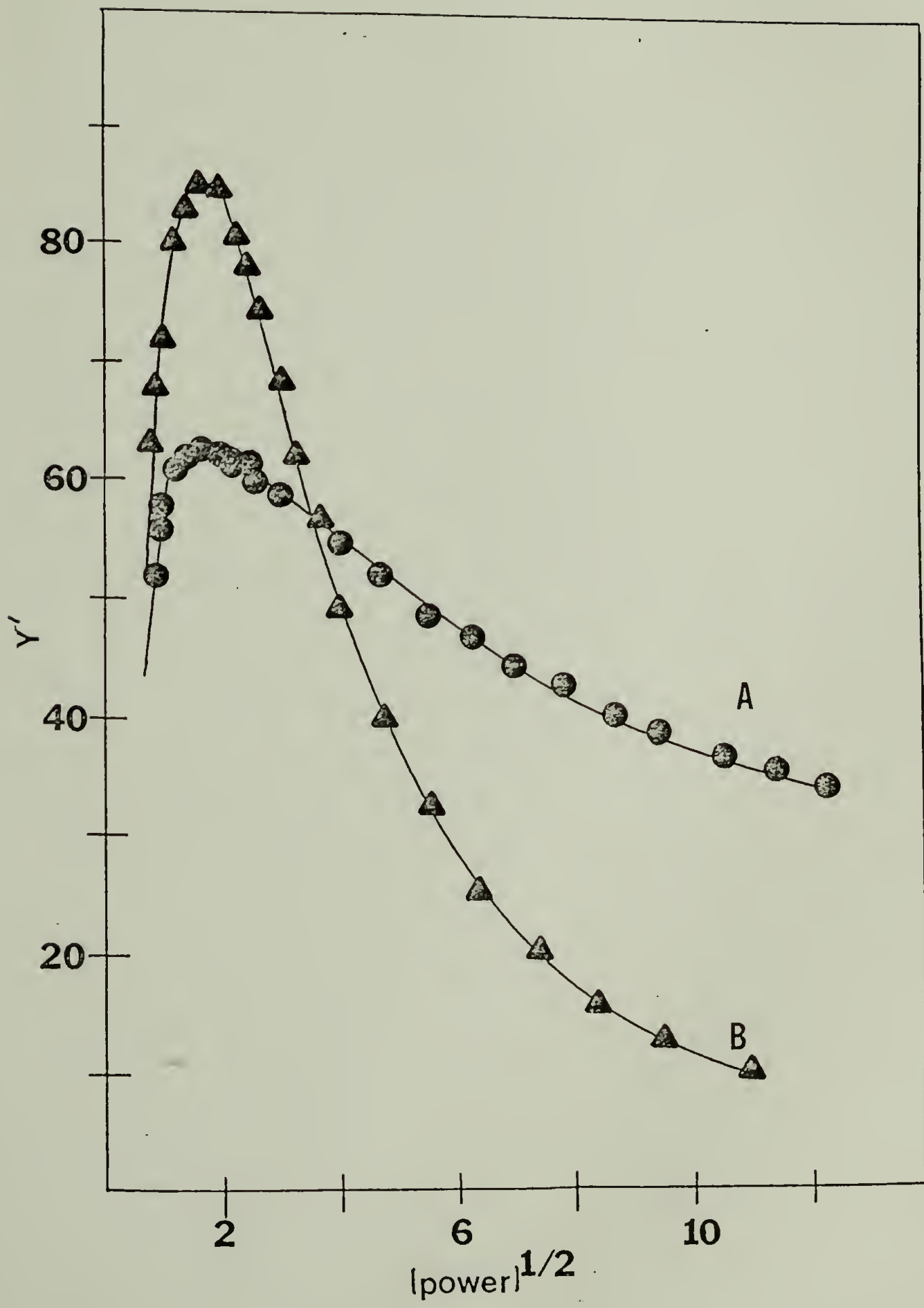


Figure 22. EPR spectra of cis $[\text{CH}(\text{AsF}_5)_y]_x$.

	<u>y</u>
A	0
B	~ 0.005
C	$\sim 0.008 \lesssim y \lesssim 0.02$
D	~ 0.08

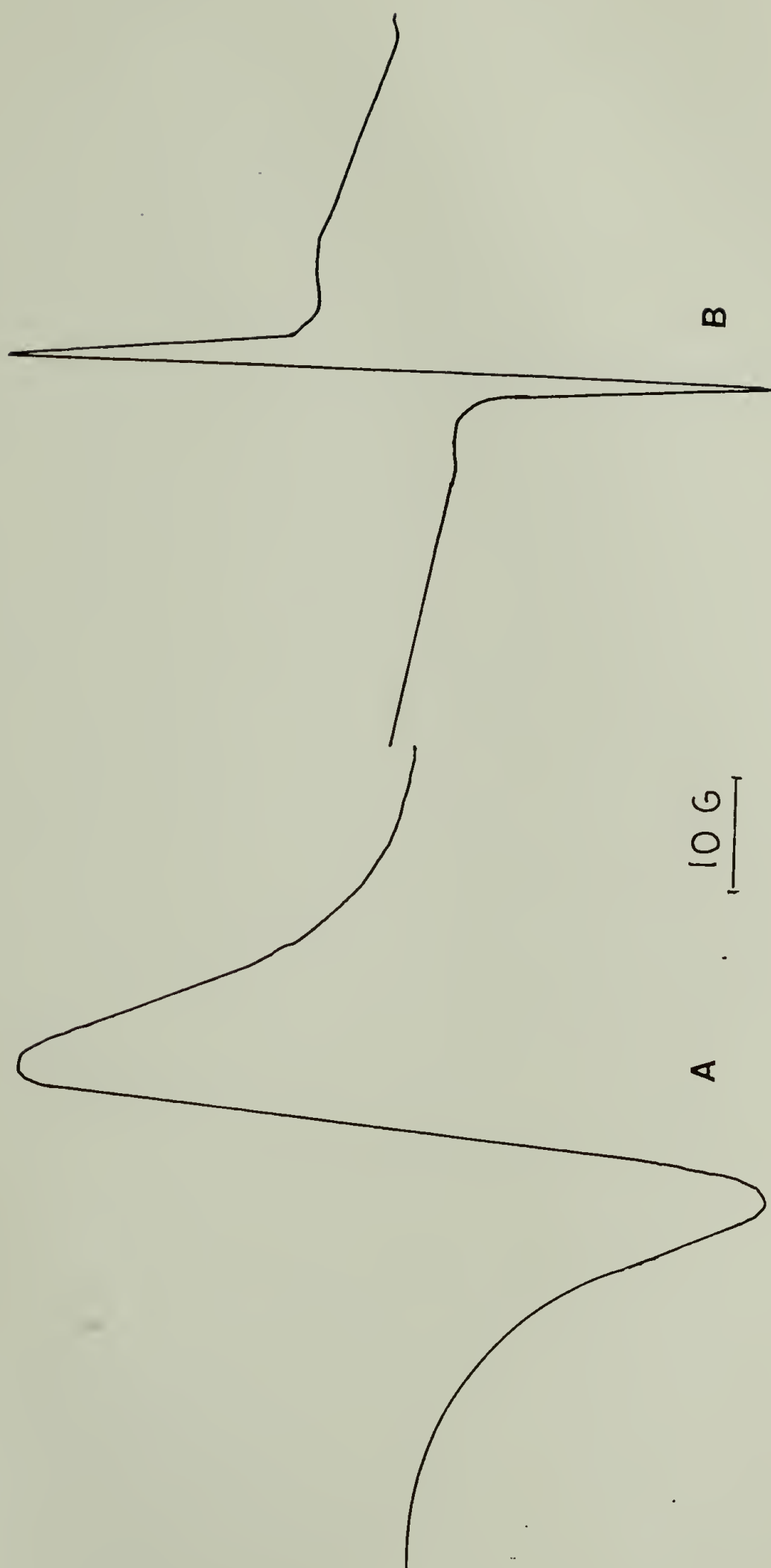


Figure 22.

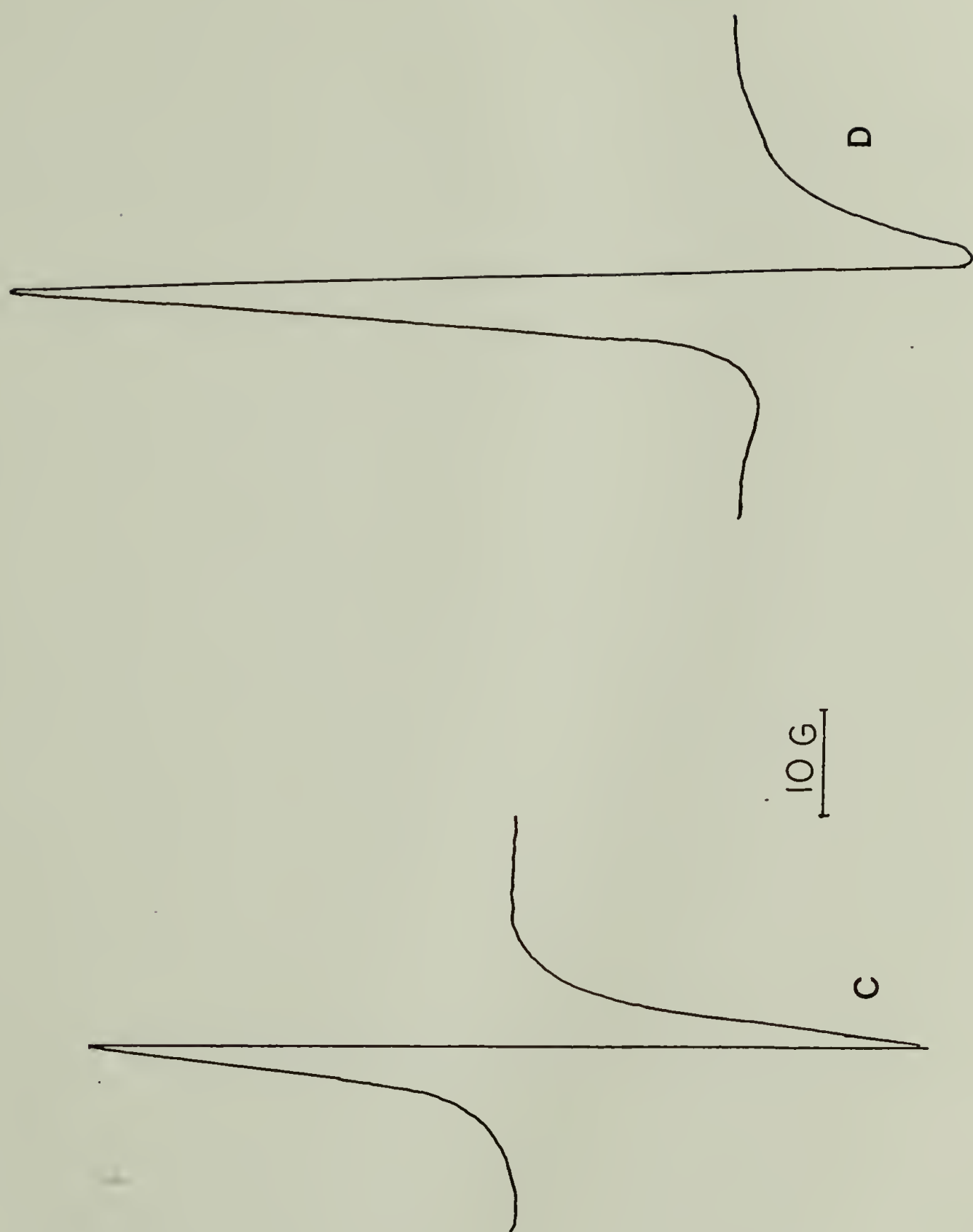


Figure 22., continued.

unity for samples having $y \leq 0.02$ and then increased with increasing y as shown in Figure 23. The EPR linewidths (ΔH_{pp}°) as a function of y are plotted in Figure 24. The ca. 7 G signal of cis $(CH)_x$ narrowed appreciably upon light doping and then progressively increased with increasing y . In all cases, g values were in the range 2.0022-2.0026. It should be noted that all EPR data described above were obtained from samples having an attached thermocouple. However, the thermocouple did not appear to affect the linewidth, A/B ratio or saturation behavior as selected samples in the absence of a thermocouple yielded similar results.

EPR saturation plots, obtained from the same thermocouple-attached samples, are shown in Figures 25a,b. The saturation maximum shifts to higher powers as y increases. The plots become essentially linear beyond $y \approx 0.02$ although some upward curvature was observed for samples having high values of y (ca. 0.08-0.10). Values of T_1 determined from samples which yielded a maximum (i.e., $y \approx 0.002$, 0.005 and 0.008) are given in Table 4. T_1 was found to decrease as y increased. Furthermore, T_2 remained essentially constant over the doping range although its magnitude was greater than T_1 , thus questioning the validity of the absolute values of T_1 .

The temperature of each sample was measured during the course of the saturation study. As indicated in Figure 26, the sample temperature increased linearly with power and in general the slope increased with y . It should be noted that since Electrodag, a fairly good conductor, was used as the thermocouple/film contact, the temperatures are probably not

Figure 23. Plot of EPR lineshape asymmetry (A/B) vs. y
for cis $[\text{CH}(\text{AsF}_5)_y]_x$

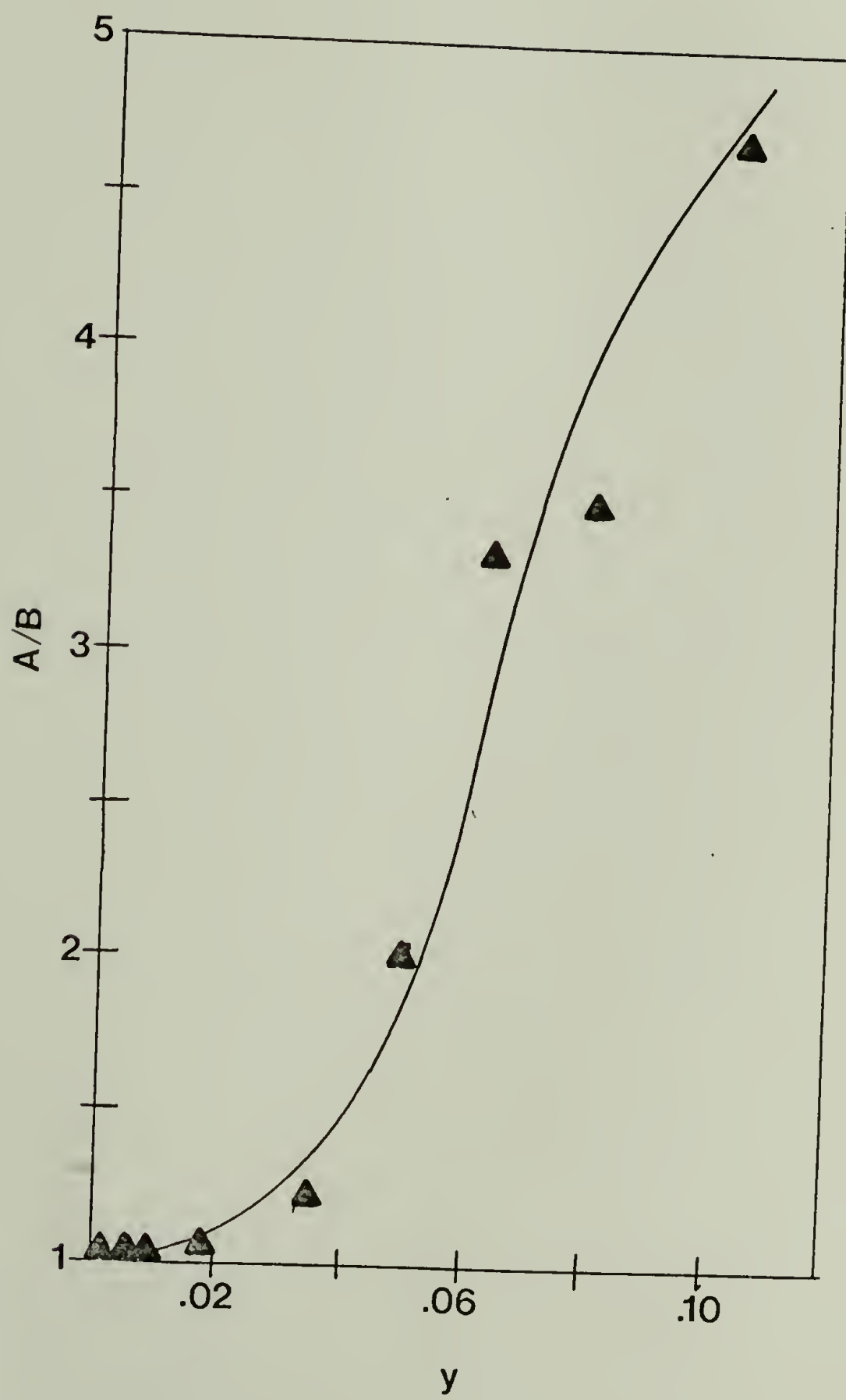


Figure 24. Plot of ΔH_{pp}° vs. y for
cis $[\text{CH}(\text{AsF}_5)_y]_x$.

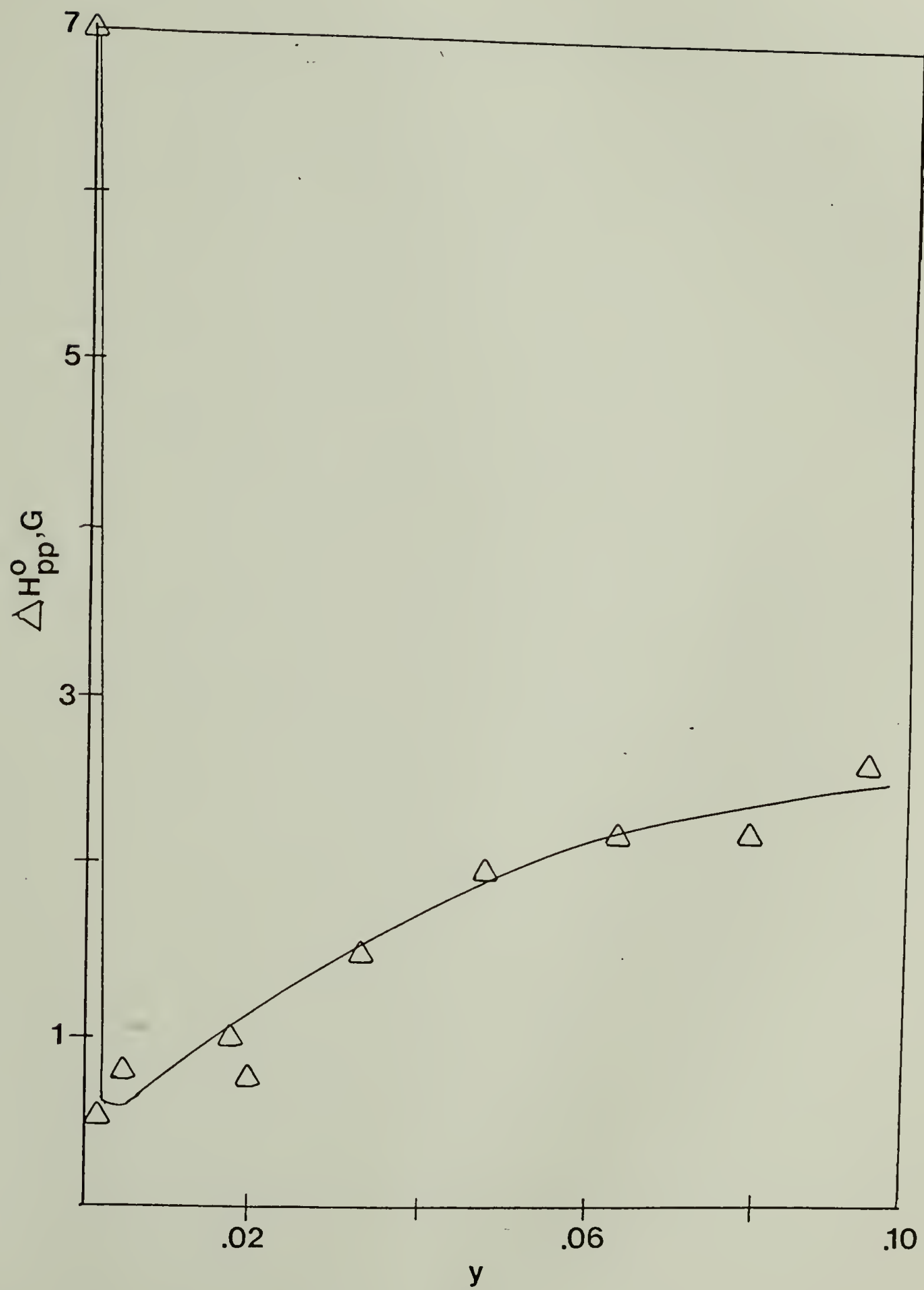


Figure 25. EPR saturation plots of
cis $[\text{CH}(\text{AsF}_5)_y]_x$.

(A)

	<u>y</u>
\triangle	0
\bigcirc	0.005
\square	0.008
\bullet	0.018
\times	0.033

(B)

	<u>y</u>
\bigcirc	0.048
\triangle	0.065
\square	0.079
\bullet	0.094

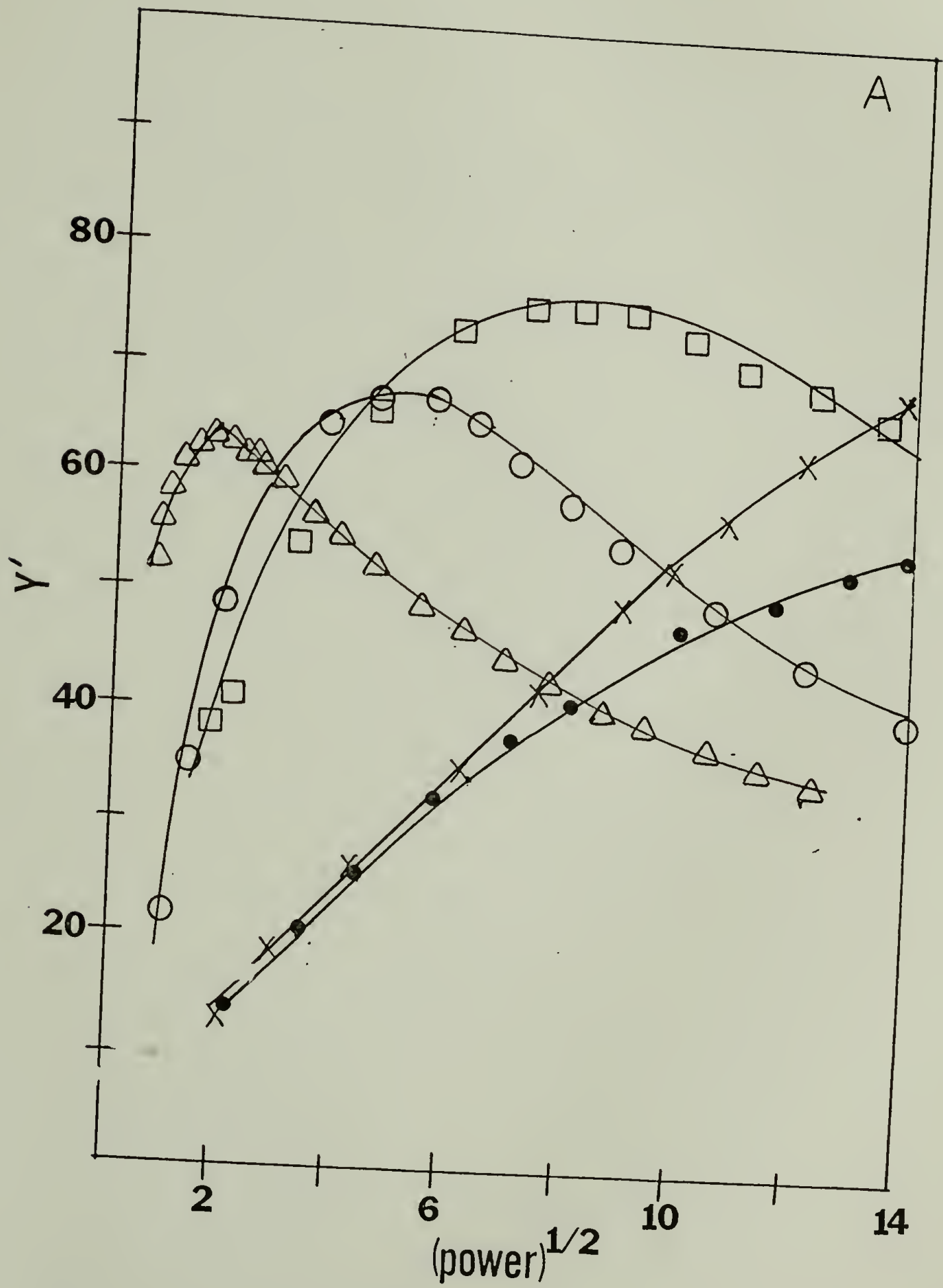


Figure 25A.

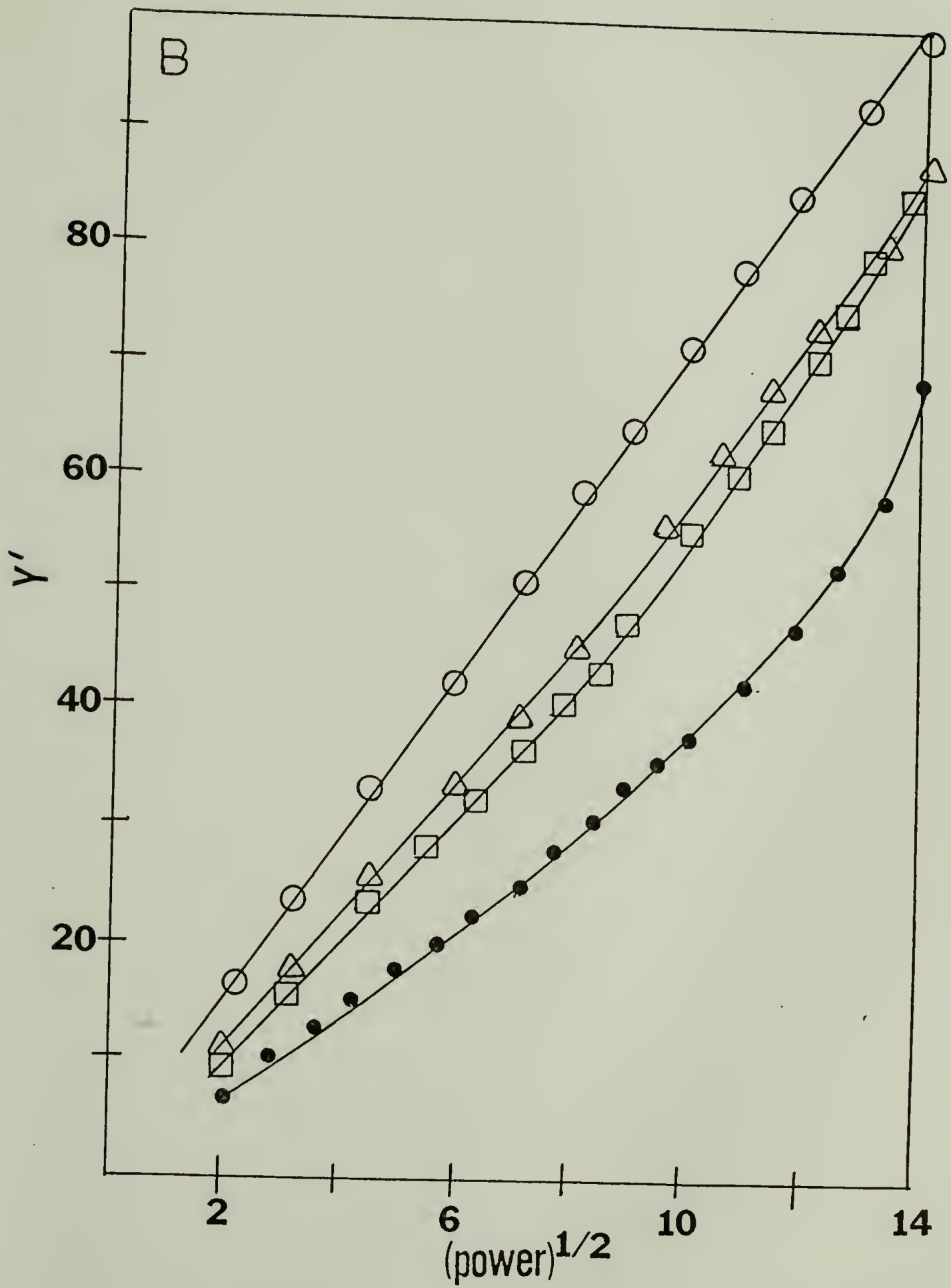


Figure 25B.

Figure 26. Plots of sample temperature vs. microwave power for cis $[\text{CH}(\text{AsF}_5)_y]_x$.

	<u>y</u>
⬡	0
○	0.005
X	0.008
□	0.018
△	0.048
●	0.094

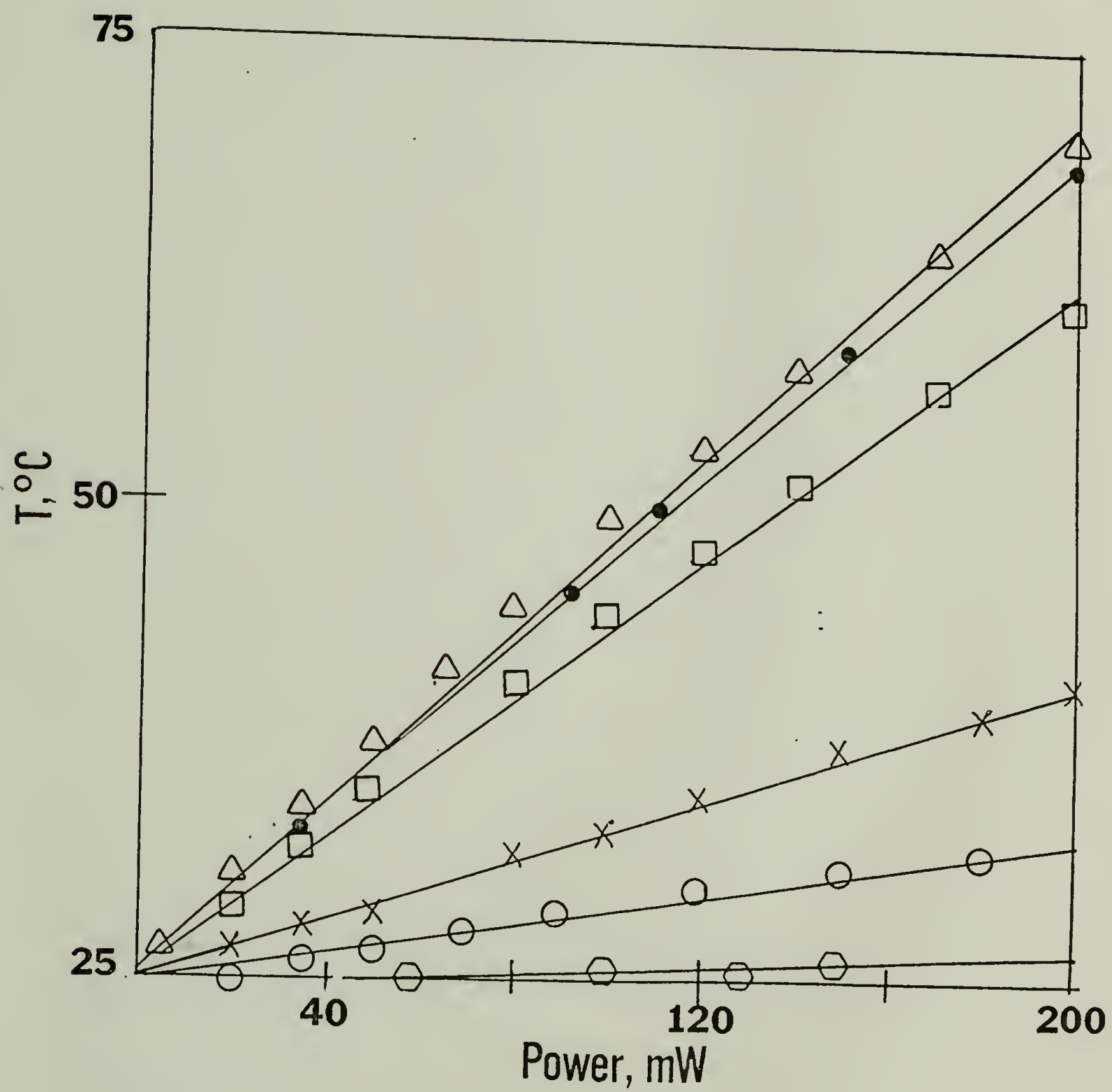


TABLE 4

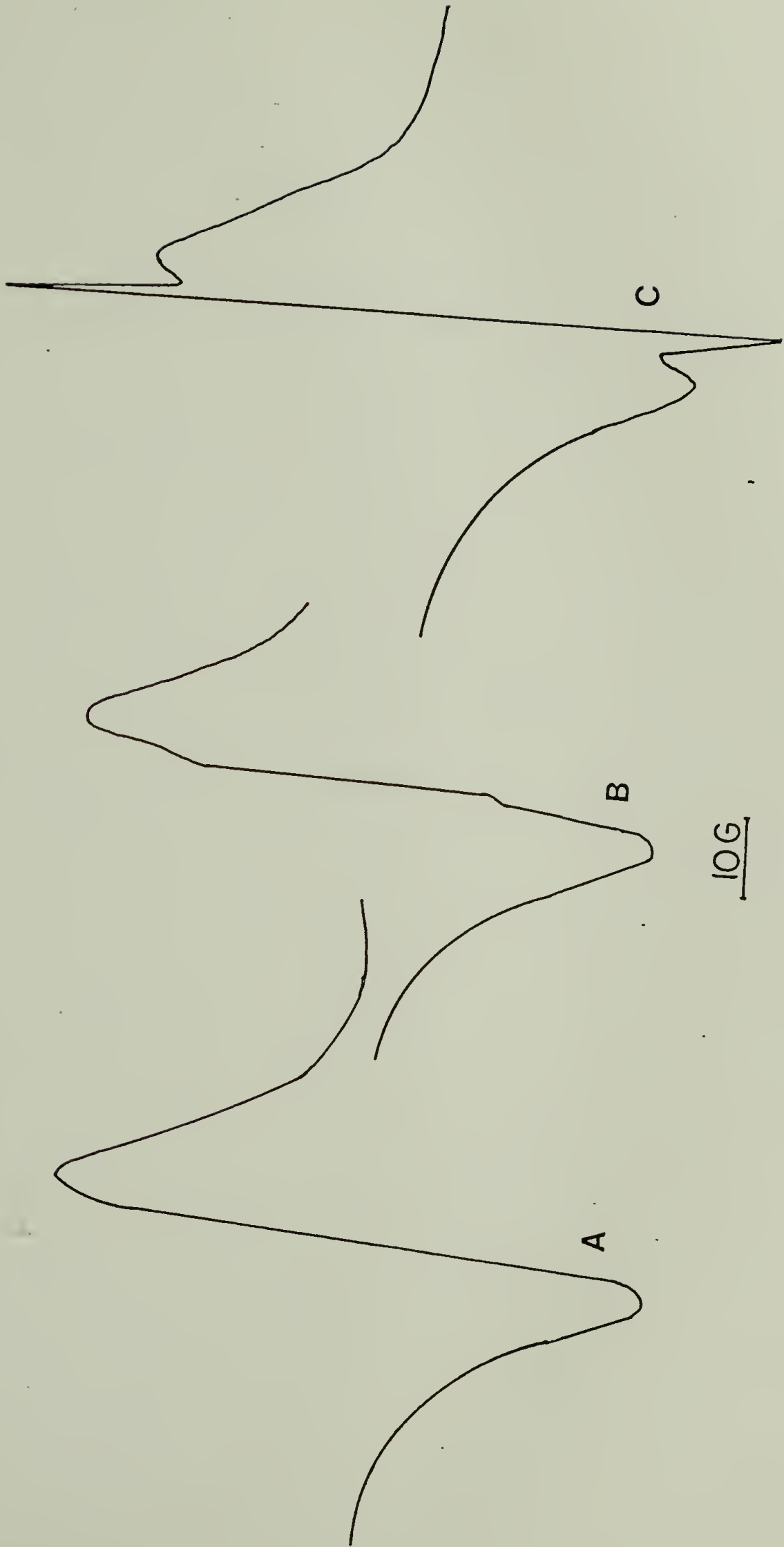
EPR Relaxation Data for cis_x, trans (CH)_x, and cis [CH(AsF₅)_y]_x.

Sample	ΔH_{pp}° , G	$(P_{\max})^{1/2}$	T_1 , sec	T_2 , sec
<u>cis</u> (CH) _x	~7	1.75	5.6×10^{-6}	9.3×10^{-9}
<u>trans</u> (CH) _x	~1	1.75	8.0×10^{-7}	6.1×10^{-8}
<u>cis</u> [CH(AsF ₅) _{0.002}] _x	~0.5	4	7.7×10^{-8}	1.3×10^{-8}
<u>cis</u> [CH(AsF ₅) _{0.005}] _x	~0.8	5	7.9×10^{-8}	8.2×10^{-8}
<u>cis</u> [CH(AsF ₅) _{0.008}] _x	~0.8	8	3.0×10^{-8}	8.2×10^{-8}

representative of a true copper-constantan junction and are likely to be somewhat lower than the actual sample temperature. However, the relative values are more important and appear to be consistent with an increase of sample temperature at a particular power as y increases. In all cases, samples which afforded fairly high temperatures (i.e., heavily doped) were noticeably warm to the touch upon completion of the saturation experiments. This qualitative observation also applied to similar samples without an attached thermocouple. The heating effect was quite reversible; "cooling" the sample by reducing the microwave power to a particular value gave a temperature very close to that from a sample which had been previously "warmed" to that power. Finally, sample heating was an off-resonance phenomenon. Thus, maintaining the spectrometer magnetic field several hundred Gauss away from the signal yielded the same temperature as obtained by scanning through the sample resonance.

The rather curious lineshape of Figure 22b, having a narrow central resonance superimposed on what appeared to be a broad resonance, prompted experiments in an effort to "trap" the narrow line in its initial stages of formation. Thus, cis $(\text{CH})_x$ samples were doped in situ (in an EPR tube on a vacuum line) with very small quantities of AsF_5 . As indicated in Figure 27b, small "bumps" were observed in the center of the cis $(\text{CH})_x$ resonance (after ca. 2-3 AsF_5 exposures) which grew into a sharp (ca. 0.4-0.5 G) line (Figure 27c) upon additional exposure. Still further AsF_5 treatment yielded a spectrum similar to Figure 22b.

Figure 27. EPR spectra of cis (CH)_x lightly doped with AsF₅. (A) undoped; (B) trace AsF₅; (C) additional AsF₅.



A saturation study (Figure 28) indicated that, while it was difficult to plot the intensity of the broad signal as a function of power due to the poor resolution of the lineshape, the narrow resonance appears to saturate at a power somewhat higher than that of the broad signal (note arrows in Figure 28). In addition, exposure of the sample to ca. 50 torr of NH_3 caused the narrow resonance to disappear although little change (possibly a small increase in intensity) of the broad signal was observed.

Iodine doping. EPR spectra of cis $(\text{CH})_x$ doped with iodine displayed considerably different behavior as compared to AsF_5 -doped $(\text{CH})_x$. The signal amplitude decreased as y increased and eventually disappeared near $y \approx 0.03$. Furthermore, the linewidth (and thus T_2) remained essentially constant ($\Delta H_{pp}^\circ \approx 6.5\text{--}7.0$ G). The saturation plots of the samples shown in Figure 29 for all intents and purposes are identical although an upward curvature is observed for $y \approx 0.02$. Although the absence of distinct maxima precluded the determination of T_1 's, it can be stated that the T_1 's are all much shorter than that of pristine cis $(\text{CH})_x$ (Table 4) and, in addition, they are relatively insensitive to y .

It should be noted that samples which were doped to fairly high levels ($y \approx 0.02$) were noticeably warm upon completion of the saturation experiments at high powers.

Figure 28. EPR spectra as a function of microwave power of cis $(CH)_x$ lightly doped with AsF_5 . The apparent saturation maxima are designated by \downarrow and \downarrow for the broad and narrow resonances, respectively.

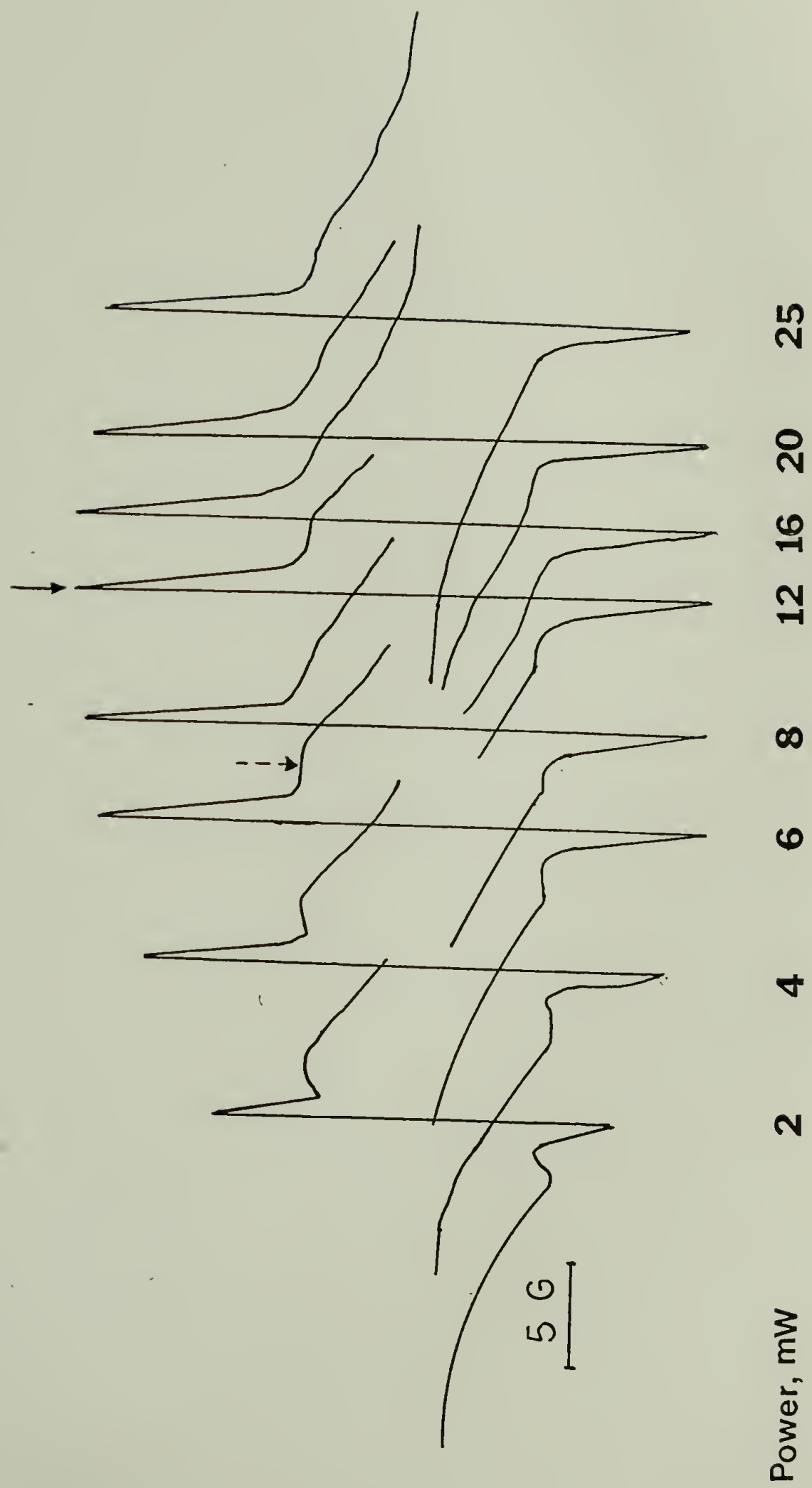
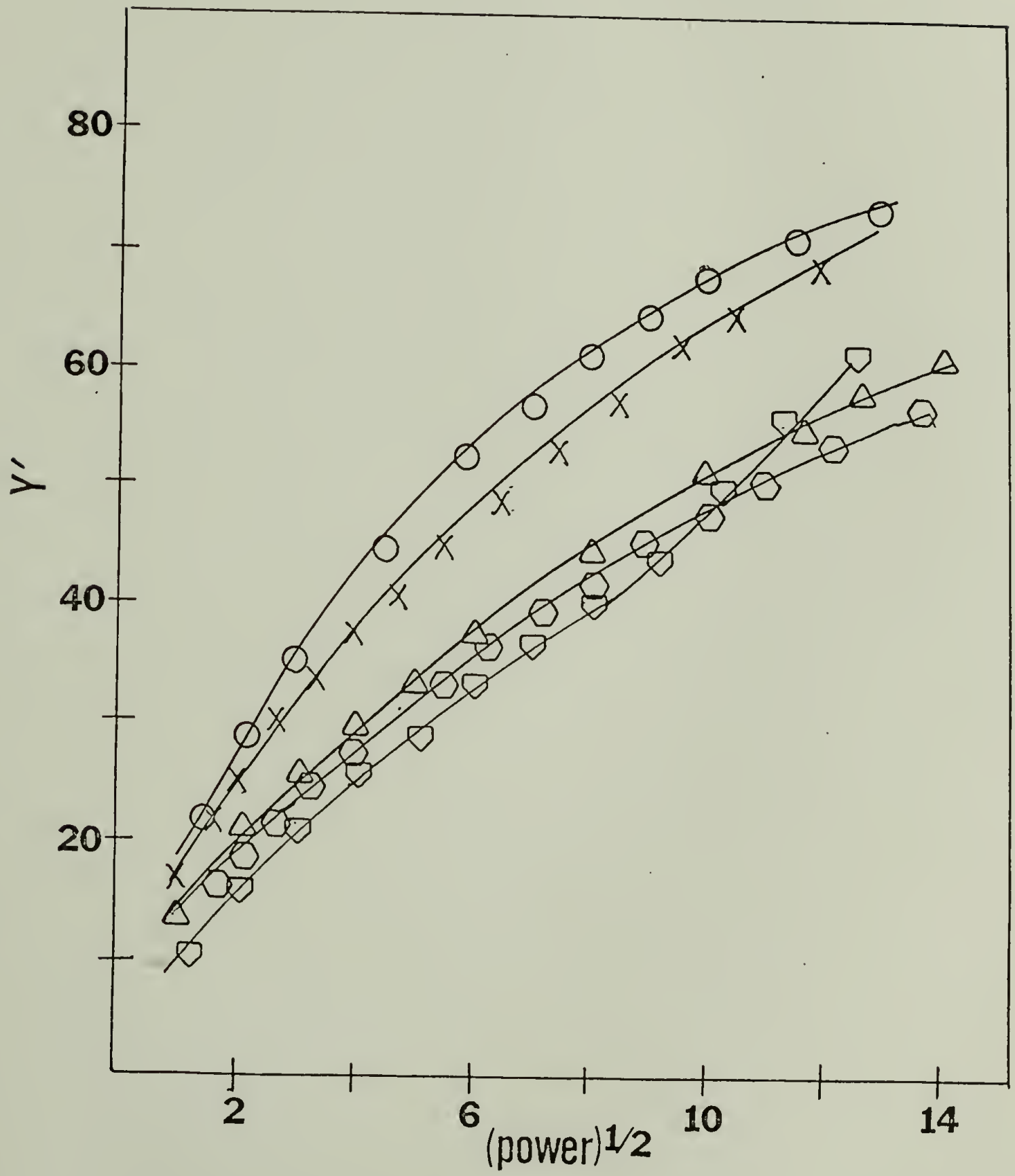


Figure 29. EPR saturation plots of
cis $[\text{CHI}_y]_x$.

	<u>y</u>
\triangle	0.0014
\hexagon	0.004
\times	0.008
\circ	0.013
\square	0.022



Discussion

Saturation behavior; undoped $(CH)_x$. Important information can be obtained from the overall slope of an EPR saturation curve.¹⁴ In some cases, Y' is linearly dependent upon $p^{1/2}$ at low powers and shows a $1/p^{1/2}$ dependence at high powers with a maximum in between (Type A saturation). Such behavior is exhibited by trans $(CH)_x$ in Figure 21b. The overall shape of this curve is suggestive of homogeneous broadening, which occurs when the magnetic resonance signal results from a transition between two spin states which are not sharply defined but rather are somewhat intrinsically broadened. A few sources of homogeneous broadening are dipolar interactions between like spins, spin-lattice interactions and motional narrowing fluctuations of local magnetic fields. Another type of saturation behavior (type B) is one in which, after the saturation maximum, Y' is independent of $p^{1/2}$. The relationship for cis $(CH)_x$ shown in Figure 21a is perhaps an admixture of both dependencies described above, with Y' being only weakly dependent upon $p^{1/2}$ at high powers. However, cis $(CH)_x$ is more representative of type B behavior suggesting that the resonance signal is inhomogeneously broadened. Such a resonance consists of a spectral distribution of individual lines merged into an overall envelope. Some sources of inhomogeneous broadening include unresolved hyperfine structure and dipolar broadening between unlike spins.¹⁴

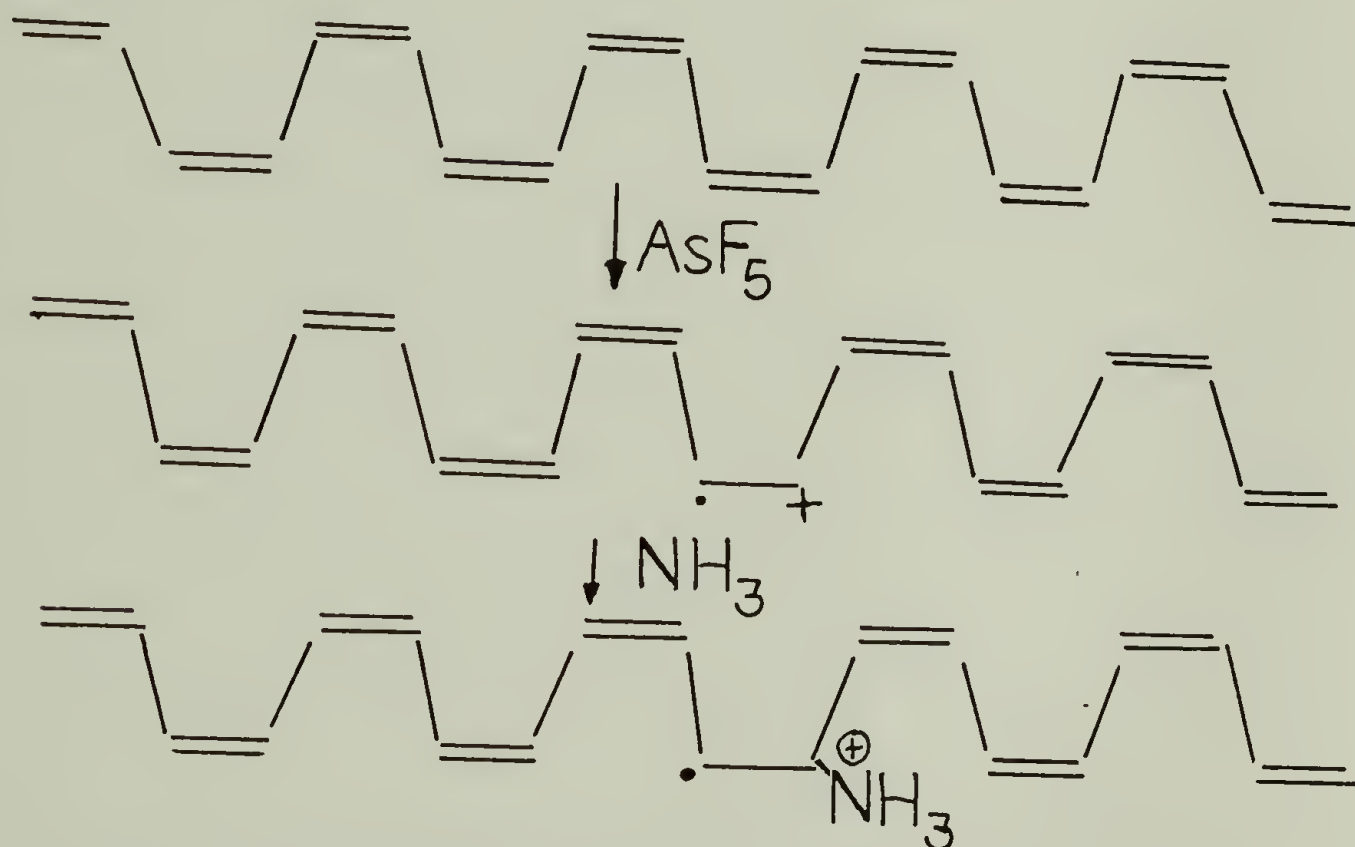
Consideration of the above discussion leads to the conclusion that the saturation data of Figure 21 are entirely consistent with previous EPR information concerning the isomers of $(CH)_x$. It has been

demonstrated, for example, that a relatively immobile¹⁶ neutral defect is present in cis (CH)_x and that the linewidth is primarily determined by unresolved hyperfine interactions,¹⁰ accounting for the observed inhomogeneous broadening. On the other hand, hyperfine interactions in trans (CH)_x are much weaker due to the greater mobility of the free spins.^{6,17} The mobility results in motional narrowing and, with concomitant local field fluctuations, could lead to homogeneous broadening. Furthermore, the value of T_1 for trans (CH)_x is increased by a factor of ≈ 7 as compared to the cis isomer due to the greater number of paramagnetic centers in trans (CH)_x. The fluctuating fields produced by such centers can be an efficient spin-lattice relaxation mechanism and thus can also contribute to homogeneous broadening.¹⁴

It should be noted that T_2 (Table 4) for trans (CH)_x is longer by a factor of ≈ 7 as compared to cis (CH)_x and is anticipated considering the narrower linewidth of the former isomer.

AsF doping. The narrow EPR signal superimposed on the broad cis (CH)_x resonance resulting from the initial in situ exposure to traces of AsF₅ (Figure 27) a priori suggests that either it arises from partial cis-trans isomerization or from the formation of radical cations via charge transfer. The two resonances are clearly different in view of their different saturation maxima (Figure 28). As noted previously, the maxima for cis and trans (CH)_x are identical; this argues against the possibility that the narrow resonance is the result of cis-trans isomerization. The argument is supported by the observation that the narrow signal disappeared upon exposure to NH₃. An independent

experiment showed that NH_3 had no effect on the intensity or the saturation behavior of pristine cis $(\text{CH})_x$. Similar results concerning signal intensity have been reported for trans $(\text{CH})_x$.⁹ Thus, it is reasonable to conclude that radical cation formation accompanies AsF_5 doping, at least under the experimental conditions employed in this work, viz.



Since no EPR signals for species such as $\text{AsF}_5^{\cdot-}$ have been observed, and chemical analysis typically yields $\text{F}/\text{As}=5$, it has been proposed that the counterion exists as the diamagnetic $\text{As}_2\text{F}_{10}^=$ ion.¹ Compensation with NH_3 may form a quaternary ammonium ion (see above). Thus, the possible small increase in the broad signal intensity observed upon NH_3 exposure may be the result of radicals which remain after charge compensation. Since $^{\oplus}\text{NH}_3$ is expected to interact with the free spins via quadrupole coupling, T_1 is in turn expected to be short, leading to a broad linewidth.

The T_1 values (Table 4) for samples doped with AsF_5 decrease as y

increases. This relationship is consistent with an increase in the number of paramagnetic species upon doping. It is interesting to note that the saturation curves (Figure 25a) are somewhat similar to that of cis (CH)_x and suggest inhomogeneous broadening. This may be the result of dipolar interactions between unlike spins¹⁴ (i.e., neutral defects and radical cations). The linearity of the plots (Figure 25b) at high doping levels suggests that T₁ of the degenerate electron gas in the "metallic" state is very short. The onset of the curvature in the plots at high doping levels may be due to "artificial" intensity increases resulting from microwave heating (see below) and, in turn, cis-trans isomerization. The onset of lineshape asymmetry (A/B) near y≈0.02 as shown in Figure 23 is consistent with the onset of metallic behavior at the semiconductor-metal transition.

The increase in paramagnetism upon doping of cis (CH)_x with AsF₅ is likely to be the result of inhomogeneous doping even when traces of the gas are employed (Figure 27). The strong electron acceptor properties of AsF₅ cause immediate formation of radical cations. Annihilation of paramagnetic centers¹⁸ may not be efficient since the free electron mobility in cis (CH)_x is lower than that of the trans isomer unless, of course, cis-trans isomerization accompanies the doping process. From the results of Figure 27, it is easy to appreciate the sensitivity question of Tomkiewicz et al. concerning cis vs. trans (CH)_x. Studies of extremely slow and homogeneous doping are essential to clarify uncertainties about radical cations and charged solitons in cis (CH)_x.

Iodine doping. The absence of a linewidth change during iodine doping suggests that the observed resonance is only due to cis $(\text{CH})_x$. The decrease of signal intensity upon doping and the saturation behavior shown in Figure 29 suggest several implications concerning the doping process. First, it is important to point out that a neutral soliton present in pristine cis $(\text{CH})_x$ resides in a non-bonding orbital and, since this corresponds to the highest filled molecular orbital (HOMO), such an electron has the lowest ionization potential. Thus, upon charge transfer between $(\text{CH})_x$ and an acceptor, the neutral solitons are the first to be removed from $(\text{CH})_x$. Iodine, an acceptor with a relatively low electron affinity (e.g., as compared to AsF_5), is anticipated to consume the neutral solitons before breaking bonds along the $(\text{CH})_x$ chain to form radical cations which incidentally requires removal of an electron from the filled valence (π -bonding) band of $(\text{CH})_x$. The latter process presumably occurs to some extent in view of the fact that the dopant concentration can exceed the (initial) neutral soliton concentration by several fold while the sample still displays an EPR signal. However, if radical cations are formed upon iodine doping, this radical would occupy the HOMO and in turn would be the most favorable electron to be removed by charge transfer. Admittedly, this rather simplified picture can be complicated by factors such as isomerization processes and quadrupole broadening due to iodine ($I=5/2$) species.

The similarity in the saturation curves for various levels of iodine doping (Figure 29) suggests that the spins in the sample have a shorter T_1 as compared to cis $(\text{CH})_x$ and relaxation behavior is essentially

independent of the doping level. The shorter T_1 might be explained as being due to quadrupole relaxation involving iodine species. It should be noted that the T_1 's, although not measurable in an absolute sense, are shorter than those from similarly doped trans $(CH)_x$ samples. This observation implies that the neutral defects in cis $(CH)_x$ are less mobile than in the trans isomer since quadrupole relaxation is expected to be enhanced if the spins are more localized.

Microwave heating. This phenomenon was brought to our attention indirectly from miscellaneous saturation studies of doped $(CH)_x$. For example, EPR spectra of "metallic" $(CH)_x$, doped with chlorosulfonic acid, showed a decrease in the A/B ratio from ≈ 3 to 1 at high (>150 mW) powers. In addition, the gold-colored film became silvery and droplets of liquid (presumably dopant) were observed in the bottom of the EPR tube. In another case, blue films of cis $[CHBr_{0.25}]_x$ became golden at high powers in qualitative analogy to the result observed by Kletter et al.²⁰ for thermolysis reactions of bromine doped $(CH)_x$. The heating phenomenon appeared to be independent of the dopant, i.e., the effect was observed in the present study of AsF_5 -doped $(CH)_x$ (Figure 26) and, qualitatively, with samples doped with iodine. Significant spectral changes, except for the curvature of saturation plots at high powers possibly suggesting thermal isomerization, were not observed in agreement with the reported stability of AsF_5 - and I_2 -doped $(CH)_x$ to temperatures of at least $100^\circ C$.

Microwave heating typically is the result of perturbations in rotational and or vibrational states in molecules in the presence of

fluctuating microwave fields. The phenomenon with regard to doped $(\text{CH})_x$ is somewhat puzzling. However, the observation¹⁹ that two new infrared modes appear in $(\text{CH})_x$ with increasing intensity upon doping, and that the frequencies are independent of the dopant, may be at least indirectly related to the microwave heating effect. Another possibility involves rotational states of the dopant molecules.

The microwave heating phenomenon is not likely to be of practical significance, although it is clear that caution should be exercised when performing what one might consider to be a "harmless" EPR saturation experiment on doped samples which are particularly sensitive to temperature.

Conclusions

EPR spectra of cis $(\text{CH})_x$ doped with AsF_5 suggest that radical cations initially form upon doping at least with the doping techniques employed. Spin-lattice relaxation times are consistent with the increase in paramagnetism upon light doping. The results are not necessarily inconsistent with a soliton doping mechanism involving non-magnetic charge carriers since the doping may very well be inhomogeneous. It is likely that AsF_5 , being a powerful electron acceptor, is non-discriminatory in terms of withdrawing electrons, i.e., neutral solitons or valence electrons. On the other hand, iodine is a weaker acceptor and preferentially removes neutral solitons accounting for the decrease in EPR signal intensity upon doping. The T_1 for the cis $(\text{CH})_x$ resonance is shortened upon doping, presumably due to quadrupole relaxation with

iodine species.

Microwave heating has been shown to be pronounced at high powers with heavily-doped samples, suggesting that caution should be exercised in applying saturation techniques to temperature-sensitive samples.

References

1. A.G. MacDiarmid and A.J. Heeger, Synth. Metals, 1, 101, (1979/80).
2. S.L. Hsu, A.J. Signorelli, G.P. Pez and R.H. Baughman, J. Chem. Phys., 69, 106 (1978).
3. W.R. Salaneck, H.R. Thomas, R.W. Bigelow, C.B. Duke, E.W. Plummer, A.J. Heeger and A.G. MacDiarmid, J. Chem. Phys., 72, 3674 (1980).
4. S. Lefrant, L.S. Lichtman, H. Temkin, D.B. Fitchen, D.C. Miller, G.E. Whitwell and J.M. Burlitch, Solid State Comm., 29, 191 (1979).
5. M. Hatano, S. Kambara and S. Okamoto, J. Polym. Sci., 51, S26 (1961).
6. H. Shirakawa, T. Ito and S. Ikeda, Makromol. Chem., 179, 1565 (1978).
7. A. Snow, P. Brant, D. Weber and N.L. Yang, J. Polym. Sci. Polym. Lett. Ed., 17, 263 (1979).
8. J.C.W. Chien, F.E. Karasz, G.E. Wnek, A.G. MacDiarmid and A.J. Heeger, J. Polym. Sci. Polym. Lett. Ed., 18, 45 (1980).
9. I.B. Goldberg, H.R. Crowe, P.R. Newman, A.J. Heeger and A.G. MacDiarmid, J. Chem. Phys., 70, 1132 (1979).
10. B.R. Weinberger, E. Ehrenfreund, A. Pron, A.J. Heeger and A.G. MacDiarmid, J. Chem. Phys., 72, 4749 (1980).
11. B.R. Weinberger, J. Kaufer, A. Pron, A.J. Heeger and A.G. MacDiarmid, Phys. Rev. B, 20, 1223 (1979).
12. Y. Tomkiewicz, T.D. Schultz, H.B. Broom, T.C. Clarke and G.B. Street, Phys. Rev. Lett., 20, 1532 (1979).
13. Y.W. Park, A.J. Heeger, M.A. Druy and A.G. MacDiarmid, in preparation.

14. C.P. Poole and H.A. Farach, Relaxation in Magnetic Resonance, Academic Press, New York, Chapter 3, (1971).
15. C.P. Poole, Electron Spin Resonance, Wiley-Interscience, New York, p. 263-304 (1967).
16. M. Nechtshein, F. Devreux, R.L. Greene, T.C. Clarke and G.B. Street, Phys. Rev. Lett., 44, 356 (1980).
17. J.C.W. Chien, F.E. Karasz and G.E. Wnek, Nature, 285, 391 (1980).
18. J.C.W. Chien, in preparation.
19. C.R. Fincher, Jr., M. Ozaki, A.J. Heeger and A.G. MacDiarmid, Phys. Rev. B, 19, 4140 (1979).
20. M.J. Kletter, T. Woerner, A. Pron, A.G. MacDiarmid, A.J. Heeger and Y.W. Park, J. Chem. Soc. Chem. Comm., 426 (1980)

C H A P T E R V I I I

POLYACETYLENE GELS AND VARIABLE DENSITY CONDUCTING POLYMERS

Recent studies have demonstrated that doping of polyacetylene, $(CH)_x$, with electron donors or acceptors yields materials whose electrical, optical and thermoelectric properties can be systematically varied over the full range from insulator to semiconductor to metal.¹⁻¹⁴ This remarkable control of electrical properties is particularly attractive in a polymer system where modified synthetic techniques combined with polymer processing can be expected to lead to a variety of novel and interesting mechanical forms.

Essentially all previous studies of the electrical properties of $(CH)_x$ have focused on the flexible films prepared by Shirakawa et al.¹⁵ These films are much more attractive for such studies as compared to powders which are the products of most other acetylene polymerizations.¹⁶⁻²⁰ Unfortunately, in all cases, the polymerization method itself determines the final form of polyacetylene due to its extreme intractability. Although the compaction of powders can be considered as a crude form of polymer processing, synthetic methods which produce $(CH)_x$ in forms other than conventional powders and films are considered to be important in order to extend the scope of the synthesis, processibility and electrical properties of polyacetylene.

An interesting method of $(CH)_x$ synthesis was recently reported by Hsu et al.²¹ employing $(C_5H_4)(C_5H_5)_3Ti_2$ as the polymerization catalyst in hexane. After exposure of this quiescent solution to acetylene for ca. 24 hours, a ca. 20 mm thick solvent-swollen, "gelatinous mass" of

$(CH)_x$ was formed. This "gel" was used to produce films by slow evaporation of the solvent and thus represented a new form of polymer processing of $(CH)_x$. Furthermore, solvent-swollen bulk polymer could be obtained if the catalyst solution was stirred. Treatment of both the gel and bulk polymer with iodine/hexane solutions followed by pumping to remove excess iodine yielded conductivities of ~ 25 and $\sim 1 \Omega^{-1} \text{cm}^{-1}$, respectively. The $(CH)_x$ gel appeared to be a potentially interesting material in that its swollen state might lead to more uniform doping, incorporation of stabilizers and more efficient post-polymerization "characterization" reactions such as hydrogenation.

In view of these anticipated advantages, a major research effort in our laboratory was directed toward the synthesis and characterization of polyacetylene gels. Unfortunately, the preparation of $(C_5H_4)(C_5H_5)_3Ti_2$ from bis-(cyclopentadienyl) titanium dichloride, or $(CP)_2TiCl_2$, and potassium naphthalide²² is rather difficult and the material is extremely air sensitive. Preparative attempts were not met with success. Efforts were then aimed at attempting to mimic the synthesis of $(C_5H_4)(C_5H_5)_3Ti_2$, or to perhaps obtain a similar derivative, through the low temperature reduction of $(CP)_2TiCl_2$ with Et_3Al . The advantage of such a procedure appeared to be direct preparation of the catalyst in a Schlenk tube followed by reaction with acetylene, thus eliminating catalyst purification and transfers.

A typical preparation involved addition of ca. 1.5 mL Et_3Al to a frozen (-196°C) solution of ca. 150 mg $(CP)_2TiCl_2$ in 50 mL toluene. Slow warming to room temperature over a period of several hours produced

a green solution, qualitatively analogous to that observed by Hsu et al.^{21,30} for $(C_5H_4(C_5H_5)_3Ti)_2$ in hexane. Exposure of this solution to acetylene (ca. 600 torr) for two days at $-78^\circ C$ gave a red, solvent-swollen "gel" of $(CH)_x$. Unfortunately, the polymer mass did not have much mechanical integrity, as pieces were easily broken away during washing with toluene. Small pieces of the gel could be squeezed between glass slides to yield silvery flakes although these were very brittle. Due to the poor integrity of these materials, the reaction was not pursued further.

Interestingly, the conversion of the red $(CH)_x$ gel to a shiny film after squeezing out solvent was reminiscent of the red \rightarrow copper change which cis $(CH)_x$ films undergo with the $Ti(OBu)_4/Et_3Al$ system during the first few minutes of the reaction (Chapter IV). The possibility seemed to exist that gel formation is perhaps a general phenomenon and not limited to the catalyst systems described previously. In $(CH)_x$ film synthesis, it is conceivable that a "gel-film" initially forms but quickly collapses to a shiny film since the small amount of toluene on the reactor wall is insufficient to maintain the film in a solvent-swollen state, especially at the high catalyst concentrations employed.

Consideration of such a possibility led to the formation of $(CH)_x$ gels having greatly improved mechanical integrity using the $Ti(OBu)_4/Et_3Al$ system at lower concentrations. These gels can be squeezed between glass slides to yield films or freeze-dried from benzene to produce low-density, "foam-like" $(CH)_x$. Thus, variable density $(CH)_x$ was prepared by novel "processing" techniques. Since the electrical con-

ductivity of $(\text{CH})_x$ is expected to be dependent upon sample density, or the number of fibrils per unit volume, it was of interest to quantitatively examine this relationship in the pristine material and doped derivatives. A preliminary account of this work has been published elsewhere.²³ In recent unpublished studies, Shirakawa²⁴ has independently shown that low-density $(\text{CH})_x$ can be synthesized by the use of gels and that the conductivity of this material can be modified by doping.

It should be noted that the term "gel" is perhaps misleading since the material cannot be rigorously defined as a colloidal dispersion of a solid in a solvent although it conveniently describes the macroscopic appearance and texture of the polymer. The term "macroporous solid" is probably more rigorously correct.

Experimental

Preparation of $(\text{CH})_x$ gels. The parent catalyst was prepared in a Schlenk tube by adding 1.7 mL $\text{Ti}(\text{OBu})_4$ and 2.7 mL Et_3Al to 20 mL of dry toluene (from the solvent still) at room temperature followed by aging at room temperature for ca. 30 minutes. This solution was diluted by transferring 1 mL of the catalyst to another Schlenk tube (the reaction vessel) containing ca. 40 mL dry toluene. The remaining parent catalyst was stored in a refrigerator at ca. 5° C for future reactions. The Schlenk tube containing the diluted catalyst was cooled to - 78° C and the solution was degassed for ca. 60 - 90 minutes on a vacuum line with occasional shaking. The quiescent catalyst solution, still at -78° C, was then exposed to acetylene (2 L bulb, ca. 650 - 700 torr initial pressure).

A reddish film (gel) appeared immediately on the surface of the catalyst solution and grew to a depth of 1 - 2 cm after ca. 18 hours. Typically, 250 - 350 torr of acetylene was consumed during the reaction. The upper surface and sides of the gel in contact with the glass reactor wall possessed a coppery luster although the bulk of the material was reddish-maroon.

Using Schlenk tube techniques, the gel (kept at -78°C) was covered with ca. 30 mL of dry toluene (or pentane), and then a syringe needle was used to free a small part of the gel from the glass reactor wall. The toluene/catalyst solution in the bottom of the reactor was removed through this opening with a syringe and was discarded. Care was taken not to allow the toluene level in the reactor to drop below the surface of the gel since partial drying and collapse of the gel can occur. This process was repeated until the toluene was colorless and then the gel was completely freed from the reactor wall using a syringe needle. The toluene-soaked gel was allowed to stand overnight at -78°C under argon.

The next day the toluene appeared yellow indicating that additional catalyst was extracted. The washing procedure was repeated until the toluene was colorless and the gel was again allowed to stand overnight in toluene at -78°C under argon. The following day, the toluene was usually colorless. However, if a yellow color was observed, the washing was repeated. The gel was stored in toluene at -78°C under argon until use.

Processing of $(\text{CH})_x$ gels; pressed films. The reaction vessel was warmed

to room temperature and taken into a glove bag. The gel was removed in one piece using forceps and then cut into sections with a razor blade. The material was quite flexible. Pieces of the gel which were not to be used immediately were placed back into the toluene to preserve the solvent-swollen state. Films were easily prepared by squeezing a piece of the toluene-soaked gel between glass slides coated with Teflon tape. The surfaces of the films displayed a dull golden or coppery luster. Solvent removal upon squeezing is completely irreversible. The thicknesses of the films were dependent upon the amount of manual pressure used to squeeze the gel. Typically, film thicknesses ranged from 0.05 - 1.0 mm. The densities of the films, determined from weight and bulk dimensions, were 0.2 - 0.4 g/cc depending upon the final thickness.

The films were easily handled with forceps although they tore easily with small stresses, unlike films prepared directly using higher catalyst concentrations. The films possessed a flaky, mica-like texture. Infrared spectra of thin films from gels prepared and washed at -78°C indicated that the cis isomer content was ca. 85% as determined by the method of Shirakawa et al.¹⁵

Removal of the toluene from the original gel by pumping at room temperature resulted in reduction of the sample volume by about one-third to one-half and yielded a dull maroon solid. The solid, as the pressed films, did not reabsorb toluene to regenerate the gel.

Processing of $(\text{CH})_x$ gels; foam-like $(\text{CH})_x$. The low density foam-like material was prepared from the original toluene-soaked gel by first removing as much toluene as possible with a syringe while still keeping

the gel "wet" followed by addition of ca. 30 mL dry benzene using Schlenk tube techniques. This process was repeated ca. eight times so as to replace the toluene in the gel with benzene. The gel was kept at room temperature during these washings. After the final benzene wash, ca. 50 mL additional benzene was added and the gel was allowed to stir gently with a magnetic bar overnight at room temperature. The benzene wash was repeated on the following day (ca. eight 30 mL portions). The Schlenk tube was then placed in an ice bath to completely freeze the benzene (mp $\sim 5.5^{\circ}\text{C}$) and then connected to a vacuum line. The frozen benzene was then sublimed by pumping. Failure of the benzene to freeze suggested that solvent exchange was incomplete, although reduction of the ice bath temperature by addition of, e.g., NaCl usually induced freezing. However, if this did not remedy the situation, the solvent exchange was repeated.

The freeze-dried, foam-like $(\text{CH})_x$ possessed essentially the same dimensions as the original gel "plug". The surface displayed a dull, silvery-gray luster while the interior possessed a maroon coloration. The material was extremely light and spongy and possessed typical densities in the range 0.02 - 0.04 g/cc. A maroon-to-black color change was observed upon cis-trans isomerization at ca. 180°C (in vacuo).

Elemental analyses of materials prepared by the procedures described above indicated high purity and agreed exactly with the formula $(\text{CH})_x$.*

* Galbraith Laboratories, Inc., Knoxville, Tenn. Anal. Calcd. for $(\text{CH})_x$: C, 92.26%; H, 7.74%. Found: C, 92.03%; H, 7.56% (Total: 99.59%).

Variable density $(CH)_x$. In order to obtain additional $(CH)_x$ bulk densities within the limits of pressed films in which the solvent was essentially completely squeezed out (ca. 0.2 - 0.4 g/cc) and the foam-like material (ca. 0.02 - 0.04 g/cc), toluene-soaked gels were pressed to various thicknesses and then were solvent-exchanged with benzene and freeze-dried as described above. Since the relationship between manual squeezing of the gel and the final density was ambiguous, it was difficult to predict a priori the density to be obtained at any "degree of squeezing" of the gel.

Observations concerning gel preparations. It is worthwhile to note that if the parent catalyst (1.7 mL $Ti(OBu)_4$, 2.7 mL Et_3Al , 20 mL toluene) was prepared at $-78^\circ C$ (Chapter IV), aged at room temperature and used immediately, there was a tendency to produce "thicker" gels which were more difficult to press to thin films as compared to gels obtained from a catalyst solution prepared at room temperature. Also, the density of the foam-like material was occasionally two-to-three times greater with the former preparation. These observations suggest that the catalyst prepared at low temperature was more active, resulting in a thicker, more dense $(CH)_x$ gel. On the other hand, permitting this catalyst to stand under argon in a refrigerator ($\sim 5^\circ C$) for several weeks seemed to give a material more like that obtained from a catalyst prepared directly at room temperature suggesting that prolonged aging results in a small decrease in activity. It is emphasized that the above statements are not meant to be absolute, but merely reflect a series of very general observations. It should be noted that all polymers studied in

this work were synthesized using catalyst solutions prepared at room temperature.

Exposure of acetylene to stirred catalyst solutions resulted in the rapid formation of red, solvent-swollen particulate (bulk) polymer. After washing the suspension several times with methanol/HCl and gradual removal of excess methanol in vacuo, continuous silvery films of $(CH)_x$ were occasionally formed on the bottom of the reactor. Furthermore, filtering of the particulate/catalyst suspension in a Buchner funnel and washing with methanol/HCl yielded a golden-silvery $(CH)_x$ "film" on the filter paper. Exposure of a piece of this surface-impregnated material to iodine vapor for one hour (assuming the $(CH)_x$ surface film thickness to be $\sim 25 \mu m$) afforded a conductivity in excess of $200 \Omega^{-1} cm^{-1}$. Although these materials were not further investigated, the techniques described above suggest yet additional routes to polymer processing of $(CH)_x$.

Finally, it should be noted that a recent perusal of the literature discovered an observation by Nicolescu and Angelescu²⁵ concerning the polymerization of acetylene at $-78^\circ C$ using low concentrations of the $Ti(OBu)_4/Et_3Al$ system. These workers reported that the resulting polymers "soak up large quantities of solvent, thus attaining elasticity, which is lost again after removal of the solvent." Thus, the techniques reported in this Chapter concerning the preparation of $(CH)_x$ gels might be considered to be a rediscovery of their observation, although no further studies by these workers were performed with the material.

Doping and electrical measurements. Doping of samples with iodine and

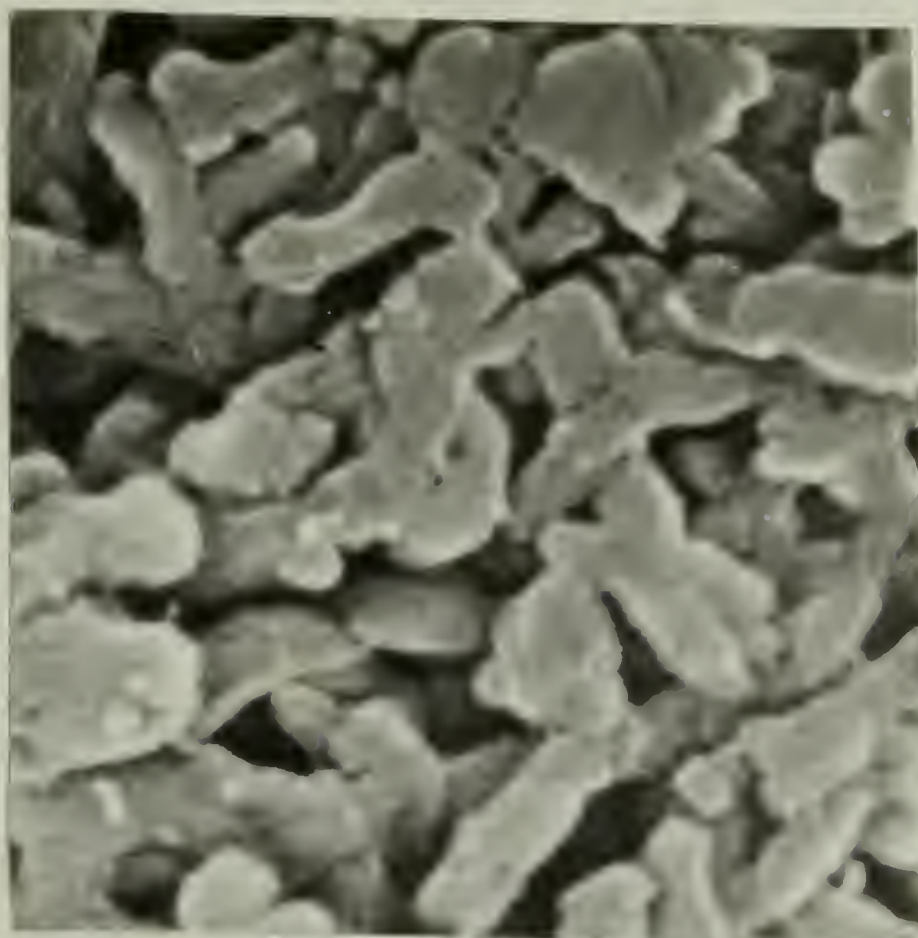
AsF_5 and measurements of electrical conductivity, temperature dependence of the conductivity and thermopower (Table 5 and Figure 32) were carried out by M. A. Druy and Y. W. Park at the University of Pennsylvania. Doping techniques were similar to those described in Chapter II; iodine doping employed the inert gas flow method. Conductivity measurements employed standard four-probe techniques. Experimental details of the thermopower measurements are described elsewhere.¹¹ The data shown in Figure 31 were obtained in our laboratory using the flow method for iodine doping and four-probe techniques (Chapter III). Densities of the materials (before doping) were determined from weight and bulk dimensions. Dopant concentrations were determined from the weight uptake of a reference sample. All conductivities reported were the saturation values.

Morphology. Electron micrographs of pressed film and foam-like $(\text{CH})_x$ samples were obtained using a JEOL 100 CX Temscan electron microscope.

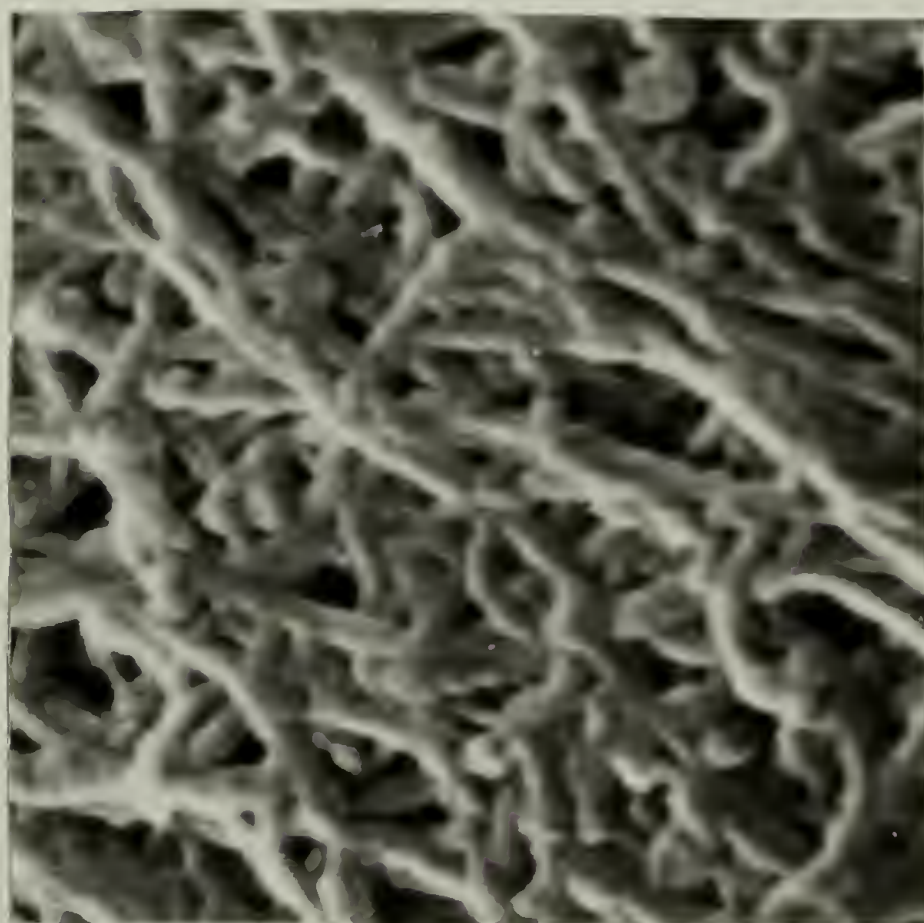
Results

Electrographs of the surface of pressed film ($\rho \sim 0.3 \text{ g/cc}$) and the interior of foam-like ($\rho \sim 0.04 \text{ g/cc}$) $(\text{CH})_x$ samples are shown in Figures 30a and 30b, respectively. The morphology of the pressed film surface is quite similar to that of the shiny side of as-grown $(\text{CH})_x$ films.^{15,26} The characteristic matted fibril morphology of the dull side of as-grown films is preserved in the foam-like material although the typical fibril diameter appears to be $600 - 800 \text{ \AA}$, i.e., somewhat larger than the ca. 200 \AA fibril diameter commonly observed with as-

Figure 30. Electron micrographs of (A) pressed film and
(B) foam-like $(CH)_x$ (x50,000)



A

 $\overline{\quad}$
 $0.1\mu m$ 

B

TABLE 5

<u>Material</u>	<u>Property</u>	<u>"Foam-like" (CH)_x</u>	<u>Pressed (CH)_x Film</u>
	<u>y</u>	<u>magnitude</u>	<u>y</u> <u>magnitude</u>
<u>trans^a (CH)_x</u> <u>(undoped)</u>	σ (RT) S (RT) Density ^c	-	-
		$1.08 \times 10^{-6} \text{ ohm}^{-1} \text{ cm}^{-1}$ +900 $\mu\text{V}/^\circ\text{K}$ 0.02-0.04 gm/cm ³	$7.9 \times 10^{-5} \text{ ohm}^{-1} \text{ cm}^{-1}$ ($\Delta E \sim 0.25 \text{ eV}$) +920 $\mu\text{V}/^\circ\text{K}$ 0.4 gm/cm ³
<u>[CHI_y]_x</u>	σ (RT) S (RT) Density ^b	0.06	0.05
		$8.14 \text{ ohm}^{-1} \text{ cm}^{-1}$ +18.7 $\mu\text{V}/^\circ\text{K}$ 0.02-0.04 gm/cm ³	$350 \text{ ohm}^{-1} \text{ cm}^{-1}$ +18.4 $\mu\text{V}/^\circ\text{K}$ 0.4 gm/cm ³
<u>[CHI_y]_x</u>	σ (RT) S (RT) Density ^b	-	0.05
		---	$11.2 \text{ ohm}^{-1} \text{ cm}^{-1}$ - 0.1 gm/cm ³
<u>[CH(AsF₅)_y]</u>	σ (RT) S (RT) Density ^b	0.08	0.06
		$81.3 \text{ ohm}^{-1} \text{ cm}^{-1}$ +8 $\mu\text{V}/^\circ\text{K}$ 0.02-0.04 gm/cm ³	$176 \text{ ohm}^{-1} \text{ cm}^{-1}$ +8.9 $\mu\text{V}/^\circ\text{K}$ 0.1 gm/cm ³

^a Isomerized by heating at 180° C for 2 hr. in vacuo in a sealed tube.

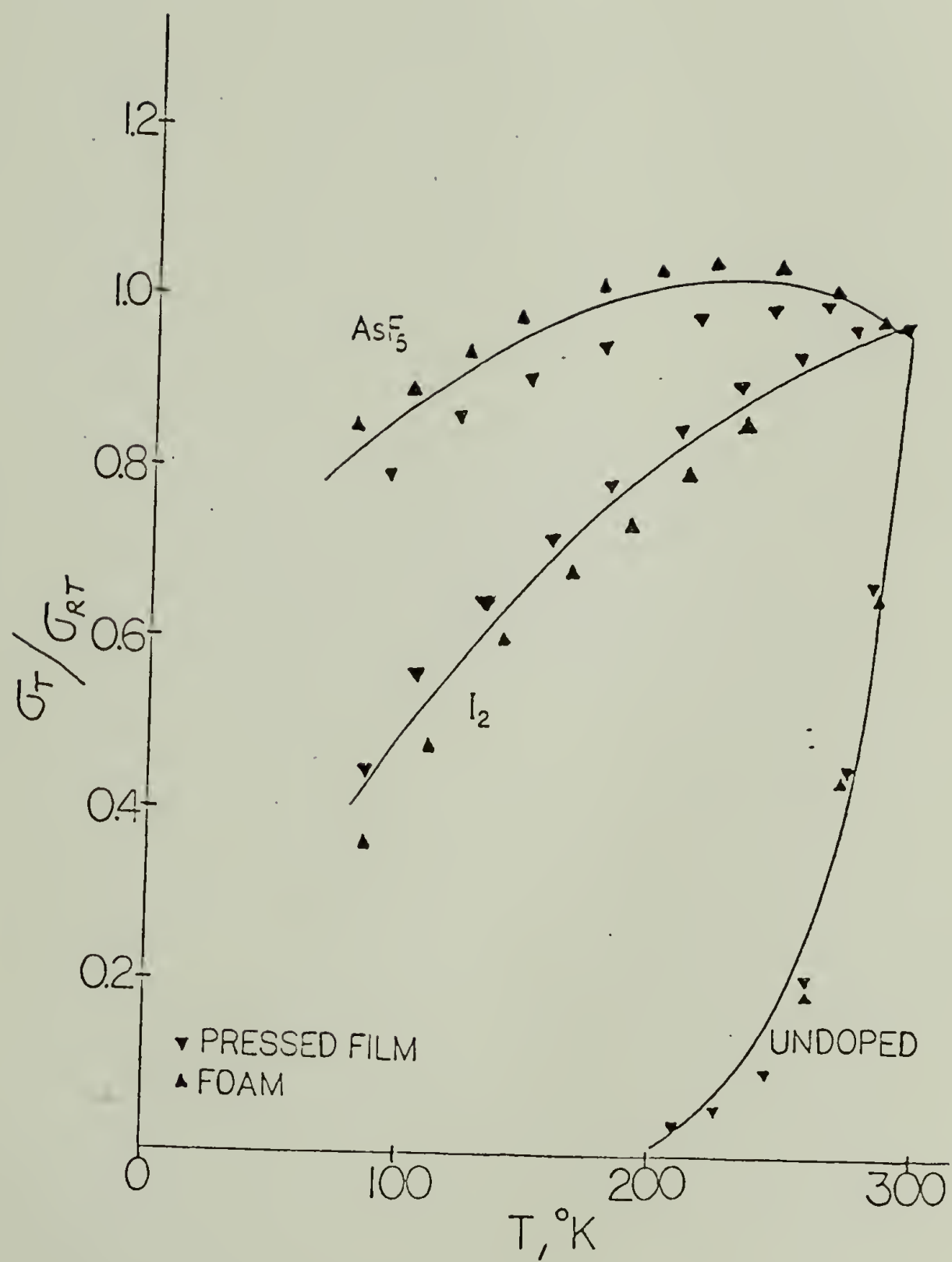
^b Density of parent film before doping.

^c Density of film before isomerizing.

Figure 31. Plot of conductivity vs. density for
iodine-doped $(CH)_x$.



Figure 32. Normalized temperature dependence of the conductivity for undoped and doped pressed film and foam-like $(\text{CH})_x$.



grown films.

Electrical conductivities and thermopower values of selected pristine and doped $(\text{CH})_x$ samples having various initial densities are given in Table 5. The data indicate that while the conductivity is very sensitive to the density, the thermopower values are essentially independent of density. The relationship between electrical conductivity and density for several $(\text{CH})_x$ samples doped with iodine is plotted in Figure 31. The results indicate that the conductivity increases with increasing density of the polymer.

The temperature dependencies of the conductivities of pristine pressed film and foam-like $(\text{CH})_x$ and corresponding samples doped with iodine and AsF_5 are shown in Figure 32. In each case the normalized conductivity depends primarily upon the dopant and the dopant concentration although the absolute value depends critically on the density of $(\text{CH})_x$.

Discussion

Morphology. The larger fibril diameter (ca. 600 - 800 Å) of the foam-like material as compared to as-grown films (ca. 200 Å) may suggest that the fibrils are slightly swollen in their nascent state during the polymerization and that subsequent freeze-drying maintains the fibril size characteristic of this swelling. However, this rationalization is purely speculative. The surface morphology of the pressed film sample (Figure 30b) is quite similar to that of the "shiny" side of as-grown $(\text{CH})_x$ film.²⁶ The fibrils appear to be flattened and merged into larger entities.

Consideration of the similar morphologies of as-grown film, pressed film and foam-like $(\text{CH})_x$ and the following observations, namely, a red \rightarrow copper color change in the initial stages of the synthesis of as-grown cis $(\text{CH})_x$ film (Chapter IV) and a similar color change upon preparing pressed films from gels, leads to the conclusion that gel formation is operative in the synthesis of as-grown films. At the high catalyst concentration employed, however, a great deal of polymer is able to rapidly form. Thus, a combination of the large number of fibril entanglements and the small amount of solvent present in these regions leads to a "desolvation" of the gel with a concomitant collapse to a film. This hypothesis is supported by the additional observation that the macroscopic fracture surface of relatively thick (ca. 180 μm) as-grown cis $(\text{CH})_x$ film displays a dull maroon coloration characteristic of the interior of both cis pressed film and foam-like $(\text{CH})_x$.

It might be argued on the basis of previous observations concerning the fibrillar morphology of other materials such as polyethylene that fibril formation is the exclusive result of the use of various heterogeneous catalysts.²⁷⁻²⁹ This necessarily assumes that the typically homogeneous catalyst system based on $\text{Ti}(\text{OBu})_4/\text{Et}_3\text{Al}$ acts as a heterogeneous system. While such behavior might be envisioned at the concentrations employed in the preparation of as-grown films ($[\text{Ti}] \sim 0.25 \text{ M}$), it is unlikely to occur at the concentrations used in gel synthesis ($[\text{Ti}] \sim 6.2 \times 10^{-3} \text{ M}$). The latter catalyst solutions in toluene are transparent and deep-orange in color and show no indication of Tyndall scattering due to the presence of colloidal material. Further-

more, a fibrillar $(CH)_x$ morphology has also been observed using the $(C_5H_4)(C_5H_5)_3Ti_2$ catalyst.³⁰ This compound affords transparent green solutions in hexane and is considered to be truly homogeneous. It appears that at least with these two catalyst systems acetylene polymerizes directly into fibrils, possibly due to the rigidity of its conjugated polymer backbone. However, upon consideration of the many types of coordination catalysts which may polymerize acetylene, particular catalyst systems may very well afford morphologies other than the fibrillar type described above. The important relationship between morphology and electrical conductivity in doped polyacetylene is anticipated to merit careful study in order to more precisely define structural variables which influence electrical transport properties.

Electrical transport studies. All previous investigations of the electrical properties of $(CH)_x$ and doped derivatives have focused on the as-grown film, having a typical bulk density of 0.4 g/cc as compared to 1.2 g/cc obtained from floatation measurements.³¹ Thus, the volume-filling fraction of fibrils, f , is approximately one-third for this material. In contrast, f is $\sim 0.015 - 0.03$ for the foam-like $(CH)_x$ whereas the variable thickness pressed films have intermediate values of f . It may be anticipated that the conductivity of $(CH)_x$ will decrease as the sample density decreases since the resistance of the sample is inversely proportional to the cross-sectional area of the conducting elements and the number of such elements per unit volume decreases as the density of the material decreases. The interfibril contacts are also expected to contribute to the observed values of the electrical conduc-

tivity.

Since the thermopower (S) is a zero-current transport coefficient, the interfibril contacts should be unimportant, allowing evaluation of the intrinsic electrical transport properties of variable density $(\text{CH})_x$. Moreover, since S can be viewed as a measure of the entropy per carrier, the results depend only upon the properties of the conducting fibrils and not on the number of fibrils per unit volume. As indicated in Table 5, the thermopower of the undoped polymer is insensitive to density; the foam-like and pressed film materials yield thermopower values of approximately $+900 \mu\text{V/K}$. Any variations are comparable with the typical variations observed earlier¹¹ in as-grown film samples from different synthetic preparations. It should be noted that the sign of S is positive for these materials, indicating that they are p-type semiconductors in agreement with previous results concerning as-grown films. Similarly, after heavy doping the results are insensitive to density with values for the foam-like material, pressed film and as-grown films in good agreement for each dopant. Comparison with the variation in S as a function of dopant concentration studied in detail earlier¹¹ leads to the conclusion that the heavily doped samples are all metallic. The thermopower results imply that the various forms of the doped and undoped polymers are microscopically identical. The lower-density materials simply consist of fibrils at a smaller filling fraction f .

The electrical conductivity data are consistent with this conclusion and demonstrate the expected dependence of conductivity on density. Thus, the conductivity of the undoped foam-like material is nearly two

orders of magnitude below that of the high density pressed film. Although there may be some increase in the interfibril contact resistance, the reduction in f is of major importance. This conclusion is strengthened by the observation that the activation energy for electrical conductivity (obtained from the temperature variation of the conductivity near room temperature) is 0.25 eV for both samples and is comparable to the value typically obtained from as-grown films.^{5,32}

Similar results are obtained with the heavily doped polymers. As indicated in Table 5, the conductivity ($176 \Omega^{-1}\text{cm}^{-1}$) of $[\text{CH}(\text{AsF}_5)_{0.06}]_x$, prepared from the low density pressed $(\text{CH})_x$ film ($\rho = 0.1 \text{ g/cc}$), is correspondingly lower than that ($560 \Omega^{-1}\text{cm}^{-1}$ and $1200 \Omega^{-1}\text{cm}^{-1}$) of $[\text{CH}(\text{AsF}_5)_{0.14}]_x$ ³ and $[\text{CH}(\text{AsF}_5)_{0.10}]_x$,³³ respectively, prepared from as-grown cis $(\text{CH})_x$ film ($\rho = 0.4 \text{ g/cc}$). Furthermore, the room temperature conductivity of $(\text{CHI}_{0.06})_x$ increases by a factor of forty in going from the low density foam-like material to the high density pressed film. In all cases, the resulting conductivity increases with the filling fraction of fibrils. This relationship is demonstrated for iodine-doped samples in Figure 31. Although dopant compositions were not determined, all samples were doped to the saturation conductivities.

The temperature dependencies of the conductivities of several samples, both doped and undoped, are shown in Figure 32. In each case the normalized temperature depends primarily on the dopant and dopant concentration, whereas the absolute value depends critically on the density (Table 5). The foam-like and pressed film samples are typical of the behavior observed earlier in as-grown films.¹⁻¹¹ For metallic sam-

ples heavily doped with iodine, σ decreases slowly with decreasing temperature. For metallic samples heavily doped with AsF_5 , σ remains nearly constant upon cooling, increasing slightly between room temperature and 250 K, then decreasing slowly as the temperature is lowered.

Conclusions

The versatility of the $\text{Ti}(\text{OBu})_4/\text{Et}_3\text{Al}$ catalyst system in the synthesis of novel forms of polyacetylene through the use of a gel as an intermediate step has been demonstrated. Polymer processing techniques have been developed for the synthesis of variable density $(\text{CH})_x$. The fibrillar morphology typical of as-grown films is preserved in freeze-dried, foam-like $(\text{CH})_x$ although the characteristic fibril diameter of the latter material is somewhat larger (ca. 600 - 800 Å) than that commonly observed in as-grown films.

Thermopower studies indicate that the various forms of the undoped and doped polymers are microscopically identical. The lower density materials simply consist of fibrils at a smaller filling fraction f . The electrical conductivity studies yield results consistent with this conclusion. The resulting doped and undoped $(\text{CH})_x$ polymers can be viewed as effective media in which the d.c. electrical transport is determined by the volume-filling fraction of conducting fibrils. Thus, experimentally-controlled density variation is yet another mechanism by which fine-tuning of the electrical properties of this interesting class of materials can be accomplished.

Potential applications of low-density, foam-like $(\text{CH})_x$, include

the use of electrically conducting and thermally insulating materials in refrigeration systems and use as microwave absorbers.³⁴ Such applications are currently under investigation at the University of Pennsylvania.

References

1. C. K. Shiang, C. R. Fincher, Jr., Y. W. Park, A. J. Heeger, H. Shirakawa, E. J. Louis, S. C. Gau and A. G. MacDiarmid, Phys. Rev. Lett., 39, 1098 (1977)
2. H. Shirakawa, E. J. Louis, A. G. MacDiarmid, C. K. Chiang and A. J. Heeger, J. C. S. Chem. Comm., 578 (1977)
3. C. K. Chiang, M. A. Druy, S. C. Gau, A. J. Heeger, E. J. Louis, A. G. MacDiarmid, Y. W. Park and H. Shirakawa, J. Amer. Chem. Soc., 100, 1013 (1978)
4. C. K. Chiang, S. C. Gau, C. R. Fincher, Jr., Y. W. Park, A. G. MacDiarmid and A. J. Heeger, Appl. Phys. Lett., 33, 18 (1978)
5. C. K. Chiang, Y. W. Park, A. J. Heeger, H. Shirakawa, E. J. Louis and A. G. MacDiarmid, J. Chem. Phys., 69, 5098 (1978)
6. Y. W. Park, M. A. Druy, C. K. Chiang, A. G. MacDiarmid, A. J. Heeger, H. Shirakawa and S. Ikeda, J. Polym. Sci., Polym. Lett. Ed., 17, 195 (1979)
7. T. C. Clarke, R. H. Geiss, J. F. Kwak and G. B. Street, J. Chem. Soc. Chem. Comm., 489 (1978)
8. J. F. Kwak, T. C. Clarke, R. L. Greene and G. B. Street, Bull. Am. Phys. Soc., 23, 56 (1978)
9. L. R. Anderson, G. Pez and S. L. Hsu, J. Chem. Soc. Chem. Comm., 1066 (1978)
10. S. Hsu, A. Signorelli, G. Pez and R. Baughman, J. Chem. Phys., 69, 106 (1978)
11. Y. W. Park, A. Denenstein, C. K. Chiang, A. J. Heeger and A. G.

- MacDiarmid, Solid State Comm., 29, 747 (1979)
12. C. R. Fincher, Jr., D. L. Peebles, A. J. Heeger, M. A. Druy, Y. Matsumura, A. G. MacDiarmid, H. Shirakawa and S. Ikeda, Solid State Comm., 27, 489 (1978)
 13. C. R. Fincher, Jr., M. Ozaki, A. J. Heeger and A. G. MacDiarmid, Phys. Rev. B., 19, 4140 (1979)
 14. C. R. Fincher, Jr., M. Ozaki, M. Tanaka, D. Peebles, L. Lauchlan, A. J. Heeger and A. G. MacDiarmid, Phys. Rev. B., 20, 1589 (1979)
 15. T. Ito, H. Shirakawa and S. Ikeda, J. Polym. Sci., Polym. Chem. Ed., 12, 11 (1974)
 16. M. Hatano, S. Kambara and S. Okamoto, J. Polym. Sci., 51, S26 (1961)
 17. L. B. Luttinger, J. Org. Chem., 27, 1591 (1962)
 18. W. E. Daniels, J. Org. Chem., 29, 2936 (1964)
 19. D. J. Berets and D. S. Smith, Trans. Faraday Soc., 64, 823 (1968)
 20. F. D. Kleist and N. R. Byrd, J. Polym. Sci. A-1, 7, 3419 (1969)
 21. S. L. Hsu, A. J. Signorelli, G. P. Pez and R. H. Baughman, J. Chem. Phys., 69, 106 (1978)
 22. D. P. Pez, J. Amer. Chem. Soc., 98, 8072 (1976)
 23. G. E. Wnek, J. C. W. Chien, F. E. Karasz, M. A. Druy, A. G. MacDiarmid, Y. W. Park and A. J. Heeger, J. Polym. Sci., Polym. Lett. Ed., 17, 779 (1979)
 24. H. Shirakawa and S. Ikeda, IBM Symposium on Conducting Polymers, March 29-30, 1979 and ACS/CSJ Chemical Congress, Honolulu, Hawaii, April 1-6, 1979
 25. I. V. Nicolescu and Em. Angelescu, J. Polym. Sci. Pt. A, 3, 1227

(1965)

26. F. E. Karasz, J. C. W. Chien, R. Galkiewicz, G. E. Wnek, A. J. Heeger and A. G. MacDiarmid, Nature, 282, 286 (1979); Chapter V, this dissertation.
27. J. Y. Guttman and J. E. Guillet, Polym. Preprints, 30, 177 (1970)
28. P. Ingram and A. Schindler, Makromol. Chem., 111, 267 (1968)
29. J. Wristers, J. Polym. Sci., Polym. Phys. Ed., 11, 1601 (1973)
30. S. L. Hsu, private conversation
31. T. Ito, H. Shirakawa and S. Ikeda, Kobunshi Ronbunshu, Eng. Ed., 5, 470 (1976)
32. H. Shirakawa, T. Ito and S. Ikeda, Makromol. Chem., 179, 1565 (1978)
33. A. G. MacDiarmid and A. J. Heeger, Synthetic Metals, 1, 101 (1979/1980)
34. A. Feldblum, Y. W. Park, A. J. Heeger, A. G. MacDiarmid, G. W. Wnek, F. E. Karasz and J. C. W. Chien, J. Polym. Sci., Polym. Lett. Ed., submitted for publication.

CHAPTER IX

ACETYLENE - METHYLACETYLENE COPOLYMER FILMS

Polyacetylene, $(CH)_x$, is the simplest linear conjugated polymer. Recent demonstration^{1,2} of the attainment of metal-like properties of $(CH)_x$ upon chemical doping has stimulated fundamental interest in this material. Polyacetylene, as well as other conducting polymers,³⁻⁵ may be anticipated to have tremendous technological potential in view of the light weight advantages and low production costs of polymers in general as compared to other materials. However, the intractability of most conducting polymer systems precludes rigorous characterization at the molecular level and attempts at processing by conventional methods. Thus, these materials pose complex problems in the context of both science and technology.

Fortunately, polymers are quite versatile. Polymerization of new monomers or post-polymerization reactions on existing materials can be expected to yield novel structures having interesting physical and mechanical properties. Various morphologies and degrees of crystallinity may be the result of subtle changes in backbone structure. Such modifications are important with regard to their influence on electrical transport properties. Furthermore, considering the intensive investigations currently underway concerning polyacetylene, modifications of this particular material are of a timely significance.

The simplest approach toward obtaining a "modified" $(CH)_x$ backbone is the polymerization of substituted acetylenes (e.g., methyl-⁶ and

phenylacetylene⁷). The resulting polymers are attractive in view of their solubility in common organic solvents. However, upon doping, electrical conductivities are several orders of magnitude smaller than those of doped $(\text{CH})_x$. Apparently, substituents promote a twisting of the polymer backbone in order to relieve steric interactions and, as a result, the effective conjugation length is considerably reduced due to poor π -orbital overlap. Recently, significantly improved conductivity has been reported upon doping of poly(1,6-heptadiyne).⁸ In this case, the "substituent" is actually a ring which bridges the polymer chain and presumably helps to fix the chain in an approximately planar configuration.

An interesting post-polymerization reaction which affords a partially substituted polyacetylene has been reported by Kletter and coworkers.⁹ They found that appropriate thermal treatment of bromine-doped $(\text{CH})_x$ afforded partial replacement of hydrogen by bromine on the polymer backbone. Subsequent doping of this material with I_2 or AsF_5 afforded conductivities two-to-three orders of magnitude lower than the corresponding doped $(\text{CH})_x$.

An alternative approach to $(\text{CH})_x$ derivatives is through copolymerization of acetylene with various monomers. Experimental control of physical properties through judicious choice of the comonomer composition is an attractive aspect of this method. It might be anticipated, for example, that the high conductivity characteristic of doped polyacetylene and the solubility of an appropriate polymer can be combined into one material through copolymerization. In addition, this approach may provide answers to fundamental questions concerning the dependence of

conductivity on the nature and the amount of defects introduced onto the $(\text{CH})_x$ backbone.

With the above considerations in mind, a portion of this dissertation work was focused on the synthesis and characterization of acetylene-methylacetylene copolymers. Methylacetylene was selected as the comonomer for three reasons. First, the homopolymer is soluble in common organic solvents. Second, the small methyl substituent was not expected to significantly disrupt interchain interactions, allowing electrical transport to be determined primarily by structural intrachain properties. Finally, methylacetylene is a gas above ca. -25°C (1 atm.) and allows the use of techniques developed for $(\text{CH})_x$ film synthesis to be applied to copolymer film preparations. The preparation of films was considered to be important in order to more easily compare electrical properties to those of the rather well-characterized $(\text{CH})_x$ films.

It should be noted that recently Wegner et al.¹⁰ reported the synthesis of copolymers of acetylene and 1-hexyne. These workers found that λ_{max} increased (i.e., the band gap decreased) with increasing acetylene content in the copolymers. However, chemical doping of these materials has not yet been investigated.

Experimental

The purifications of solvents and gases used in the copolymer film preparations have been described in Chapter II.

Comonomer feed. A 2 L storage bulb was used to contain the comonomer feed gases. The total pressure of the gas mixture in the bulb was ca.

720 torr for all copolymer preparations. The gases were assumed to be ideal and mole ratios were determined simply by the partial pressures of the gases in the bulb.

Typically, after pumping the bulb and the sub-manifold of the vacuum line, methylacetylene was allowed to fill the bulb to a pressure a few torr above that desired for a particular feed composition. For example, for a 1:1 acetylene/methylacetylene feed, the bulb was filled to a pressure just above 350 torr. The slight excess was employed to compensate for potential false pressure readings due to small amounts of air which may enter the system during the gas transfer. The gas was dried as described in Chapter II and then was condensed into the cold finger of the bulb (-196°C) followed by pumping to remove traces of air. After isolating the sub-manifold from the remainder of the vacuum line, the methylacetylene was warmed to room temperature and small amounts of the gas were pumped away in order to achieve the desired pressure. The gas was then condensed back into the bulb and the stopcock of the bulb was closed. Next, the connection between the acetylene purification train and the sub-manifold was pumped while the train was purged (Chapter II). After isolating the sub-manifold from the remainder of the vacuum line and expanding the methylacetylene in the bulb into the sub-manifold, acetylene was allowed to enter the system to bring the total gas pressure to ca. 720 torr. The gas mixture was then condensed into the cold finger of the bulb (-196°C) and the bulb was pumped to remove traces of air. The stopcock to the bulb was then closed and the gases were allowed to warm to room temperature. It should be noted

that if a relatively large (> 5 torr) amount of air was observed in the system after admission of the acetylene (as determined by the failure of the manometer arm to register "vacuum" upon condensing the gas mixture), additional acetylene was admitted following degassing and warming of the gas mixture to room temperature. The mixture was then once again degassed.

The acetylene/methylacetylene mixture was additionally degassed at least once immediately prior to the polymerization reaction.

Copolymer film syntheses. The techniques described in Chapter IV concerning $(CH)_x$ film preparations provided the foundation for the synthesis of copolymer films. However, a considerable amount of time was expended in the development of specific synthetic methods in order to obtain reasonable and workable copolymer films. Thus, a brief description of the salient features of the initial film preparations is worthwhile before proceeding with an account of the most successful method.

Initial film syntheses employed catalyst solutions prepared as described in Chapter IV. Polymerizations were carried out at -10°C (ice-salt bath) in order to preclude condensation of the methylacetylene fraction of the comonomer feed (b.p. methylacetylene ca. -23°C at 1 atm.). The catalyst solution at -10°C was considerably less viscous than that at -78°C . Thus, upon wetting the reactor walls with the catalyst, the solution was observed to "thin out" very rapidly. As a result, extremely thin (ca. $15 - 40\ \mu\text{m}$) copolymer films were obtained, even after immediate introduction of the feed gases. In many cases, the film could not be removed from the reactor walls in workable pieces;

rather, thin "flakes" were usually obtained. In addition, pentane was found to be a poor solvent for removal of soluble residues. It was observed that the colorless pentane in the reactor, after what was believed to be the completion of the washing process (ca. 12 cycles), slowly assumed a yellow-orange color upon standing at room temperature.

The most serious problem was clearly the inability to obtain large sections of free-standing film. It appeared evident that the viscosity of the catalyst solution needed to be increased. Addition of various amounts of mineral oil to the catalyst solution did yield an observable increase in viscosity although the quality of the films produced did not improve. The use of a more concentrated catalyst solution, however, did afford reasonable amounts of free-standing films. Apparently, the viscosity of the $\text{Ti}(\text{OBu})_4$ component was responsible for the formation of the thicker and more tractable films.

This more concentrated catalyst was prepared by adding 2.5 mL of $\text{Ti}(\text{OBu})_4$ to 10 mL of toluene (previously distilled into the reactor from a solvent storage tube) at 0° C. Next, 4.0 mL of Et_3Al was added dropwise to this solution. All transfers employed Schlenk tube techniques. The dark orange-brown catalyst solution was then allowed to age at room temperature for 30 minutes. Meanwhile, the comonomer mixture in the bulb was degassed one final time.

The reactor was attached to the vacuum line via flexible stainless steel tubing and the catalyst solution was cooled to -78° C. The solution was degassed for 30 - 60 minutes while occasionally agitating the reactor. The reactor was then warmed to room temperature and immersed

up to the stopcock "arms" in an ice-salt bath (ca. -10°C). After shaking the reactor in order to coat the walls with the catalyst solution, the feed gas mixture was immediately admitted. Typical reaction times were 20 - 40 minutes.

After the desired time period, the reactor was disconnected from the vacuum line and argon was introduced. The catalyst solution remaining at the bottom of the reactor was removed with a syringe and discarded. [It was observed that this solution was occasionally somewhat viscous if the methylacetylene content of the feed gas was high (i.e., $> 1:1$) suggesting that polymerization occurred in the solution. In a few cases, attempts were made to isolate this polymer according to techniques to be described shortly concerning the preparations and isolation of poly(methylacetylene).]

The reactor was closed under argon, cooled to -78°C and pumped. In view of the poor solubility of low molecular weight polymer products in pentane at -78°C , toluene was chosen as a washing solvent. Thus, ca. 30 mL toluene was distilled into the reactor and the films were washed as described in Chapter IV. It was observed that a tremendous amount of deep red-colored soluble material was removed during the toluene wash, the amount of which increased with increasing methylacetylene content in the feed. Upon warming of the toluene in the reactor to room temperature the color was usually deeper. The films were typically subjected to 15 - 20 wash cycles over a period of two days. Even after this extensive treatment, the toluene was occasionally observed to be orange and probably the result of continued extraction of low molecular

weight polymer. Due to the considerable time expenditure involved, the washing was not carried further than ca. 20 cycles.

The copolymers were handled primarily in a drybox although a glove bag was used on occasion. The films were found to peel off the reactor walls more readily when wetted with solvents such as pentane or toluene. The films were stored in Schlenk tubes in vacuo or under nitrogen at -78°C .

For comparative purposes, a $(\text{CH})_x$ film was also prepared using the method described above. The qualitative characteristics of the various polymer films will be described in the next section of this Chapter.

Preparation of poly(methylacetylene), $(\text{C}_3\text{H}_4)_x$.⁶ The catalyst solution was prepared in a Schlenk tube at room temperature by adding 1.7 mL of $\text{Ti}(\text{OBu})_4$ and 2.7 mL of Et_3Al to 20 mL of dry toluene using syringe and Schlenk tube techniques. A stir bar was also placed in the tube. A mercury bubbler was connected via butyl rubber tubing to the balljoint of the Schlenk tube top (while argon was flowing through the tube and top) and the stopcock to the argon supply was closed. The bubbler served to relieve pressure generated from the exothermic reaction of the catalyst components and the gaseous reaction products. The solution was allowed to age at room temperature for ca. 30 minutes. Meanwhile, the methylacetylene (ca. 700 - 740 torr) in a gas storage bulb was degassed one final time.

After removing the bubbler, the Schlenk tube was attached to a vacuum line and the catalyst solution was cooled to -78°C and degassed

for ca. 30 - 60 minutes. The tube was gently agitated during the degassing while loosening the balljoint connection to the vacuum line. Next, the -78°C bath was replaced with an ice bath (0°C) and the catalyst solution was stirred vigorously. After the solution came to thermal equilibrium with the ice bath, the methylacetylene was admitted. The orange-brown catalyst solution assumed a dark brownish-red color and became viscous as the polymerization proceeded. Typical reaction times were 60 - 90 minutes. The reaction consumed ca. 300 - 400 torr of methylacetylene.

While the polymerization was in progress, ca. 150 mL of anhydrous methanol (previously distilled from methylmagnesium iodide and stored under argon in a Schlenk-type round bottom flask) was transferred via a syringe to another Schlenk tube which contained a stir bar. Ca. 10 mL of conc. HCl was then added and the solution was stored under argon until use. In addition, ca. 50 mL of toluene was transferred from the solvent still into yet another Schlenk tube under argon.

After the desired time period, the reaction vessel was disconnected from the vacuum line and argon was introduced. The polymer/catalyst mixture was then syringed dropwise into the stirring methanol/HCl solution. The mixture was brown-black and viscous. Upon completion of the transfer, stirring was discontinued to allow the precipitated $(\text{C}_3\text{H}_4)_x$ to settle to the bottom of the tube. As much as possible of the supernatant was then removed with a syringe and discarded. The polymer was observed to be an orange-brown, tacky mass. Ca. 50 mL of toluene was then added from the corresponding Schlenk tube to the polymer with a

syringe. The polymer/toluene mixture was stirred overnight to dissolve the $(C_3H_4)_x$.

A Schlenk tube equipped with a female $\frac{29}{42}$ joint was attached to a Schlenk filter (coarse frit filter with a side arm and stopcock). The remaining $\frac{24}{40}$ female joint of the filter was connected to a Schlenk tube top and the entire apparatus was pumped overnight on a vacuum line.

The next morning, the filtration apparatus was connected to an argon line via the side arm on the filter section and to a vacuum line via butyl rubber tubing and the side arm of the Schlenk tube. While argon was flowing through the apparatus and the Schlenk tube containing the polymer/toluene mixture, a small (ca. 10 mL) portion of this mixture was syringed onto the frit filter. The upper end of the filter section was capped, the stopcock to the argon supply was closed and the stopcock of the Schlenk (collection) tube was opened to the vacuum line allowing soluble polymer to be collected in the tube. This process was repeated until all of the polymer/toluene mixture was filtered. The filtered solution was deep orange in color. Various amounts of gummy, black insoluble polymer were collected on the filter and eventually discarded.

Ca. 150 mL of anhydrous methanol was transferred to a clean Schlenk tube containing a stir bar and then ca. 10 mL of conc. HCl was added. The polymer/toluene solution was transferred to the methanol/HCl to once again precipitate the $(C_3H_4)_x$. The supernatant was removed and the orange polymer mass was washed several times with anhydrous methanol. The Schlenk tube was then connected to a vacuum line and the polymer

was dried by pumping overnight. Yields ranged from 300 - 600 mg.

The poly(methylacetylene), a flaky orange powder, was stored in a Schlenk tube in vacuo at -78°C .

Doping. Polymer samples were doped and conductivities were measured by techniques described in Chapter III. In the case of iodine doping, the in vacuo method was usually employed. The polymer films were typically mounted in air although exposure times were kept very short (< 5 minutes) due to the sensitivity of the copolymers and $(\text{C}_3\text{H}_4)_x$ toward oxidation. A "film" of the soluble $(\text{C}_3\text{H}_4)_x^6$ (and in one case the soluble fraction from a copolymerization) was cast onto small rectangular glass slides in a glove bag and contacts to the four-probe apparatus were made with Electrodag. Since these polymers are soluble in common organic solvents, the Electrodag was used sparingly.

All samples were doped to their saturation conductivities. Dopant concentrations were determined from the weight uptake of reference samples.

Spectra. IR spectra were recorded on a Perkin-Elmer 283 grating spectrophotometer. EPR spectra were obtained using a Varian E-9 X-Band spectrometer equipped with a variable temperature probe; g values were determined as described in Chapter VI.

Results

Copolymer compositions. Table 6 summarizes pertinent data concerning feed compositions and chemical analyses of the copolymer films and ap-

TABLE 6

Comonomer Feed and Copolymer Composition

Sample ^b	Mole Ratio C_2H_2/C_3H_4 in Feed	Mole % C_2H_2 in Feed	% C	% H	Total C,H %	Chemical Analysis of Polymers ^a H/C	Mole % C_2H_2 in Polymer
$(CH)_x$	∞	100	84.16	7.61	91.77	1.08 (1.00 theor.)	(100)
AMA-61	6	85	86.31	8.15	94.46	1.13	70
AMA-31	3	75	87.31	8.61	95.92	1.18	55
AMA-11	1	50	86.36	8.94	95.30	1.24	33
AMA-13	0.33	25	84.53	9.30	93.83	1.31	15
$(C_3H_4)_x^c$	0	0	88.81	10.95	99.76	1.48 (1.33 theor.)	(0)

a - Galbraith Laboratories, Inc., Knoxville, Tenn.

b - Code = Acetylene - MethylAcetylene - mole ratio C_2H_2/C_3H_4 in feed

c - Courtesy of Mr. J. M. Warakowski, this laboratory

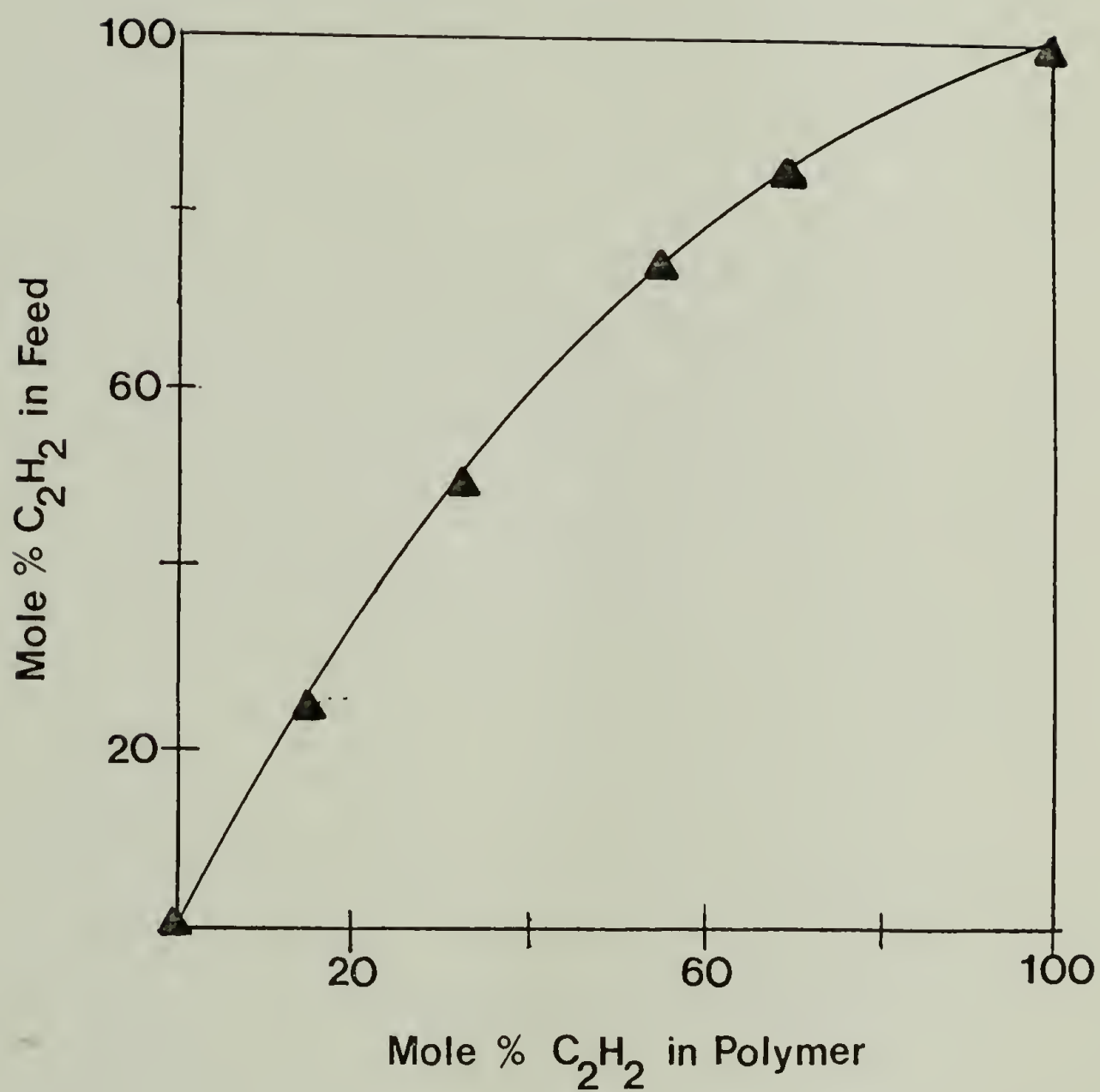


Figure 33. Plot of copolymer feed vs. copolymer composition.

appropriate homopolymers. Copolymer compositions were determined from H/C ratios. Three general statements can be made concerning the data. First, the acetylene content of the copolymers increases with increasing acetylene content in the feed. Second, the total C, H contents of all of the materials are low. Third, the H/C ratios of $(CH)_x$ and $(C_3H_4)_x$ are considerably greater than those anticipated for the "pure" homopolymers. These last two results are disappointing since they cast serious doubts about the validity of determining copolymer compositions from H/C ratios. However, plotting the feed composition vs. copolymer composition (Figure 33) affords a reasonable relationship with only a moderate amount of scatter. It is doubtful that this relationship is merely fortuitous and suggests that the copolymer compositions are not grossly in error. It should be noted, however, that since the H/C ratios of the homopolymers are larger than the anticipated values, it is likely that the copolymers are somewhat more rich in acetylene content than the data indicate.

Qualitative comparisons. A $(CH)_x$ film was prepared using the catalyst system employed for copolymer film syntheses simply for comparative purposes. The $(CH)_x$ film so prepared was quite different in appearance than the "typical" films described in Chapter IV. First, the film possessed poor integrity and broke into several small pieces during washing. Second, the film was very thin (ca. 20 μm) and extremely brittle. In addition, although the side of the film which grew against the reactor wall (referred to as "front side") possessed the coppery luster

characteristic of cis $(\text{CH})_x$, the backside displayed a shiny green coloration. Finally, the film surfaces were very irregular and displayed a macroscopic "rippled" appearance as indicated by the electron micrograph in Figure 34a. A region of the film between a surface crack is magnified in Figure 34b.

Copolymer sample AMA-61 exhibited similar lustrous and rippled surfaces as the $(\text{CH})_x$ film described above. The material was also very brittle and disintegrated into several small pieces during washing.

Sample AMA-31 more resembled typical $(\text{CH})_x$ films; the front side, although shiny green, possessed a relatively smooth macroscopic surface while the backside displayed a dull grey-black coloration. However, the electron micrographs in Figures 35a-b show no evidence of the fibrillar texture of typical $(\text{CH})_x$ films. Rather, irregular and ill-defined "clumps" are observed.

Copolymer AMA-11 displayed a dull greenish-gold luster on both sides of the film. The morphology of this material (Figure 36a) is similar to that observed for AMA-31. It is important to point out that the luster was lost and the film became black upon wetting with a solvent (e.g., pentane, toluene), suggesting solvent swelling of the polymer occurred. The luster was recovered upon evaporation of the solvent.

It was also observed that the AMA-11 film became very elastic upon wetting with a solvent. In fact, wetted films could be stretched to extension ratios as high as ~ 7 and, upon solvent evaporation, a fixed elongation could be achieved. Alternatively, wetting of a stretched, dried film resulted in considerable retraction. It is interesting to

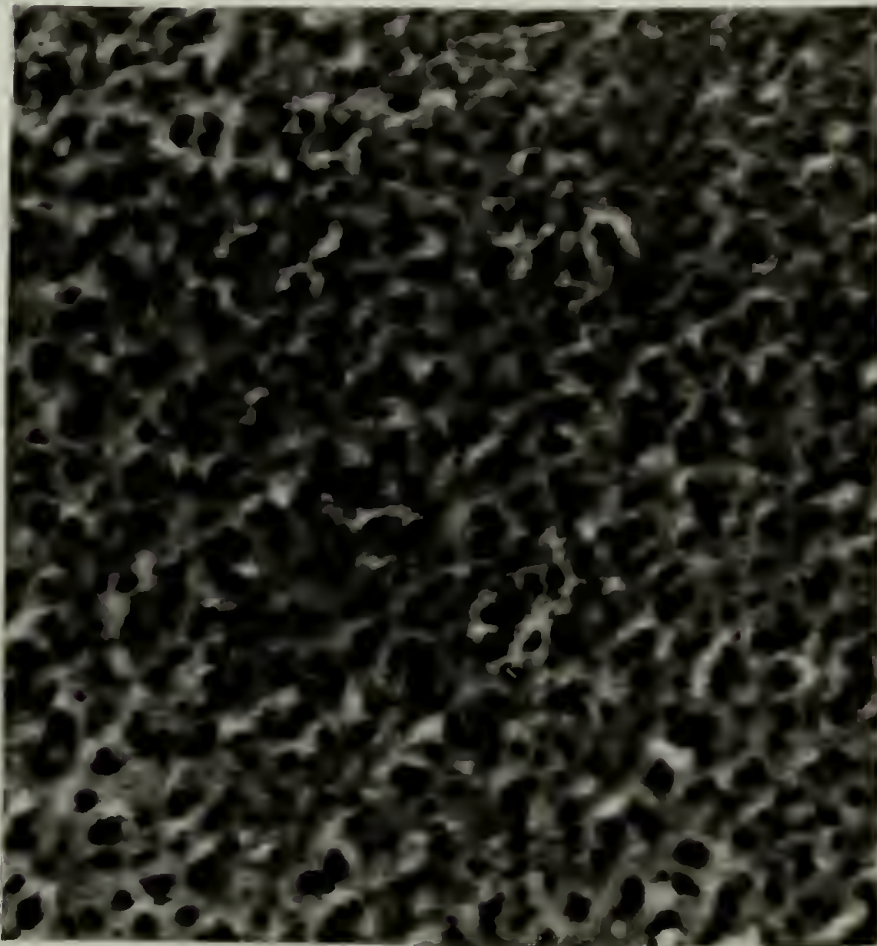
Figure 34. Electron micrographs of $(\text{CH})_x$ films prepared using high concentrations of $\text{Ti}(\text{OBu})_4/\text{Et}_3\text{Al}$.

(A) Film surface (x10)

(B) Crack in film surface (x4,000)



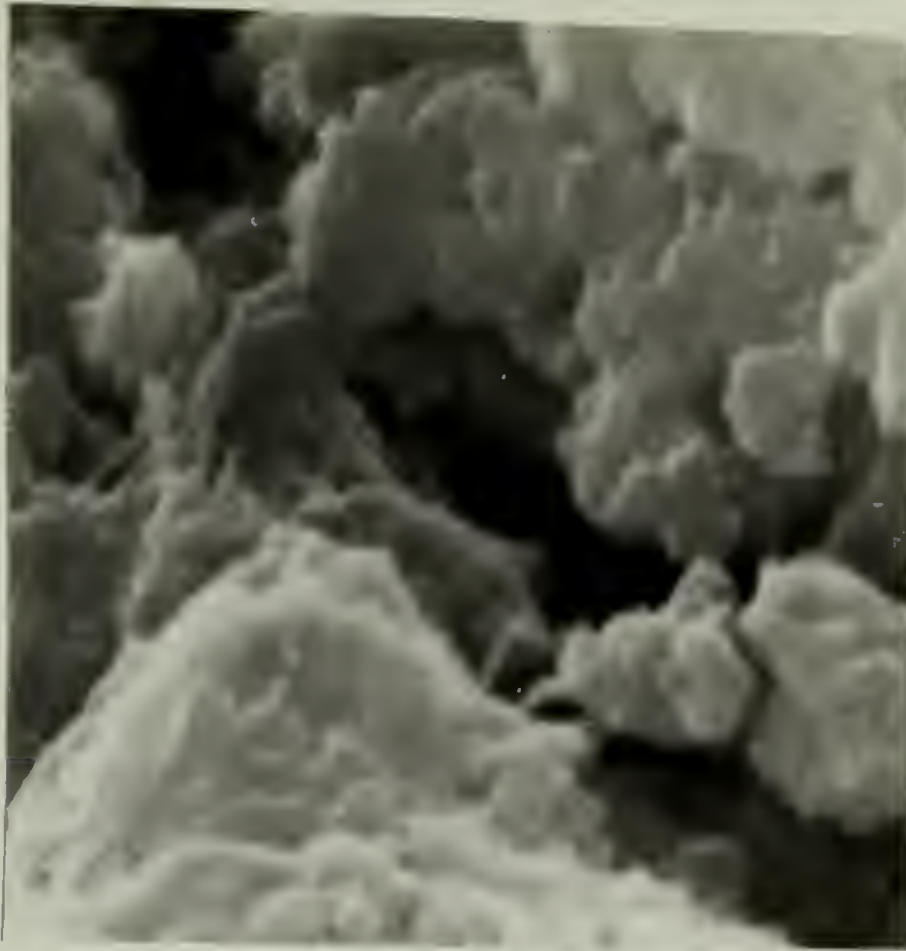
A

 $100\mu m$ 

B

 $1\mu m$

Figure 35. Electron micrographs of AMA-31 copolymer film.
(A) Shiny side (x50,000)
(B) Dull side (x20,000)



A

 $0.1\mu m$ 

B

 $0.1\mu m$

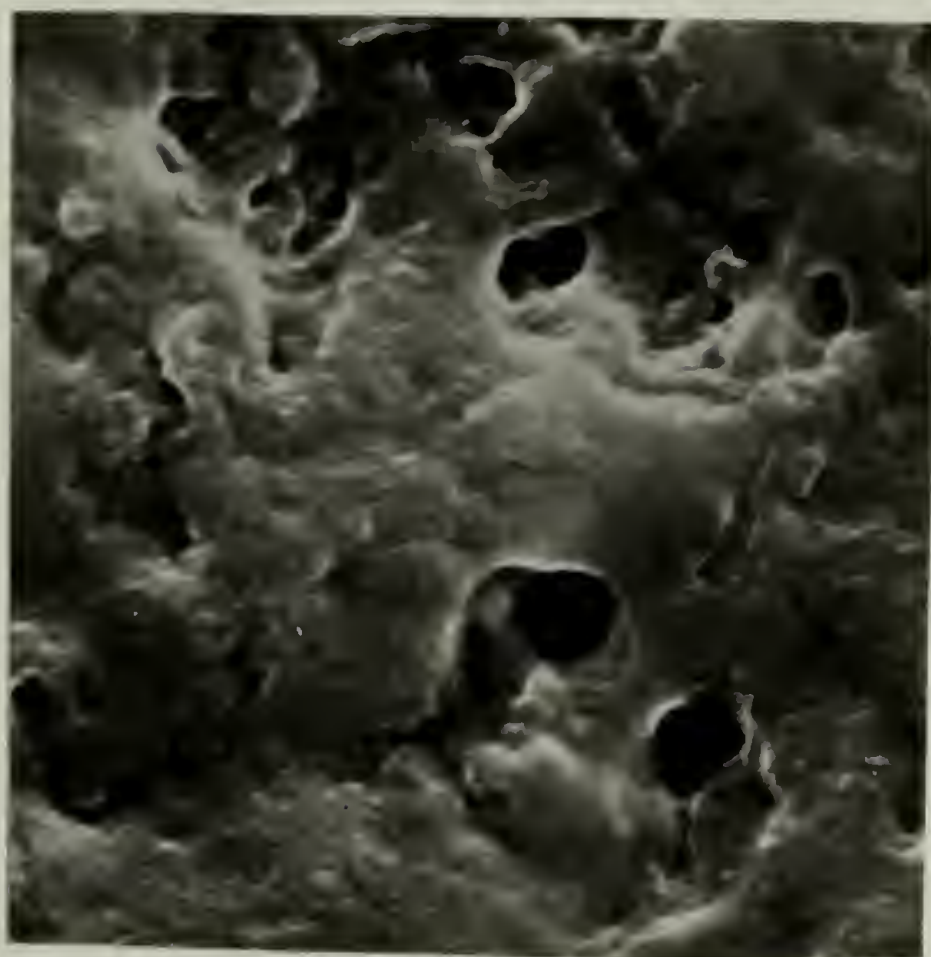
Figure 36. Electron micrographs of AMA-11 and
AMA-13 copolymer films.

(A) AMA-11 (x2,000)

(B) AMA-13 (x4,000)



A

 $1\mu m$ 

B

 $1\mu m$

note that the wet films are somewhat tacky and stick together tenaciously upon drying. This was observed, for example, during the washing process when fairly large sections of film separated from the reactor walls and folded over on themselves. The film sections could usually be separated with tweezers when contacted with a solvent.

The same general observations concerning sample AMA-11 apply to the characteristics of the AMA-13 film although the latter was less lustrous and even more elastic when wetted with solvent. The irregular, "clump-like" morphology of the film is exemplified in Figure 36b. It should be noted that an attempted preparation of an AMA-14 copolymer failed to produce a tractable film. The material was extremely rubbery and tacky when wetted with solvent and, as the result of poor mechanical integrity, was washed away from the reactor walls as black, tacky masses. Thus, it appeared that the methylacetylene content of AMA-13 (Table 6) was nearly the upper limit for the production of free-standing films.

Poly(methylacetylene), $(C_3H_4)_x$, was obtained as a brittle orange powder. As was mentioned in the experimental section, the insoluble fraction from a $(C_3H_4)_x$ preparation is black and rubbery in the presence of a solvent. Thus, the reversible swelling and color of various copolymer films is in qualitative agreement with the presence of C_3H_4 units in these materials. The morphology of $(C_3H_4)_x$ was not investigated. An infrared spectrum of $(C_3H_4)_x$ (evaporated from toluene on a NaCl plate) is shown in Figure 37. The two IR bands at 1020 and 960 cm^{-1} are probably related to the = C - H out of plane deformation of trans

Figure 37. Infrared spectrum of poly(methylacetylene).



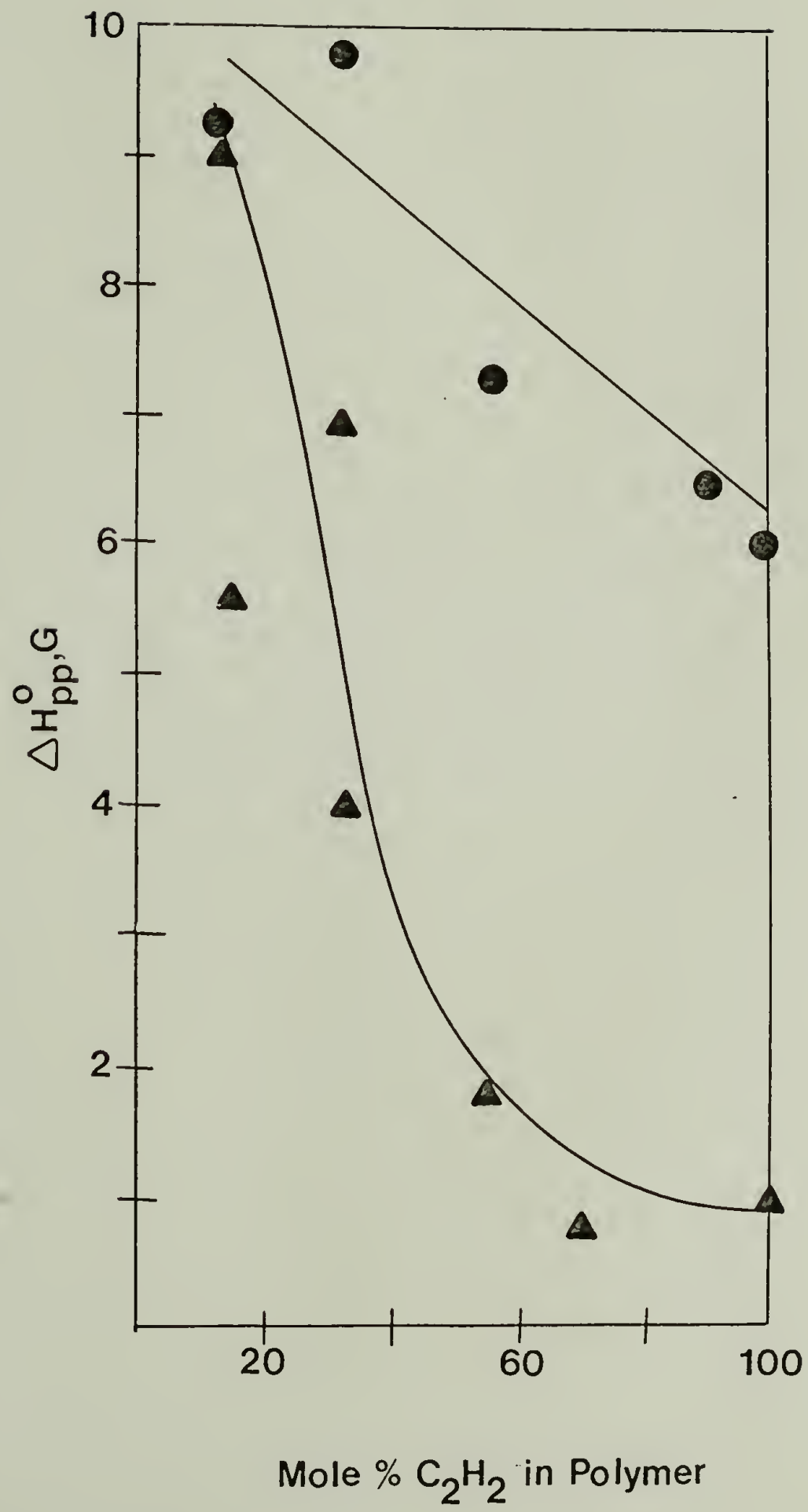
units in the polymer. No bands characteristic of cis units in the range $700 - 750 \text{ cm}^{-1}$ are observed. This result is not surprising in view of the unfavorable steric interactions anticipated between the methyl and hydrogen substituents in cis $(\text{C}_3\text{H}_4)_x$. The bands at 2960, 2920, 2875, 1440 and 1370 cm^{-1} are consistent with the presence of methyl groups in the polymer.

It is important to point out that $(\text{C}_3\text{H}_4)_x$ is much more sensitive to oxidation than $(\text{CH})_x$. The orange powder became white-yellow in color upon overnight exposure to oxygen suggesting that the conjugated backbone was considerably disrupted. In contrast, $(\text{CH})_x$ lost its luster and became discolored after several weeks of air exposure. Copolymers rich in methylacetylene content (e.g., AMA-11, AMA-13) became yellow-white and extremely brittle merely upon overnight air exposure resembling $(\text{C}_3\text{H}_4)_x$.

All copolymer samples and $(\text{CH})_x$ (Table 6) displayed Lorentzian EPR resonances with g values in the range 2.0023 - 2.0026. Linewidths ranged from ca. 10 G to ca. 7 G and in general increased with increasing methylacetylene content in the copolymers (Figure 38a). Heating each sample to 150°C for ca. 30 minutes in the EPR probe followed by cooling to room temperature resulted in the relationship shown in Figure 38b. It is important to note that $(\text{C}_3\text{H}_4)_x$ did not display any observable resonance even when heated to 150°C , although the material melted during heating.

Miscellaneous properties. AMA-11 was the copolymer investigated in the

Figure 38. Plot of EPR linewidth as a function of acetylene content in copolymer films.
(●) room temperature; (▲) after heating to 150° C for 30 min. followed by cooling to room temperature.



greatest detail since it could be prepared fairly easily and reproducibly. Figure 39 shows an infrared spectrum of an AMA-11 film. Comparison of this spectrum with that of $(C_3H_4)_x$ (Figure 37) and $(CH)_x$ (Figure 15, Chapter IV) indicates that bands characteristic of both polymers are present in the copolymer. The intense bands observed at ca. 1010 and 730 cm^{-1} in Figure 39 are characteristic of the = C - H out of plane deformations of cis and trans $(CH)_x$, respectively.¹¹ A shoulder at ca. 960 cm^{-1} may be due to a similar deformation in trans $(C_3H_4)_x$. Figure 39 also shows three IR scans of AMA-11 recorded in air at approximately 10 minute intervals. In this short period of time, carbonyl absorptions in the region 1650 - 1750 cm^{-1} appear in high intensity and demonstrate the sensitivity of the copolymer toward oxidation. Of particular interest, however, is the observation that the 1010 cm^{-1} band increases in intensity while that at 730 cm^{-1} decreases, indicating that cis - trans isomerization occurred. Such an effect has never been observed with $(CH)_x$ under similar conditions. The role of oxygen in catalyzing cis - trans isomerization in $(CH)_x$ has been discussed in Chapter VI. This effect is clearly more pronounced in the copolymer sample as the result of its enhanced sensitivity toward oxidation.

Thermal gravimetric analyses in nitrogen (courtesy of J. - L. Fan) of $(CH)_x$, $(C_3H_4)_x$ and AMA-11 are shown in Figure 40. The onset of decomposition of $(CH)_x$ is near 350° C and is in good agreement with the calorimetric study of Shirakawa et al.¹² In comparison, poly(methylacetylene) has a greatly reduced thermal stability with decomposition being observed near 180 - 200° C. Furthermore, much less residue from

Figure 39. Infrared spectra of AMA-11 film.

———— initial scan
- - - - after 10 min. in IR beam
- · - · - after 20 min. in IR beam

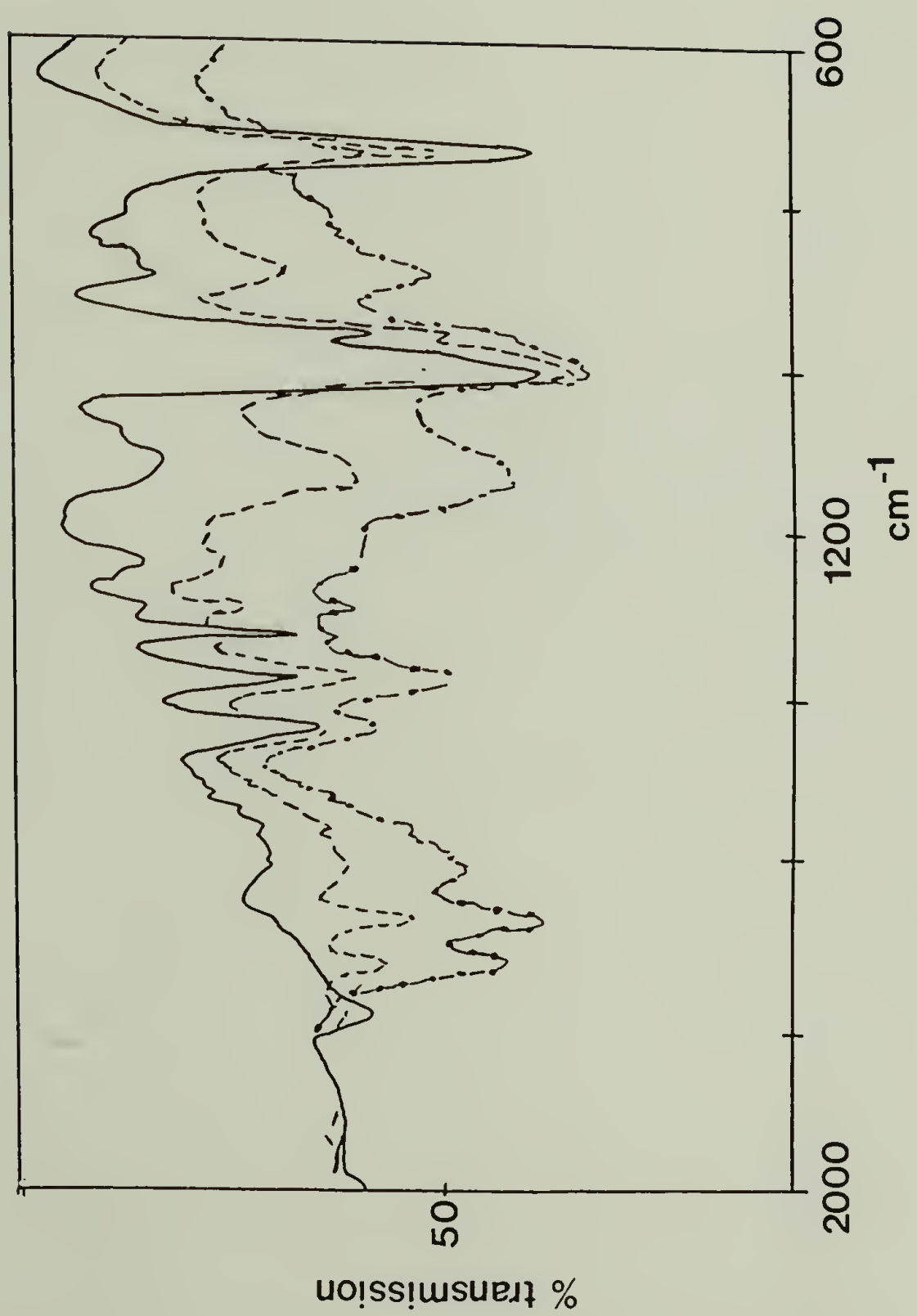
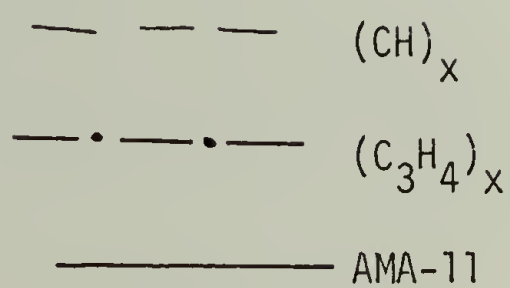
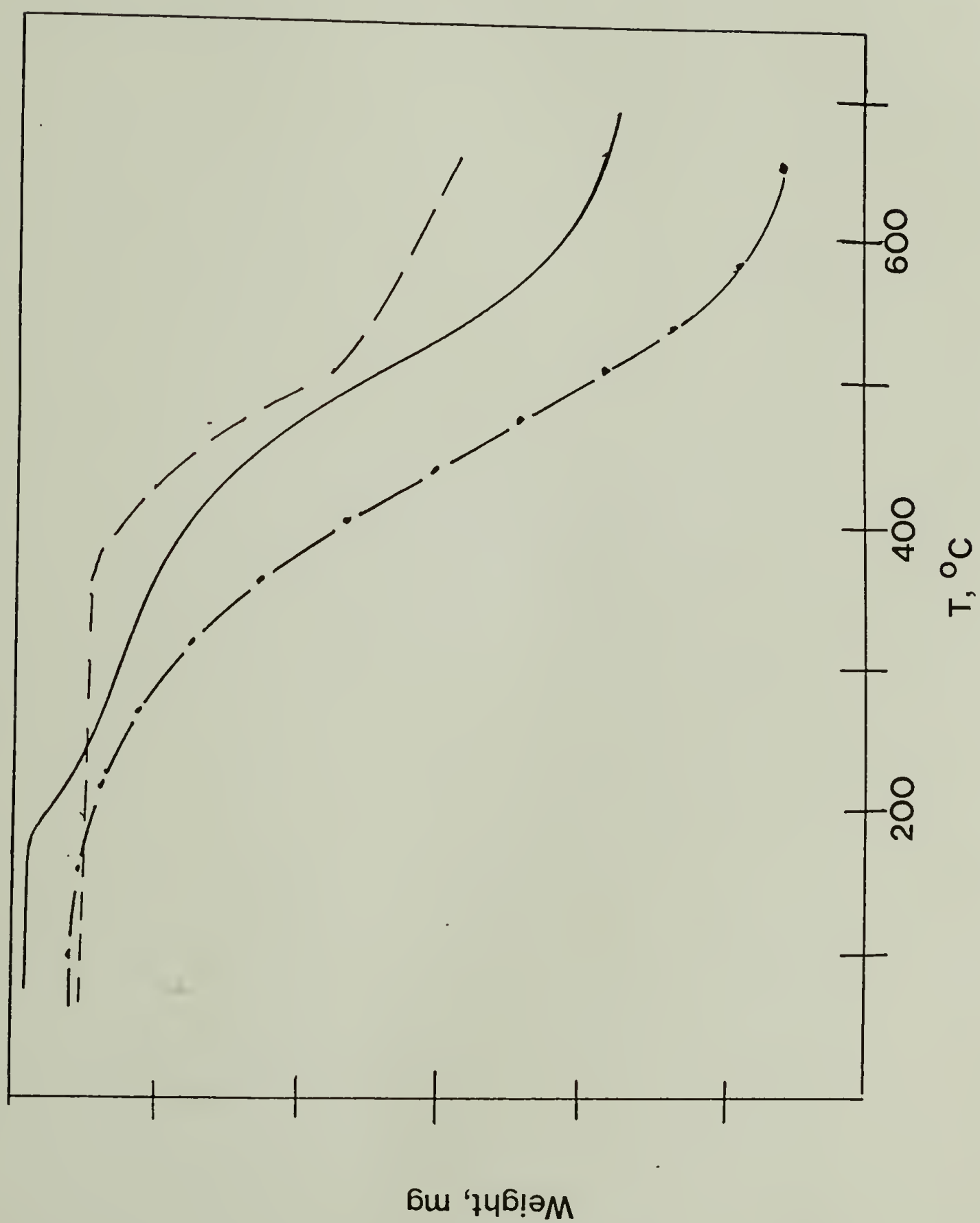


Figure 40. TGA curves of $(\text{CH})_x$, $(\text{C}_3\text{H}_4)_x$ and AMA-11.





$(C_3H_4)_x$ is observed after completion of the pyrolysis as compared to $(CH)_x$ suggesting that chain scission with concomitant formation of volatile products occurs to a greater extent in $(C_3H_4)_x$. The copolymer AMA-11 displays somewhat intermediate behavior. The TGA curve of AMA-11 shows a two-step decomposition process and is nearly a superposition of the curves for $(C_3H_4)_x$ and $(CH)_x$.

Electrical conductivity. Conductivities and dopant concentrations for $(CH)_x$, $(C_3H_4)_x$ and various copolymer samples are given in Table 7. The conductivities are observed to decrease with decreasing acetylene content. This relationship is shown graphically in Figure 41 in the case of polymers doped with iodine and AsF_5 . Iodine becomes a progressively better dopant than AsF_5 as the methylacetylene content of the polymers increases. It should be noted in passing that the conductivity of the red, soluble residue from an AMA-11 preparation was essentially the same as that of doped $(C_3H_4)_x$. Due to the oily (low molecular weight) nature of this material and the low conductivity, little effort was made to characterize the soluble fractions.

Doping of partially oriented AMA-11 (stretched while wetted with pentane) with iodine did not yield a measurable increase in conductivity as compared to the doped, unoriented polymer (Table 8).

TABLE 7

Conductivities and Compositions of Doped Homo- and Copolymers

Sample ^a	Mole % C ₂ H ₂ in Polymer	Composition of Doped Polymer	$\sigma, \Omega^{-1} \text{cm}^{-1}$
(CH) _x	100	[CH(AsF ₅) _{0.12}] _x	~400
AMA-31	~55	[CH _{1.18} I _{0.24}] _x	~36
		[CH _{1.18} I _{0.16}] _x - after pumping above sample overnight	~18
		[CH _{1.18} (AsF ₅) _{0.08}] _x	~45
		[CH _{1.18} Br _{0.17}] _x	~4x10 ⁻²
		Na-doped; composition not determined	~2.5x10 ⁻¹
AMA-11	~33	[CH _{1.24} I _{0.16}] _x	~1.5
		[CH _{1.24} (AsF ₅) _{0.1}] _x	~1.0
AMA-13	~15	[CH _{1.31} I _{0.11}] _x	~2x10 ⁻²
		[CH _{1.31} (AsF ₅) _{0.05}] _x	~2x10 ⁻³
(C ₃ H ₄) _x ^b		[CH _{1.33} I _{0.17}] _x ^b	~10 ^{-3b}

a - Table 6

b - Reference 6

Figure 41. Plot of conductivity vs. copolymer composition
for films doped with iodine and AsF_5 .

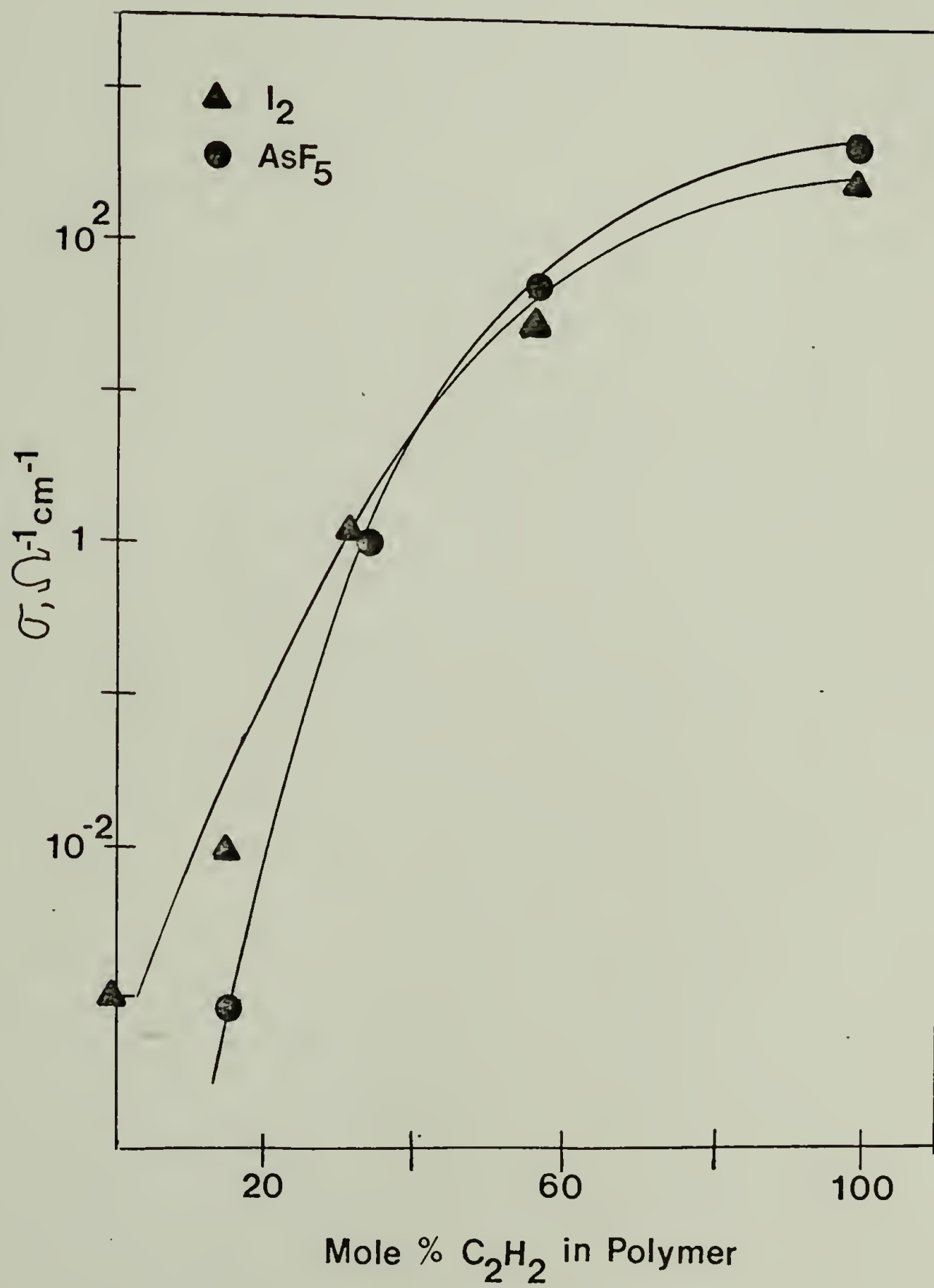


Table 8

Effect of Elongation Ratio (l/l_0) on σ for an AMA-11 Copolymer film doped with Iodine.

<u>l/l_0</u>	<u>$\sigma, \Omega^{-1} \text{ cm}^{-1}$</u>
1	1.5
3.5	1.2

Discussion

The poor purity of the samples investigated (Table 6) is probably the result of considerable catalyst "entrapment" in the materials due to the high catalyst concentrations employed in their preparation. This effect was most pronounced in the $(\text{CH})_x$ sample since it is not swellable with solvents and thus an unusually large quantity of catalyst could remain in the material. However, the conductivity of this AsF_5 -doped $(\text{CH})_x$ sample (Table 7) is comparable¹ to that obtained with typical as-grown films. Furthermore, this $(\text{CH})_x$ sample displayed identical EPR behavior compared to typical as-grown films¹³ (Figure 38); i.e., the ca. 6 G resonance narrows to ca. 1 G upon isomerization. Thus, the purity of the $(\text{CH})_x$ appears to affect neither its "dopability" or its EPR behavior to any great degree and suggests that results regarding the copolymers are not particularly dependent upon sample purity.

The oxidative instability of $(\text{C}_3\text{H}_4)_x$ and the copolymers is a direct consequence of the methyl substituent on the conjugated backbone. These hydrogens are readily susceptible to radical attack since the formation

of $\cdot\text{CH}_2-$ is facilitated by delocalization of the radical in an allyl-type system.

The qualitative results described previously suggest the presence of true copolymers as opposed to "blends" of $(\text{CH})_x$ and $(\text{C}_3\text{H}_4)_x$. However, definitive proof of copolymer formation was difficult especially in view of the insolubility of the films. The effective conjugation length of $(\text{C}_3\text{H}_4)_x$ is expected to be severely reduced as compared to $(\text{CH})_x$ due to steric interactions between methyl and hydrogen substituents, causing a "twist" of the backbone. In fact, a uv-visible spectrum of $(\text{C}_3\text{H}_4)_x$ in heptane shows two λ_{max} absorptions at ca. 220 and 290 nm; these are well into the uv region as compared to $(\text{CH})_x$ (λ_{max} ca. 600 - 700 nm). In other words, the band gap of $(\text{C}_3\text{H}_4)_x$ is considerably larger than that of $(\text{CH})_x$. As a result of these steric factors, the $(\text{C}_3\text{H}_4)_x$ polymer backbone is rendered less rigid and, in conjunction with the disruption of intermolecular interactions, the polymer is soluble. Apparently, the methylacetylene content of copolymers AMA-11 and AMA-13 is insufficient to induce a great deal of solubility although interchain interactions are disrupted to the extent that solvents can plasticize the materials.

It might be anticipated that the effective conjugation length of the copolymers, if they are in fact copolymers, will increase with increasing acetylene content as demonstrated by Wegner et al.¹⁰ with acetylene/1-hexyne copolymers. Unfortunately, uv-visible spectra for the "AMA" polymers are not yet available. However, the EPR data of Figure 38 argue in favor of the presence of "true" copolymers. It is important to note that no EPR resonance for $(\text{C}_3\text{H}_4)_x$ was observed even when the sample

was heated to 150° C. In view of this result, any EPR behavior (from a polymer blend) would be characteristic of the highly conjugated $(CH)_x$ itself. On the other hand, true copolymers are expected to possess reduced effective conjugation lengths which should be manifested by a reduced mobility of the unpaired spins in the polymers. The EPR linewidth¹⁴ in turn qualitatively reflects the mobility of the spins. Inspection of Figure 38a indicates that the linewidth does increase (and thus the mobility decreases) with increasing methylacetylene content in the polymers. This dependence is even more pronounced with samples which have been isomerized to 150° C (Figure 38b). These results suggest that samples AMA-31, AMA-11 and AMA-13 are not simply mixtures of homopolymers. The absence of an observable EPR resonance for $(C_3H_4)_x$ is difficult to rationalize since a resonance is observed in the related material poly(phenylacetylene).¹⁵ It is interesting to note that the EPR linewidth of poly(phenylacetylene) is ca. 10 - 12 G; i.e., consistent with the anticipated linewidth of poly(methylacetylene) (Figure 38a).

The electrical conductivity data of Table 7 and Figure 41 are consistent with predictions concerning the dependence of conductivity on copolymer composition. An increase in the methylacetylene content of the polymer is anticipated to increase both its band gap ($\pi \rightarrow \pi^*$ transition) and its ionization potential, making free carrier generation more difficult. In addition, the reduction of the effective conjugation length with increasing methylacetylene content is expected to reduce carrier mobility. Thus, the methylacetylene units would act as barriers to conductivity. Carrier migration through (or around) these barriers

should become progressively more difficult as the number of these barriers in creases. The absence of an increased conductivity in the case of stretch-oriented AMA-11 doped with iodine (Table 8) might be explained in a similar manner. In this case, potential anisotropy could be quenched by the methylacetylene barriers. However, additional studies of anisotropic electrical properties are needed before definitive statements concerning anisotropy in these copolymers can be offered.

Additional factors which may contribute to the magnitude of the electrical conductivity in a particular sample include morphology and the degree of crystallinity. As described previously, all of the copolymer films display a similar "clump-like" morphology and thus the morphology should not play an important role in affecting the conductivity of the copolymer samples. In addition, it is interesting to note that the $(CH)_x$ sample studied in this work possessed a morphology quite different from the fibrillar character¹⁶ of typical as-grown $(CH)_x$ films, although doping with AsF_5 afforded a comparable conductivity¹ (Table 7). The degree of crystallinity of the samples, on the other hand, may play a very important role in determining electrical transport properties. Unfortunately, data concerning the degrees of crystallinity of the copolymers are not available at this time.

It is worthwhile to note that as the acetylene content of the copolymers decreases, AsF_5 becomes a progressively poorer dopant than I_2 (Figure 41). In fact, AsF_5 produces no change in conductivity with $(C_3H_4)_x$.⁶ This phenomenon might be due to a complicated combination of steric and electronic factors with regard to polymer-dopant interactions.

Furthermore, these interactions appear to be weak in $(C_3H_4)_x$ doped with iodine; essentially all of the iodine can be removed from the sample by pumping with a six order of magnitude decrease in conductivity.⁶ This effect was not investigated in detail with the copolymer samples although it was found that iodine could be partially removed by pumping in the case of AMA-31 with a small decrease in conductivity (Table 7). This behavior is similar to that observed in iodine-doped $(CH)_x$.

It is important, for future studies, to consider measurements of thermopower in order to complement electrical conductivity measurements. As mentioned in the previous chapter, the thermopower is representative of intrinsic electrical properties and would be very useful in properly assessing the influence of copolymer composition on electrical characteristics.

Conclusions

The applicability of copolymerization in the synthesis of novel electrically conducting materials having interesting properties (e.g., solvent plasticization) has been demonstrated. The electrical conductivity of the doped copolymers increased with increasing acetylene content. It is suggested that the methylacetylene units in the polymers are the predominant barriers to electrical conductivity.

Admittedly, the acetylene-methylacetylene copolymers are not practical in view of their extreme sensitivity toward oxidation. However, the observation that partial backbone substitution of $-CH_3$ for hydrogen can induce swellability is important and suggests the possibility of

incorporating oxidative stabilizers into such materials. Upon consideration of the enormous number of potential copolymers which may be prepared, a large new class of organic polymers is envisioned possessing electrical properties which can be controlled over the full range from insulator to semiconductor to metal.

References

1. C. K. Chiang, M. A. Druy, S. C. Gau, A. J. Heeger, E. J. Louis, A. G. MacDiarmid, Y. W. Park and H. Shirakawa, J. Amer. Chem. Soc., 100, 1013 (1978)
2. C. K. Chiang, S. C. Gau, C. R. Fincher, Jr., Y. W. Park, A. G. MacDiarmid and G. J. Heeger, Appl. Phys. Lett., 33, 18 (1978)
3. D. M. Ivory, G. G. Miller, J. M. Sowa, L. W. Shacklette, R. R. Chance and R. H. Baughman, J. Chem. Phys., 71, 1506 (1979)
4. K. K. Kanazawa, A. F. Diaz, R. H. Geiss, W. D. Gill, J. F. Kwak, J. A. Logan, J. F. Rabolt and G. B. Street, J. Chem. Soc. Chem. Comm., 854 (1979)
5. T. Yamamoto, K. Sanechika and A. Yamamoto, J. Polym. Sci., Polym. Lett. Ed., 18, 9 (1980)
6. Y. Matsumura, A. G. MacDiarmid and A. J. Heeger, private communication.
7. P. Cukor, J. I. Krugler and M. F. Rubner, ACS Polymer Preprints, 21, 161 (1980)
8. H. W. Gibson, F. C. Bailey and J. M. Pochan, Org. Coat. Plast. Chem., 42, 603 (1980)
9. M. J. Kletter, T. Woerner, A. Pron, A. G. MacDiarmid, A. J. Heeger and Y. W. Park, J. Chem. Soc. Chem. Comm., 426 (1980)
10. V. Enkelmann, H. Muller and G. Wegner, Synthetic Metals, submitted
11. H. Shirakawa and S. Ikeda, Polym. J., 2, 231 (1971)
12. T. Ito, H. Shirakawa and S. Ikeda, J. Polym. Sci., Polym. Chem. Ed., 13, 1943 (1975)

13. H. Shirakawa, T. Ito and S. Ikeda, Makromol. Chemie., 179, 1565 (1978)
14. Cf. J. C. W. Chien, F. E. Karasz and G. E. Wnek, Nature, 285, 391 (1980)
15. G. M. Holob, P. Ehrlich and R. D. Allendoerfer, Macromolecules, 5, 569 (1972)
16. F. E. Karasz, J. C. W. Chien, R. Galkiesicz, G. E. Wnek, A. J. Heeger and A. G. MacDiarmid, Nature, 282, 286 (1979)

CHAPTER X

AROMATIC CONDUCTING POLYMERS

The high intractability of polyacetylene has prompted the search for other materials which may also yield highly conducting derivatives in combination with enhanced thermal and oxidative stability and processibility. Two approaches, namely the synthesis of homopolymers of substituted acetylenes and copolymers with acetylene, have been described in the previous Chapter. Another approach involves the use of polymers which are rich in aromatic functionalities. In particular, such materials are anticipated to display excellent thermal and oxidative stability and thus have recently come under intensive investigation.

The foremost examples of this class of materials are the poly(phenylenes).¹⁻³ The parent poly(p-phenylene), besides possessing enhanced stability compared to polyacetylene, can be processed through various sintering techniques. Furthermore, its conductivity can be varied over seventeen orders of magnitude upon doping with strong electron acceptors such as AsF_5 . Ultimate conductivities as high as $500 \Omega^{-1} \text{ cm}^{-1}$ can be achieved. The doped polymer possesses similar free electron-like absorption in the infrared and similar conductivities and thermopower values when compared with doped polyacetylene. Donor doping with sodium or potassium yields ultimate conductivities near $10 \Omega^{-1} \text{ cm}^{-1}$. In addition, the acceptor and donor dopants can compensate one another. The stability of AsF_5 -doped poly(p-phenylene) is particularly attractive; its conductivity decreases by only a factor of two upon exposure to moist air. Poly(m-phenylene)⁴ is both solution and melt processible

and can also be doped with acceptors such as AsF_5 , although conductivities are six orders of magnitude lower than that of the doped para polymer. The lower conductivity undoubtedly reflects the reduced conjugation in the meta polymer. The ionization potentials⁴ of poly(p-phenylene) and poly(m-phenylene) have been calculated to be 5.4 and 6.5 eV, respectively, and are much larger than that reported for trans polyacetylene (ca. 4.7 eV).⁵ The ionization potentials probably account for the fact that dopants such as iodine form highly conducting derivatives with polyacetylene but not with the poly(phenylenes).

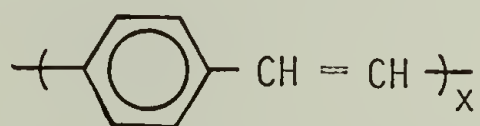
Polymers containing heterocyclic aromatic units have recently been reported to possess good electrical properties upon doping. For example, the electrochemical oxidation of pyrrole⁶ has produced conducting polymers ($\sigma \sim 10 - 100 \, \Omega^{-1} \text{ cm}^{-1}$). The oxidized polymer backbone is stabilized by anions such as BF_4^- . The polymer is extremely stable in air although, unfortunately, it is intractable. Poly(2, 5 - thienylene) has been doped with iodine⁷ to yield conductivities of ca. $10^{-5} \, \Omega^{-1} \text{ cm}^{-1}$. It might be anticipated that even higher conductivities may result upon doping with more powerful oxidizing agents such as AsF_5 .

The most recent and perhaps most surprising results have been obtained from the phenylene chalcogenide polymers. Poly(p-phenylene sulfide), a material which is both melt and solution processible, has been found to yield conductivities near $1 \, \Omega^{-1} \text{ cm}^{-1}$ upon doping with AsF_5 .^{8,9} The surprising aspect is that in contrast to polyacetylene and the aromatic systems mentioned above, this polymer possesses no continuous carbon chain in the backbone. Furthermore, the neighboring phenyl rings

are displaced $+45^\circ$ and -45° with respect to the planar zig-zag polymer backbone.¹⁰ Thus, overlap of orbitals between phenyl rings is expected to be extremely poor. It may be that the spatially extended d-orbitals of the sulfur atoms provide overlap between the phenyl rings. The processibility and commercial availability (Ryton, Phillips Petroleum Co.) of poly(p-phenylene sulfide) makes this material particularly attractive as a viable and economical conducting polymer system. Unfortunately, as with many other doped polymers, poly(p-phenylene sulfide) becomes intractable and sensitive to air and moisture upon doping.^{8,9}

Considering the polymer systems mentioned above in a collective sense, the positive results obtained are at least encouraging and suggest that these materials merit further exploration.

In order to obtain additional insight into the chemistry of aromatic macromolecular structures which can be doped to yield highly conducting materials, a portion of this dissertation work was focused on poly(p-phenylene vinylene), or PPV, having the structure



This polymer can be considered as a regularly alternating copolymer of p-phenylene and acetylene. Since the homopolymers of these materials yield highly conducting derivatives upon doping, it was anticipated that the same might be true for PPV. In addition, PPV appeared to offer distinct advantages over other polymer systems currently under investigation. Materials such as polyacetylene and poly(p-phenylene) are structurally rather ill-defined since their intractability precludes

the straightforward determination of important parameters such as molecular weight. Poly(p-phenylene vinylene) is readily prepared by the Wittig reaction and, since this is a step growth polymerization, chain ends can be effectively "labeled" by employing a small excess of one reactant. Typically, PPV is prepared from p-xylylene-bis-(triphenylphosphonium chloride) and terephthalaldehyde.¹¹ Thus, the use of excess dialdehyde results in polymers with terminal aldehyde groups and allows a reasonable determination of molecular weight from elemental analysis of the oxygen content. Furthermore, this work was motivated by the synthetic versatility of the Wittig reaction, allowing the preparation of a wide range of substituted PPV analogs. Besides offering potential processibility, such materials were of interest for studies concerning the effect of substituents on the ultimate conductivity of doped derivatives. It should be noted that the electrical properties of pristine PPV and related materials have been extensively studied^{15,16} although the work reported here represents the first attempt at modifying the electrical properties through chemical doping. In addition, the conductivities attainable through doping of organic "model compounds" such as naphthalene, stilbene, etc., were investigated for comparative purposes. Preliminary accounts of this work have been published elsewhere.¹²

Experimental

The organic compounds which were studied in this work are illustrated in Figures 42a-b. Commercial grades of naphthalene (1), anthra-

Figure 42. Structures of aromatic polymers and model compounds (see text).

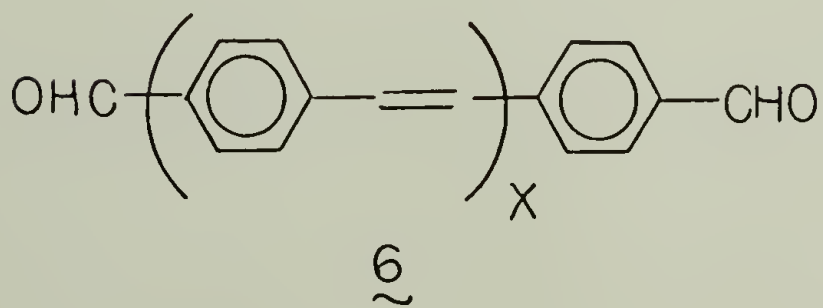
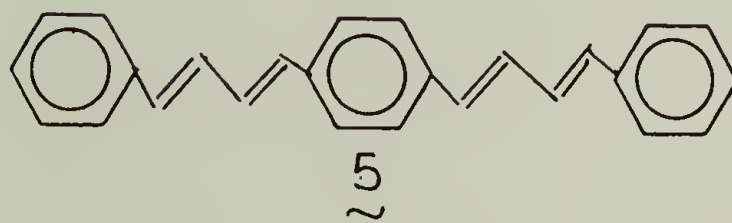
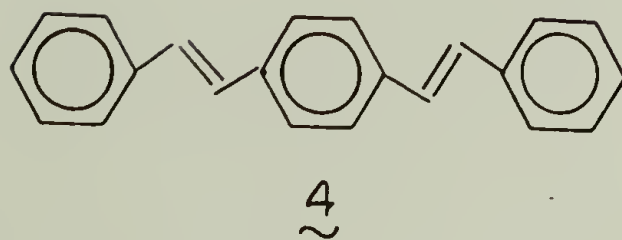
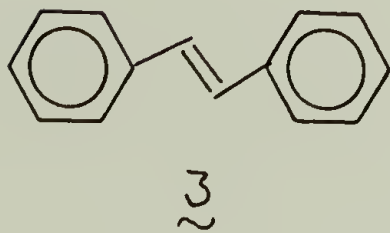
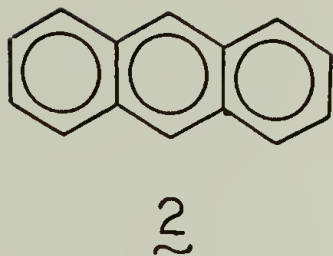
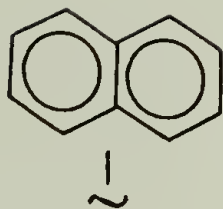


Figure 42.

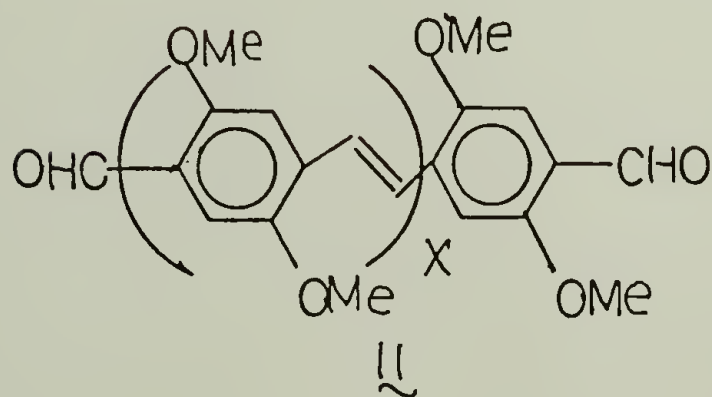
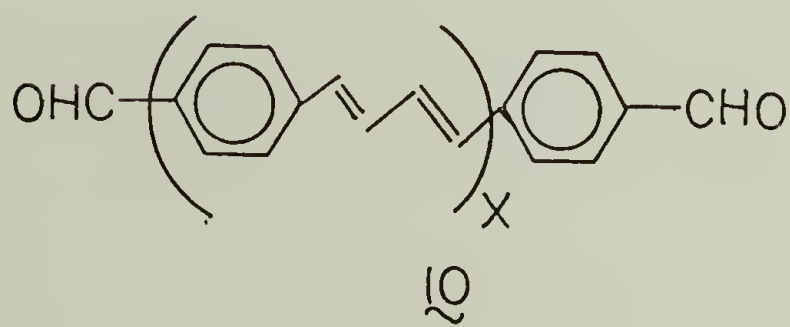
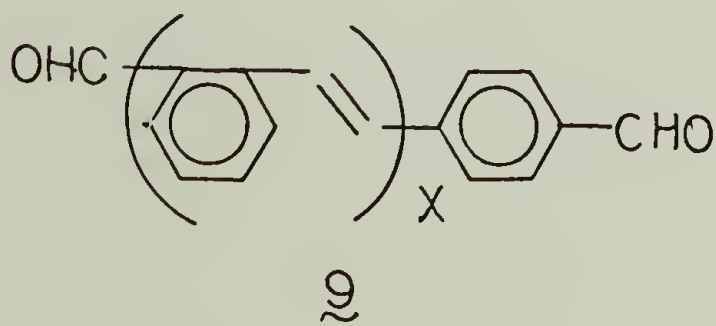
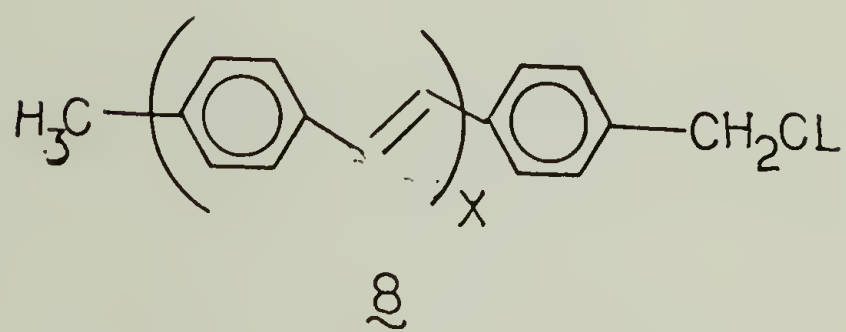
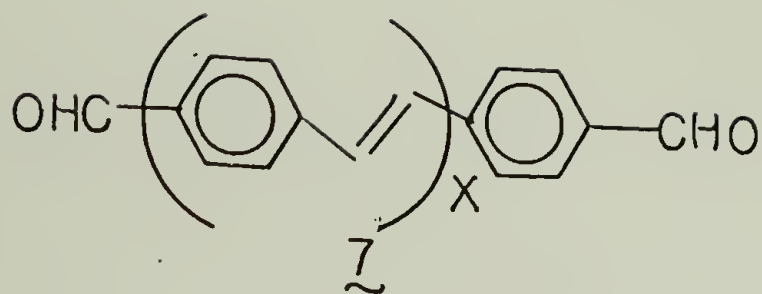


Figure 42., continued.

cene (2) and trans-stilbene (3) were used without further purification. Compounds 4 - 11 were prepared by Dr. K. Yao and Messers. R. Gooding and M. Samolis under the direction of Prof. C. P. Lillya, University of Massachusetts Chemistry Department. The preparations of these materials employed well-established techniques and will not be described in detail. Trans-trans-distyryl benzene (4),¹³ 1,4-bis-(4-phenyl-1,3-butadienyl) benzene (5),¹⁴ poly(p-phenylene vinylene), or PPV, containing a mixture of cis and trans vinyl linkages (6),¹¹ trans-PPV (7),¹¹ trans-poly(m-phenylene vinylene) (9),¹⁵ trans-poly(p-phenylene butadienylene) (10)^{14a} and trans-poly(2,5-bis-methoxy-p-phenylene vinylene) (11)¹⁶ were prepared via the Wittig reaction of the appropriate phosphonium chloride ylids and aldehydes. It should be noted that the Wittig reaction produces materials containing a statistical mixture of cis and trans vinyl linkages. Thus, all materials designated as trans (with the exception of 3) were isomerized by refluxing in xylene with a trace of iodine for several hours. The degree of isomerization was undetermined. Polymers 6 - 11 were typically washed of residues with benzene in a Soxhlet extractor for ca. 48 hours.

PPV (8) was additionally prepared¹⁷ by the reaction of p-bis-(chloromethyl) benzene and sodium hydride. Since this method presumably yields PPV with occasional -CH₂ - CHCl - linkages, pyrolysis at 300° C in vacuo was carried out to afford the elimination of HCl and concomitant extension of the conjugated system.

Elemental analyses of two PPV samples (7 A and B), polymer 10 and polymer 8 before and after pyrolysis are given in Table 9. Although

Table 9
Elemental Analyses of Selected Polymers*

<u>Sample</u>	<u>Analysis, %</u>			<u>Empirical Formula</u>	<u>X</u>
	<u>C</u>	<u>H</u>	<u>O</u>		
7A	90.6	5.74	3.40	$\sim \text{C}_{72}\text{H}_{54}\text{O}_2$	~ 8
7B	87.71	6.07	6.20	$\sim \text{C}_{32}\text{H}_{24}\text{O}_2$	~ 3
10	88.92	6.58	2.28	$\sim \text{C}_{108}\text{H}_{86}\text{O}_2$	~ 10
	<u>C</u>	<u>H</u>	<u>Cl</u>		
8 before pyrolysis	84.40	6.15	7.50	$\text{C}_{8.00}\text{H}_{6.94}\text{Cl}_{0.24}$	
8 after pyrolysis	88.7	6.20	2.75	$\text{C}_{8.00}\text{H}_{6.70}\text{Cl}_{0.08}$	$\sim 11^{**}$

* Galbraith Laboratories, Inc., Knoxville, Tenn.

** Assuming one $-\text{CH}_2\text{Cl}$ end group per chain

polymers 9 and 11 were not subjected to analysis, it is reasonable to assume from comparison of results (see Table 9) that the degree of polymerization, x , for these two materials is in the range 5 - 10. Precipitation of the polymers from solution during the syntheses undoubtedly played a major role in determining their ultimate degrees of polymerization.

Preparation of samples for doping and spectroscopy. Samples for electrical conductivity studies were typically prepared by compression of powders into 1.25 cm diameter pellets at ca. 10,000 psi in a standard infrared KBr pellet press. The thicknesses of the pellets ranged from 0.5 - 1.5 mm.

PPV samples were usually prepared somewhat differently. The yellow powder was placed between two Teflon sheets (ca. 0.01" thickness) and compressed to ca. 300 psi to produce irregularly-shaped wafers. Rectangular specimens well-suited for electrical conductivity studies (ca. 2 cm x 0.3 cm) were obtained by cleaving the wafers edge-on with a razor blade. This method was not successful with other polymer samples as the wafers were extremely brittle and could not be easily cleaved to appropriate geometries.

Infrared spectra of PPV were obtained from a thin film pressed onto Teflon film at ca. 300 psi. A Teflon film was placed in the reference beam of the Perkin-Elmer 283 grating infrared spectrophotometer.

Doping. All samples were mounted in air on the four-probe apparatus with Electrodag (Chapter III). Samples were typically pumped at least

one hour prior to doping. The four-probe apparatus usually contained samples for weight uptake of dopant and EPR spectroscopy.

Doping of samples with AsF_5 did not follow any general procedure although the techniques described in Chapter III applied to the initial stages of doping. Typically, PPV samples were doped by exposing them to the full vapor pressure of AsF_5 at -98°C (ca. 30 torr). It was found useful to begin the doping in stages with a few torr of AsF_5 , since immediate initial exposure occasionally resulted in fracture of the material. Other materials were doped similarly. For samples which responded slowly to AsF_5 (e.g., 3, 4 and 5), the AsF_5 pressure was usually increased to 100 - 200 torr by removing the slush bath from the cold finger of the bulb until the conductivity reached the saturation value. The AsF_5 was then condensed back into the bulb at -196°C . It should be noted that the slush bath serves to trap HF which may be formed in the vacuum line from the reaction of AsF_5 with moisture. Thus, the use of higher pressures of AsF_5 allowed HF to enter the vacuum line and the four-probe apparatus, and on occasion the glass walls of the apparatus became clouded with a white film presumably due to the reaction with HF. To avoid this problem, it is recommended for future studies that the AsF_5 be purified by trap-to-trap distillation to remove HF and also that the vacuum line be pretreated with AsF_5 prior to doping.

All AsF_5 -doped samples were handled in a glove bag (prepurified nitrogen gas). Reference samples were weighed in pre-weighed vials capped in the glove bag. Samples for EPR spectroscopy were placed in

EPR tubes in the glove bag and the tubes were sealed with a torch after pumping on a vacuum line for at least one hour.

Selected polymers were doped with iodine, sodium naphthalide and H_2SO_4 as described in Chapter III. Compensation experiments were carried out with ca. 100 torr of NH_3 (contained in a gas storage bulb and degassed prior to use).

Due to the fairly low electrical conductivity of the doped samples, conductivities were usually determined from the two-probe method. However, for samples which attained resistances of $< 10^3 \Omega$ upon doping, the four-probe method was employed. The undoped conductivities of most samples were beyond the range of measurement (ca. $< 10^{-10} \Omega^{-1} \text{ cm}^{-1}$) with the instruments in our laboratory.

EPR spectra. EPR spectra of doped materials were obtained using a Varian E-9 X-band spectrometer. The determination of g values (DPPH reference) has been described in Chapter VI. Saturation plots (signal amplitude vs. microwave power) were obtained as described in Chapter VII.

Results

PPV. The room temperature conductivity of a PPV wafer was ca. $10^{-10} \Omega^{-1} \text{ cm}^{-1}$, somewhat larger than the value of $10^{-14} \Omega^{-1} \text{ cm}^{-1}$ reported by Manecke et al. More precise measurements (Y.W. Park, University of Pennsylvania) yielded $\sim 10^9 \Omega^{-1} \text{ cm}^{-1}$. The effect of doping of PPV with AsF_5 is qualitatively analogous to that observed with polyacetylene¹⁸

and poly(p-phenylene).¹ Exposure of a PPV wafer to ca. 30 torr AsF₅ for 2 - 3 hours resulted in a conductivity increase of ten orders of magnitude.

The yellow sample developed an olive greenish hue and eventually assumed a dark brown coloration with a slight brassy luster. The dependence of the amount of AsF₅ incorporated into the polymer as determined by weight uptake of a reference PPV wafer is given in Table 10.

Table 10

Room Temperature Conductivity of AsF₅-Doped PPV (7A).

<u>$\sigma \quad \Omega^{-1} \text{ cm}^{-1}$</u>	<u>AsF₅ (wt %)</u>
4.3×10^{-5}	5.6
1.3×10^{-3}	8.9
6.2×10^{-2}	16.4
~ 3	57.0

Final molar composition: $[\text{C}_8\text{H}_6(\text{AsF}_5)_{0.92}]_x$

A significant and surprising observation was that essentially no difference in conductivity was found between the doped higher and lower molecular weight samples (Table 11, 7A and 7B).

It is worthwhile to note that exposure of a pressed pellet of PPV to AsF₅ resulted in the immediate color change of yellow to lustrous gold on the surface of the pellet. The conductivity of this sample was typically found to be ca. one order of magnitude lower than those ob-

Table 11. Conductivity and EPR data for doped aromatic polymers and model compounds.

TABLE 11

Compound	Dopant	$\sigma_{\text{doped}}, \Omega^{-1} \text{cm}^{-1}$	Molar ratio, dopant/ monomer units	EPR g value	EPR linewidth (G)
1	AsF ₅	$\sim 10^{-4}$	-	2.0025	0.6
2	AsF ₅	$\sim 10^{-6}$	-	-	-
3	AsF ₅	$\sim 10^{-6}$	0.20	2.0024	0.9
4	AsF ₅	$\sim 10^{-5}$	0.21	2.0022	1.0
5	AsF ₅	$\sim 10^{-4}$	0.37	2.0026	0.5
6	AsF ₅	$\sim 10^{-2}$	-	-	-
7A	AsF ₅	~ 3	0.92	2.0024	1.5
	Na	$\sim 10^{-2}$	-	-	-
	H ₂ SO ₄	$\sim 10^{-3}$	-	-	-
	I ₂	$< 10^{-7}$	-	-	-
7B	AsF ₅	~ 3	-	-	-
8	AsF ₅	~ 0.7	0.13	-	-
9	AsF ₅	$< 10^{-7}$	-	2.0024	-

(continued)

TABLE 11 (continued)

Compound	Dopant	$\sigma_{\text{doped}}, \Omega^{-1} \text{cm}^{-1}$	Molar ratio, dopant/ monomer units	EPR g value	EPR linewidth (G)
10	AsF ₅	$\sim 10^{-7}$	-	-	-
11	AsF ₅	$\sim 10^{-7}$	-	-	-
	H ₂ SO ₄	$\sim 10^{-4}$	-	-	-
	I ₂	$\sim 10^{-5}$	-	-	-

tained upon doping of PPV wafers. Furthermore, even after doping to the saturation conductivity, fracture of the pellet revealed a yellow and essentially undoped interior.

The AsF_5 -doped PPV samples were very unstable to oxygen and/or moisture and conductivity decayed rapidly upon room temperature exposure to air. The materials became black and several small liquid droplets, presumably moisture, were observed on their surfaces. However, the conductivity was reduced by less than 25% when the sample was held under dynamic vacuum for 18 hours. The conductivity of AsF_5 -doped PPV was electronic; passage of ca. 0.5 mA through the sample for 14 hours caused almost no change in sample resistance.

It has been shown that chemical compensation of donor and acceptor species readily occurs in polyacetylene¹⁹ and poly(p-phenylene).¹ This compensation effect was also observed in PPV. Thus, exposure of AsF_5 -doped PPV ($\sigma \sim 3 \Omega^{-1} \text{ cm}^{-1}$) to ~ 100 torr of the donor, NH_3 , resulted in a rapid decrease in conductivity. The light brown material assumed insulator-like properties after several minutes.

Exposure of PPV to iodine vapor for several hours resulted in no measurable conductivity change ($R > 10^7 \Omega$), although the yellow sample adopted a brown coloration. Treatment of a PPV pellet with a solution of sodium naphthalide radical anion in THF resulted in a rapid increase in conductivity to ca. $10^{-2} \Omega^{-1} \text{ cm}^{-1}$ (Table II). The surfaces of the pellet immediately assumed a golden luster. Continued exposure to the solution caused rapid deterioration of the pellet due to its poor mechanical integrity. Exposure of a PPV wafer to the vapor of H_2SO_4 result-

ed in a black coloration of the sample surface. The conductivity rose to ca. $10^{-3} \Omega^{-1} \text{ cm}^{-1}$ after several hours. However, the resistance of the sample was found to increase during the measurement (ohm-meter) suggesting that polarization of ionic charges occurred. This was presumably due to the presence of adsorbed H_2SO_4 on the surface of the sample. It should be noted that even after 48 hours exposure to H_2SO_4 , the interior of the sample after fracture was yellow (undoped).

Doping of PPV (8) with AsF_5 yielded a conductivity of ca. $0.7 \Omega^{-1} \text{ cm}^{-1}$. The value is comparable to that from samples prepared by the Wittig reaction indicating that the ultimate conductivity of PPV attained through doping is not dependent upon variations in trace impurities or end groups. In addition, pyrolyzed 8 showed a similar conductivity to that of the parent material upon doping. Although the pyrolysis treatment is expected to increase the conjugation length of the material, the above results are consistent with those reported previously (Table 11, 7A and 7B) and again imply that the conductivity of AsF_5 -doped PPV is not very sensitive to the degree of polymerization of the material.

Infrared spectroscopy was used to obtain evidence of metal-like properties in doped PPV. The IR spectrum of pristine PPV (7A) pressed on Teflon film (with Teflon film in the reference beam of the spectrophotometer) is shown in Figure 43a. Exposure of this sample to AsF_5 (30 torr) for ~ 3 hours produced a featureless spectrum (Figure 43b), the high transmission being due to incomplete coverage of the sample on the Teflon film. The spectrum was recorded in air with sample exposure

Figure 43. Infrared spectra of undoped
and AsF₅-doped PPV.

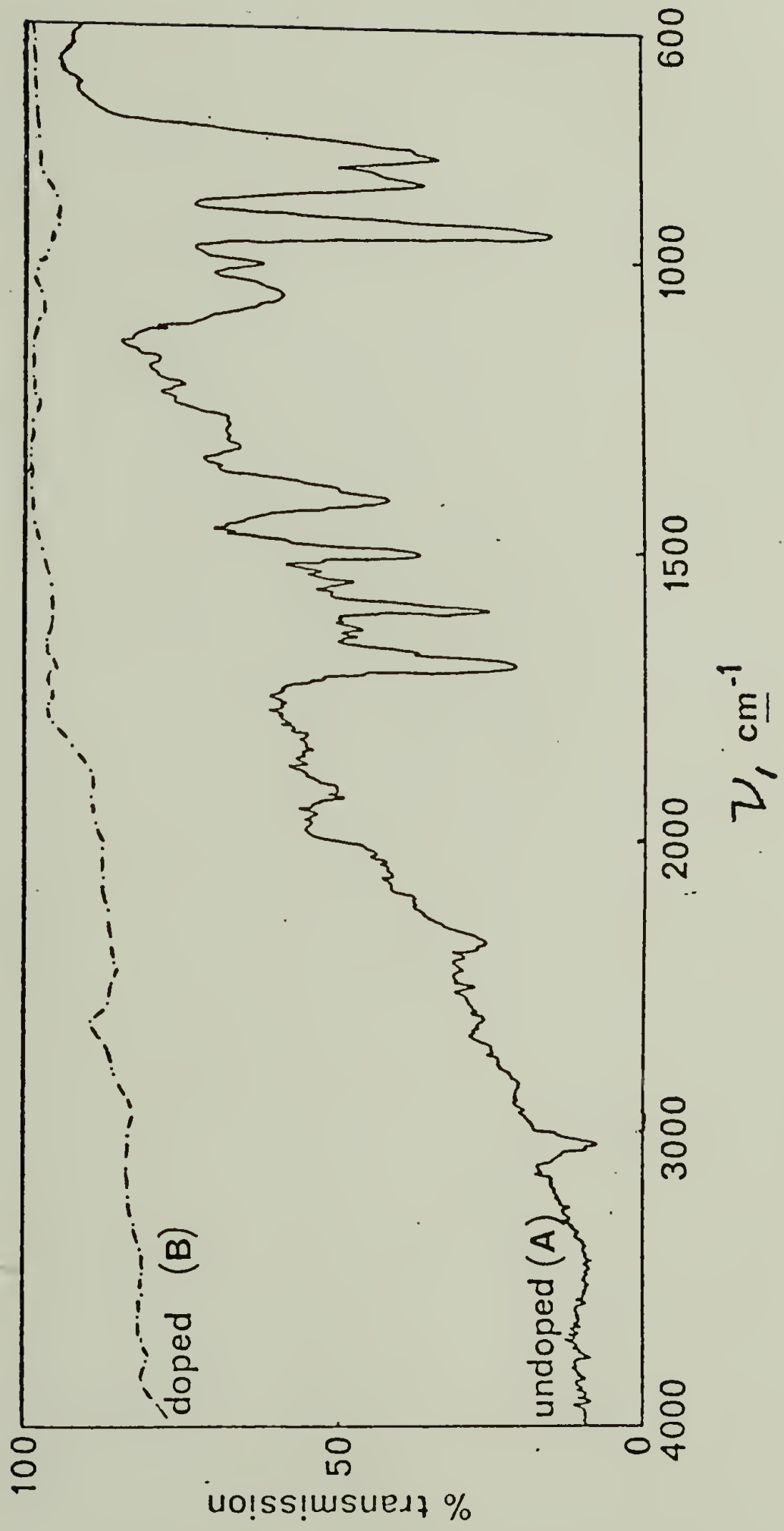


Figure 44. EPR spectra of PPV doped with AsF_5 .
(a) Lightly doped
(b) Heavily doped

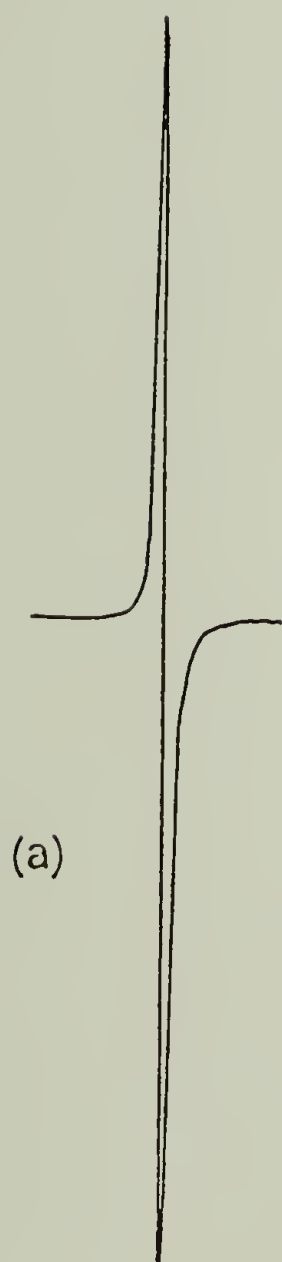


Figure 45. EPR saturation plots of AsF_5 -doped PPV.

\triangle Lightly doped

\circ Heavily doped

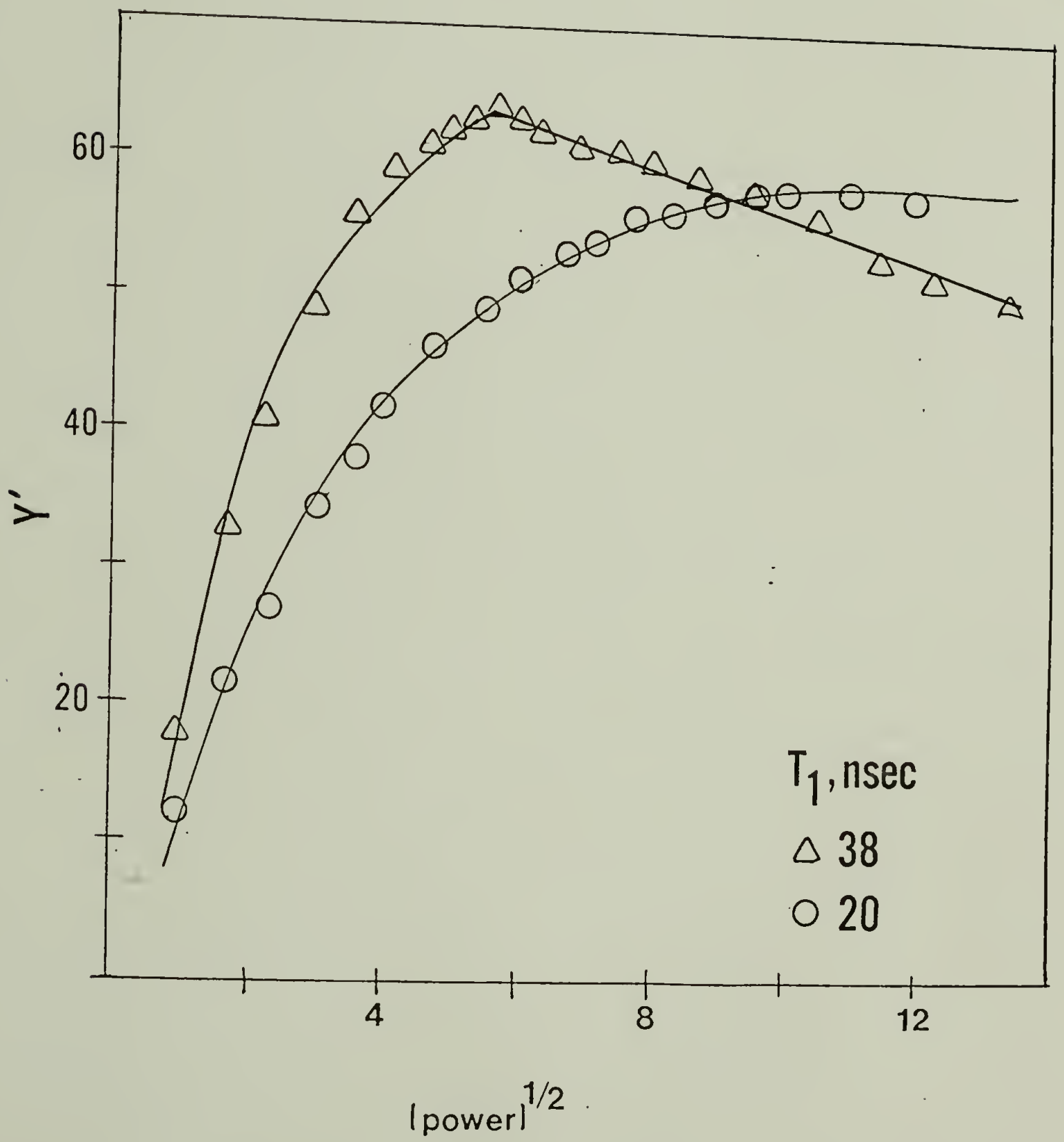
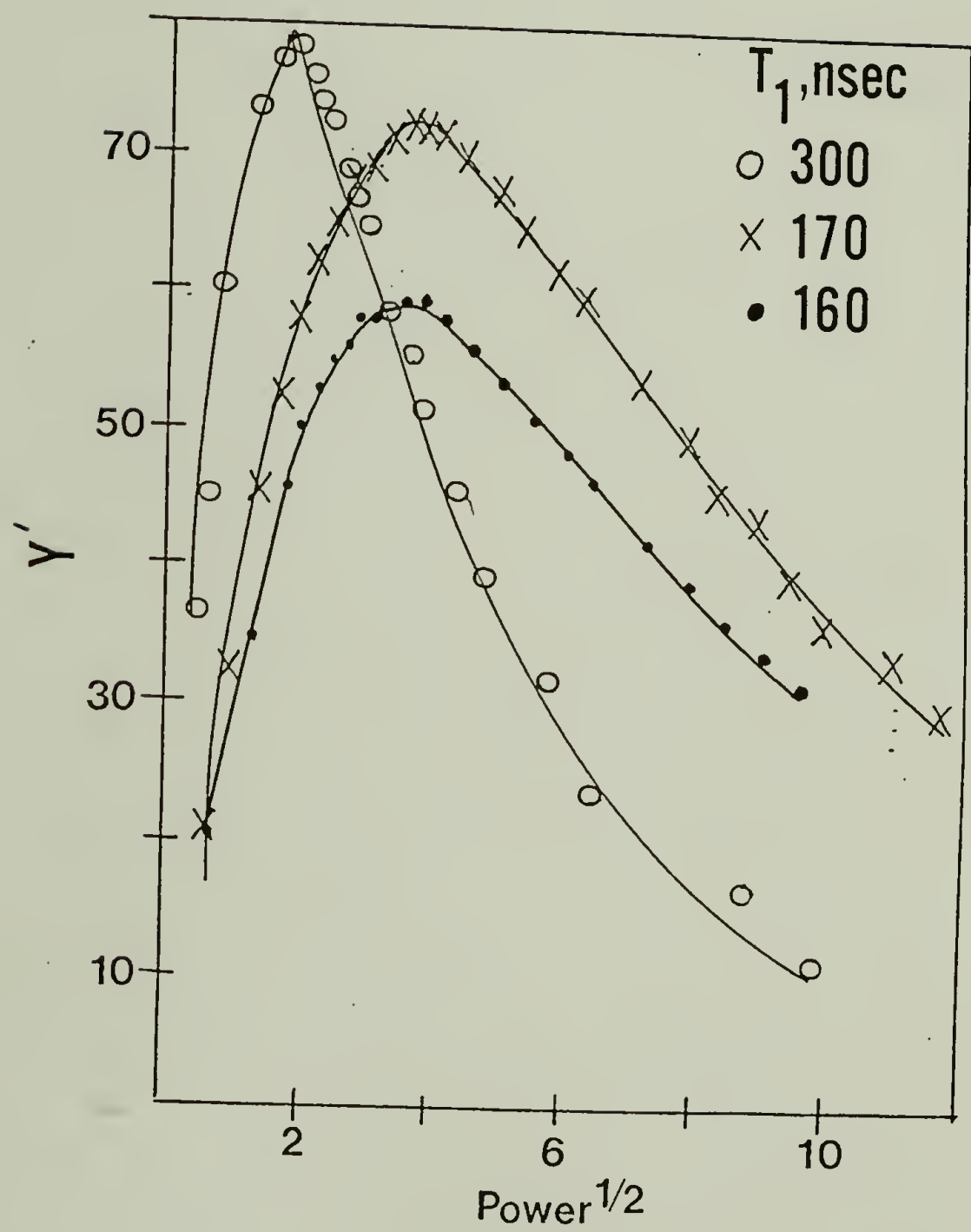


Figure 46. EPR saturation plots of AsF_5 -doped model compounds (see Table 11 for compositions)

- compound 3
- x compound 4
- compound 5



time kept to a minimum. The featureless spectrum is consistent with metallic behavior.

EPR spectroscopy was used to study the effect of doping and the nature of the free spins in PPV. Undoped PPV possessed an extremely weak EPR line (even at high spectrometer gains) although exposure to < 1 torr AsF_5 for ~ 1 minute produced a narrow (0.5 G), intense EPR signal (Figure 44a). Heavily doped PPV ($\sigma \sim 3\Omega^{-1}\text{ cm}^{-1}$) exhibited a broadened signal (1.5 G) which was asymmetric (Figure 44b). This Dysonian lineshape, which has also been observed with AsF_5 -doped polyacetylene,²⁰ is consistent with metallic behavior.

EPR saturation plots of lightly AsF_5 -doped (7A) and heavily doped (8) PPV samples are shown in Figure 45. Heavy doping resulted in a saturation maximum at a higher microwave power as was observed in doping of $(\text{CH})_x$ with AsF_5 (Chapter VII). However, the saturation maximum of heavily doped PPV occurs at a much lower microwave power than that observed in heavily doped, "metallic" $(\text{CH})_x$. It is interesting to note that in one case (heavily AsF_5 -doped 7A), upon recording saturation behavior for pieces of a pressed pellet having a lustrous coppery surface and a yellow (undoped) interior, the A/B ratio of the Dysonian lineshape increased from ca. 1.6 to ca. 3.1 at high microwave powers (> 60 mW). Furthermore, the surface of the previously undoped interior possessed a black coloration upon completion of the experiment and the EPR sample tube was noticeably warm.

Model compounds and PPV derivatives. The results of doping of several

organic model compounds and polymers are summarized in Table 11. Compounds 3, 4 and 5 can be considered as low molecular weight analogs of PPV (7) and poly(p-phenylene butadienylene) (10). Exposure of compressed pellets of compounds 1 - 5 to AsF_5 typically resulted in uptake of AsF_5 and the development of a gold or copper luster on the surfaces of the pellet. Stilbene (3) became shiny black and naphthalene (1) became pink-red and finally violet-black during doping. The data indicate that the limiting value of the conductivity upon doping of compounds 3 - 5 increases as the size of the conjugated system increases. In all cases, the interior of the pellets remained undoped, even when relatively high (200 - 300 torr) pressures of AsF_5 were employed. The g values from EPR spectra (Table 11) were in the range 2.0022 - 2.0026. EPR saturation plots (Figure 46) for compounds 3 - 5 doped with AsF_5 show saturation at relatively low microwave powers in contrast to doped PPV (Figure 45).

Polymers 9 - 11 yielded conductivities in the range $< 10^{-7}$ - $\sim 10^{-3} \Omega^{-1} \text{cm}^{-1}$ depending on the dopant. All pellets exposed to AsF_5 displayed undoped interiors. Doping of 11 with H_2SO_4 was qualitatively analogous to the similar doping of PPV; namely, an increase in sample resistance occurred during two-probe measurements suggesting polarization of ionic species.

Discussion

The data of Table 11 indicate that large increases in conductivity (assuming σ of the undoped materials to be $< 10^{-10} \Omega^{-1} \text{cm}^{-1}$) generally

result upon doping of these compounds. However, perhaps the most important observation in this work was that in all cases only a thin surface layer of the pressed pellets appeared to be doped with AsF_5 . This suggests that a chemical change occurs at the surface of the pellets, forming a "skin" which prevents diffusion of AsF_5 into the interior of the pellet. Upon considering the strong electron acceptor (Lewis acid) properties of AsF_5 and the susceptibility of aromatic units to electrophilic attack, it seems quite reasonable to suggest that the "skin" is formed as the result of polymerization of the model compounds or polymers via Friedel-Crafts type chemistry catalyzed by AsF_5 . In fact, Lewis acids such as AlCl_3 are used as catalysts in the polymerization of benzene to poly(p-phenylene).²¹ An observation concerning naphthalene doped with AsF_5 supports the formation of a "polymer" on the surface of the pellet. It was observed that placement of an AsF_5 -doped, NH_3 -compensated naphthalene pellet into ether resulted in solubilization of the undoped pellet interior although a brown "disk" from the surface of the pellet was insoluble. Furthermore, recent studies²² of doping of paraphenylene oligomers (e.g., biphenyl, terphenyl, etc.) with AsF_5 have unambiguously shown that the final product in all cases is poly(p-phenylene). Thus, it appears that AsF_5 serves as both a dopant and a "chain extender" in these aromatic systems.

This interesting chemistry exhibited by AsF_5 affords one obvious and rather serious implication concerning doping studies of the compounds illustrated in Figure 42. As mentioned earlier, an important impetus for initiating these studies was the use of rather well-defined

starting materials in order to examine the influence of parameters such as molecular weight, ring substitution, etc., on the ultimate conductivity attainable through doping. However, the observation that polymerization occurs to some undetermined degree upon doping with AsF_5 indicates that these materials become very ill-defined and thus specific conclusions concerning this work are limited. The AsF_5 -catalyzed polymerization reaction may well account for the observation that the conductivity of doped PPV is essentially independent of the (initial) degree of polymerization or nature of the end groups if the same final product ("polymerized" PPV) is obtained. At least in the case of oligomers 3 - 5, the limiting value of the conductivity upon doping increases as the size of the conjugated system increases. Unfortunately, the mole ratios of dopant to monomer units listed in Table 11 are not very meaningful in view of the fact that only the surfaces of the pellets were doped. The relatively high dopant concentration obtained in the case of a PPV wafer (Table 11, sample 7a) is probably due to the relatively large surface-to-volume ratio of the thin wafers as compared to the somewhat thicker pressed pellets employed with the other materials.

PPV doped with AsF_5 clearly afforded the highest conductivities of all of the materials investigated. The featureless IR spectrum (Figure 43b) and the Dysonian EPR signal (Figure 44b) suggest that heavily doped PPV is metallic. Iodine was observed to be a poor dopant, probably due to the relatively high ionization potential of PPV. Similar behavior has been reported for poly(p-phenylene).¹⁻³ Methoxylated PPV (11) is expected to have a lower ionization potential than PPV itself and, in

fact, iodine is a better dopant for 11 than for PPV. On the other hand, the lower conductivity of 11 doped with AsF_5 as compared to PPV might be due to coordination of the strong Lewis acid AsF_5 with the relatively basic $-\text{OCH}_3$ substituents. This coordination could increase the ionization potential of the polymer, making the creation of charge carriers more difficult. The low conductivity obtained upon doping of 9 is probably the result of decreased conjugation in the meta PPV isomer.

All materials studied by EPR (Table 11) did not possess detectable spin resonances in their pristine states although intense and narrow resonances appeared even after only mild exposure to AsF_5 . The EPR spectra of all materials heavily doped with AsF_5 (with the exception of PPV) displayed symmetrical lineshapes. The g values ranged from 2.0022 - 2.0026 indicating that the free spins created upon doping are due to π -electron radicals.²⁰ Undoubtedly, radical cations are formed upon doping. Dimerization of radical cations is likely to occur and may also account in part for the formation of a "skin" on the surfaces of the materials. The EPR saturation plots of AsF_5 -doped PPV (Figure 45) and similarly doped model compounds 3 - 5 (Figure 46) may contain important information. In the case of the model compounds, saturation occurs at fairly low microwave powers and seems to suggest that the free carriers in these materials are very localized even after heavy doping; i.e., T_1 is relatively long, suggesting that the free electrons do not "see" each other to any great extent. This saturation behavior is similar to that of undoped $(\text{CH})_x$, although upon doping with AsF_5 the saturation maximum becomes progressively shifted to higher microwave powers (see Chapter

VII). PPV doped with AsF_5 displays somewhat intermediate behavior. The value of T_1 for heavily doped PPV is about an order of magnitude smaller than those of the doped compounds 3 - 5, perhaps suggesting that the free electrons in PPV interact with each other more readily (i.e., they are more delocalized). Admittedly, this "localized-delocalized" carrier hypothesis is speculative. However, the saturation behavior is at least somewhat consistent with conductivity in these doped aromatic materials. It might be interesting, for example, to compare the saturation behavior of, say, doped stilbene to that of the doped material compensated with NH_3 and then re-doped with AsF_5 . The latter material, presumably a doped "polystilbene", is anticipated to display higher conductivity and may also show saturation behavior which suggests greater delocalization of free electrons in the extended, conjugated system.

It is worthwhile to note that the surfaces of the undoped interior of a previously AsF_5 -doped PPV pellet became colored upon recording EPR spectra at high powers and was apparently the result of microwave heating. A portion of the AsF_5 originally present in the material was driven off and doped additional available surfaces. More importantly, the A/B ratio of the Dysonian lineshape increased by a factor of ~ 2 . This may suggest that the conductivity concomitantly increased upon heating. It may be possible that chain extension is favored at high temperatures and, upon heating, the length of the conjugated PPV system increased. Although this phenomenon was not investigated in any greater detail, it may be worth considerable attention. Experimental control of the degree and the kinetics of the chain extension and doping reactions is impor-

tant for developing an understanding of the relationship between these factors and electrical transport properties.

Conclusions

Doping of PPV with AsF_5 yields new materials of greatly enhanced conductivities, with values of the latter parameter ($\sim 3 \Omega^{-1} \text{ cm}^{-1}$) in the lower part of the range associated with classical metals. IR and EPR evidence substantiates the contention that heavily doped PPV assumes a metallic-like state. In several respects, the phenomena investigated are qualitatively analogous to those previously observed in polyacetylene and poly(p-phenylene).

In all cases, only the surface of pressed pellets were observed to be doped with AsF_5 . This implies that a change must occur upon doping at the pellet surface which forms a "skin" and prevents diffusion of AsF_5 into the pellet interior. Evidence suggests that polymerization of the materials occurred via Friedel-Crafts type chemistry catalyzed by AsF_5 . Thus, AsF_5 is apparently able to act as both a dopant and a chain extender. The observation that the limiting conductivity of AsF_5 -doped PPV is independent of the "initial" degree of polymerization may be due to this phenomenon.

Unfortunately, all materials investigated became ill-defined upon AsF_5 doping in terms of molecular weight, degree of chain branching, etc., thus precluding studies of quantitative relationships between these parameters and the ultimate conductivity attainable upon doping. In view of the sensitivity of conductivity measurements to defects, in-

terparticle contacts, etc., thermopower measurements are anticipated to be useful in future studies in order to properly evaluate intrinsic electrical properties in these materials.

References

1. D. M. Ivory, G. G. Miller, J. M. Sowa, L. W. Shacklette, R. R. Chance and R. H. Baughman, J. Chem. Phys., 71, 1506 (1979)
2. R. H. Baughman, D. M. Ivory, G. G. Miller, L. W. Shacklette and R. R. Chance, Org. Coat. Plast. Chem., 41, 139 (1979)
3. L. W. Shacklette, R. R. Chance, D. M. Ivory, G. G. Miller and R. H. Baughman, Synth. Metals, 1, 307 (1980)
4. R. H. Baughman, Org. Coat. Plast. Chem., 43, 762 (1980)
5. W. R. Salaneck, H. R. Thomas, C. B. Duke, A. Paton, E. W. Plummer, A. J. Heeger and A. G. MacDiarmid, J. Chem. Phys., 71, 2044 (1979)
6. K. K. Kanazawa, A. F. Diaz, R. H. Geiss, W. D. Gill, J. F. Kwak, J. A. Logan, J. F. Rabolt and G. B. Street, J. Chem. Soc. Chem. Comm., 854 (1979)
7. T. Yamamoto, K. Sanechika and A. Yamamoto, J. Polym. Sci. Polym. Lett. Ed., 18, 9 (1980)
8. R. R. Chance, L. W. Shacklette, G. G. Miller, D. M. Ivory, J. M. Sowa, R. L. Elsenbaumer and R. H. Baughman, J. Chem. Soc. Chem. Comm.
9. J. F. Rabolt, T. C. Clarke, K. K. Kanazawa, J. R. Reynolds and G. B. Street, J. Chem. Soc. Chem. Comm.
10. B. J. Tabor, E. P. Magre and J. Boon, Eur. Polym. J., 7, 1127 (1971)
11. R. N. MacDonald and T. W. Campbell, J. Amer. Chem. Soc., 82, 4669 (1960)
12. G. E. Wnek, J. C. W. Chien, F. E. Karasz and C. P. Lillya, Polymer,

- 20, 1441 (1979); J. C. W. Chien, R. D. Gooding, F. E. Karasz, C. P. Lillya, G. E. Wnek and K. Yao, Org. Coat. Plast. Chem., 43, 886 (1980)
13. a.) G. Kossmehl, Ber. Bunsenges. Phys. Chem., 83, 417 (1978);
b.) S. Misumi et al., Bull. Chem. Soc. Japan, 34, 1833 (1961)
14. S. Misumi et al., Bull. Chem. Soc. Japan, 36, 399 (1963)
15. G. Kossmehl, M. Hartel and G. Manecke, Makromol. Chem., 131, 37 (1970)
16. G. Manecke, D. Zerpner and G. Kossmehl, Makromol. Chem., 137, 35 (1971)
17. G. Drefahl, R. Kuhnstedt, H. Oswald and H-H. Horhold, Makromol. Chem., 131, 89 (1970)
18. C. K. Chiang, M. A. Druy, S. C. Gau, A. J. Heeger, E. J. Louis, A. G. MacDiarmid, Y. W. Park and H. Shirakawa, J. Amer. Chem. Soc., 100, 1013 (1978)
19. C. K. Chiang, S. C. Gau, C. R. Fincher, Jr., Y. W. Park, A. G. MacDiarmid and A. J. Heeger, Appl. Phys. Lett., 33, 18 (1978)
20. I. B. Goldberg, H. R. Crowe, P. R. Newman, A. J. Heeger and A. G. MacDiarmid, J. Chem. Phys., 70, 1132 (1979)
21. Cf. P. Kovacic and A. Kyriakis, J. Amer. Chem. Soc., 85, 454 (1963)
22. R. R. Chance, L. W. Shacklette, G. G. Miller, D. M. Ivory and R. H. Baughman, Bull. Amer. Phys. Soc., 25, 399 (1980)

C H A P T E R X I

CONCLUSIONS

The novelty of electrically conducting polymers and their potential for a wide variety of applications implies that this class of materials will be a focal point of scientific investigation for many years. Synthetic organic chemistry is anticipated to play a most important role in the development of materials which possess a wide range of desirable properties (i.e., processibility, stability, etc.). A more thorough understanding of polymer-dopant interactions and conduction mechanisms is essential in order to properly predict the polymer structures which can yield highly conducting derivatives. Of particular importance are studies concerning polyacetylene and related materials.

Copolymerization has been shown to be an effective method for producing novel polymers having interesting properties (i.e., solvent plasticization) and a range of attainable conductivities through chemical doping. Additional studies concerning morphology and degree of crystallinity are required to understand the relationship between these properties and copolymer composition. Furthermore, thermoelectric power measurements would be useful in evaluating the intrinsic effect of backbone substitution on electrical properties of the copolymers. Besides being of practical value in terms of the potential to experimentally control polymer structure and properties, copolymerization is anticipated to afford important information of theoretical interest as

well. The question of how often the conjugated π -system of polyacetylene can be interrupted while still maintaining good conductivity can be addressed through studies of acetylene/ethylene copolymers. Thermopower measurements would be particularly useful. The importance of electrical conductivity along the polyacetylene chain (one-dimensionality) as opposed to between chains could be examined using copolymers of acetylene with, for example, $\text{HC}\equiv\text{CR}$, where R is an alkyl group of variable length (ethyl, propyl, etc.). The larger substituents should disrupt interchain interactions to a greater degree. Thus, if interchain conduction is of major importance, copolymers having larger substituents (at a particular copolymer composition) may be expected to afford lower conductivities upon doping than those materials possessing smaller substituents.

Introducing saturation into the $(\text{CH})_x$ backbone has another implication; namely, enhanced oxidative stability. It is likely that protonic acid dopants such as H_2SO_4 actually add a hydrogen to the $(\text{CH})_x$ chain and probably accounts for the increased stability of this type of doped $(\text{CH})_x$ as compared to other derivatives. In miscellaneous studies, we have found that $(\text{CH})_x$ film is significantly swelled in the presence of chlorosulfonic acid. This might suggest the possibility of synthesizing polyacetylene derivatives having eventual solubility, stability and high conductivity. Thus, the chemistry of protonic acid-doped $(\text{CH})_x$ merits careful study.

The potential of polyacetylene gels has not yet been realized. The solvent-swollen state suggests the possibility of incorporating

stabilizers into the polymer. Post-polymerization reactions such as hydrogenation, hydrochlorination, etc., may be more efficient with the gel leading to better structural characterization of the parent material. In view of recent concerns and controversies about the homogeneity of dopant distribution in polyacetylene, doping in the gel state may be important as a simple method to achieve a homogeneous dopant distribution.

Studies of magnetic properties with regard to doped polyacetylene are of paramount importance in understanding polymer-dopant interactions. Additional electron paramagnetic resonance studies are needed to assess the influence of the nature of the dopant and the rate of doping on soliton generation and annihilation. Such studies need to focus on four classes of dopants; namely, halogens, protonic acids, alkali metals and the class of Lewis acids consisting of AsF_5 , SbCl_5 , etc. Additional spectroscopic studies (IR, Raman, NMR) are necessary to evaluate the charge transfer doping mechanism, the structure and oxidation state of the dopant and the homogeneity of dopant placement.

Finally, the chemistry of polymer-dopant interactions in aromatic materials needs to be investigated. It is unfortunate that polymerization occurs in conjunction with doping (at least in the case of AsF_5) thereby rendering the materials intractable. It may be possible to control the degree and kinetics of the chain extension process in order to allow charge transfer to predominate. Other dopants having lesser tendencies to induce polymerization should be explored. The enhanced thermal and oxidative stability of aromatic polymers as compared to

polyacetylene indicates that these materials will play a major role in the development of practical polymeric conductors.

